Synthesis of Green Transportation Fuel: Investigations in Ultrasonic Route to Biodiesel Production

A
Thesis
Submitted in
Partial fulfillment of the
Requirements for the Degree of

DOCTOR OF PHILOSOPHY

By

Hanif A. Choudhury

Centre for Energy
Indian Institute of Technology Guwahati
Guwahati – 781039, Assam, India
May 2014

Dedicated
To
My
Parents
&
My Mentors

Certificate

It is certified that the work contained in the thesis entitled "**SYNTHESIS OF GREEN TRANSPORTATION FUEL: INVESTIGATIONS IN ULTRASONIC ROUTE TO BIODIESEL PRODUCTION**", by **Hanif A. Choudhury** (Roll No. 08615106), has been carried out under my supervision and that this work has not been submitted elsewhere for a degree.

Date:

Dr. V. S. Moholkar
Professor
Department of Chemical Engineering &
Center for Energy

CONTENTS

LIST OF TABLES i

LIST OF FIGURES v

LIST OF SCHEMES ix

ABBREVIATIONS AND NOTATIONS xi

CHAPTER 1: GENERAL INTRODUCTION AND MOTIVATION 1

1.1 Introduction 1

1.2 Global Production Scenario Of Biodiesel 9

1.3 Biofuels Policy of India 11

1.4 National Biodiesel Mission 14

1.5 Aim and Scope of Present Thesis 18

References 20

CHAPTER 2: ULTRASONIC BIODIESEL SYNTHESIS: BACKGROUND AND LITERATURE REVIEW 23

2.1 Introduction 23

2.2 Biodiesel 24

2.3 Biodiesel from Different Vegetable Oil 25

2.3.1 Blending/Dilution of Vegetable Oil with Petrodiesel 25

2.3.2 Micro-emulsion with Short Chain Alcohols 26

2.3.3 Pyrolysis and Catalytic Cracking 26

2.3.4 Transesterification 27

2.4 Emission and Combustion Characteristic of Biodiesel: A Brief Review 27

2.5 Literature Review Biodiesel Synthesis 35

2.6 Synthesis of Biodiesel by Transesterification Process 51

2.7 Overview, Inferences and Justification of Present Thesis Work 56

2.8 Basic Principles of Ultrasound Wave Phenomenon and Cavitation Bubble Dynamics 59

2.8.1 What is an Acoustic Wave? 59

2.8.2 Intensity of Acoustic Wave 59

2.8.3 Cavitation Bubble Dynamics 60

2.8.4 Physical and Chemical Effect of Ultrasound and Cavitation 73

References 75

CHAPTER 3: ULTRASONIC BIODIESEL SYNTHESIS FROM SOYBEAN OIL WITH BASIC HETEROGENEOUS (CaO) CATALYST **93**

3.1 Introduction 93
3.2 Experimental and Mathematical Modeling 95
3.2.1 Approach 95
3.2.2 Material and Methods 96
3.2.3 Experimental Setup and Protocol 97
3.2.4 Mathematical Modeling of Cavitation Bubble Dynamics 102
3.3 Result and Discussion 104
3.3.1 XRD and BET Data of The Solid Catalyst 106
3.3.2 NMR Analysis of Reaction Mixture 108
3.3.3 Experimental Results and Statistical Analysis 108
3.4 Optimization of the Process 113
3.5 Kinetic Analysis of the Process 113
3.6 Simulation Results 115
3.7 Discussion and Analysis 118
3.8 Conclusion 121
References 121

CHAPTER 4: ULTRASONIC SYNTHESIS OF BIODIESEL FROM JATROPHA OIL USING HETEROGENEOUS BASE CATALYST **127**

4.1 Introduction 127
4.2 Approach, Materials, Methods and Analysis 129
4.3 Experimental Setup 130
4.4 Experimental Protocol 130
4.5 Mathematical Modeling of Cavitation Bubble Dynamics 139
4.6 Results and Discussion 142
4.6.1 Characterization of CaO catalyst 142
4.6.2 NMR analysis 143
4.6.3 Experimental results and statistical analysis 144
4.6.4 Optimization of the process 149
4.6.5 Kinetic analysis of the process 150
4.7 Simulation Results 154
4.8 Analysis 154
4.9 Conclusion 158
References 159

CHAPTER 5: ULTRASONIC JATROPHA OIL BIODIESEL SYNTHESIS USING SULFURIC ACID **165**

5.1 Introduction 165
5.2 Material and Methods 166
5.2.1 Materials 166
5.2.2 Experimental Setup 167
5.2.3 Experimental Protocol 167
5.2.4 Analysis 171
5.2.5 Simulations of Cavitation Bubble Dynamics 172
5.3 Results and Discussion 174
5.3.1 NMR Analysis of Reaction Mixture 174
5.3.2 Experimental Results 175
5.3.3 Simulation Results 183
5.4 Analysis 184
5.5 Conclusions 188
References 189

CHAPTER 6: ULTRASONIC JATROPHA OIL BIODIESEL SYNTHESIS USING CHLOROSULFONIC ACID **191**

6.1 Introduction 191
6.2 Theoretical Contemplation 192
6.3 Materials and Methods 196
6.3.1 Materials 196
6.3.2 Experimental Setup 197
6.3.3 Experimental Protocol 198
6.4 Results & Discussion 203
6.4.1 Statistical Analysis 203
6.4.2 Kinetic and Thermodynamic Analysis 209
6.4.3 Thermodynamic Analysis 212
6.5 Conclusion 213
References 214

CHAPTER 7: OVERVIEW AND SCOPE FOR FURTHER RESEARCH **217**

7.1 Overview 217
7.2 Scope for Future Work 224
References 225

ACKNOWLEDGEMENTS **227**

RESEARCH OUTPUT FROM THESIS **229**

List of Tables

CHAPTER 1

Table 1.1	Time trend production of crude oil in India (in thousand Tonnes)	2
Table 1.2	Statistics of crude oil import in India (2011-12)	2
Table 1.3	Consumption of petroleum products in India (in thousand Tonnes)	4
Table 1.4	Time history of Indian petroleum industry at a glance (2011-12)	5-6
Table 1.5	State wise total registered motor vehicle in India	7-8
Table 1.6	Renewable energy in India at a glance	13
Table 1.7	Area (ha) under major tree born oilseeds for production of biodiesel in India.	15
Table 1.8	Estimated yield of non-edible oil seeds plants	16
Table 1.9	Diesel & biodiesel demand, area required under Jatropha for different blending rates	16

CHAPTER 2

Table 2.1	Country wise feedstock for production for biodiesel	29
Table 2.2	Fatty acid compositions of different vegetable oils	31
Table 2.3	Summary of results of published literature on biodiesel synthesis from *Jatropha Curcas* oil using conventional techniques	49
Table 2.4	Summary of published literature on ultrasonic biodiesel synthesis from *Jatropha curcas* oil with different catalysts	50
Table 2.5	FAME and FAEE chemical formulae	53
Table 2.6	Chemical formulae of different glycerides	53

CHAPTER 3

Table 3.1	Experimental range and levels of independent variables	96
Table 3.2A	Box–Behnken experimental design matrix	100
Table 3.2B	Composition of reaction mixture in Box–Behnken experimental design matrix	100
Table 3.3A	Model for the radial motion of cavitation bubble	105
Table 3.3B	Thermodynamic properties of various species	106
Table 3.4A	Estimated regression coefficients for % FAME yield	110
Table 3.4B	Analysis of variance (ANOVA) for transesterification of soybean oil using ultrasound	111
Table 3.4C	Analysis of surface plots	111
Table 3.5	Kinetic analysis of reaction data	115
Table 3.6	Summary of the simulation results	118

CHAPTER 4

Table 4.1	Composition of reaction mixture for esterification reaction	132
Table 4.2A	Experimental range and levels of independent variables	135
Table 4.2B	Box–Behnken experimental design matrix*	136
Table 4.2C	Composition of reaction mixture in Box–Behnken experimental design matrix	136
Table 4.3A	Parameters of simulations	141
Table 4.3B	Results of simulations	141
Table 4.4A	Estimated regression coefficients for % FAME yield	147
Table 4.4B	Analysis of variance (ANOVA) for transesterification of soybean oil using ultrasound	147
Table 4.4C	Analysis of contour plots	148
Table 4.5A	Results of integral analysis of reaction kinetics data	152
Table 4.5B	Kinetic analysis for 3rd order reaction	152

CHAPTER 5

Table 5.1	Levels of independent variables in statistical design of experiments	169
Table 5.2A	Box–Behnken experimental design matrix	170
Table 5.2B	Composition of reaction mixture in Box–Behnken experimental design matrix	171
Table 5.3A	Estimated regression coefficients for % FAME yield	180
Table 5.3B	Analysis of variance (ANOVA) for transesterification of *Jatropha curcus* oil	180
Table 5.3C	Analysis of surface plots	180
Table 5.4	Kinetic analysis of reaction data	183
Table 5.5	Summary of simulation results	185

CHAPTER 6

Table 6.1	Experimental range and levels of independent variables	200
Table 6.2A	Box–Behnken experimental design matrix	200
Table 6.2B	Composition of reaction mixture in Box–Behnken experimental design matrix	201
Table 6.3A	Estimated regression coefficients for % FAME yield	205
Table 6.3B	Analysis of variance (ANOVA) for transesterification of Jatropha oil	205
Table 6.3C	Analysis of surface plots	205
Table 6.4	Kinetic analysis of transesterification process	211
Table 6.5	Thermodynamic analysis	213

CHAPTER 7

Table 7.1	Summary of results of different components of ultrasonic biodiesel process development as described in preceding chapters	220

List of Figures

CHAPTER 1

Figure 1.1	A) Global biodiesel production, (B) Country wise biodiesel production	10
Figure 1.2.	Cost of biodiesel Production	17

CHAPTER 3

Figure 3.1	Results of the control experiments with mechanical stirring (reaction parameters: alcohol to oil molar ratio = 12:1, temperature = 65^{o}C, catalyst concentration = 8 wt% oil, agitation speed = 600 rpm)	98
Figure 3.2	Schematic of the experimental setup	99
Figure 3.3	(A) XRD spectrum of the CaO catalyst Characterization of catalyst, (B) Particle size distribution of the CaO catalyst. Summary of distribution: D(10%) – 957.2 nm, D(50%) – 1124.7 nm, D(90%) – 1325.2 nm, Average- 1176.7 nm, (C) N_2 adsorption–desorption isotherms for the CaO catalyst and the corresponding BJH pore size distribution curve.	107
Figure 3.4	^{1}H NMR spectrum of fatty acid methyl esters (FAME) of soybean oil	110
Figure 3.5	Response surface plots for % FAME yield as a function of reaction temperature, catalyst loading and methanol-to-oil molar ratio.	112
Figure 3.6	Kinetic analysis of experiment under optimum conditions. (A) Time history of conversion of triglycerides at different temperatures for methanol to oil molar ratio of 10:1 and catalyst concentration 6 wt%, (B) First order kinetic model fitted to the conversion data for determination of kinetic constants, (C) Arrhenius plot of ln (k) vs 1/T for the transesterification for methanol to oil molar ratio of 10:1 with catalyst concentration of 6 wt%	114
Figure 3.7	Simulation results for radial motion of a 5 µm cavitation bubble (air) in methanol at 65^{o}C. Time variation of (A) normalized bubble radius (R/R_o), (B) temperature in the bubble, (C) number of methanol molecules in the bubble, (D) pressure inside the bubble, (E) micro-convection (or oscillatory liquid velocity) generated by the cavitation bubble, (F) acoustic (or shock) waves emitted by the bubble.	116 - 117

CHAPTER 4

Figure 4.1	Schematic of experimental setup: (1) Transducers, (2) Sonication bath, (3) Sonication medium (water), (4) Reaction mixture, (5) Reflux condenser, (6) Electrical motor, (7) Electrical immersion heater, (8) Stand holder	131
Figure 4.2	Time history of conversion of triglycerides with mechanical agitation for methanol to oil molar ratio of 12:1 and catalyst concentration 4 wt% at 65^{o} C.	134
Figure 4.3	XRD spectrum of (a) CaO and (b) $Ca(OMe)_2$	143
Figure 4.4	^{1}H NMR spectrum of (A) pure *Jatropha Curcas* oil, (B) esterification product with 18% FAME and (C) fatty acid methyl ester (FAME) of *Jatropha Curcas* oil after trans–esterification	145
Figure 4.5	Contour plots showing variation of transesterification yield (or % FAME yield) as a function of any two experimental parameters. (A) temperature & molar ratio, (B) molar ratio & catalyst concentration, (C) catalyst concentration and temperature.	148
Figure 4.6	Results of integral analysis of the kinetic data for determination of kinetic constant and order of transesterification (with respect to triglycerides)	152
Figure 4.7	Kinetic analysis of transesterification under optimum conditions determined from statistical analysis, (A) Time history of conversion of triglycerides at different temperatures for methanol to oil molar ratio of 11:1 and catalyst concentration 5.5 wt%, (B) Fitting of 3rd order kinetics to the transesterification data to determine the kinetic constant of the reactions, (C) Arrhenius plot of ln (k) vs 1/T for transesterification reaction considering 3rd order reaction kinetics (with respect to triglyceride) for optimum conditions of methanol to oil molar ratio (11:1) and catalyst concentration (5.5 wt%) as determined by statistical analysis	153
Figure 4.8	Simulation results for radial motion of a 5 μm cavitation bubble (air) in methanol at 55^{o}C. Time variation of (A) normalized bubble radius (R/R_o), (B) acoustic (or shock) waves emitted by the bubble, (C) micro–convection (or oscillatory liquid velocity) generated by the cavitation bubble.	155

LIST OF FIGURES

CHAPTER 5

Figure 5.1 ^{1}H NMR spectrum of (A) pure Jatropha oil, and (B) fatty acid methyl ester(FAME) of Jatropha oil after trans–esterification. 176

Figure 5.2 Response surface plots for % FAME yield as a function of reaction temperature, catalyst loading and methanol–to–oil molar ratio. 179

Figure 5.3 Kinetic analysis of transesterification of Jatropha oil under sonication. (A) Time history of conversion of triglycerides at different temperatures for methanol to oil molar ratio of 7:1 and catalyst concentration 6 wt%, (B) Pseudo 1st order kinetic model fitted to the conversion data for determination of kinetic constants at different reaction temperatures, (C) Arrhenius plot of ln (k) vs 1/T for the transesterification for methanol to oil molar ratio of 7:1 with catalyst loading of 6 wt%. 182

Figure 5.4 Simulation results for radial motion of a 10 μm cavitation bubble (air) in methanol at 55 ^{o}C. Time variation of (A) normalized bubble radius (R/R_o), (B) temperature in the bubble, (C) number of methanol molecules in the bubble, (D) pressure inside the bubble; (E) micro–convection (or oscillatory liquid velocity) generated by the cavitation bubble; (F) acoustic (or shock) waves emitted by the bubble. 186 - 187

CHAPTER 6

Figure 6.1 Experimental setup: (1) ultrasound probe, (2) refrigerated and heating bath circulator, (3) reaction mixture, (4) water in the refrigerated bath (5) ultrasonic processor. 197

Figure 6.2 Control experiment for transesterification with mechanical agitation. Reaction conditions: temperature = 65^{o}C, molar ratio = 20:1, catalyst concentration = 5 wt% oil, Agitation = 300 rpm. Reaction mixture: Oil = 13.6 mL, MeOH = 11.4 mL, Catalyst = 0.4 mL. 198

Figure 6.3 Response surface plots for % FAME yield as a function of reaction temperature, catalyst loading and methanol–to–oil molar ratio. 208

Figure 6.4 (A) Time history of FAME yield at different reaction temperatures for single–step transesterification process, (B) Fitting of pseudo first order kinetic model to the conversion data for single–step transesterification process. Best fit equations: For 30 ^{o}C, $y = 0.00472\ x$, $R^2 = 0.92$; For 45 ^{o}C, $y = 0.00976\ x$, $R^2 = 0.94$; For 60 ^{o}C, $y = 0.0133\ x$, $R^2 = 0.954$, (C) Time history of FAME yield at different reaction temperature for 2–step transesterification process. (D) Fitting of pseudo first order kinetic model to the conversion data for 2–step transesterification process. Best fit equations: For 30 ^{o}C, $y = 0.00485\ x + 0.22$, $R^2 = 0.99$; For 45 ^{o}C, $y = 0.00787\ x + 0.22$, $R^2 = 0.99$; For 60 ^{o}C, $y = 0.0137\ x + 0.22$, $R^2 = 0.945$. 210

Figure 6.5 Arrhenius plot for determination activation energy of transesterification process. (A) Single step process, Best fit: $y = -6895.1\ x + 16.57$, $R^2 = 0.89$, (B) Double step process with intermediate water removal after esterification, Best fit: $y = -3764.2\ x + 7.0357$, $R^2 = 0.99$. 211

Figure 6.6 Eyring plots to determine change in enthalpy (ΔH) and change in entropy (ΔS) during transesterification process. (A) Single–step process, Best fit: $y = -4023\ x + 1.8621$, $R^2 = 0.99$, (B) Double step process (with intermediate removal of water after esterification), Best fit: $y = -3168.8\ x - 0.603$, $R^2 = 0.99$. 213

List of Schemes

Chapter 2

Scheme 2.1	Transesterification reaction of TG molecule with methanol	53
Scheme 2.2	Esterification reaction of FFA with methanol	54
Scheme 2.3	Homogeneous alkali catalysed transesterification reaction	54
Scheme 2.4	Homogeneous acid catalysed transesterification reaction	55
Scheme 2.5	Simultaneous esterification and transesterification by heterogeneous acid	56

Chapter 3

Scheme 3.1	Chemical mechanism of calcium oxide catalyzed trans-esterification for biodiesel synthesis.	119

Chapter 4

Scheme 4.1	Proposed mechanism of calcium oxide catalyzed trans–esterification reaction.	150

Chapter 6

Scheme 6.1(A)	Reaction of chlorosulfonic acid induced esterification process.	194
Scheme 6.1(B)	Removal of water formed during esterification by chlorosulfonic acid	195
Scheme 6.1(C)	Plausible mechanism of chlorosulfonic acid induced transesterification process	195

ABBREVIATIONS

Abbreviation	Full Form
ATF	Aviation turbine fuel
ANOVA	Analysis of Variance
bbl	Barrel
BTE	Break Thermal Efficiency
BSEC	Brake Specific Energy Consumption
CGPL	Combustion, Gasification and Propulsion Laboratory
CNG	Compressed Natural Gas
DF	Degrees of Freedom
DG	Diglyceride
DOE	Design of Experiments
EIA	Energy Information Administration
FAME	Fatty Acid Methyl Ester
FAEE	Fatty Acid Ethyl Ester
FFA	Free Fatty Acid
FDI	Foreign Direct Investment
F & W	Forest and Wasteland
GC	Gas Chromatography
GDP	Gross Domestic Product
GHG	Green House Gas
HHS	High Sulfur Heavy Stock

Abbreviation	Full Form
HC	Hydrocarbon
HSD	High Speed Diesel
IEA	International Energy Agency
IISC	Indian Institute of Science
JVC/Private	Joint Ventures Contracts
LDO	Light Diesel Oil
LSHS	Low Sulfur Heavy Stock
LPG	Liquid Petroleum Gas
MMT	Million Metric Ton
MS	Mean of Squares
MSP	Minimum Support Price
MMTPA	Million Metric Tons Per Annum
NREGP	National Rural Employment Guarantee Programme
NABARD	National Bank of Agriculture and Rural Development
NIST	National Institute of Science and Technology (USA)
OIL	Oil India Limited
ONGC	Oil and Natural Gas Corporation
PM	Particulate Matter
SKO	Kerosene
SFC	Specific Fuel Consumption
SIDBI	Small Industries Development Bank of India
SMP	Statutory Minimum Price

CHAPTER 1

General Introduction and Motivation

1.1 Intoduction

Major energy needs of a developing nation are in terms of electricity and transportation fuels. A developing country like India with population of 1 billion is a major producer and consumer of energy. Currently, India ranks fifth in global list of energy consumer and fourth largest petroleum consumer next to United States, China and Japan [1]. As a result of global economic slowdown, the growth of Indian economy has remained at modest rate of 6–8% [1]. Despite this, growing infrastructural and socio –economic development has lead to significant rise in energy consumption across all major sectors (especially industrial and agricultural) of Indian economy. For past 67 years after independence, India has remained one of the most energy deficit nations of the world. As per the statistics produced by National Statistical Organization (Ministry of Statistics and Programme Implementation), the total domestic energy production is projected at 669.7 MTOE (million tonnes of oil equivalent), which puts India among top 10 energy producer nation globally [1]. However, per capita consumption is at a meagre 600 KGOE (kg of oil equivalent). This is far lesser than the global average of

Table 1.1: Time trend production of crude oil in India (in thousand Tonnes)

Item	2005–06	2006–07	2007–08	2008–09	2009–10*	2010–11
(a) Onshore						
Gujarat	6251	6212	6177	5946	5960	5905
Assam/Nagaland	4474	4400	4357	4674	4740	4719
Arunachal Pradesh	104	109	102	102	131	116
Tamil Nadu	385	353	298	265	239	234
Andhra Pradesh@	216	252	279	289	304	305
Rajasthan	–	–	–	–	447	5149
Total (a)	11430	11326	11213	11276	11821	16428
Organization wise Production						
OIL	3234	3107	3100	3468	3572	3582
ONGC	8095	8058	7921	7565	7515	7446
JVC/Private	101	161	192	243	734	5400
(b) Offshore						
ONGC	16309	17993	18020	17801	17340	17002
JVC/Private	4451	4669	4885	4431	4529	4282
Total (b)	20760	22662	22905	22233	21869	21284
Grand Total (a + b)	32190	33988	34118	33508	33690	37710

Source: [2]

Table 1.2: Statistics of crude oil import in India (2002)

Year	Crude oil import (MMT)	Average crude oil price (US $/bbl.)
2002–03	81.99	26.59
2003–04	90.43	27.98
2004–05	95.86	39.21
2005–06	99.41	55.72
2006–07	111.50	62.46
2007–08	121.67	79.25
2008–09	132.78	83.57
2009–10	159.26	69.76
2010–11	163.59	85.09
2011–12*	171.729	111.89

* Provisonal. **Source**: [2]

Note: Imports of Crude Oil during 2011–12, in terms of quantity was 171.729 MMT valued at Rs.6,72,220 crore, this marked an increase by 4.97% in quantity terms w.r.t. 163.595 MMT during the year 2010–11, but increased by 47.65% (w.r.t.Rs.4,55,276crore) in value terms over the year of 2010–11. In terms of US$, the extent of increase in value of Crude imports was 33.58%. During the year 2004–05 the imports of crude oil was 95.861 MMT that increased to 171.729 MMT in 2011–12 i.e. an increase of 79.14% as compared to imports during 2004–05.

over 2000 KGOE [3]. Per capita electricity consumption in India (as estimated in March 2012) was 819 kWh, which is less than that of global average of more than 2000 kWh [4]. Scenario on the front transportation fuel is even worse. As per statistics provided by Ministry of petroleum and Natural Gas [5], India have total reserves of 760 million metric tons of crude oil and 1330 billion cubic meters of natural gas. However, the actual production of these resources is very small, i.e. crude oil production stood at 38.09 millions tons and natural gas production was 47.56 billion cubic meters during 2011–2012. Tables 1.1–1.4 give the quantitative details of the petroleum and natural gas statistics in past few years [5]. The petroleum consumption, however, has been far higher than production. The total consumption of petroleum products in India was 147.995 million metric tons in 2011–2012, which was 4.93% higher than the previous year. The net value of crude oil imports for the year was 6.69 trillion, which has created an enormous burden on country's economy. A typical distribution of consumption of petroleum products is as follows [6]:

(1) Transportation sector: 51%

(2) Industry sector 14%

(3) Commercial sector 13%

(4) Domestic sector 18%

(5) Agriculture 4%

As evident from above figures, the energy demand of the transport sector is the highest. Road transport (both passenger and freight) constitutes the major fraction of the total traffic in India. In addition, economic growth, increasing urbanization, increasing purchase power and improved road infrastructure have lead to a significant rise in vehicle ownership across all states of India. The statistics of the registered motor vehicles in India are given in Table 1.5 [7]. It could be inferred from Table 1.5 that the total number of registered motor vehicles in India has exceeded 140 million by 2012 [7]. With increasing vehicle ownership, the demand

Table 1.3: Consumption of petroleum products in India (in thousand Tonnes)

Products	2006–07	2007–08	2008–09	2009–10	2010–11	2011–12*
Light Distillates Components	**37076**	**38557**	**39878**	**39086**	**41433**	**43657**
LPG	10849	12165	12344	13121	14328	15358
Mogas	9286	10332	11258	12818	14192	14992
Naphtha	13886	13294	13911	10239	10691	11105
Others	3055	2766	2365	2908	2222	2202
Middle Distillates Components	**57595**	**62823**	**66378**	**71198**	**74949**	**79407**
SKO	9505	9365	9303	9304	8928	8229
ATF	3983	4543	4423	4627	5079	5536
HSDO	42896	47669	51710	56320	59990	64742
LDO	720	667	552	457	455	415
Others	491	579	390	490	497	458
Heavy Ends Components	**26078**	**27568**	**27343**	**27911**	**25402**	**23588**
Total	**120749**	**128948**	**133599**	**138195**	**141784**	**146652**
Refinery Fuel	10920	11751	11912	11607	15873	15422
Grand total	**131669**	**140699**	**145511**	**149802**	**157657**	**162074**

* Provisional and not included data in respect of RIL SEZ Refinery as it is presumed that all products have been exported and not consumed domestically.

Notes: Consumption includes sales by all companies & direct private imports. SKO – Kerosene, LDO – Light Diesel Oil, LSHS – Low Sulfur Heavy Stock, HHS – High sulphur heavy stock, ATF – Aviation turbine fuel
Source: [5]

for petroleum products, especially diesel and gasoline, is bound to grow. Although, many new vehicles have CNG (compressed natural gas) engines, the primary fuel for the vehicles remains diesel and gasoline, which constitute >95% of total fuel consumption. The demand of diesel and petrol is likely to grow at a rate of 6–8% in coming years [6].

Another major problem associated with petroleum fuels is the environmental pollution and the emission of green house gases (GHG) leading to global warming. India is the fourth largest global contributor to carbon emissions. As per the statistics provided by Indian Network for Climate Change Assessment [8], the net greenhouse gas emission from India was 1729.91 million metric tons of CO_2 equivalents. The contribution from Energy, Industry, Agriculture and Waste sectors were 58%, 22%, 19% and 3%, respectively. The energy sector

Table 1.4: Time history of Indian Petroleum Industry at a Glance

Item	Unit	2004–05	2005–06	2006–07	2007–08	2008–09	2009–10	2010–10	2011–12
1. (Balance Recoverable)									
(i) Crude Oil	Million Tonnes	739	756	725	770	773	775	757	760
(ii) Natural Gas	Billion Cubic Meters	923	1075	1055	1090	1115	1149	1278	1330
2. Consumption									
(i) Crude Oil (in terms of refinery crude throughput)	Million Tonnes	127.42	130.11	146.55	156.10	160.77	192.77	206.00	211.42
(ii) Petroleum Products (excl. RBF)	–do–	111.63	113.21	120.75	128.98	133.60	137.81	141.04	148.00
3. Production									
(i) Crude Oil	–do–	33.98	32.19	33.99	34.12	33.51	33.69	37.68	38.09
(ii) Petroleum Products	–do–	118.58	119.75	135.26	144.93	150.52	179.77	190.32	196.71
(iii) LPG from natural gas	–do–	2.24	2.19	2.09	2.06	2.16	2.24	2.17	2.21
4. Imports & Exports									
(i) Gross Imports:	–do–								
(a) Qty: Crude Oil	–do–	95.86	99.41	111.50	121.67	132.78	159.26	163.59	172.11
LNG	–do–		5.06	6.81	8.32	8.06	8.83	8.95	9.7
(b) Value: Crude Oil	Rs. Billion	1170.30	1717.02	2190.29	2726.99	3481.49	337.54	558.12	482.88

Contd...

Item	Unit	2004–05	2005–06	2006–07	2007–08	2008–09	2009–10	2010–10	2011–12
LNG	–do–		33.66	56.50	71.97	95.48	102.97	127.19	203.73
(ii) Net Improts									
(a) Qty : Crude Oil	Million Tonne	95.86	99.41	111.50	121.67	132.78	159.26	163.59	172.11
(b) Value: Crude oil	Rs. Billion	1170.03	1717.02	2190.29	2726.99	3481.49	3753.78	4559.09	6690.68
(iii) Unit Value of Crude oil imports (gross)	Rs./MT	12205.6	17272	19643.5	22412.63	26220.98	23570.28	27868.29	38873.54
5. India's Total Imports	Rs. Billion	5010.65	6604.09	8405.06	10123.12	13744.36	13637.04	16834.67	23422.17
6. India's Total Exports	Rs. Billion	3753.40	4564.18	5717.79	6558.64	8407.55	8455.34	11429.20	14540.66
7. Petroleum imports as % of India's total imports	%	26.33	30.74	31.63	33.67	30.45	30.76	31.15	31.50
8. Petroleum Exports as % of India's total Exports	%	7.97	10.95	14.18	16.89	14.51	17.04	17.16	18.33
9. Natural Gas:									
(i) Gross Production	Billion Cubic Meters	31.76	32.20	31.75	32.42	32.85	47.496	52.22	47.56
(ii) Utilisation	"	30.775	31.325	30.791	31.749	31.746	46.521	51.248	46.482

Source: [2, 5]

Table 1.5: State wise total registered motor vehicle in India

State/ Union Territory	2001	2002	2003	2004	2005	2006	2007	2008	2009	2010	2011
Andhra Pradesh	3966	4389	5002	5720	6458	7218	6367	7208	8059	8923	10189
Arunachal Pradesh	21	21	21	21	22	22	22	22	22	22	145
Assam	542	596	657	727	815	914	1021	1116	1235	1384	1582
Bihar	949	1024	1121	751	1352	1432	1577	1739	1960	2357	2673
Chhatisgarh	857	948	1076	1216	1375	1541	1734	1935	2115	2436	2766
Goa	341	366	397	436	482	529	579	624	674	727	790
Gujarat	5576	6008	6508	7087	7817	8622	9497	10289	10999	11873	12993
Haryana	1949	2122	2279	2548	2854	3087	3528	3973	4425	4792	5377
Himachal Pradesh	217	244	269	289	301	334	342	371	494	538	622
Jmmu & Kashmir	330	364	399	439	478	524	570	620	668	739	927
Jharkhand	909	984	1101	1217	1357	1505	1686	1850	2038	2767	3113
Karnataka	3537	3636	3738	3977	5436	6220	5486	6217	6953	9044	9930
Kerala	2112	2315	2552	2792	3122	3559	3957	4430	4860	5398	6072
Madhya Pradesh	3095	3173	3459	3804	4188	4609	5047	5523	6011	6591	7356
Maharashtra	6760	7414	8134	8969	9936	10966	12171	13335	14451	15768	17434
Manipur	77	90	97	106	114	124	133	147	147	194	207
Meghalaya	62	67	73	73	92	104	117	128	142	158	176
Mizoram	31	34	37	42	47	52	61	66	70	80	93
Nagaland	160	177	162	172	172	184	210	226	240	254	273
Orissa	1096	1215	1359	1525	1715	1932	2148	2370	2607	2932	3338
Punjab	2910	3103	3308	3529	3876	4035	4294	4573	4832	5274	5274
Rajasthan	2943	3197	3487	3834	4261	4754	5336	5902	6490	7166	7986
Sikkim	12	13	15	17	20	22	25	26	29	34	39
Tamil Nadu	5162	5658	8005	8575	9257	10054	10981	11930	12891	14062	15638
Tripura	50	57	66	76	73	106	120	131	144	160	188
Uttarakhand	364	406	457	516	573	643	643	731	787	831	997
Uttar Pradesh	4921	5171	5928	6460	7344	7989	9086	9826	10779	11988	13287
West Bengal	1690	1690	2366	2548	2681	2827	3198	2762	3044	2747	3261
TOTAL STATES	50639	54482	62073	67466	76218	83953	89936	98072	107163	119240	132725

Continued…..

State/ Union Territory	2001	2002	2003	2004	2005	2006	2007	2008	2009	2010	2011
A. & N. Islands	25	28	28	28	37	41	48	53	60	62	69
Chandigarh	386	386	562	586	617	647	678	712	747	949	1008
D. & N. Haveli	13	13	31	35	40	45	51	58	63	69	76
Daman & Diu	37	41	44	48	51	55	62	68	70	72	78
Delhi	3635	3699	3971	4237	4187	4487	5492	5899	6302	6747	7228
Lakshadweep	4	5	5	5	5	6	7	7	7	8	9
Puducherry	252	270	293	313	347	384	432	484	538	599	673
TOTAL UNION TERRITORIES	4352	4442	4934	5252	5283	5665	6771	7281	7788	8506	9140
GRAND TOTAL	**54991**	**58924**	**67007**	**72718**	**81502**	**89618**	**96707**	**105353**	**114951**	**127746**	**141866**

Source: [7]

(mainly the coal based thermal power plants) emitted 1100 million tons of CO_2, while 142 million tons of CO_2 equivalent were contributed by transportation sector. In order to control these emissions, in view of rapidly growing vehicle population on rode, Government of India transport policy has targeted Euro–III & IV vehicle emission norms. However, effective implementation of these norms usually requires adoption of clean and green fuels. Therefore, the Government of India's energy economics and security policy is focused at alternate fuels, which are technically efficient, economically viable and environmentally sustainable. Biomass is the only renewable and abundant natural resource that has capability of supplying energy in various forms such as electric power and fuel (in various forms like solid, liquid and gas). Biomass based energy is, thus, a major issue in the energy security policy of the nation.

The major source of biomass in India is the agro and forest residues. A survey conducted by Combustion, Gasification and Propulsion Laboratory (CGPL) of Indian Institute of Science Bangalore has estimated the total agro residue production in India as 125 MMTPA, which has a potential of 16 GW of electricity generation. The total biomass in the form of forest residue is estimated at 249 million tons, which has capability of power generation equivalent to 33.29 GW [9]. Other resources of renewable power are wind, solar (both photovoltaic and thermal) and micro–hydro. The current scenario of the renewable energy in India is summarized in Table 1.6 [10].

1.2 Global production scenario of biodiesel

Driven by fast depletion of fossil fuels, sky rocketing international prices of crude oil and concerns of climate change (global warming) due to green house gas emissions, biodiesel industry has observed very rapid growth all over the world. The total annual global biodiesel production was around 5.1 billion gallons (or 15.1 MMTPA) in 2009, and the largest (~ 80%)

share of this production 80% was in the European Union [11]. Fig. 1.1 depicts the biodiesel production scenario in the world by region as well as the total annual production (current as well as projected, as shown in Fig. 1.1(A)).

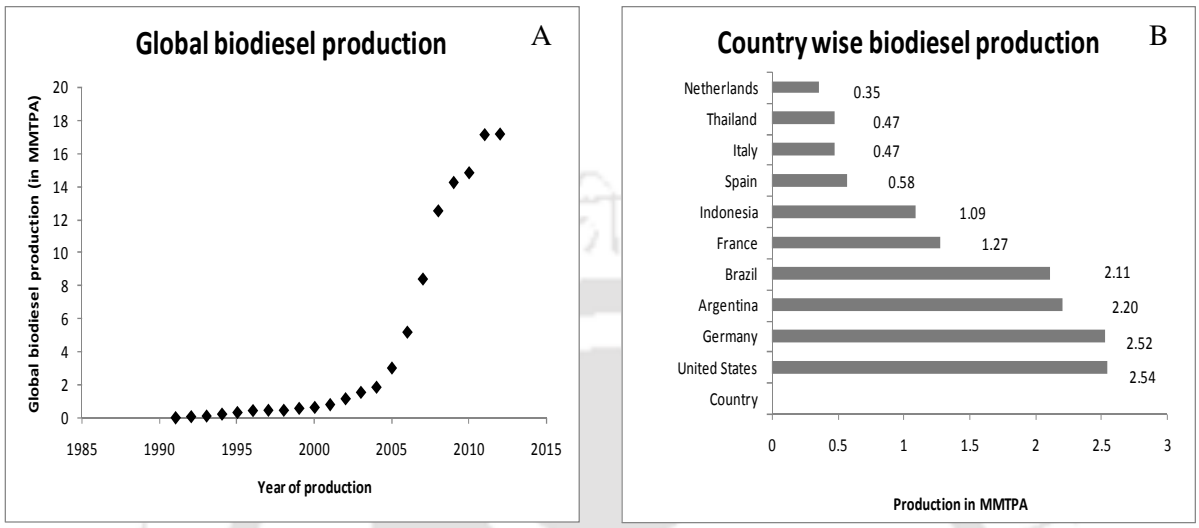

Figure 1.1 (A) Global total biodiesel production, (B) Country wise biodiesel production [12]

Although, Europe and United States are the leaders in biodiesel production, but almost every developing nation has included biodiesel production and implementation of use of biodiesel blends in the vehicles as a part of their renewable energy policies. In 2005 Energy Policy Act, Renewable Fuels Standard (RFS) was established in United States for blending of biofuels in transport fuels. The mandated use of renewable fuels by 2012 in the United States was 7.5 billion gallons (or 22.68 MMTPA). This was further increased to a target of 36 billion gallons (106.56 MMPTA) by 2022 under the Energy Independence and Security Act (EISA) of 2007. In the US, biodiesel production reached 650 million gallons (1.9 MMTPA) in 2008. EISA had set a target of production of 12.95 billion gallons (38.33 MMTPA) of transportation biofuels, of which 6.5 million gallons (1.92 MMTPA) is cellulosic biofuel (mainly ethanol to be blended with gasoline) and 1.15 billion gallons (3.4 MMTPA) biodiesel (to be blended with diesel) for 2010. Biofuels programme of Brazil stated in 1975 with the nation's Alcohol

Programme. In addition to Alcohol Programme, Brazil has started its National Biodiesel Programme in 2008 to ensure 2% biodiesel blend and 5% biodiesel blend in 2013. Following the mandate of National Biodiesel Programme, Brazil's production of biodiesel rises from 736 m^3 (588.8 MMTPA) in 2005 to 2.39 million m^3 (1.91 MMTPA) in 2010 making Brazil as world 2nd largest biodiesel producer [13]. In Europe the most important liquid biofuel for transportation is biodiesel that represents 82% of the total biofuels production. Germany is the largest producer of biodiesel with 150,000 tons/year (0.15 MMTPA) in 2004. France biodiesel production was around 520,000 tons/year (0.52 MMTPA) making it to be the 2nd largest producer of biodiesel in Europe. According to the European Commission's 2004 report, Germany produced an estimated 715,000 tons (0.71 MMTPA) of biodiesel in 2003, France produced 357,000 tons (0.357 MMTPA), and Italy produced 273,000 tons (0.273 MMTPA). Fig 1.1(B) gives the biodiesel production in ten leading countries in world in 2011. Countries like Australia, China, India, Indonesia, Malaysia, Philippines, South Korea, Taiwan and Thailand have also set national or partial mandates to blend biofuels. Indian biodiesel mission was started in 2003 with an am to ensure 20% blending of biodiesel by 2012. Commercial biodiesel production has not been started in any major scale in India. There are only a few small commercial biodiesel production units. To the best of our knowledge, Aatmiya Biofuels Pvt. Ltd. in Vadodara, Gujarat has been producing 1000 L/day (292 MT/Y) biodiesel. British Petroleum has been producing 9 million L per annum of biodiesel in Andhra Pradesh. Some other small scale producers of biodiesel in India (to the best of our knowledge) are: Biodiesel Technologies, Kolkata with production of 450 L/day (131.4 MT/Y) and Mint Biofuels, Pune with production of 400 L/day (116.8 MT/Y) [14].

1.3 **Biofuels Policy of India** [15]

In order to effectively utilize the renewable energy resources in India, the Government of India approved National Policy on Biofuels in December 2009. The salient

features and objectives of this policy are as follows:

To achieve optimum mix of primary resources of energy generation: Although fossil fuels continue to play dominant role in satisfying energy needs of the nation, these resources are limited and also contribute to pollution. The renewable energy resources are non–polluting and practically perpetual. India is blessed with abundant renewable energy resources, which should be used judiciously.

Mainstreaming of biofuels: This objective is aimed at having central role of biofuels in the energy and transportation sector of the country. The policy aims at accelerated development and promotion of cultivation, production and use of biofuels as alternative for conventional diesel and petrol. This will contribute to energy security and climate change mitigation in addition to creating new employment opportunities, which can lead to environmentally sustainable developments.

Stimulation of rural development with creation of new employment opportunity: The policy aims at promotion of non–food feed stocks (in view of fuel vs. food security). Another aim is to promote use of degraded or wasteland not suited for agriculture.

The policy also aims at making available minimum level of bio fuels in the market to meet the demand at any time. A target of implementing up to 20% blends biodiesel and ethanol with conventional petro–diesel and gasoline is envisaged till 2017.

The policy aims at development of new technologies for efficient synthesis of biofuels from non–food feed stocks. Research and development in this area should be promoted for all aspects of feedstock production and biofuels processing. Policy proposes to undertake intensive R&D in advanced conversion technologies for first generation biofuels and emerging technologies for second generation biofuels including conversion of lignocellulosic and non food grade feed stocks .The policy also emphasises development of technologies for end–use applications including modification and development of engines for the transport

Table 1.6: Renewable energy in India at a glance*

Sl. No.	Source / System	Cumulative achievement (as on 31 Aug 2013) (MW)
I.	**Power From Renewables**	
A	*Grid interactive renewable power*	
1.	Wind power	19779.15
2.	Small hydropower (≤ 25 MW)	3711.75
3	Biomass Power	1264.80
4.	Bagasse Cogeneration	2337.43
5.	Waste to Poewe–Urban–industrial	99.08
6.	Solar power (SPV)	1968.84
SUBTOTAL A		**29161.05**
B	*Off grid/Captive power*	
7.	Wind Power–Urban Industrial	115.57
8	Biomass (Non–Bagasse) Cogeneration	486.84
9.	Biomass Gasifier (Rural and Industrial)	160.30
10.	Aero–Generators/Hybrid Systems	2.14
11	SPV Systems (>1 kW)	131.86
12.	Water Mills/Micro Hydel	10.65(2131 nos).
SUBTOTAL B		907.36
TOTAL (A + B)		**30,068.41**
II.	**Remote Village Electrification**	
III.	**Decentralized Energy Systems**	
1.	Family type biogas plants (in lakhs)	46.55
2.	Solar Water Heating Systems – Collector Area (million sq m)	7.16

* Data as of August 2013 (kW = kilowatt; MW = megawatt; Sq m = square meter)
Source: [10]

sector based on large scale centralized approach, and for non–stationary applications such as electricity production through decentralized approach.

Appropriate financial and fiscal measures should be devised and implemented for achievement of policy objectives. This includes contract farming on private wasteland through minimum support price mechanism. The policy identifies Minimum Support Price (MSP) for oil seeds as major instrument to promote plantation of oil seeds by farmers. This will, of course, be decided after consultation with Government agencies, states, local bodies such as *Gram Panchayat* or *Gram Sabha* and other stakeholders. Policy also purposes extension of Statutory Minimum Price (SMP) mechanism (similar to that for sugarcane procurement) for oil seeds to be purchased by biodiesel processing units.

Coverage for the labours and other employees in plantations of non–edible oil seeds under National Rural Employment Guarantee Programme (NREGP).

Creation of new infrastructure for storage and distribution through financing farm institutions and banks like National Bank of Agriculture and Rural Development (NABARD), Indian Renewable Energy Development Agency (IREDA), Small Industries Development Bank of India (SIDBI).

Promotion of investment and joint ventures: Biofuels technologies and projects should be made eligible for availing 100% foreign equity thorough automatic approval route to attract Foreign Direct Investment (FDI).

1.4 National Biodiesel Mission [6, 18]

Government of India implemented the first phase of National Biodiesel Mission as a demonstration project during 2003–2007. The Ministry of Rural Development was appointed as the nodal ministry for plantation of 4,00,000 hector of Jatropha, which was identified as the most suitable non–edible oil seed (referring to the Report of the Committee on Development of Biofuels published by Planning Commission). With involvement of public and private sector organisations, state government and research institutions, this programme achieved moderate level of success.

In October 2005, Ministry of Petroleum and National Gas announced the biodiesel purchase policy, under which oil marketing companies would centrally purchase biodiesel from local manufacturers. Twenty purchase centres were set up across country by January 2006. The purchase price of biodiesel was set at Rs. 26.5 per litre. In 2008, the second self–sustaining execution phase of National Biodiesel Mission was launched for 4–year term 2008–12. This phase targeted at producing sufficient biodiesel for 20% blending by the end of 11^{th} 5–year plan. Under this programme, an estimated half–million hectors of Jatropha plantation has already been done, and it is expected to bear fruits by 2013.

Table 1.7: Area (ha) under major tree born oilseeds for production of biodiesel in India.

Sr. No.	Name of State	Jatropha *(Jatropha curcas)*	Neem *(Azadirechta indica)*	Karanja *(Pongamia pinnata)*	Mahua *(Mashuca indica)*	Simarouba *(Simarouba glauca)*
1.	Andhra Pradesh	1,500	59,856	7,009	5,620	–
2.	Assam	100	3,101	712	3	
3.	Arunachal Pradesh	235	12	28	34	
4.	Bihar	200	7,979	180	1301	
5.	Chattisgarh	304,152	14,657	1,895	7,793	
6.	Dadra Nagar Haveli	45	232	53	245	
7.	Gujarat	1,300	42,794	718	1,554	10
8.	Delhi		3,333	168		
9.	Haryana	1,405	12,534	553	55	–
10.	Himachal Pradesh	489	845	843	10	
11.	Jammu & Kashmir	9	212	5		
12.	Jharkhand	800	9,940	1,416	2,570	
13.	Karnataka	670	41,666	3,580	3,037	1,860
14.	Kerala	50	16,457	685	1,047	
15.	Madhya Pradesh	374,648	50,066	4,235	15,884	
16.	Maharashtra	2,360	59,903	2,201	5,341	15
17.	Manipur	450	668	19		
18.	Meghalaya	446	216	347	3	
19.	Mizoram	380				
20.	Nagaland	490				
21.	Orissa		13,324	1,506	5,367	
22.	Puduchery		17,207	1,830	37	
23.	Punjab	300	12,836	319	37	
24.	Rajasthan	10,554	60,768	595	3,257	
25.	Sikkim	150	51		3	
26.	Tamilnadu	900	96,413	4,176	1324	
27.	Tripura	150	440.21	3.93		
28.	Uttar Pradesh	12,000	70,193	1,929	6,482	
29.	Uttarakhand	13,500	2,527	513	838	
30.	West Bengal	21,500	19,125	481	658	
Total		**748,782**	**617,359**	**36,000**	**62,500**	**1,885**

Source: [16]

Table 1.8: Estimated yield of non–edible oil seeds plants

Sr. No.	Scientific name	Plant type	Plant part	Oil yield (kg/ha)
1.	*Azadirachta indica* (Neem)	Tree	Seed	2670
2.	*Calophyllum inophyllum* (Polanga)	Tree	Seed	4680
3.	*Hevea brasiliensis* (Rubber)	Tree	Seed	40–50
4.	*Jatropha curcas* (Physic nut)	Tree/shrub	Seed	1900–2500
5.	*Pongamia(Millettia)pinnata/Pongamia glabra* (Koroch, karanja)	Tree	Seed	225–2250
6.	*Ricinus communis* (Castor)	Tree/shrub	Seed	450
7.	*Simarouba glauca* (Paradise tree)	Tree	Seed	900–1200
8.	*Thevetia peruviana* (Yellow oleander)	Shrub	Seed	1575

Source: [17]

Table 1.9: Diesel & biodiesel demand, area required under Jatropha for different blending rates

Year	Diesel Demand MMTPA	Biodiesel Demand @5% blend MMTPA	Plantation Area @5% blend (MHa)	Biodiesel Demand @10% blend MMTPA	Plantation Area @10% blend (MHa)	Biodiesel Demand @10% blend MMTPA	Plantation Area @10% blend (MHa)
2001–02	39.81	1.99	N.A.	3.98	N.A.	7.96	N.A.
2006–07	52.33	2.62	2.19	5.23	4.38	10.47	8.76
2011–12	66.9	3.35	2.79	6.69	5.58	13.38	11.19

Source: [18]

A recent report from Global Agricultural Information Network (GAIN) [6] puts the biodiesel production requirement (for just 5% blending level) at 3.21million tons. If the target of 20% blend is to be achieved, it should necessitate Jatropha cultivation on 18.6 million ha (assuming an average seed yield of 2.5 tons/ha with 30% oil content) by 2017. Table 1.7 shows cultivation area (ha) under major tree born oilseeds for production of biodiesel in different states of India. Table 1.8 shows the estimated yield of non–edible oil seeds from different plants species. Table 1.9 shows diesel demand and corresponding biodiesel requirement for 5 and 10% blending rate. The area required under Jatropha cultivation to achieve 5 and 10% blending rates is also given in Table 1.9.

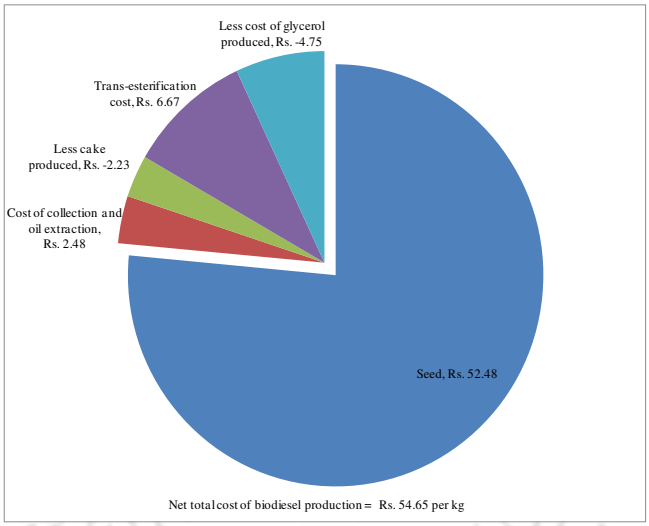

Figure 1.2.Cost of biodiesel Production. Source [19]

The major impediments for achieving goals of National Biodiesel Mission have been smaller land holdings and ownership issues with Government or community–owned wasteland to stimulate large–scale Jatropha plantation. This has also lead to smaller or negligible investment in biodiesel manufacture by private or public sector companies. In order to give a boost to biodiesel production, the Government has plans of increasing the MSP for biodiesel to Rs. 34/litre (as compared to Rs. 26.5/litre as done at the beginning of the biodiesel mission). The oil marketing companies have recommended an even higher MSP of Rs. 36/litre for biodiesel. This price is still much smaller than the actual production cost of biodiesel to attract handsome investment. Fig. 1.2 shows typical contribution of various cost components in biodiesel manufacturing [19]. It could be seen from this analysis that the cost of feedstock is the single largest contribution to the production cost of biodiesel. It is also noteworthy that the side products of biodiesel manufacture, i.e. oil cake remaining after extraction of oil from seeds and the glycerol formed during transesterification reaction, also attract revenue that help in reduction of total production cost. The glycerol resulting from biodiesel industry is contaminated with alkali and alcohol, and hence, not useful for conventional applications. Forward integration of the biodiesel plant to convert this glycerol

can boost the overall economy of the biodiesel industry. Another thesis from our group [20] has addressed the issue of bioconversion of biodiesel derived glycerol to value added products like 1,3–propanediol and butanol.

1.5 Aim and Scope of the Present Thesis

This thesis work is undertaken in the spirit of achieving two important goals of the National Biofuels Policy, viz. effective utilization of non–edible feedstocks for biodiesel production, and secondly, development of an efficient technology for biodiesel synthesis for such feedstocks. As noted earlier, Jatropha has already been identified as the major non food (non–edible) oil feedstock for biodiesel. Other such feedstocks are basically animal fats or waste grease. A major problem with these feed stocks is their high content of free fatty acids. Due to this, the conventional alkali catalyst cannot be used for esterification of these feedstocks, as it leads to soap formation. Therefore, acid catalyst needs to be used for esterification of such feedstocks. The esterification process with acid catalyst suffers from very slow kinetics, and hence, the batch time is large. Sonication of the esterification/transesterification system can enhance the kinetics of the process enormously. Moreover, use of heterogeneous catalysts can significantly reduce the contamination of the glycerol, and increase its sale value and also the revenue of the biodiesel industry. The present thesis addresses these crucially important issues for making biodiesel a valuable attractive fuel for the future. The approach in this thesis work is twofold: First optimization of the ultrasonic biodiesel synthesis process, and secondly, establishment of its physical mechanism. The results of the first objective can form useful guidelines for designing of large–scale ultrasonic process, while results of the second objective can be useful for future research in this area.

The thesis comprises of 7 chapters (including the present one) and the contents of the

each of these chapters are briefly outlined below:

1. **Chapter 2** gives the literature review of various aspects biodiesel synthesis. In addition, an introduction to basic principles of ultrasound and cavitation is also given, which could be useful for readers not much conversant with this subject.

2. **Chapter 3** presents studies in ultrasound assisted synthesis of biodiesel form soybean oil using CaO as heterogeneous catalyst. This chapter essentially demonstrates the feasibility of heterogeneous catalyst for transesterification with ultrasonic techniques. Soybean oil, although being edible grade, has been used only as model feed stock.

3. **Chapter 4** extends the theme developed in Chapter 3 for non–edible Jatropha oil. Here, the process has been carried out in two stages, as per conventional norms, i.e. esterification followed by transesterification.

4. **Chapter 5** presents the studies in biodiesel synthesis with Jatropha oil using homogeneous acid catalyst. Although the process has been carried out in two stages, viz. esterification and transesterification, same acid catalyst has been used in both steps.

5. In **Chapter 6**, we have presented a novel single step biodiesel synthesis process using chlorosulfonic acid catalyst. This catalyst has distinct and unique merit of catalyzing esterification process, followed by in–situ removal of water and finally catalyzing the transesterification process.

6. **Chapter 7** presents summary and overview of the various individual studies presented in the preceding chapters and an attempt is made to give gross and collective interpretations of these results from viewpoint of developing a viable ultrasonic process with non–edible feedstocks. Based on the results of the chapters, some guidelines have been identified for developing and optimizing large scale ultrasonic process for biodiesel synthesis. The merits as well as limitations of the ultrasonic–technology have been highlighted. Some suggestions for future work have also been given.

References

[1] Energy Statistics 2013. Central Statistics Office, National Statistical Organization, Ministry of Statistics and Programme Implementation, Government of India, New Delhi, 2013 (http://www.mospi.gov.in)

[2] Basic Statistics on Indian Petroleum and Natural Gas, Economic Division, Ministry of Petroleum and Natural Gas, Government of India, New Delhi, 2010–11.

[3] Key World Energy Statistics 2013. International Energy Agency, Paris, France (http://www.iea.org).

[4] Central Electricity Authority, Ministry of Power, Government of India. http://www.cea.nic.in (accessed December 2013).

[5] Indian Petroleum & Natural Gas Statistics, 2012–13. Economic Division, Ministry of Petroleum & Natural Gas, Government of India, New Delhi.

[6] A. Mustard, A. Aradhey, India Biofuels Annual 2012. GAIN (Global Agricultural Information Network) Report No. IN2081, USDA Foreign Agricultural Service, Washington DC, USA, June 2012.

[7] Statistical Year Book, India 2013. Ministry of Statistics and Programme Implementation, Research and Publications Unit, Government of India, New Delhi.

[8] India Greenhouse Gas Emission 2007. Indian Network for Climate Change Assessment, Ministry of Environment and Forests, Government of India, May 2010.

[9] J. R. Meshram, S. Mohan, (2007) Biomass power and its role in distributed power generation in India. In: 25 Years of Renewable Energy in India, Ministry of New and Renewable Energy, New Delhi, pp. 109–134.

[10] Akshay Urja, Vol.7 (Issue 1), Ministry of New and Renewable Energy, Govt. of India, New Delhi, August 2013 (Available online at http://mnre.gov.in).

[11] K. Bozbas, Biodiesel as an alternative motor fuel: Production and policies in the European Union. Renew. Sust. Energ. Rev. 12 (2008) 542–552

[12] Compiled by Earth Policy Institute from F.O. Licht, World Ethanol and Biofuels Report, vol. 10, no. 14 (27 March 2012), p. 281.

[13] Recent developments of biofuels/bioenergy sustainability certification: A global overview, Energ. Policy 39 (2011) 1630–1646.

[14] P. K. Biswas, S. Pohit, R. Kumar, Biodieselfromjatropha:Can India meet the 20% blending target? Energ. Policy 38 (2010) 1477–1484.

[15] National Biofuels Policy, Ministry of New and Renewable Energy, Government of India, New Delhi, September 2008 (available online at http://mnre.gov.in/file–manager/UserFiles/biofuel_policy.pdf).

[16] S. K. Lohan, T. Ram, S. Mukesh, M. Ali, S. Arya, Sustainability of biodiesel production as vehicular fuel in Indian perspective, Renew. Sust. Energ. Rev., 25 (2013) 251–259.

[17] Kumar A, Sharma.S, Potential non–edible oil resources as biodiesel feedstock: An Indian perspective, Renew. Sust. Energ. Rev. 15 (2011) 1791–1800.

[18] Report of the Committee on Development of Biofuels, Planning Commission, Government of India, New Delhi – 110 001, April 2003.

[19] S. Kumar, A. Chaube, S. K. Jain, Critical review of Jatropha biodiesel promotion policies in India, Energ. Policy 41 (2012) 775–781.

[20] S. Khanna, Bioconversion of Glycerol by Immobilized Clostridium pasteurianum: Process Development, Optimization and Intensification. Ph.D. Dissertation, Center for Energy, Indian Institute of Technology Guwahati, Guwahati, India, April 2013.

Ultrasonic Biodiesel Synthesis: Background and Literature Review

2.1 Introduction

In the previous chapter, we outlined the energy scenario in India, which clearly showed urgent need for development and commercial implementation of technology for transportation fuel production from renewable sources like biomass. These biofuels can provide viable solution to both issues of energy security and climate change risks. Biodiesel has emerged as a potential liquid biofuel for transportation. Despite the merits and benefits offered by biodiesel over other liquid biofuels (such as biomethanol and bioethanol), the economy of large scale production is not attractive, as noted in last chapter. This thesis has addressed the important issue of developing faster transesterification processes with use of ultrasound using cheaper feedstock that have high content of free fatty acids. Before proceeding to the main chapters of the thesis that describe various components and outcome of the thesis research, we shall briefly review various aspects and facets of biodiesel production in this chapter, with review of related literature. Over past several years, all aspects of biodiesel have been intensively investigated that

has resulted in a very large volume of literature. Our review in each aspect of biodiesel is only representative and not a comprehensive one. Nonetheless, it still gives the readers idea of the state-of-the-art in the particular aspect of biodiesel synthesis. For readers not conversant with the concepts of ultrasound and cavitation, we have also given a brief description of the physics of these two phenomena. We have essentially defined and explained some basic concepts of ultrasound wave phenomena and cavitation bubble dynamics.

2.2 Biodiesel

According to the chemical composition, biodiesel is fatty acid methyl or ethyl ester, which has properties very similar to those of petroleum derived diesel. The principal merits of biodiesel as renewable liquid transportation fuel are: (1) moderate cetane number in the range of 48-60, (2) low sulfur content (< 15 ppm), (iii) low hydrocarbon, CO and polyaromatic hydrocarbon (PAC) emission during combustion, and (iv) low particulate matter (PM) emission (25-50%). Thus, biodiesel is not only a carbon neutral fuel, but also has combustion characteristics that are environmentally friendly. Another peculiar feature of biodiesel is super lubricity even at very low sulfur content. Blending of biodiesel with ultra-low sulfur diesel and gasoline can obviate the need of addition of lubricating agent. As far as safety point of view is concerned, biodiesel has special merit that it has a high flash point of > 100^{o}C. Blending of biodiesel with petro-diesel can increase the flash point of diesel leading to safer operations. The only problem with biodiesel is higher viscosity than petroleum diesel that can lead to gum formation in the injector. However, diesel-biodiesel blends up to 20% have been reported give problem free operation. Storage, transportation as well as blending of biodiesel with diesel can be carried out using simple and inexpensive infrastructure. Finally, in addition to providing a viable solution to energy security and climate change risks (by reducing the net carbon emission), large-scale biodiesel manufacture can also have several other beneficial issues such as creation of employment (especially in rural areas where the oil seed plantation will be done),

rehabilitation and greening of degraded lands and reduction in oil import reducing the burden on national economy.

2.3 Biodiesel from Different Vegetable Oil

Use of vegetable oil and animal fats as potential liquid fuels for motor engines were investigated much before the energy crisis of nineteen century. Rudolf Diesel (1858–1913) in the year 1900 demonstrated successful operation of his diesel engine on peanut oil in Paris Exposition. Since then, many vegetable oils have been tested, among which palm oil has received the most attention along with other vegetable oils such as cottonseed, soybean oil, and castor oil. Despite smooth operation of diesel engines, use of vegetable oils as diesel fuel was ceased with growth of petroleum industry. The obvious reason being high cost of oil as compared to the petroleum fuel. There were also other technical features that inhibited the direct use of vegetable oils as fuels for diesel engines. Main disadvantages of direct use of vegetable oil as diesel were: (1) higher viscosity, (2) lower volatility, and (3) the reactivity of unsaturated hydrocarbon chains [1]. Prolong use of vegetable oils led to (a)coking and formation, (b) carbon deposits, (c) oil ring sticking and (d) thickening and gelling of the lubricating oil, as a result of contamination by the vegetable oils [2]. Thus, direct use of vegetable oil requires modifications of the engines [3]. Nevertheless, high viscosity of vegetable oils can be reduced by four different methods: (1) Blending/dilution of vegetable oil with petroleum diesel; (2) Micro–emulsion with short chain alcohols; (3) Pyrolysis and catalytic cracking to produces alkanes, cycloalkanes, alkenes, and alkylbenzenes; and (4) Transesterification with alcohol (methanol/ethanol), which produces biodiesel.

2.3.1 Blending/dilution of vegetable oil with petroleum diesel

Dilution of vegetable oils with solvents like ethanol may reduce the viscosity of oil but also reduce the fuel property like brake specific fuel consumption. A blend of 25 parts sunflower oil and 75 parts diesel have been used as diesel fuel by Ziejewski et al. [4] with kinematic

viscosity of 4.88×10^{-6} m^2/s at 40°C, while the maximum specified ASTM value is 4×10^{-6} m^2/s. This blend was also not suitable for long–term use in a direct injection engine. Bilgin et al. [5] also studied 4% ethanol blend and found reduced brake specific fuel consumption.

2.3.2 Micro–emulsion with short chain alcohols

Billaud et al. [6] has studied micro emulsion of vegetable oils with immiscible liquids such as methanol, ethanol, and ionic or non–ionic amphiphiles. Ziejewski et al. [7] prepared an emulsion of 53% v/v alkali–refined and winterized sunflower oil, 13.3% v/v 190–proof ethanol and 33.4% v/v 1–butanol. Micro–emulsion of vegetable oil was also studied with butanol, hexanol, and octanol that met the maximum viscosity requirement by Schwab et al. [8], Goering [9], and Ma and Hanna [2]. However, in laboratory screening endurance test many problems were reported such as irregular injector needle sticking, heavy carbon deposits, incomplete combustion, and an increase of lubricating oil viscosity.

2.3.3 Pyrolysis and catalytic cracking

Pyrolysis is essentially thermal decomposition of material (or cleavage of chemical bonds to yield small molecules) in complete absence or scarcity of oxygen (or air) either in presence or absence of a suitable catalyst [10]. Liquid products obtained by pyrolysis of vegetable oils can be used as alternative engine fuel. Vegetable oils may be converted to liquid product containing gasoline boiling range hydrocarbons. Vegetable oils are converted to lower molecular products by two simultaneous reactions: cracking and condensation. First step of pyrolysis is the conversion of triglycerides into carboxylic acids, which are further decomposed by decarboxylation (leading to alkanes and carbon dioxide) or decarbonylations. Pioch et al. [11] studied the catalytic cracking of vegetable oils (viz. copra oil and palm oil) to produce biofuels. This was carried out in presence of a catalyst SiO_2/Al_2O_3 at 450°C to produce biogasoline and biodiesel fuel.

The pyrolysis oils have high water content typically in the range of 15–30 wt% oil that cannot be removed by conventional methods like distillation. The water content of pyrolysis oils

has many adverse impacts such as reduction in energy density and flame temperature of the oils, which could lead difficulties in ignition and injection. The higher heating value (HHV) of pyrolysis oils is below 26 MJ/kg (compared to 42–45 MJ/kg for conventional petroleum fuel oils) [12].

2.3.4 Transesterification

Walton [13] suggested that the glycerides have no fuel value, and hence, recommended the elimination of glycerol from the liquid fuel, termed as "Biodiesel" today. Trans-esterification is a solution to reduce viscosity of oil, and also to remove the glycerol from the oil. Chemical transformation of triglyceride (TG) present in the vegetable oil to its corresponding fatty ester is called transesterification [14]. A catalyst is usually used to improve the reaction rate and yield, since the reaction is reversible. An excess of alcohol is used to shift the equilibrium towards the products side. Vegetable oils have been converted to methyl, ethyl, 2–propyl and butyl esters through transesterification using potassium and/or sodium alkoxides as catalysts. The transesterification reaction system is essentially a liquid-liquid heterogeneous system which forms two immiscible phases after reaction: organic one containing the ester product and aqueous one containing glycerol. This makes separation of biodiesel rather easy and straightforward, as side products of glycerol, water and catalyst remain in aqueous phase. Biodiesel thus obtained is a clear amber–yellow liquid with a viscosity almost similar to diesel produced from petroleum. It is used as blend in formulations of diesel to increase the lubricity of pure ultra–low sulphur petro–diesel (ULSD) fuel. The blends of biodiesel and petrodiesel are often coded as “B” to represent the percent volume of the blend. For example, fuel containing 20% biodiesel and 80% of petrodiesel is labelled B20. Pure biodiesel is referred to as B100. The common international standard for biodiesel is EN 14214 and ASTM D 6751[15].

2.4 Emission and Combustion Characteristics of Biodiesel: A brief review

Biodiesel can be synthesized from large variety of lipid feedstock available across the

globe. However, biodiesel properties and cost depend on the type of lipid and alcohol used for transesterification. Majority of lipids are used for human food (80%), animal feed (5%) and industrial applications (15%). Use of lipids for biodiesel production poses the famous food vs. oil controversy for the food security in developing countries. Recently, oils from other organisms such as micro–algae and cyano-bacteria have also been explored. [16]. Table 2.1 gives a broad description of different feedstock used in various countries for biodiesel production, while Table 2.2 gives the fatty acid compositions of different vegetable oils that have been employed as feedstock for biodiesel. The major raw materials for biodiesel production are food–grade canola oil in Europe, soybean oil in North–South America and palm oil in South–East Asia and in Africa. Cheap resources for biodiesel production are waste oils such as waste cooking and frying oils, rendered animal fat and new non–edible resources such as *Jatropha curcas* and *Pongamina pinnata* and lipids derived from microalgae. Among 350 identified oil–bearing crops, only a few such as soybean, palm, sunflower, safflower, cottonseed, rapeseed, and peanut oils have been considered as potential alternative fuels for diesel engines. Various vegetable oils have been tested in the internal combustion (IC) engines in USA, Europe, India, Malaysia and Germany [19]. A review of representative literature on engine performance and emissions such as NO_x, hydrocarbons (HC), particulate matters (PM) and carbon monoxide (CO) with use of biodiesel from different feedstock has been presented below. This review is by no means a thorough one, but it gives an idea of the research and outcome thereof on the combustion properties of biodiesel in an IC engine as a green transportation fuel.

Ng et al. [20] studied the performance of IC engine using biodiesel obtained from palm oil, at different speeds and load conditions. Their result revealed that due to lower energy contents of palm oil methyl ester, specific fuel consumption (SFC) was higher than conventional diesel fuel.

Table 2.1: Country wise feedstock for production for biodiesel [17]

Country	Feedstock
USA	Soybean/ peanut/ waste oil
Canada	Rapeseed/ animal fat/ soybean/ yellow grease/ mustard
Mexico	Animal fat/ waste oil
Italy	Rapeseed/ sunflower
France	Rapeseed/ sunflower
Spain	Linseed oil/ sunflower
Greece	Cottonseed
Sweden	Rapeseed
UK	Rapeseed/ waste cooking oil
Ireland	frying oil/ animal fat
India	Jatropha/ Pongamiapinnata(karanja)/ soybean/ rapeseed/ sunflower/ peanut
Malaysia	Palm oil
Singapore	Palm oil
Indonesia	Palm oil/ Jatropha/ coconut
Singapore	Palm oil
Philippines	Coconut/ Jatropha
Thailand	Palm/ Jatropha/ coconut
China	Jatropha/ waste cooking oil/ rapeseed
Brazil	Soybeans/ Palm oil/ Castor/ Cotton oil
Argentina	Soybeans
Japan	Waste cooking oil
New Zealand	Waste cooking oil/ tallow

The authors concluded that despite the shortcoming of palm oil methyl ester, it is technically viable alternative to fossil diesel in both neat and blended forms for use in light–duty diesel engines.

Karavalakis et al. [21] investigated exhaust emissions and fuel consumption of blends of diesel fuel and palm oil derived biodiesel at proportions of 5%, 20% and 40% (v/v). Their result

revealed that use of palm oil methyl ester increases NO_x emission, while reduce the carbonyl emission. Similar results were also reported by Leevijit and Prateepchaikul [22].

Hazar [23] studied the engine emission and performance of canola oil derived biodiesel. The author found significant decrease in carbonyl emission with a slight increase in both NO_x and particulate matter emission. The authors also reported higher power output from engine with use of canola oil biodiesel as fuel. Ekrem [24] has also reported the performance, emission and combustion characteristics of a diesel engine using pure rapeseed biodiesel. Author reported lower power output from engine using biodiesel blend as compared to pure biodiesel. The biodiesel blend also caused lower CO emission. But higher exhaust gas temperature lead to higher NO_x emission. The highest brake thermal efficiency of the engine was obtained with B_{20} blend.

Nwafor et al. [25] have concluded that diesel blends (ranging from 25–75%) of methyl ester of rapeseed oil emitted high CO_2 compared to diesel. However, a significant reduction in emissions of hydrocarbons (HC) was reported with the blends. The author also reported lower engine output power with the blend. There was no marked difference noted for the exhaust temperatures of the diesel-biodiesel blends and diesel alone.

Fontaras et al. [26] reported the effect of soybean oil biodiesel and its blend 50% (v/v) on engine performance. Authors reported higher specific fuel consumption with B_{50} blend. Moreover, there was increase in CO as well as NO_x emission with the B_{50} blend. Combustion and performance characteristics of biodiesel from soybean oil and its different blend (B_0, B_{30}, B_{50}, B_{80}, B_{100}) were studied by Qi et al. [27]. This study reported higher specific fuel consumption, lower CO and hydrocarbon emission and higher NO_x emission.

Table 2.2: Fatty acid compositions of different vegetable oils [18]

Types of oil	Species	Main chemical composition (fatty acid composition)	Density (g/cm^3)	Flash point (^oC)	Kinematic viscosity (Cst, at 40 ^oC)	Acid value (mg KOH/g)	Heating value (MJ/Kg)
Edible oil	Soybean	C16:0, C18:1, C18:2	0.91	254	329	0.2	39.6
	Rapeseed	C16:0, C18:0, C18:1, C18:2	0.91	246	35.1	2.92	39.7
	Sunflower	C16:0, C18:0, C18:1, C18:2	0.92	274	32.6	–	39.6
	Palm	C16:0, C18:0, C18:1, C18:2	0.92	267	39.6	0.1	–
	Corn	C16:0, C18:0, C18:1, C18:2, C20:0, C22:0	0.90	271	22.72	3	39.8
	Camelina	C16:0, C18:0, C18:1, C18:2, C18:3, C20:0, C20:0, C20:3	0.91	–	–	0.76	42.2
	Canola	C16:0, C18:0, C18:2, C18:3			38.2	0.4	
	Cotton	C16:0, C18:0, C18:1, C18:2	0.91	234	18.2		39.5
	Pumpkin	C16:0, C18:0, C18:1, C18:2	0.92	>230	35.6	0.55	39
Non–edible oil	*Jatropha curcas*	C16:0, C16:1, C18:0, C18:2	0.92	225	29.4	28	38.5
	Pongamina pinnata	C16:0,C18:0,C18:1,C18:2,C18:3	0.91	205	27.8	5.06	34
	Sea mango	C16:0,C18:0,C18:1,C18:2	0.92	–	29.6	0.24	40.86
	Palanga	C16:0,C18:0,C18:1,C18:2	0.90	221	72	44	39.25
	Nile tilapia	C16:0,C18:1,C20:5,C22:6,other acids	0.91	–	32.1	2.81	–
	Poultry	C16:0,C16:1,C18:0,C18:2, C18:3	0.90	–	–	–	39.4
	Used Cocking oil	Depends on fresh cooking oil	0.90	–	44.7	25	–

Ulusoy et al. [28] reported the emission characteristics of sunflower oil methyl ester at different speeds and full load condition in an IC engine. This study showed that smoke, hydrocarbon and CO emissions of sunflower oil methyl ester are generally lower than diesel fuel for different engine speeds. The authors concluded that biodiesel has more favourable effects on air quality, since biodiesel's exhaust emissions are lower than diesel fuels.

Godiganur et al. [29] studied the performance and emission characteristics of *Mahua* oil methyl ester and its blend at different load and constant speed (1500 rpm). The test results showed that higher biodiesel blends significantly reduces CO and hydrocarbon emissions due to complete combustion of biodiesel. However, there is slight increase in NO_x emissions due to higher temperature of exhaust gas, which is a possible consequence of higher oxygen presence in biodiesel. There was a small reduction in brake specific energy consumption (BSEC) and slight increase in break thermal efficiency (BTE) of engine compared to diesel fuel was observed, when it was run on 20% biodiesel.

Puhan et al. [30] reported emission properties and engine performance of biodiesel from Mahua oil in a constant speed (1500 rev/min) four stroke direct injection compression ignition diesel engine. A reduction in CO, hydrocarbon and NO_x emission was observed for Mahua oil biodiesel than petroleum diesel. However, CO_2 emission and brake specific fuel consumption (BSFC) was found to be higher than diesel. Higher BSFC of Mahua oil biodiesel is due to lower heating value of esters.

Saravanan et al. [31] also reported emission properties and engine performance of biodiesel from Mahua oil in diesel engine. The CO and hydrocarbon emission was found to be less for Mahua oil biodiesel than diesel. Authors reported a lower power output of engine and higher fuel consumption, when Mahua oil biodiesel was used. This result is attributed to lower heating value and higher viscosity of biodiesel of Mahua oil. A 4% reduction in NOx emission was also reported due to lower exhaust gas temperature of Mahua oil biodiesel.

Baiju et al. [32] studied the performance and exhaust emission characteristics of biodiesel blends from *Karanja* oil. Lower engine power output, lower brake thermal efficiency (BTE) and higher brake specific fuel consumption (BSFC) was reported due to lower heating value of ester. The authors reported an increase in NO_x emissions (10-25%) for biodiesel blends compared to normal diesel at partial load. However, at full load reduced emission of CO, hydrocarbon and NO_x was observed for biodiesel of *Karanja* oil.

Nurun Nabi et al. [33] studied the exhaust emission of *Karanja* oil biodiesel and compared with diesel. They reported reduction of CO emission up to 50% and smoke up to 43% for biodiesel as compared to diesel fuel. However, they reported a higher NO_x emission for biodiesel at high load condition. Higher emission of NO_x was due to the presence of oxygen in the *Karanja* oil biodiesel molecular structure. The brake thermal efficiency of the *Karanja* oil biodiesel and its blend are almost similar to that of diesel fuel.

Raheman and Phadatare [34] also studied the engine performance and emission property of *Karanja* oil biodiesel blends. The reported reduction in CO and NO_x emission for *Karanja* oil biodiesel blends. They reported a lower brake specific consumption of fuel (BSFC) for B_{20} and B_{40} blends, whereas higher brake specific consumption of fuel (BSFC) for $B_{60\text{-}100}$ blends. They suggested a 40% blend of *Karanja* oil biodiesel to have potential to replace diesel for diesel engine with lesser emission and comparable engine power out put.

Aydin and Bayindir [35] studied the performance and emission characteristic of cottonseed oil methyl ester and its various blends. The authors reported lower brake specific fuel consumption (BSFC) at lower engine speed. At higher engine speed, higher brake specific fuel consumption (BSFC) was observed due to higher viscosity and lower calorific value of biodiesel. The emission of CO and SO_2 has been reported to be less with higher biodiesel blends, whereas NO_x emission was reduced by use of all blends of cottonseed oil methyl ester except B_{100} and B_5.

Chauhan et al. [36] studied the performance and exhaust emissions using different blends of Jatropha biodiesel (5, 10, 20 and 30%) and diesel fuel. Their results show that engine performance with Jatropha biodiesel and its blends were comparable to the performance of diesel fuel. All fuel blends are reported to have lower brake thermal efficiency, lower HC, CO, CO_2 emission and lower smoke density, while brake specific fuel consumption (BSFC) and NO_x emission were higher than that of diesel. On a whole, this study has recommended direct use of Jatropha biodiesel and its blend for diesel engine without any modification.

Agarwal and Agarwal [37] have reported the study on performance and emission characteristics of Jatropha oil and its blends in a direct injection compression ignition engine. They reported a higher brake specific fuel consumption (BSFC) and exhaust gas temperature for unheated Jatropha oil compared to diesel. Thermal efficiency was lower for unheated Jatropha oil compared to heated Jatropha oil and diesel. CO_2, CO, HC, and smoke opacity were higher for Jatropha oil compared to that of diesel. Heating the engine with exhaust gases improved the emission characteristics and engine performance. Blends of Jatropha oil has higher emission and brake specific fuel consumption (BSFC) than diesel fuel. Based on this study, the authors have suggested use of preheated Jatropha biodiesel in diesel engines.

Mumtazab et al. [38], Hirkude et al. [39] and Lin et al. [40] have investigated the performance and emission characteristics of methyl ester from waste cooking oil. The results indicated that the performance parameters for different methyl ester of cooking oil blends were found to be very close to diesel. They reported a lower brake thermal efficiency coupled with lower CO emission in the exhaust gases and suggested that waste cooking oil methyl ester can be cheap fuel option for diesel engines.

The above representative literature demonstrates that biodiesel derived from numerous sources can be effectively used in IC engines, although with varying emission characteristics.

One general conclusion that can be drawn from this literature is that biodiesel can be a potential blend substitute. There are almost 350 oil bearing crops available in the world that can support biodiesel industry. From review of representative literature given above, it could be understood that use of biodiesel in the diesel engine can significantly reduce emission of particulate matter, hydrocarbon and carbon monoxide due to higher oxygen content in the biodiesel and higher cetane no of biodiesel as compared to conventional diesel. However, higher combustion temperature due to higher oxygen content in the biodiesel increases the NOx emission. Other engine related issues like lowered brake power and brake thermal efficiency is also attributed to the higher viscosity, density and lower heating value of biodiesel. Nevertheless, biodiesel production from different feedstock has huge potential to support transportation industry, and would be a promising renewable energy source. Pure biodiesel can be used with some modification in the engines, whereas blended biodiesel can be used without or little modification in the existing engines. It can reduce burden on fossil fuel demand, and also reduce pollution that has great impact on the environment.

2.5 Literature Review on Biodiesel Synthesis

Vast literature (more than 1000 papers) has been published in the past one and half decade in the area of biodiesel synthesis through many feedstocks, using many catalysts and techniques of synthesis. A detailed review of this literature is rather impractical and also irrelevant from the theme of this thesis. This thesis is mainly aimed at investigating the sonochemical route to biodiesel using cheap feedstocks and heterogeneous catalyst. As noted earlier in the thesis, cheaper feedstock lowers the production cost, advanced synthesis techniques such as ultrasound enhances kinetics of the process and use of heterogeneous catalysts enhances purity of glycerol and hence its resale value. In concurrence with this theme, given below is a review of ***representative literature*** in the area of biodiesel synthesis

with two feedstocks that have been used in the present thesis, viz. soybean oil and Jatropha oil. Again, in concurrence with the theme of thesis, we have selected references that fall in either or both of these categories, viz. (1) heterogeneous catalysis with conventional synthesis technique of mechanical agitation, and (2) ultrasonic synthesis with either homogeneous or heterogeneous catalysts. In each of these categories, both acid and base type catalysts have been considered.

For more detailed review and analysis of literature we refer the reader to the following state-of-art reviews published in recent past: Lottero et al [41], Gole and Gogate [42], Maddikeri et al. [43], Jain and Sharma [44], Pandey et al. [45], Koh et al. [46], Jain and Sharma [47], Janaun and Ellis [48], Jothiramalingam and Wang [49], Borugadda and Goud [50], Kumar and Sharma [51], Lam et al [52], Al-Zuhair [53] and Gole and Gogate.[54].

Silva et al. [55] reported synthesis of biodiesel for by using hydrotalcites as catalyst and soybean as feedstock. Author reported Mg–Al hydrotalcite as potential catalyst for biodiesel synthesis. Conventional transesterification reaction was carried out at a reaction temperature of 230^{o}C with catalyst loading of 5 wt%, 13:1 methanol molar ratio and reaction time of 1 h. This method gave 90% biodiesel yield within 1 h. However, the temperature and pressure requirement for the method was very high, viz. 180–230^{o}C and 27–34 atm.

Dias et al. [56] studied biodiesel synthesis from waste frying oil, sunflower and soybean refined oil using KOH, NaOH and CH_3ONa as catalysts. Results of this study revealed that the use of virgin oils resulted in higher yields (reaching 97%) as compared to waste frying oils (reaching 92%). The synthesis was carried out using conventional transesterification method, where the reaction mixture containing virgin oils, methanol and catalyst were vigorously stirred at 60^{o}C for 1 h. Under optimum condition author reported a 94% biodiesel yield which met the European biodiesel standard EN 14214.

Dias et al. [57] studied methanolysis of soybean oil over magnesia supported SrO

heterogeneous catalysts. A moderate reaction condition of 67^{o}C, 9:1 alcohol molar ratio and 5 wt% of catalyst loading was required for a FAME yield of 94%. No soap formation was observed using the same catalyst and maximum biodiesel yield was obtained in 3 h. However, the catalyst performance was drastically reduced after 3rd reuse due to the loss of Sr from the catalyst.

Fan et al. [58] has studied biodiesel synthesis from soybean oil using KF modified CaO–MgO catalyst. A high yield ~ 98% biodiesel was obtained within 2.5 h of reaction time with 2% catalyst loading, 9:1 alcohol molar ratio and a reaction temperature of 65^{o}C. The catalyst performance was good for up to 4th reuse with biodiesel yield of 87%.

Guo et al. [59] studied synthesis of biodiesel from soybean oil using calcined sodium silicate. A very high yield of 95% biodiesel was obtained with this method. The catalyst showed a consistent performance even after 5th reuse with slight deactivation due to loss of Na^{+} form the catalyst surface.

Guzatto et al. [60] studied transesterification double step process (TDSP) for the production of biodiesel from vegetable oils like linseed, soybean and waste cooking oil. 1.1 g of potassium hydroxide as homogeneous catalyst was used with 10:1 methanol molar ratio and reaction temperature of 65^{o}C for transesterification reaction. A high biodiesel yield of 87-93% was obtained by this method.

Li et al [61] have developed solid superbase of Eu_2O_3/Al_2O_3 for transesterification reaction of soybean oil for production of biodiesel. Result of this study showed that Eu_2O_3/Al_2O_3 is an excellent catalyst for the transesterification of soybean oil, and the conversion of soybean oil can reach 63.2% at 70^{o}C for 8 h.

Li et al. [62] synthesized KOH supported neodymium oxide catalyst for biodiesel synthesis from soybean oil. The transesterification reaction was carried out at reflux of methanol, with molar ratio of methanol to oil of 14:1, reaction time 1.5 h, reaction

temperature 60°C and catalyst amount 6 wt% oil, the highest biodiesel yield reached was 92.41%.

Liang et al. [63] developed a novel method for production of biodiesel from soybean oil with chloroaluminate ionic liquid as catalyst. This method was found to be very efficient with biodiesel yield of 98.5%, when the reaction was carried out under the conditions of soybean oil = 5 g, methanol = 2.33 g, reaction time = 9 h, temperature = 70°C. The the key features of this methodology were: simple procedure, low catalyst cost and higher reusability, high yields, and no saponification.

Liu et al. [64] synthesized biodiesel using $Ca(OCH_2CH_3)_2$ as catalyst using both methanol and ethanol as alcohol for transesterification of soybean oil and presented a comparison study of catalyst performance of $Ca(OCH_2CH_3)_2$ and CaO. The authors have reported better catalytic performance of $Ca(OCH_2CH_3)_2$ with 95% biodiesel yield at 65°C within 1 h. The kinetic study was also done and activation energy of ~ 55 kJ/mol was reported for $Ca(OCH_2CH_3)_2$ catalyzed transesterification reaction of soybean oil.

Liu et al. [65] studied biodiesel synthesis of soybean oil using SrO as catalyst. A very high yield of biodiesel (> 95%) was obtained with SrO as a catalyst at temperatures < 70°C within 30 min. SrO had a long catalyst lifetime, and could maintain sustained activity even after 10 cycles. This study proved that transesterification of soybean oil to biodiesel using SrO as a catalyst is a commercially viable process with low cost of production.

Liu et al. [66] studied the synthesis of biodiesel form soybean oil using CaO as solid base catalyst. Effect of various parameters and presence of water in methanol was reported on the yield of biodiesel synthesis. The results of this study showed that a 12:1 molar ratio of methanol to oil, addition of 8% CaO catalyst, 65°C reaction temperature and 2.03% water content in methanol gave the best results, and the biodiesel yield exceeded 95% at 3 h. The catalyst deactivation was negligible and a consistent activity was reported for more than 20

cycles of reuse.

Moradi et al. [67] studied the transesterification of soybean oil to biodiesel using KOH as homogeneous catalyst under different conditions. Influence of different process parameter like molar ratio of methanol/oil, catalyst amount and reaction temperature was studied. Optimal conditions were found to be methanol/oil molar ratio, 9:1; catalyst amount, 1 wt%; reaction temperature, 60^{o}C. Biodiesel yield of 93.2% was obtained in 1 h. The artificial neural network has been applied to estimate the biodiesel yield.

Pasupulety et al. [68] studied production of biodiesel from soybean oil on CaO/Al_2O_3solid base catalysts. The molar ratio for the highest biodiesel yield of 90% was 9:1 at 150^{o}C. The process took 6 h to produce 90% biodiesel at 150 psig pressure and 3 wt% of catalyst. The kinetic study was also done for the transesterification reaction and very low activation energy of ~ 30 kJ/mol was reported.

Rashtizadeh et al. [69] studied biodiesel production via transesterification of soybean oil using KOH loaded on double alumino-silicate layers, microporous and mesoporous materials as catalyst. This study reports optimum biodiesel synthesis with 70:1 methanol molar ratio, 30wt% of catalyst, reflux temperature of methanol and 6 h of reaction time.

Samart et al. [70] developed calcium supported on mesoporous silica catalyst for biodiesel production by methanolysis of soybean oil. The authors reported an optimized conditions for synthesis as 15 wt% of Ca loading on the mesoporous silica catalyst, catalyst concentration of 5% w/w oil, 16:1 alcohol molar ratio and a reaction temperature of 60^{o}C. For these conditions, biodiesel yield of 95.2% was obtained within 8 h.

Shu et al. [71] studied synthesis of biodiesel from soybean oil using La/zeolite catalyst. The catalyst was synthesized by ion exchange method and transesterification reaction was done at reflux temperature of methanol using conventional stirring method. The highest yield of ~ 49% biodiesel was achieved within a reaction time of 4–8 h.

Silva et al. [72] studied optimization of biodiesel production by transesterification of soybean oil with ethanol as alcohol and NaOH as homogeneous catalyst employing response surface methodology. In this work, a 2^4 factorial design was adopted to optimize the biodiesel production process. The effect of process parameter like reaction temperature, catalyst concentration, reaction time and alcohol molar ratio has been investigated. Optimum conditions for the production of ethyl esters were: temperature = 56.7°C, reaction time = 80 min, molar ratio = 9:1 and catalyst concentration = 1.3 M.

Meneghetti et al. [73] studied the production of biodiesel from a mixed vegetable oil of soybean oil, cottonseed oil and castor oil. Transesterification reactions were carried out in different mixture ratios of oils and conventional string of reaction mixture was used for biodiesel synthesis. The reaction mixture containing methanol, the homogeneous catalyst (NaOH), vegetable oils (castor, cottonseed, or soybean oil) or their mixtures, with the molar ratio of alcohol/oil/catalyst of 34:6:1 was used at reflux condition of alcohol used for a reaction time of (1–10 h).

Tang et al. [74] developed a technique for biodiesel synthesis using glyme as co–solvent for CaO catalysed transesterification of soybean oil. The effect of different catalyst loading with different co–solvent ratio was studied, and a high reaction yield of 98% biodiesel within 4–8 h was reported. This study also reported a new method to activate the commercial lime with glyme only without external calcination. The dissolution–agglomeration process of CaO surface in the presence of glyme was reported to be responsible for removal of the $CaCO_3$ and $Ca(OH)_2$ layer coated on the surface of lime.

Xie et al. [75] have studied biodiesel production from soybean oil transesterification using tin oxide–supported WO_3 catalysts. Catalyst was synthesized by impregnation method and maximum conversion to FAME of 79.2% was achieved for conditions: time = 5 h, temperature = 383 K, molar ratio = 30:1, and catalyst concentration 5 wt%. Catalyst was also

capable of esterify the FFA present in the oil. The reusability of catalyst was reported to be consistent up to four reaction cycles.

Xie et al. [76] have reported CaO-supported tin oxide catalyzed biodiesel synthesis of soybean oil. Catalyst was prepared by precipitation method, and the transesterification reaction was done using conventional stirring of the reaction medium using methanol as alcohol. Maximum yield of 89% of biodiesel was achieved within 6 h with 12:1 molar ratio and catalyst loading of 8 wt%. The catalyst was reported to show consistent activity ever after 5 cycles of reaction.

Xie et al. [77] have developed biodiesel production process from soybean oil using aminopropyl silica as catalyst. Catalyst was synthesized using wet impregnation method, whereas transesterification reaction was carried out in 250 mL stainless steel high–pressure autoclave reactor fitted with a temperature controller and a mechanical stirrer. High yield of methyl esters up to 94.5% was reported at a molar ratio of methanol to soybean oil of 30:1, catalyst concentration 8 wt%, reaction temperature of 150^{o}C. A small decrease in the catalytic activity was reported after reuse for at least five cycles. Catalyst activity was affected by the FFA and water present in the reaction medium.

Kalva et al. [78] studied ultrasound assisted synthesis of biodiesel with NaOH as alkali catalyst. This study investigates the chemical and physical effect on ultrasound on biodiesel synthesis. Different molar ratios of alcohol were employed for biodiesel synthesis and simulation of bubble dynamics model was done to investigate the physical mechanism of ultrasonic enhancement in biodiesel yield. Authors reported that influence of ultrasound on the transesterification reaction system was of mere physical nature. Micro-turbulence generated by ultrasound and cavitation produced large interfacial area between oil and alcohol, which accelerated the transesterification reaction.

Batistella et al. [79] studied ultrasound–assisted lipase–catalyzed transesterification of

soybean oil. Two commercial immobilized lipases, Novozym 435 from *Candida Antarctica* (immobilized on a macroporous anionic resin, 1.4 wt% water) and Lipozyme RM IM from *Rhizomucor miehei* (immobilized on a macroporous anion exchange resin, 3 wt% water) were investigated for production of biodiesel under ultrasound irradiation. The Lipozyme RMIM showed a higher yield up to 90% biodiesel in comparison to Novozym 435, which gave only 57% biodiesel. However, in terms of enzyme activity, Novozym 435 showed better performance with consistent eight repeated reuse, whereas Lipozyme RMIM was only active for two reusable cycles.

Chand et al. [80] have developed enhanced biodiesel production technique from soybean oil using ultrasound. Methanol was used as alcohol, with NaOH as catalyst, and the transesterification reaction was carried out at 60^{o}C. Authors reported a high biodiesel yield of 96% within 90 s in continuous mode of sonication and 86% biodiesel within 15 s with pulse mode.

Cintas et al. [81] have reported biodiesel synthesis from soybean oil with ultrasound in a pilot flow reactor. This study reported development of a high power ultrasound reactor with tuneable frequency of ultrasound from 17 and 45 kHz. The biodiesel synthesis from soybean oil using this reactor was reported to be ~ 100%.

Santos et al. [82] have reported optimization of ultrasound assisted synthesis of biodiesel from soybean oil. The optimisation study was done by RSM method and biodiesel yield of 100% with NaOH catalyst was reported by this method.

Guo et al. [83] have reported ultrasound assisted biodiesel synthesis using Brønsted acidic ionic liquid as catalyst. Authors reported optimal conditions for biodiesel synthesis as: methanol/oil molar ratio of 9:1, 1 wt% catalyst in oil, ultrasound power of 200 W, and reaction temperature of 60^{o}C. Maximum conversion of triglycerides to fatty acid methyl esters (about 93.2%) was obtained within the reaction time of 1 h for the optimum conditions.

Parkar et al. [84] have reported ultrasound assisted biodiesel synthesis from soybean oil using sulfuric acid catalyst. This study also investigated the kinetics of the transesterification reaction with acid catalyst. The activation energy of the transesterification reaction was reported to increase with increasing alcohol molar ratio. This study also reported interrelation between mechanics of ultrasound/cavitation, and the intrinsic behavior of the transesterification reaction.

Mahamuni and Adewuyi [85] studied the ultrasound assisted synthesis of biodiesel form soybean oil. Authors used Taguchi method to optimize the biodiesel synthesis process. The optimum conditions reported were: frequency = 581 kHz, power = 143 W, catalyst concentration = 0.75% w/w KOH, oil/methanol molar ratio = 1:6. For these conditions, more than 92.5% biodiesel yield was obtained in less than 30 min.

Yu et al. [86] developed ultrasound assisted synthesis of biodiesel from soybean oil using Novozym 435 catalyst. Authors investigated effects of reaction parameters, such as ultrasonic power, water content, organic solvents, ratio of solvent/oil, ratio of methanol/oil, enzyme dosage and temperature on the activity of Novozym 435. The optimum conditions were found as follows: 50% of ultrasonic power, 50 rpm vibration, water content of 0.5%, tert–amyl alcohol/oil volume ratio of 1:1, methanol/oil molar ratio of 6:1, 6% Novozym 435 and 40^{o}C for 96% yield of fatty acid methyl ester (FAME) for a reaction time of 4 h. The biocatalyst was reported to be reusable up to four cycles without any loss of activity.

Jain et al. [87] studied synthesis of biodiesel from Jatropha oil using a two-step approach. The Jatropha oil contained high FFA ≈ 22.5%, and hence, esterification of this FFA was carried out by acid pre–treatment, prior to transesterification with NaOH catalyst. Kinetics of the esterification and transesterification reaction has also been reported by the authors. Optimum temperature for transesterification reaction was reported as 65^{o}C for esterification, and 50^{o}C for transesterification. Maximum biodiesel yield obtained by this method was 91%.

Berchmans et al. [88] studied biodiesel production from mixture of Jatropha oil (FFA ~ 5 wt%) and waste food oil. The mixture was so prepared to keep the FFA content of mixed oil below 1 wt%. A 9:1 ratio of Jatropha oil: waste food was mixed to make the feedstock for biodiesel synthesis. The overall biodiesel yield was reported to be 97% in 2 h with NaOH as catalyst for transesterification.

Berchmans et al. [89] have reported synthesis of biodiesel from Jatropha oil with FFA content ~ 15%. The authors reported a two-step approach, where first step was sulphuric acid catalyzed esterification, and second step was NaOH catalysed transesterification reaction. Final biodiesel yield was 90% within 2 h of reaction with methanol as alcohol.

Corro et al. [90] have reported biodiesel production from *Jatropha curcas* crude oil using ZnO/SiO_2 photocatalyst for free fatty acid esterification. The activity of the catalyst was consistent up to 10 cycles of esterification. Transesterification was done with NaOH as base catalyst.

Corro et al. [91] studied biodiesel production from *Jatropha curcas* crude oil using in a two-step process. The FFA esterification reaction was catalyzed by SiO_2-HF solid catalyst, whereas transesterification reaction was catalyzed by NaOH. Biodiesel synthesized by this process was highly pure and met ASTM D6584.

Deng et al. [92] have reported biodiesel synthesis form Jatropha oil using nano–sized Mg–Al catalyst. Author reported a two-step method, in which first step was FFA reduction with sulphuric acid, and the second step comprised of transesterification reaction with solid Mg–Al catalyst. A high biodiesel yield of 95% was obtained in 6 h with 8 cycles of reuse of catalyst.

Endalew et al. [93] have studied biodiesel production from *Jatropha curcas* oil using heterogeneous catalyst. In this study, authors employed different type of heterogeneous catalyst like CaO, Li–CaO, La_2O_3/ZnO, La_2O_3/Al_2O_3 and $La_{0.1}Ca_{0.9}MnO_3$ for

transesterification reaction. Mixture of solid base catalysts (CaO and Li–CaO), and solid acid catalyst, $Fe_2(SO_4)_3$, were found to give complete conversion to biodiesel in a single–step simultaneous esterification and trans–esterification process.

Guo et al. [94] have studied biodiesel production from high FFA containing Jatropha oil in a single step process. Biodiesel synthesis was done using ionic liquids with metal chlorides. 1–butyl–3–methylimidazolium tosylate was reported to have the highest catalytic activity with 93% esterification rate for oleic acid at 140^{o}C, but only 63.7% Jatropha biodiesel yield was obtained at 200^{o}C. With addition of $ZnCl_2$ to ionic liquid, Jatropha biodiesel yield increased to 92.5% at 180^{o}C. The catalyst was reported to be easily separable from the reaction mixture for reuse.

Kay et al. [95] have studied production of biodiesel from Jatorpha oil using modified natural zeolite as a solid catalyst. The authors investigated various reaction parameter like reaction time, molar ratio of methanol to oil, reaction temperature, mass ratio of catalyst to oil and catalyst reusability. Maximum yield of 96% biodiesel was obtained within 6 h of reaction time with 20:1 molar ratio, 5 wt% of catalyst loading at temperature of 70^{o}C. The reusability of the catalyst was also tested, and it was reported that the catalyst showed a consistent activity at least for 3 cycles of separation and reuse. The biodiesel synthesized by this method met European standard EN14214 for biodiesel.

Kitakawa et al. [96] have studied production of high quality biodiesel and glycerin from Jatropha oil using ion–exchange resins as catalysts and adsorbent. This study reports complete conversion of FFA and triglyceride to biodiesel. All byproducts were adsorbed on the resin and the resulting biodiesel met the industrial standards. This method is also reported to overcome several problems of upstream refining of crude oil and downstream processing for separation of catalyst and byproducts.

Helwani al. [97] have reported process biodiesel production using re-crystallized

hydrotalcite. The highest conversion of jatropha oil to biodiesel at 75.2% was achieved using re-crystallized HT at 65 ^{o}C with a methanol:Jatropha oil molar ratio of 12:1, a reaction time of 6 h and a catalyst loading of 4 wt.%.

Mazumdar et al. [98] studied the physico–chemical characteristics of *Jatropha curcas* derived biodiesel from 20 genotypes. The oil content of these genotypes varied from 23.7% to 46.6%. Transesterification reaction was carried out using KOH as catalyst. The synthesized biodiesel was reported to meet the ASTM D 6751 specification.

Yee et al. [99] have studied biodiesel production from Jatropha oil using SO_4^{2-}/ZrO_2 catalyst. Authors used response surface methodology to optimize the biodiesel synthesis process. It was reported that 4 h of reaction at 150^{o}C, alcohol molar ratio of 9.9 and 7.6 wt% for catalyst loading gave an optimum biodiesel yield of 90.3 wt%. The fuel properties of Jatropha biodiesel is reported to meet the specifications for biodiesel according to ASTM D6751.

Taufiq–Yap et al. [100] have reported transesterification reaction of Jatropha oil using mixed calcium based metal catalyst. This study reports use of mixed oxide catalysts (CaMgO and CaZnO) for transesterification reaction. Conventional stirring method was employed. Biodiesel yield of ~ 80% was achieved with 4 wt% of catalyst within 6 h of reaction time. The catalysts showed a decrease in activity with reuse due to leaching of the catalyst with consecutive run.

Zanette et al. [101] carried out optimization studies of biodiesel synthesis from Jatropha oil. The study also investigated the kinetics of transesterification reaction. A large number of heterogeneous catalysts, viz. resins, zeolites, clays, hydrotalcites, alumina and niobium oxide, were screened for transesterification reaction. Authors reported that Amberlyst 15 and KSF clays showed the highest catalytic activity, and hence, the factorial design for optimization of biodiesel was carried out with these catalysts. The optimum reaction conditions reported for

both catalysts were: oil to methanol molar ratio of 1:12, 5 wt% of catalyst, 160°C temperature and 6 h of reaction time with a FAME yield of about 70 wt%.

Badday et al. [102] have studied ultrasound assisted synthesis of biodiesel form Jatropha oil using activated carbon–supported tungsto-phosphoric acid catalyst. Authors reported a full factorial design to optimize the transesterification process with ultrasound. A yield of 91% was reported in 40 min at a moderate ultrasonic amplitude (60%), high molar ratio (25:1) and low reaction temperature (65°C).

Badday et al. [103] reported ultrasound assisted synthesis of biodiesel from Jatropha oil using cesium doped heteropolyacid catalyst. The highest yield was reported to be 90.5% within 34 min under the optimum reaction conditions of: ultrasonic amplitude ~ 60%, and molar ratio of 25:1.

Badday et al. [104] have reported transesterification of crude Jatropha oil in an ultrasound–assisted reactor system by alumina–supported heteropolyacid catalyst. A response surface methodology was employed to optimize the biodiesel synthesis process. For optimum conditions, the highest biodiesel yield of 84% was achieved under optimum conditions of ultrasonic amplitude of 60%, molar ratio of 19:1, and a reaction temperature of 65°C in just 50 min.

Deng et al. [105] have reported a two-step approach for ultrasonic biodiesel synthesis from Jatropha oil. The study reported esterification with sulphuric acid and transesterification reaction with NaOH catalyst. The biodiesel yield was reported to be more than 96% within 30 min of reaction time.

Kumar et al. [106] studied ultrasound assisted synthesis of biodiesel from Jatropha oil. Ethanol was used as alcohol and KOH was the base catalyst used for transesterification reaction. Biodiesel yield with this method was 97% within 7 min. The biodiesel produced with this method met the international standards.

Kumar et al. [107] reported ultrasound assisted transesterification of *Jatropha curcus* oil using solid catalyst, Na/SiO_2. Effect of various process parameters like catalyst loading, ultrasound energy, molar ratio, reaction time on the biodiesel yield was investigated. Biodiesel yield of ~ 99% was reported with oil to methanol molar ratio of 1:9, catalyst concentration of 3 wt% and 15 min reaction time.

Zou and Lei [108] have studied ultrasound assisted pre-esterification of Jatropha oil under ultrasound irradiation. Pre–esterification by 1.2% sulfuric acid under ultrasound field has been reported to yield 98% FFA conversion with 18:1 methanol: oil molar ratio and reaction time of 1.5 h.

The literature on biodiesel synthesized from different reaction parameters are summarized in the two table viz. Table 2.3 and Table 2.4. Table 2.3 summarizes results published in literature on conventional process where as Table 2.4 summarizes results published on ultrasound assisted process on biodiesel.

Table 2.3: Summary of results of published literature on biodiesel synthesis from *Jatropha Curcas* oil using conventional techniques

Vegetable oil source	Alcohol	Methanol /Oil ratio	Catalyst	Amount of Catalyst (wt%)	Optimum Condition	% FAME	References
Jatropha Curcas	Methanol	5.9:1	H_2SO_4	15	60°C, 24 h	99.8	109
Jatropha Curcas	Methanol	1:1	Lipase	4	30°C, 60 h	80	110
Jatropha Curcas	Ethanol	4:1	Lipase	10	50°C, 8 h	98	111
Jatropha Curcas	Methanol	6.7:1	H_2SO_4/ NaOH	1.4	65°C, ½ h	90	112
Jatropha Curcas	Methanol	9.6:1	H_2SO_4/ NaOH	1	50°C, 2 h/2 h	90	113,114
Jatropha Curcas	Methanol	4:1	H_2SO_4/ KOH	0.55	60°C, 88 min/ 24 min	99	115
Jatropha Curcas	Methanol	9:1	H_2SO_4/ KOH	4.5	60°C, 2 h/2 h	90–95	116
Jatropha Curcas	Methanol	6:1	(SO_4^{2-}/ TiO_2) / KOH	1.3	64°C, 2 h/2 h	98	117
Jatropha Curcas	Methanol	6:1	SiO_2·HF/ NaOH	1	60°C, 2 h/2 h	99.5	118
Jatropha Curcas	Methanol	12:1	KSF clay and Amberlyst 15	5	160°C, 6 h	70	119
Jatropha Curcas	Methanol	15:1	SO_4^{2-}/ SnO_2^{-} SiO_2	3	180°C, 2 h	97	120
Jatropha Curcas	Methanol	6:1	CaO + $Fe_2(SO_4)_3$	5	60°C, 3 h	100	121
Jatropha Curcas	Methanol	6:1	Li–CaO + $Fe_2(SO_4)_3$	5	60°C, 3 h	100	121
Jatropha Curcas	Methanol	6:1	La_2O_3–ZnO	5	60°C, 3 h	100	121
Jatropha Curcas	Methanol	10:1	SO^{2-}_4 /ZrO_2	7.61	150°C, 4 h	90	99
Jatropha Curcas	Methanol	40:1	CaO–MgO	3.6	115°C, 3.4 h	95	122

Table 2.4: Summary of published literature on ultrasonic biodiesel synthesis from *Jatropha curcas* oil with different catalysts

Vegetable Oil Source	Alcohol	Methanol / Oil ratio	Catalyst	Amount of Catalyst (wt%)	Optimum Condition	% FAME	References
Jatropha Curcas	Methanol	24:1	H_2SO_4/ NaOH	1.4	1 h /0.5 h	96.4	105
Jatropha Curcas	Methanol	25:1	Heteropolyacid	4.5	65°C, 1 h	91	102
Jatropha Curcas	Methanol	10:1	NaOH	1	27°C, 80 min	94	123
Jatropha Curcas	Methanol	15:1	H_2SO_4/ NaOH	1	30°C 30 min /30 min	98	124
Jatropha Curcas (FFA free oil)	Methanol / Ethanol	6:1	KOH	0.75	50°C, 11 min	94–96%	125
Jatropha Curcas (Low FFA)	Methanol	9:1	NaOH	1	50°C, 30 min/ 24 min	93	126
Jatropha Curcas (FFA free oil)	Methanol	4:1	Lipase	5	30 min	84	127
Jatropha Curcas (FFA free oil)	Methanol	9:1	Na/SiO_2	3	15 min	98.54	128
Jatropha Curcas	Methanol	4:1	H_2SO_4/Mg–Al	1	45°C, 1 h/ 1.5 h	94.2	92

2.6 Synthesis of Biodiesel by Transesterification Process

Due to the limitation of the various methods described in the section 2.3 most common and favourable method for biodiesel synthesis is transesterification reaction. The transesterification reaction progresses in three consecutive and reversible reactions steps as follows: (1) reaction of triglyceride (TG) and methanol to produce diglycerides (DG) and 1 molecule of methyl ester, (2) further reaction of diglycerides to yield monoglycerides (MG) and another molecule of methyl ester, and finally (3) reaction of monoglyceride to yield one mole of methyl ester and one mole of glycerol. Chemical composition of biodiesel is fatty acid methyl esters or ethyl esters, produced via transesterification of triglycerides (TG) or esterification of fatty acids. Table 2.5 and 2.6 represents the chemical structures of molecules involved in biodiesel synthesis. Biodiesel typically comprises long alkyl fatty acid with chain length C_{14}–C_{22}, and esters of short–chain alcohols, primarily, methanol or ethanol. Schemes 2.1 and 2.2 show the production of fatty acid mono alkyl esters from triglyceride and fatty acid. The transesterification reaction is reversible in nature, and a catalyst is used to shift the equilibrium towards product side. The catalyst may be homogeneous alkali, acid or heterogeneous base or acid catalyst. Enzymes like lipase are also used as catalyst for transesterification reaction. Nevertheless, biocatalysts are more expensive (thus necessitating complete recovery and recycle) and reaction kinetics is extremely sluggish. Hence, they are less popular in large (industrial) scale production of biodiesel. The most popular catalyst for transesterification reaction is homogenous alkali catalyst, since the rate of transesterification reaction with alkali catalyst is very fast. NaOH and KOH are the widely used and studied homogenous alkali catalysts so far. These catalysts produce > 99% biodiesel yield in few min of reaction time. Although, homogenous alkali catalysts are very efficient in producing biodiesel in shorter reaction time and higher biodiesel yield, major limitation for use of such catalyst is requirement of a pure and FFA-free feedstock. This makes the biodiesel synthesis

process costly, as it involves refined vegetable oils containing only triglycerides. It has been reported by numerous studies that FFA present in vegetable oil (or any similar feedstock for biodiesel) would react with alkali catalyst producing soap, which could render biodiesel yield poor, in addition to complicating downstream separation process. Scheme 2.3 [41] represents the mechanism of methanolysis of TG with alkali catalyst. Thus, for a crude vegetable oil with higher FFA content, use of homogenous alkali catalyst is ruled out. To make biodiesel process economic, use of non–edible oil and other cheap feedstock has been suggested by Zhang et al. [129]. But the problem with these feedstocks is their higher FFA content. Esterification reaction of FFA with methanol in presence of an acid catalyst can convert the FFA to FAME. This will reduce the acid value of the vegetable oil and evade problem of soap formation. Acid catalysts are also capable of catalyzing transesterification reaction. Thus, vegetable oil with high acid value (high FFA content) can be converted to biodiesel using an acid catalyst, which can simultaneously catalyze both esterification and transesterification reaction. Scheme 2.4 [41] depicts the biodiesel synthesis mechanism by an acid catalyst. Although acid catalysts are popular for their efficacy in catalyzing two reactions (esterification and transesterification) simultaneously, as represented by Scheme 2.5 [130], the reaction rates are extremely slow (typically 4000× slower than that of alkali catalyst). Use of both homogenous alkali and acid catalyst is also associated with higher downstream separation and purification cost. A large volume of water is required to remove traces amount of acid and alkali present in the biodiesel samples. Moreover, the catalysts are not reusable, which also adds to process economy. Therefore, a large number of studies focused on biodiesel synthesis using heterogeneous catalyst. Heterogeneous catalysts are easily separable from reaction mixture, and simple technique like filtration, sedimentation or centrifugation can be used to separate the catalyst from the processed biodiesel. Major attraction of heterogeneous catalyst for biodiesel synthesis is their reusability. The catalyst can be

separated very easily for the reaction mixture and reused with simple reactivation process like washing of catalyst then drying or in some cases calcination. Moreover, the catalyst also does not contaminate the glycerol phase (as in case of homogeneous alkali catalyst). This increases the sale price of the glycerol and enhances the revenue of the biodiesel industry making it economically attractive.

Table 2.5: FAME and FAEE chemical formulae

Fatty Acid Methyl Ester (FAME)	Fatty Acid Ethyl Ester (FAEE)
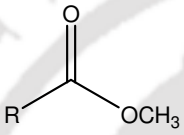	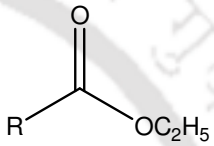
R= Fatty acid chain	

Table 2.6: Chemical formulae of different glycerides

Glycerol	Monoglyceride	Diglyceride	Triglyceride
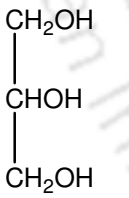	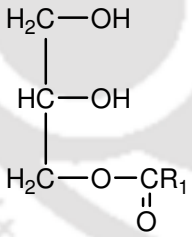	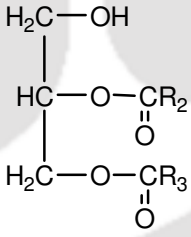	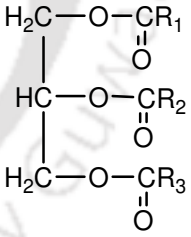

R_1,R_2,R_3= Fatty acid chain

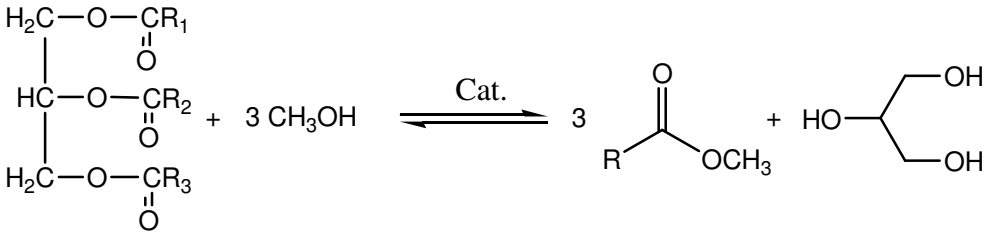

Scheme 2.1: Transesterification reaction of TG molecule with methanol

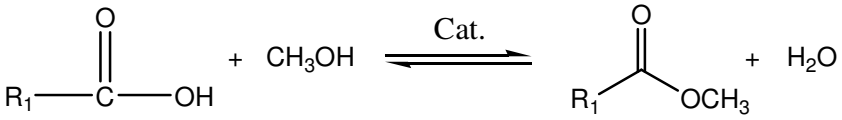

Scheme 2.2: Esterification reaction of FFA with methanol

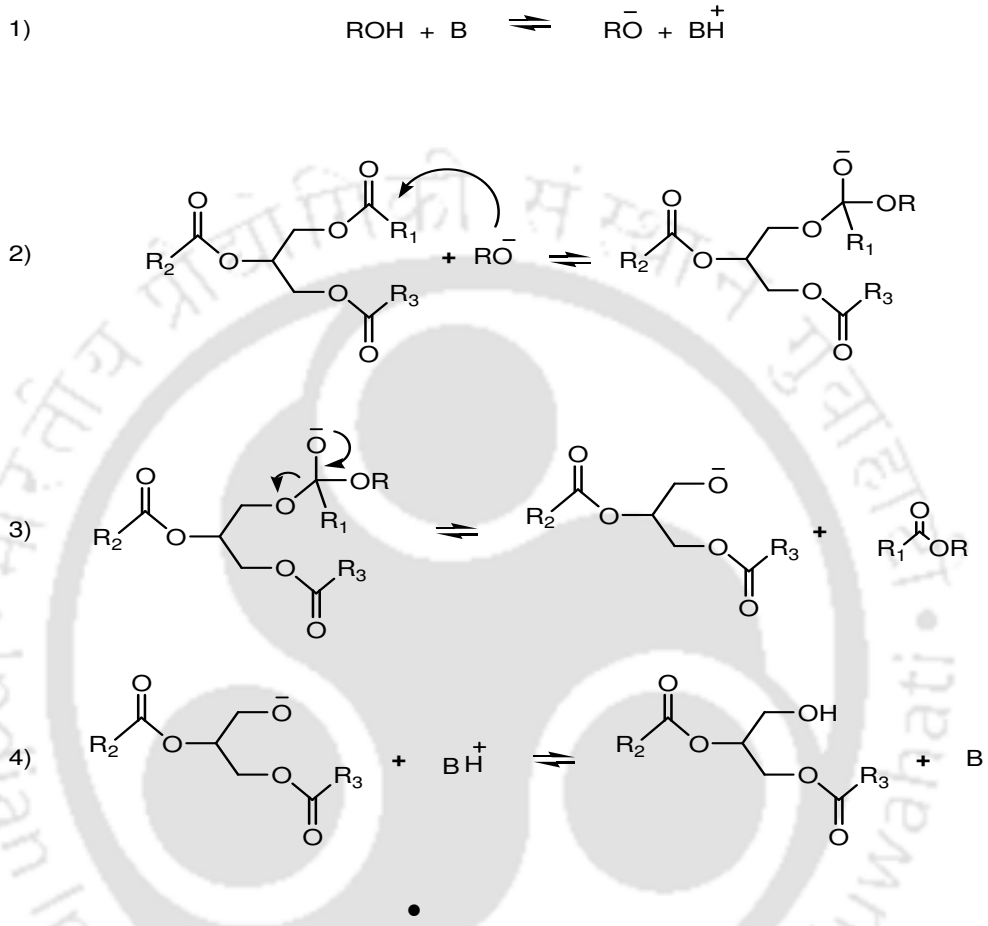

- R_1, R_2, R_3 = Carbon chain of fatty acid, R = Alkyl group of alcohol

- **Scheme 2.3:** Homogeneous alkali catalysed transesterification reaction

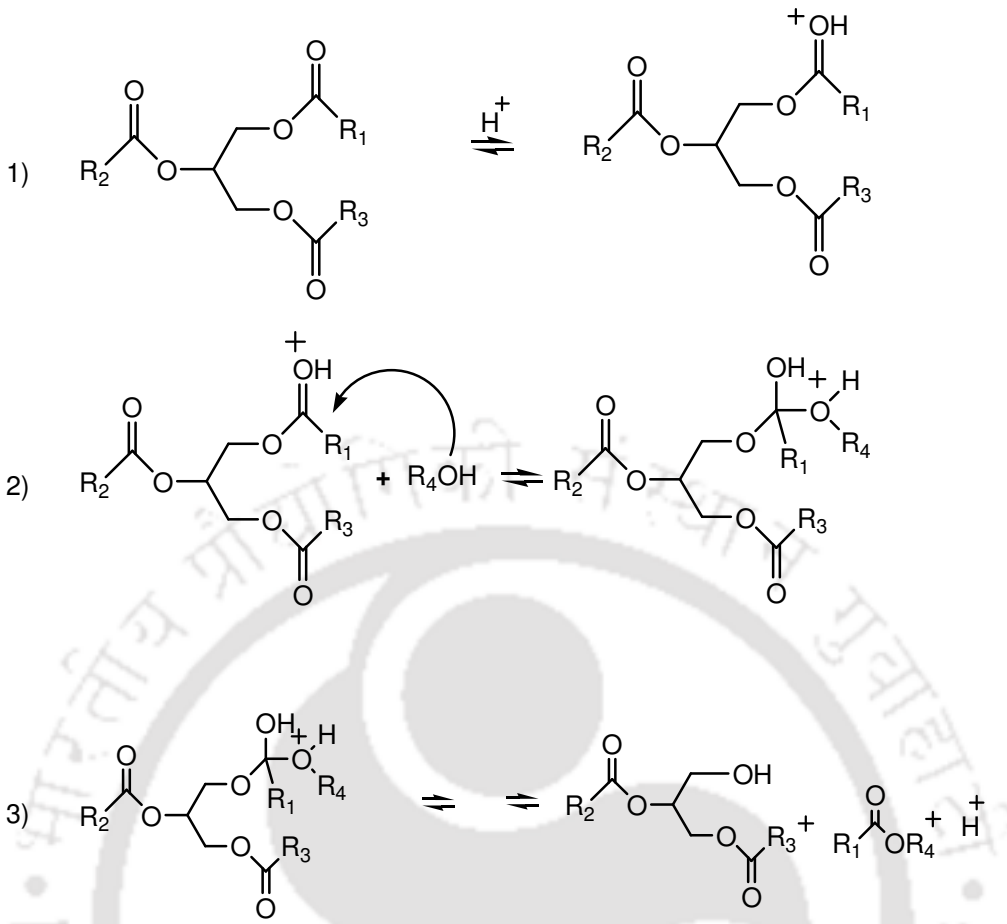

R_1, R_2, R_3 = Carbon chain of fatty acid, R_4 = Alkyl group of alcohol

Scheme 2.4: Homogeneous acid catalysed transesterification reaction

In general, various reaction parameters influence the performance of transesterification reaction. The parameters are type of alcohol used, alcohol to oil molar ratio, FFA and water content of feedstock, reaction temperature, reaction time, catalyst type and methodology (or technique) employed for agitation of reaction mixture (for example, simple mechanical agitation, ultrasound or microwave). Ultrasound can boost kinetics of the transesterification reaction by better dispersion, homogenization and emulsification of reactants and catalysts as the results of micro–convection and strong shockwaves generated by ultrasonic cavitation.

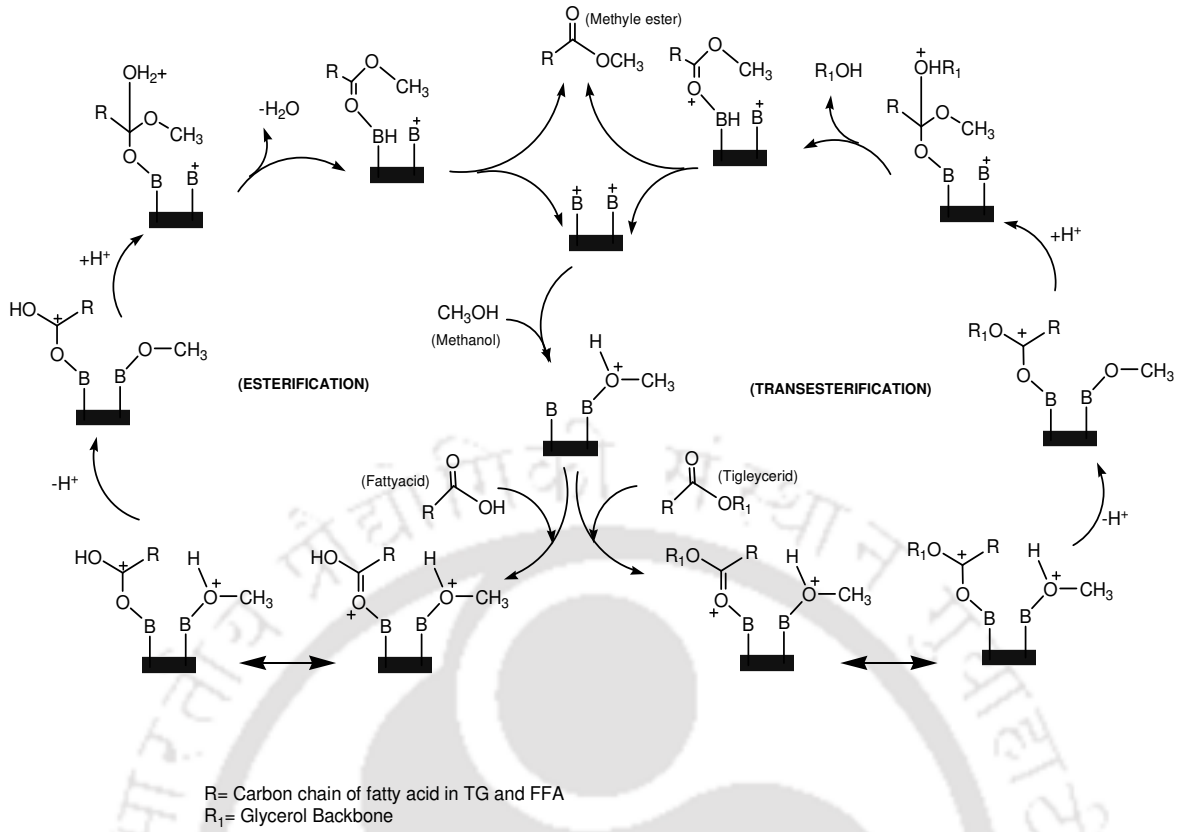

Scheme 2.5: Simultaneous esterification and transesterification by heterogeneous acid catalyst

2.7 Overview, Inferences and Justification of Present Thesis Work

Literature review presented in this chapter gives a clear picture of the biodiesel research and development. A very large number of studies have been published using different feedstocks, catalysts and synthesis techniques. However, major focus of this research is on the results and not the rationale. Therefore, as far as mechanistic issues of biodiesel synthesis are concerned, there is significant knowledge gap as the actual mechanisms of many new catalysts and synthesis techniques (that lead to higher yield as reported by the inventors) is not known. This makes the scale-up of the process to industrial scale rather difficult. The economic analysis of biodiesel is also not very attractive. The manufacturing cost of biodiesel is at par with petroleum derived diesel. There are two solutions to this: (1) use of cheaper feedstock that would reduce the production cost, and (2)

biodiesel industry start marketing side products such as the glycerol formed during transesterification reaction or the oil cake that remains after extraction of oil from seeds, which would fetch additional revenue. As far as the first solution is concerned, non-edible oils are potential low price feedstocks. However, due to their high free fatty acid (FFA) content, conventional alkali catalyzed transesterification is not feasible. This necessitates two-step process, first acid catalyzed esterification to convert the FFA, separation of the oil phase, followed by transesterification with alkali catalyst. Another problem with acid catalyzed biodiesel process is its extremely slow kinetics, which can put limit to production rate. For the second solution, heterogeneous catalysts are the potential solution. Cheaper basic solid catalysts such as CaO can drastically reduce the contamination of glycerol (as seen with homogeneous alkali catalysts) that will help improve its quality and also the sale price. However, the bottleneck in this case is slow kinetics of the solid catalyzed transesterification system due to the triphasic nature of the reaction system (liquid-liquid-solid). The mass transfer limitations can bring down the kinetics drastically, which is again a hurdle for effective scale-up of the process.

In this thesis, we have addressed these issues. Using ultrasound as a means of intensification of the process, we have studied several biodiesel synthesis systems with conventional feedstock of Soybean oil, cheaper alternate non-edible feedstock of Jatropha oil and heterogeneous catalysts. In addition, we have also presented a novel single step process for high FFA content feedstocks. Our approach in the thesis work has been that of coupling experiments of biodiesel synthesis with simulations of cavitation bubble dynamics. This approach helps in getting a physical or mechanistic insight into the process to deduce the exact nature of interaction or links between chemistry of esterification / trans-esterification and the physics of cavitation bubble dynamics. Such mechanistic insight can form crucial guidelines for effective scale-up of the process. Moreover, we have also used the statistical

tools such as response surface methodology (with fitting of quadratic model to experimental data) and ANOVA to identify the optimum combination of operating parameters for the process that would lead to maximum biodiesel yield. We believe that the results of this thesis will not only form useful inputs for further research in biodiesel synthesis, but will also form crucial guidelines for scale-up of ultrasonic biodiesel process. Ultrasound and cavitation as a means of intensifying diverse physical, chemical and biological processes has been investigated for many years. However, most of the literature in the area focuses on results than rationale. In other words, this means that a small fraction of the literature attempts to discern the actual physical mechanism of the process forming link between physics of ultrasound and cavitation and chemistry of the reaction system. In general it is accepted that all physical and chemical effects of ultrasound are attributed to cavitation, which generally is described as nucleation, growth and implosive transient collapse of tiny gas or vapor bubbles driven by pressure variation induced by ultrasound wave. But this is too broad and hazy description of the process. Our attempt in this thesis is to explore and establish mechanics of the ultrasonic biodiesel synthesis, which could form basis for effective scale up and optimization of the process.

In the consecutive section of this chapter, we have given some basic information about principles of ultrasound and cavitation. This chapter will be quite useful for those readers who are not very conversant with this topic. The contents of this chapter are largely derived from standard textbooks [131-137] and popular reviews [138-141] in the area of acoustics, cavitation and sonochemistry.

2.8 Basic Principles of Ultrasound Wave Phenomena and Cavitation Bubble Dynamics

2.8.1 What is an Acoustic Wave?

Sound passes through a compressible medium, such as air or water, in the form of a longitudinal wave. The pressure as well as density of the medium undergoes periodic variation with passage of wave. The particles or molecules of the medium undergo an oscillatory motion around a mean position with passage of sound wave. The general wave equation that describes the propagation of the acoustic wave is [142]:

$$\nabla^2 P - \frac{1}{c^2}\frac{\partial^2 P}{\partial t^2} = 0, \; where \; c^2 = \left(\frac{\partial P}{\partial \rho}\right)_{S\,=\,constant} \tag{2.1}$$

The solution of this equation can be written in the simplest form as:

$$P(x,t) \; = \; P_A \; \cos(\omega t - kx) \tag{2.2}$$

Notation: $P(x, t)$ = instantaneous pressure of the wave at any point x in the path at time t, ω ($2\pi f$) = the angular frequency of the acoustic wave, k ($2\pi/\lambda$) = wave number, λ = wavelength, f = frequency. A relation between particle velocity (v) and acoustic pressure amplitude (P_A) is given as (Mason and Lorimer, 2002): $P_A = \rho v c$ or $P_A / \rho c = v$

2.8.2 *Intensity of the Acoustic Wave*

Acoustic intensity is basically the measure of rate at which energy in the wave crosses a unit area perpendicular to the direction of propagation. The total energy density in a plane progressive acoustic wave is: $\frac{1}{2}\rho\left|\dot{\varepsilon}\right|^2_{\max}$, where ε is the displacement of the particle and $\dot{\varepsilon}$ is its time derivative, indicating velocity [136]. The total energy crossing a segment of area A in time Δt is: total energy density $\times Ac\Delta t$, where c is the velocity of the acoustic wave. On this basis, we can identify that the energy crossing a unit area in unit time is:

$I = total\ energy\ density \times c = \frac{1}{2}\rho\left|\dot{\varepsilon}\right|_{\max}^{2} c$. The velocity of the particles, $\left|\dot{\varepsilon}\right|_{\max}$ is written as impedance as: $\left|\dot{\varepsilon}\right|_{\max} = P_A/\rho c$. Substituting this in above equation gives the intensity of acoustic wave as: $I = P_A^2/2\rho c$. The intensity of the acoustic wave is proportional to the square of the pressure amplitude of the acoustic wave.

2.8.3 Cavitation Bubble Dynamics

Although cavitation has been known as a fluid transportation problem that caused damage to transport machinery like pipes and pumps. However, research in the past several decades has conclusively proven that controlled cavitation can be a useful tool in intensification of several physical and chemical processes. Cavitation is essentially a phenomenon of nucleation, growth, oscillation and collapse of small gas or vapor bubbles, which is induced and driven by the pressure variation in the system. Cavitation creates extreme concentration of energy on extremely small temporal and spatial scales. Using the criterion of cause of cavitation, this phenomenon is broadly categorized into four types as follows:

(1) **Acoustic Cavitation**, which results due to pressure variation generated due to passage of an acoustic wave.

(2) **Hydrodynamic Cavitation**, which results due to pressure variation in the liquid flow due to changing flow geometry.

(3) **Optic Cavitation**, which is a result of local evaporation of liquid due to an intense energy dissipation, such as laser.

(4) **Particle Cavitation**, which is produced by any elementary particle (such as proton) rupturing the liquid.

As far as generation of cavitation for physical and chemical processing is concerned, only the two types of cavitation are practical and feasible. Optic and particle cavitation have

been mainly employed in laboratory research on cavitation, due to the high costs associated with them.

Inception of cavitation: Theoretically, cavitation phenomenon involves creation of voids in the liquid. With progression of sound wave in the medium, the molecules of the liquid oscillate about mean position. In the compression phase, the distance between the molecules decreases, while during rarefaction the molecules are pulled apart and the distance between them increases. If the amplitude of the acoustic wave is large enough, the distance between molecules may exceed the critical distance to hold the liquid intact (also known as van der Waal's distance), resulting in creation of voids. Typically, this pressure amplitude required for this phenomenon is $2\sigma/R$, where σ is the surface tension and R is the van der Waal's distance. For water, the values are σ = 0.072 N/m and $R = 4\times10^{-10}$ m. Thus, the theoretical pressure and amplitude required for creation of void is ~ 1500 atm.

However, actual cavitation phenomenon occurs at far lower pressure amplitude. This is attributed to the phenomenon of nucleation. Nucleation occurs due to presence of solid particles, or tiny free-floating bubbles present in the liquid that act as weak spots. Another source of nucleation is the gas pockets trapped in the crevices of the solid boundaries in the medium. These solid boundaries could be walls of the reactor or tip of the ultrasound horn. These gas pockets have a concave meniscus. The radius of curvature of the gas pocket, as seen from liquid, is negative. Therefore, the surface tension force (or Laplace pressure) acts in the liquid. The pressure inside the bubble is lesser than the ambient pressure. Due to this pressure difference, the dissolved gas in the medium diffuse into the gas pocket, thus stabilizing it. These gas pockets can grow in response to reduction in ambient pressure with passage of acoustic wave. The phenomenon of nucleation broadens the definition of cavitation as growth, oscillation and collapse of gas bubbles already present in the medium or vapor bubbles generated out of passage of ultrasound wave.

***Radial Motion of Cavitation Bubbles*:** Under the influence of the acoustic wave, which creates periodic pressure variation in the medium, the cavitation bubble undergoes volume oscillations. The amplitude of these volume oscillations depends on the amplitude of the acoustic wave. For relatively small pressure amplitudes, the volume oscillations of the bubbles are also small and essentially in phase with the acoustic pressure wave. However, for larger pressure amplitude, the volumetric oscillations become nonlinear comprising of an explosive initial growth followed by a transient collapse and a few afterbounces. The subject of radial motion of cavitation bubble has been extensively investigated in past 100 years. The first ever analysis of the collapse of an "empty" cavity under constant ambient pressure was given by Lord Rayleigh [143]. This analysis used the definition of cavity given by Besant [144] as "a spherical portion of liquid suddenly annihilated". The equation for radial motion of bubble, derived in its simplest form using energy balances, can be written as (for detained derivation please refer to Leighton, 1994): $\frac{(P_L - P_\infty)}{\rho} = \frac{3}{2}\dot{R}^2 + R\ddot{R}$. P_L, the pressure in the liquid just outside bubble surface is determined as follows: If the is initially comprised of mixture of gas and vapor, the pressure inside the bubble is $P_i = P_g + P_V$. Due to surface tension forces, the pressure inside the bubble is greater than pressure in liquid outside bubble surface by Laplace pressure = $2\sigma/R_o$. Thus, $P_i = P_L + 2\sigma/R_0$. If the bubble is initially in static equilibrium, then pressure throughout the liquid medium (including the region immediately outside the bubble surface) is P_0. Thus: $P_i = (P_0 + 2\sigma/R_0)$. Once set into the radial motion, the bubble radius changes from an initial value R_0 to any value R at time t. The pressure of gas in the liquid falls, however, vapor pressure stays the same. Assuming that gas present in the bubble obeys polytropic law, we can write:

$$P_i = (P_0 + 2\sigma/R_0 - P_V)(R_0/R)^{3K} + P_V, \tag{2.3}$$

where k is the polytropic constant. Inserting expressions for P_i in equation 2.18, we get:

$$R\frac{d^2R}{dt^2}+\frac{3}{2}\left(\frac{dR}{dt}\right)^2=\frac{1}{\rho}\left\{\left(P_0+\frac{2\sigma}{R_0}-P_V\right)\left(\frac{R_0}{R}\right)^{3K}+P_V-\frac{2\sigma}{R}-\left(P_0+P(t)\right)\right\} \tag{2.4}$$

The above expression ignores the effect of viscosity of the medium. Plesset [145], Poritsky [146], Noltingk and Neppiras [147] later extended the above approach to include effect of viscosity of the medium. We give herewith the final equation (popularly known as Rayleigh-Plesset equation) and refer the reader to original papers for detailed derivation.

$$R\frac{d^2R}{dt^2}+\frac{3}{2}\left(\frac{dR}{dt}\right)^2=\frac{1}{\rho}\left\{\left(P_0+\frac{2\sigma}{R_0}-P_V\right)\left(\frac{R_0}{R}\right)^{3K}+P_V-\frac{2\sigma}{R}-\frac{4\mu}{R}\frac{dR}{dt}-\left(P_0+P(t)\right)\right\} \tag{2.5}$$

These equations assume constant density of the medium in which bubble undergoes radial motion and thus these equations do not account for the compressibility of liquid. However, as noted earlier, during transient collapse of the bubble (or large amplitude volume oscillations), the velocity of bubble wall (dR/dt) reaches or even exceeds the sonic velocity (1500 m/s for water as liquid medium). For these conditions, the compressibility effect needs to be taken into account.

***Equation Accounting for Liquid Compressibility*:** In past six decades several authors have attempted to incorporate liquid compressibility into mathematical formulation for radial bubble motion. An excellent review of these developments has been given by Leighton [136] and Brenner et al. [141]. We present below a brief summary of the development of models cavitation bubble dynamics that account for liquid compressibility.

The first attempt in this regard was done by Gilmore [148] who used the Kirkwood-Bethe hypothesis [149] as the basis. This hypothesis stated that for spherical waves with finite amplitude, the quantity $r\phi$ (r - radial coordinate, ϕ - velocity potential) propagates with velocity equal to sum of the liquid velocity and sound velocity. The local velocity of sound is expressed as a function of the free enthalpy on the surface of the bubble.

In an alternate approach, Keller and coworkers proposed the following equation (Keller and Kolodner, [150]; Keller and Miksis, [151]; Prosperetti and Lezzi, [152]; Brennen, [153]):

$$\left(1-\frac{\dot{R}}{c}\right)R\rho\frac{d^2R}{dt^2}+\frac{3}{2}\left(\frac{dR}{dt}\right)^2\rho\left(1-\frac{\dot{R}}{3c}\right)=\left(1+\frac{\dot{R}}{c}\right)\left(P_g-P_0-P(t)\right)+\frac{R}{c}\frac{dP_g}{dt}-4\mu\frac{dR/dt}{R}-\frac{2\sigma}{R} \tag{2.6}$$

Prosperetti and Lezzi (1986) presented a general form of the cavitation bubble dynamics equation as one-parameter family of equations. Lofstedt *et al.* [154] and Barber *et al.* [155] have presented a simplified form of the general equation of Prosperetti and Lezzi [152] by deleting prefactors in parenthesis containing $\dot{R}/c$. This gives the following equation for the radial motion of bubble, which has gained immense popularity in the sonoluminescence and sonochemistry community (for further details see the original paper of Prosperetti and Lezzi [152], and the review by Brenner *et al.* [141]):

$$\rho\left[R\frac{d^2R}{dt^2}+\frac{3}{2}\left(\frac{dR}{dt}\right)^2\right]=\left[P_g-P_0-P(t)\right]-4n\frac{\dot{R}}{R}-\frac{2\sigma}{R}+\frac{R}{c}\frac{dP_g}{dt} \tag{2.7}$$

Transport Phenomena in the Bubble: In transient cavitation, the change in the temperature and pressure of the bubble contents with radial motion show peculiar features. In this case, the bubble motion is highly uneven in terms of time scales. The growth phase occurs relatively slowly over a period of few tens of microseconds; followed by a transient collapse which occurs in few tens of nanoseconds (Storey and Szeri, 2000). This unusual feature of motion imparts some peculiar characteristics to the transport phenomena in the bubble (basically heat and mass transfer). At the instance of maximum compression (or minimum radius) during radial motion, the bubble volume is extremely small and is comparable (on order of magnitude basis) to the hard core volume of the gas molecules in the bubble. Therefore, the pressure inside the bubble is given by the following expression, which

accounts for the finite volume of gas molecules:

$$P_g = \left(P_0 + \frac{2\sigma}{R_0}\right)\frac{\left(R_0^3 - h^3\right)^{\gamma}}{\left(R^3(t) - h^3\right)^{\gamma}} \tag{2.8}$$

R_0 is the initial or equilibrium radius and h is the van der Waal's hard core radius. γ is the characteristic constant that describes the thermal behavior of bubble contents, as discussed subsequently.

***Heat Transfer*:** The radial motion of the cavitation bubble occurs on extremely small time scales and also comprises uneven phase of expansion and compression, as stated above. Due to this thermal behavior of the bubble content (or the extent of heat transfer during radial motion of the bubble) is governed by the relative time scales of heat transfer and radial motion. If the heat transfer time scale is shorter than bubble dynamics time scales, the gas in the bubble remains at constant temperature (equal to the ambient temperature in liquid). This isothermal behavior allows value of γ in the expression for pressure inside the bubble to be set to 1. Conversely, if the time scale of bubble motion is smaller than that of heat transfer, the bubble contents would behave adiabatically. Thus, value of γ in expression for pressure inside the bubble should be replaced with polytropic constant. Hilgenfeldt *et al.* [156] have argued that the radial motion of bubbles contains very small time scales, and the condition for which thermal Pé number of the bubble content >> 1 (which essentially implies adiabatic behavior of bubble content) lasts for very short duration (~ 10 ns). Therefore, Hilgenfeldt *et al.* [156] have suggested setting $\gamma = 1$ uniformly in time in bubble motion.

***Gas and Vapor Transport in Bubble*:** During radial oscillations both gas and vapor diffuse across bubble. However, the extent of gas transport and vapor transport differs as a result of different time scales for diffusion of gas and evaporation/condensation of vapor. In this section, we describe the features (along with essential equations) of the gas and vapor transport in the bubble.

Gas Diffusion: Comparison of the timescales of diffusion of gas and that of the bubble motion helps identifying the influence of gas diffusion on the bubble motion. The time scale for the diffusion of gas estimated as R_0^2/D is in milliseconds. The time scale of bubble motion is almost same as the period of the ultrasound wave. The period of 20 kHz ultrasound is 50 microseconds, which is much shorter than the time scale of gas diffusion. Therefore, net diffusion of gas across bubble wall is a period of few acoustic cycles is negligible. However, diffusion of gas for longer periods needs to be taken into account. The slow pumping of the dissolved gas in liquid in the bubble is called rectified diffusion. The phenomenon of rectified diffusion has been investigated by numerous researchers over past 6 decades mainly for small amplitude oscillations of cavitation bubbles [157-160].

The landmark development in analysis of rectified diffusion was the paper of Fyrillas and Szeri 161], in which they presented a general formulation of the rectified diffusion applicable to large amplitude non-linear motion of cavitation bubbles. This analysis was based on the idea of "separation of time scales" to account for the rectified diffusion. Fyrillas and Szeri [161] proposed that the dissolved gas content in the liquid can be divided in two parts. First, the oscillatory part (in close vicinity of bubble) that changes on a fast time scale (which is essentially the time scale of the acoustic wave), and secondly, the smooth part (at large distance from bubble wall) that changes on a time scale given by R_0^2/D. Fyrillas and Szeri [161] solved the diffusion equation coupled to the equation for radial motion of cavitation bubble using singular perturbation analysis and found that the contribution by the oscillatory portion of dissolved gas to the overall mass transport was negligible. The smooth part, however, makes contribution to the change in gas content of the bubble over larger time periods (for example a few thousand acoustic cycles).

It must however be mentioned that transient cavitation comprises of bubble motion only for few acoustic cycles. At the point of minimum radius (or maximum compression), the

temperature and pressure inside the bubble is extreme (~ 5000 K, 500 bar), and the bubble is in extremely energetic, and hence, unstable state. Any instability in the medium surrounding the bubble can cause fragmentation of the bubble into smaller pieces, some of which can further grow. Therefore, for transient cavitation bubbles, the phenomenon of rectified diffusion is of relatively smaller relevance than for the stable cavitation, in which bubble motion lasts for much longer duration (few thousand acoustic cycles as mentioned above) so as to have effective rectified diffusion. Due to these reasons, most of the transient cavitation models used in literature ignore rectified diffusion.

***Vapor Transport*:** During the expansion phase, evaporation of liquid occurs at the bubble interface and the vapor molecules diffuse towards the bubble core. Several authors have attempted to model the vapor transport in the bubble and its influence on radial motion [138,162-165]. In a previous publication from our group [166], a detailed review of this literature has been published. Given below are some extracts of this review.

Yasui [167,168] considered non-equilibrium phase change at the bubble wall during condensation of vapor, and also 25 chemical reactions occurring between various species produced in the bubble at the time of transient collapse. Yasui assumed that the vapor transport in the bubble was condensation limited and diffusion of vapor to the bubble wall was instantaneous. The principal result of Yasui's study was that some water vapor remained in the bubble at the amount of transient collapse. Endothermic dissociation of water vapor reduced the final temperature peak reached in the bubble. Another physical factor that influences the vapor transport in the bubble is the accommodation coefficient (denoted as σ_a). The accommodation coefficient represents resistance to condensation at the bubble interface. Lower values of σ_a indicate greater resistance to condensation, and thus, non-equilibrium phase change at bubble interface. The most general treatment of the vapor transport in the cavitation bubble was given by Storey and Szeri [169], who showed that

vapor transport in the bubble is a two-step process: (1) diffusion of vapor molecules to the bubble wall, and (2) the condensation at bubble wall. Therefore, time scales of both of these steps (viz. t_{dif} and t_{cond}), and their relative magnitudes with time scale of bubble motion (t_{osc}), influence the vapor transport. In the initial phase of bubble collapse, time scales of both of the steps mentioned above are smaller than the time scale of bubble oscillation (or $t_{cond}, t_{dif} < t_{osc}$). However, as the bubble wall accelerates during collapse, the above inequality reverses. The time scale of vapor diffusion becomes greater than the time scale of bubble dynamics ($t_{osc} << t_{dif}$). Consequently, the vapor in the bubble has insufficient time to diffuse towards bubble interface (or bubble wall) at which it can condense. The vapor present in the bubble at this moment gets "*frozen*" in the bubble due to which the composition of the bubble remains fixed (or in other words the bubble becomes a "closed system" on which work is being done by the converging fluid elements that compress the bubble). Another mechanism that contributes parallely to the entrapment of water vapor is the inequality between time for condensation of vapor and time scale of bubble motion (i.e. $t_{cond} >> t_{osc}$). The extent of vapor entrapment by this mechanism is a function of the accommodation coefficient. Both of the mechanisms stated above can contribute to the entrapment of vapor. However, as shown by Storey and Szeri [169] the condition $t_{diff} >> t_{osc}$ is reached in the bubble motion much earlier than $t_{cond} >> t_{osc}$. Therefore, Storey and Szeri [169] concluded that the vapor transport was diffusion (and not condensation) limited. On the basis of results of Storey and Szeri [169-170], Toegel *et al.* [171] developed a simplified diffusion limited model using boundary layer approximation, which was validated against the full numerical model of Storey and Szeri [169]. The model of Toegel *et al.* [171] has been used in our study for correlation the experimental results.

***Stable and Transient Cavitation*:** Radial motion of cavitation bubble is broadly categorized

into two types: stable and transient. *Stable cavitation* refers to small amplitude oscillatory radial motion around a mean for several acoustics cycles. In transient cavitation, the radial motion comprises of an explosive growth (several times the initial radius) followed by an extremely rapid transient collapse. The cavitation bubble can be made up of gas or vapor or a mixture of both. If the cavitation bubble contains non-condensable gas, the pressure inside the bubble continuously rises as the bubble undergoes compression. Due to this pressure, the bubble may undergo several after-bounces subsequent to an initial collapse. The nature of bubble motion, whether transient or stable, depends on four factors: (1) pressure amplitude of ultrasound wave (P_A), (2) frequency of ultrasound wave (f), (3) initial bubble radius (R_o) and (4) ambient or static pressure in the liquid (P_o). In general, when $P_A << P_0$, the bubble motion is oscillatory and also in phase with the driving pressure. With increase in P_A, the amplitude of the radial motion of the bubble increases, and the motion becomes more-and-more nonlinear and inertial (for example, the expansion of the bubble continues even after end of the rarefaction half cycle). Obviously, the intensity of the ensuing transient collapse of the bubble also increases. Transient cavitation threshold (denoted as P_T) is defined as the minimum amplitude of the acoustic wave (for a given value of P_0) at which the bubble motion becomes transient.

Given below are some of the quantitative criteria for defining and distinguishing transient bubble motion.

Flynn's [172] *analysis*: Flynn defined a critical expansion ratio for the bubble $\left(R_{max}/R_0\right)_c$, exceeding which the bubble collapse is dominated by the inertial forces. In this case, the spherical convergence of the liquid surrounding the bubble transfers ever increasing quantities of kinetic energy to the contracting bubble. Flynn calculated $\left(R_{max}/R_o\right)_c$ value for bubbles of size smaller than the resonant size corresponding to frequency of the acoustic wave (but not so small that surface tension becomes dominant) using simulations of radial

motion of bubble. As the P_A approaches P_T, the velocity of the transient collapse increased very sharply. If the bubble expands twice of its initial size during expansion phase (or $R_{max}/R_o \sim 2$), the velocity of the bubble wall in the final moments of transient collapse reaches or even exceeds the sonic velocity. Due to an extremely rapid collapse, the bubble behaves adiabatically, with temperature and pressure inside the bubble reaching extreme. Flynn proposed two criteria for distinguishing transient cavitation: (1) a radial expansion of > 2× (which corresponds to volumetric expansion of 8×); (2) bubble wall velocity in the final moments of transient collapse reaching or exceeding sound velocity.

Neppiras [173] *analysis:* Neppiras has given an analytical expression for the transient cavitation threshold as:

$$P_T > P_o + \frac{4}{3}\sqrt{\frac{2\sigma^3}{3R_o^3\left(P_o + 2\sigma/R_o\right)}} \tag{2.9}$$

For detailed derivation of this expression, we refer the reader to the original paper. The basis of the derivation is essentially the balance between pressure just outside the bubble (or the gas-liquid boundary) and the pressure in the bulk liquid at the instance of minimum bubble radius (or maximum compression) during radial motion. The expression given by Neppiras can be simplified for two cases as follows:

(1) In case of very small bubbles, where $2\sigma/R_o >> P_o$. Thus, $P_T \approx P_0 + \frac{4\sigma}{3\sqrt{3}R_o}$.

(2) For medium to large size bubbles (for which $P_o >> 2\sigma/R_o$): $P_T \approx P_0$

Other criteria: Apfel [174] and Holland and Apfel [175] defined a mechanical index, representative of the likelihood of occurrence of transient cavitation. This index was a ratio of max negative pressure in the bulk to the insonation frequency, and was proportional to the mechanical work that needs to be performed on the bubble during negative phase of acoustic cycle. With this analysis, Apfel corrected the critical expansion ratio for transient collapse as

2.3 (instead of 2, as defined by Flynn [172]).

***Factors Affecting Cavitation Bubble Dynamics*:** Several factors such as properties or characteristics of ultrasound wave and physical properties of the liquid medium influence radial motion of cavitation bubble. Given below is a brief qualitative description of the influence of these factors. Greater details on this can be obtained in several monographs [135,136,137].

***Frequency of ultrasound*:** The intensity of the transient collapse cavitation bubble decreases with increasing frequency of ultrasound, provided all other factors remain unaltered (especially the pressure amplitude of the wave). The physics behind this phenomenon can be explained as follows: with rise in the frequency of the acoustic wave, the period of the acoustic wave (comprising of a rarefaction and a compression) decreases. With this, the bubble is exposed to reduced pressure for a smaller duration due to which the extent of bubble expansion decreases. As a consequence, the ensuing collapse is also less intense as less energy is imparted to the bubble by the converging liquid elements around it.

***Pressure amplitude of ultrasound*:** The intensity of the cavitation bubble collapse increases with increasing acoustic pressure amplitude, for a constant ultrasound frequency, initial bubble radius and other factors such as temperature of the liquid medium. With higher acoustic pressure amplitude, the energy content of the ultrasound wave increases, as noted in previous sections. As a result, the expansion of the bubble during rarefaction half period of the wave increases. The ensuing collapse of the bubble (in the compression half period) is also more intense.

***Liquid medium related parameters*:** As seen from the equation of cavitation bubble dynamics, the main physical properties of the liquid medium that influence the radial bubble motion are:

Viscosity: Viscosity of the medium acts as a break on the radial motion of bubbles as it is

representative of the natural cohesive forces present in the liquid. In this way, viscosity also contributes to the attenuation of the acoustic wave during its passage through the medium. Increase in liquid viscosity dampens the radial motion of the bubbles, thus limiting the maximum size attained by the bubble during radial motion. Obviously, the intensity of the transient collapse (which essentially is the temperature and pressure peaks reached inside bubble during collapse) also decreases with increasing viscosity of the liquid.

Surface tension: Surface tension determines the Laplace pressure of the liquid (given as $2\sigma/R$, where R is the radius of the void or bubble generated in the liquid), and thus, represents the difficulty in generation of cavitation in the liquid. An increase in surface tension of the liquid increases the cavitation threshold, i.e. the minimum acoustic pressure amplitude for creation of cavitation in liquid. Higher Laplace pressure causes greater expansion of the bubble during rarefaction half cycle of ultrasound, and hence, intensity of transient cavitation is higher in liquid with high surface tension. For example, water has far higher surface tension (0.072 N/m) than organic liquids (which have surface tension in the range 0.02–0.03 N/m), and hence, water is the preferred solvent for sonochemical reactions.

Vapor pressure and Temperature: The expansion of cavitation bubble is accompanied by evaporation and diffusion of vapor inside the bubble. The larger the vapor pressure of the liquid, the greater the diffusion of vapor molecules into the cavitation bubble. A fraction of this vapor gets entrapped in the bubble during transient collapse, as noted earlier. The heat capacity of the bubble contents increases due to the presence of vapor molecules, as a result of which the temperature peak attained during collapse reduces. Moreover, endothermic reactions occurring during dissociation of the vapor also contribute to lowering of temperature peak. Vapor pressure of liquid varies directly with the bulk temperature of the liquid, and thus, cavitation intensity reduces with increase in the bulk temperature of liquid.

2.8.4 Physical and Chemical Effects of Ultrasound and Cavitation

Sonochemical effect: In the preceding section, we described the features of vapor transport in the bubble during radial motion. Due to large difference in time scales of diffusion, condensation and the bubble at the final moments of transient collapse, not all of the vapor that enters the bubble during expansion can escape in the ensuing compression. Moreover, the compression of the bubble is adiabatic and the temperature and pressure conditions inside the bubble reach exteme (~ 5000 K, ~ 500 bar). The fraction of the water vapor trapped in the bubble is subjected to the extreme temperatures and pressure conditions generated in the bubble at the transient collapse. The vapor molecules undergo dissociation in the bubble to generate radicals such as $H^{\bullet}$, $O^{\bullet}$, $^{\bullet}OH$ and $HO^{\bullet}_2$, with $^{\bullet}OH$ being the dominant radical species. The rate of radical generation is dependent on the total number of water vapor molecules present in the bubble during collapse, the intensity of the collapse (i.e. the magnitude of the temperature and pressure reached in the bubble at the moment of collapse), and the number of bubbles in the medium. At the instance of maximum compression, the bubble may get fragmented with release of radicals into the bulk medium, where these radicals induce and accelerate chemical reactions. This is the well-known sonochemical effect.

Sonophysical effect: The main physical effect of ultrasound and cavitation is generation of strong convection in the bulk liquid medium through several mechanisms, as described below:

Micro-streaming**:** The propagation of ultrasound waves through the liquid medium creates small amplitude oscillatory motion of fluid elements around a mean position. This is phenomenon is called micro-streaming. The velocity of the micro-streaming is: $v = P_A / \rho C$, as described in the preceding section.

Microturbulence**:** Radial motion of cavitation bubble induces high velocity oscillatory motion of the fluid in its vicinity, called microturbulence. This phenomenon is explained as follows:

during the expansion phase of radial motion, the fluid is displaced away from the bubble center. During the collapse phase, the liquid is pulled towards the bubble as it fills in the vacuum created in liquid with size reduction of the bubble. The mean velocity of the microturbulence depends on the amplitude of the oscillation of the bubble. It should, however, be noted that phenomenon of microturbulence is restricted only in the region in close vicinity of the bubble. The velocity of the microturbulence diminishes very rapidly away from the bubble.

Acoustic waves (or shock waves): As mentioned above, during the compression phase of radial motion, the fluid elements in the vicinity of the bubble wall spherically converge towards bubble wall. For a gas bubble (containing non-condensable gas such as air), the adiabatic compression results in rapid rise of the pressure inside the bubble. At the point of minimum radius (or maximum compression), the bubble wall comes to a sudden halt and rebounces with high velocity. At this instance, the converging fluid elements are reflected back from the bubble interface. This reflection creates a high-pressure shock wave that propagates through the medium.

Microjets: If the bubble is located close to a phase boundary (either solid-liquid or gas-liquid or liquid-liquid), the motion of liquid in its vicinity is hindered, resulting in development of pressure gradients around it. This non-uniformity of pressure results in the loss of spherical geometry of the bubble. During the asymmetric radial motion, the portion of the bubble exposed to higher pressure collapses faster than the rest of the bubble, which gives rise to formation of a high speed liquid jet. However, the direction of this jet depends on the characteristics of the solid boundary. For a rigid boundary (e.g. metal surfaces), the microjet is directed towards the boundary, while for a free boundary (or pressure release boundaries, e.g. gas-liquid interface), the microjet is directed away from the boundary. The velocity of the microjet has been estimated in the range of 120–150 m/s. In case of rigid boundaries, these

jets can cause severe mechanical damage such as erosion of the surface.

For a homogeneous chemical reaction system, only the chemical effects of cavitation bubbles are relevant. However, for a liquid-liquid heterogeneous reaction system such as the transesterification system for biodiesel synthesis, both physical and chemical effects of cavitation influence kinetics and yield of the reaction. Intense microturbulence created by the cavitation bubbles disrupts the liquid-liquid interface and creates very fine emulsion between the phases. This greatly enhances the interfacial area leading to large mass transfer enhancement that boosts the kinetics of the reaction system.

References

[1] G. Knothe, J. V. Gerpen, The Biodiesel Hand book, AOCS press, Germany 2004.

[2] F. Ma, M. A. Hanna, Biodiesel production: a review, Bioresour. Technol. 70 (1999) 1–15.

[3] S. Kerschbaum, G. Rinke, Measurement of the temperature dependent viscosity of bio–diesel fuels, Fuel 83 (2004) 287–291.

[4] M. Ziejewski, K. Kaufman, R. Tuppa, Laboratory endurance testing of a 25/75 sunflower oil-diesel blend treated with fuel additives, SAE technical paper 840236, 1984.

[5] A. Bilgin, O. Durgun, Z. Sahin, The effects of diesel–ethanol blends on diesel engine performance, Energ. Source. 24 (2002).431–440.

[6] F. Billaud, V. Dominguez, P. Broutin, C. Busson, Production of hydrocarbons by pyrolysis of methyl esters from rapeseed oil, J. Am. Oil Chem. Soc. 72 (1995) 1149-1154.

[7] M. Ziejewski, H. Getter, G. L. Pratt, International Congress and Exposition, Detroit, MI, Paper No. 86031, 1986

[8] A. W. Schwab, M. O. Bagby, B. Freedman, Preparation and properties of diesel fuels from vegetable oils, Fuel 66 (1987) 1372–1378.

[9] C. E. Goering, Final report for project on effect of nonpetroleum fuels on durability of direct–injection diesel engines. Under Contract 59–2171–1–6–057–0, USDA, ARS, Peoria, IL (1984).

[10] N. O. V. Sonntag, Reactions of fats and fatty acids, In: Bailey's Industrial Oil and Fat Products (Vol. 1, 4th ed., Editor: D. Swern), Wiley, New York, 1979, p. 99.

[11] D. Pioch, M. Lozawa, C. Rasoanatoandro, S. Graile, P. Geneste, A. Guida, Biofuels from catalytic cracking of tropical vegetable oils, Oleagineaux 48 (1993) 289–291.

[12] A. Demirbas, The influence of temperature on the yields of compounds existing in bio–oils obtaining from biomass samples via pyrolysis, Fuel Proc. Technol. 88 (2007) 591–597.

[13] J. Walton, The fuel possibilities of vegetable oils, Gas Oil Power 33 (1938) 167– 168.

[14] B. K. Bala, Studies on biodiesels from transformation of vegetable oils for diesel engines, Energ. Edu. Sci. Technol. 15 (2005) 1–45.

[15] E. H. Pryde, Vegetable oil as diesel fuel: Overview, J. Am. Oil Chem. Soc. 60 (1983) 1557–1558.

[16] R. Verhe, C. V. Stevens, Production of Biodiesel from Waste Lipids, In: Biofuel (Eds. W. Soetaert, E. J. van Damme), Chapter 9, John Wiley and Sons Ltd., Belgium, 2009.

[17] M. Mofijur, A. E. Atabani, H. H. Masjuki, M. A. Kalam, B. M. Masum, A study on the effects of promising edible and non–edible biodiesel feedstocks on engine performance and emissions production: A comparative evaluation, Renew. Sust. Energ. Rev. 23 (2013) 391–404.

[18] D. Y. C. Leung, X. Wu, M. K. H. Leung, A review on biodiesel production using catalyzed transesterification, Appl. Energ. 87 (2010) 1083–1095.

[19] A. S. Ramadhas, S. Jayraj, C. Muraleedharan, Use of vegetable oil as I.C. engine fuels: a review, Renew. Energ. 2003 (29) 727–742.

[20] J. H. Ng, H. K. Ng, S. Gan, Characterisation of engine–out responses from a light–duty diesel engine fuelled with palm ethyl ester (PME), Appl. Energ. 90 (2012) 58–67.

[21] G. Karavalakis, F. Alvanou, S. Stournas, E. Bakeas, Regulated and unregulated emissions of a light duty vehicle operated on diesel/palm–based methyl ester blends over NED Candanon–legislated driving cycle, Fuel 88 (2009) 1078–1085.

[22] T. Leevijit, G. Prateepchaikul, Comparative performance and emissions of IDI– turbo automobile diesel engine operated using degummed, deacidified mixed crude palm oil–diesel blends, Fuel 2011; 90: 1487–1491.

[23] H. Hazar, Effects of biodiesel on a low heat loss diesel engine, Renew. Energ. 34 (2009) 1533–1537.

[24] B. Ekrem, Effects of biodiesel on a DI diesel engine performance, emission and combustion characteristics, Fuel 89 (2010) 3099–3105.

[25] O. M. I. Nwafor, Emission characteristics of diesel engine operating on rapeseed methyl ester, Renew. Energ. 29 (2004) 119–129.

[26] G. Fontaras, G. Karavalakis, M. Kousoulidou, T. Tzamkiozis, L. Ntziachristos, E. Bakeas, Effects of biodiesel on passenger car fuel consumption, regulated and non–regulated pollutant emissions over legislated and real–world driving cycles, Fuel 88 (2009) 1608–1617.

[27] D. H. Qi, H. Chen, L. M. Geng, Y. Z. Bian, Experimental studies on the combustion characteristics and performance of a direct injection engine fuelled with biodiesel/diesel blends, Energ. Convers. Manag. 51 (2010) 2985–2992.

[28] Y. Ulusoy, R. Arslan, C. Kaplan, Emission characteristics of sunflower oil methyl ester, Energ. Source. Part A 31 (2009) 906–910.

[29] S. Godiganur, C. H. S. Murthy, R. P. Reddy, 6BTA 5.9 G2–1 Cummins engine performance and emission tests using methyl ester Mahua (Madhuca indica) oil/diesel blends, Renew. Energ. 34 (2009) 2172–2177.

[30] S. Puhan, N. Vedaraman, B. V. B. Ram, G. Sankarnarayanan, K. Jeychandran. Mahua oil (Madhuca indica seed oil) methyl ester as biodiesel–preparation and emission characterstics, Biomass Bioenerg. 28 (2005) 87–93.

[31] N. Saravanan, G. Nagarajan, S. Puhan, Experimental investigation on a DI diesel engine fuelled with Madhuca indica ester and diesel blend, Biomass Bioenerg. 34 (2010) 838–43.

[32] B. Baiju, M. K. Naik, L. M. Das. A comparative evaluation of compression ignition engine characteristics using methyl and ethyl esters of karanja oil, Renew. Energ. 34 (2009) 1616–1621.

[33] M. NurunNabi, S. M. NajmulHoque. M. S. Akhter. Karanja (Pongamia pinnata) biodiesel production in Bangladesh, characterization of karanja biodiesel and its effect on diesel emissions, Fuel Process. Technol. 90 (2009) 1080–1086.

[34] H. Raheman, A. G. Phadatare, Diesel engine emissions and performance from blends of karanja methyl ester and diesel, Biomass Bioenerg. 27 (2004) 393–397.

[35] H. Aydin, H. Bayindir, Performance and emission analysis of cotton seed oil methyl ester in a diesel engine, Renew. Energ. 35 (2010) 588–592.

[36] B. S. Chauhan, N. Kumar, H. M. Cho. A study on the performance and emission of a diesel engine fuelled with Jatropha biodiesel oil and its blends, Energy 37 (2012) 616–22.

[37] D. Agarwal, A. K. Agarwal, Performance and emissions characteristics of Jatropha oil (preheated and blends) in a direct injection compression ignition engine, Appl. Therm. Eng. 27 (2007) 2314–2323.

[38] M. W. Mumtazab, A. Adnana, Z. Mahmoodc, H. Mukhtard, M. F. Malike, F. A. Q., A. Raza, Biodiesel From Waste Cooking Oil: Optimization of Production and Monitoring of Exhaust Emission Levels From its Combustion in a Diesel Engine, Int. J. Green Energy 9 (2012) 685–701.

[39] J. B. Hirkude, A. S. Padalkar, Performance and emission analysis of a compression ignition: engine operated on waste fried oil methyl esters, Appl. Energ. 90 (2012) 68–72.

[40] Y. C. Lin, K. H Hsu, C. B. Chen, Experimental investigation of the performance and emissions of a heavy duty diesel engine fuelled with waste cooking oil biodiesel/ultra low sulfur diesel blends, Energy 36 (2011) 241–248.

[41] E. Lotero, Y. Liu, D. E. Lopez, K. Suwannakarn, D. A. Bruce, J. G. Jr. Goodwin, Synthesis of biodiesel via acid catalysis, Ind. Eng. Chem. Res.44 (2005) 5353-5363

[42] V. L. Gole, P. R. Gogate, Intensification of synthesis of biodiesel from non-edible oils using sonochemical reactors, Ind. Eng. Chem. Res. 51 (2012) 11866–11874.

[43] G. L. Maddikeri, A. B. Pandit, P. R. Gogate, Intensification approaches for biodiesel synthesis from waste cooking oil: a review, Ind. Eng. Chem. Res. 51 (2012) 14610–14628.

[44] S. Jain, M. P. Sharma, Prospects of biodiesel from Jatropha in India: a review, Renew. Sust. Energ. Rev. 14 (2010) 763–771.

[45] V. C. Pandey, K. Singh, J. S. Singh, A. Kumar, B. Singh, R. P. Singh, *Jatropha curcas*: a potential biofuel plant for sustainable environmental development, Renew. Sust. Energ. Rev. 16 (2012) 2870–2883.

[46] M. Y. Koh, T. I. M. Ghazi, A review of biodiesel production from *Jatropha curcas* L. oil, Renew. Sust. Energ. Rev. 15 (2011) 2240–2251.

[47] S. Jain, M. P. Sharma, Biodiesel production from *Jatropha curcas* oil, Renew. Sust. Energy Rev. 14 (2010) 3140–3147.

[48] J. Janaun, N. Ellis, Perspectives on biodiesel as a sustainable fuel, Renew. Sust. Energ. Rev. 14 (2010) 1312–1320.

[49] R. Jothiramalingam, M. K. Wang, Review of recent developments in solid acid, base, and enzyme catalysts (heterogeneous) for biodiesel production via transesterification, Ind. Eng. Chem. Res. 48 (2009) 6162–6172.

[50] V. B. Borugadda,V. V. Goud, Biodiesel production from renewable feedstocks: Status and opportunities, Renew. Sust. Energ. Rev. 16 (2012) 4763–4784.

[51] A. Kumar, S. Sharma, Potential non-edible oil resources as biodiesel feedstock: An Indian perspective, Renew. Sust. Energ. Rev. 15 (2011) 1791–1800

[52] M. K. lam, K. T. Lee, Homogeneous, heterogeneous and enzymatic catalysis for transesterification of high free fatty acid oil (waste cooking oil) to biodiesel: A review, Biotech. Adv. 28 (2010) 500–518.

[53] S. Al-Zuhair, Production of biodiesel: possibilities and challenges, Biofuels Bioprd. Bioref. 1 (2007) 57–66.

[54] V. L. Gole, P. R. Gogate, A review on intensification of synthesis of biodiesel from sustainable feed stock using sonochemical reactor, Chem. Eng. Process: Process Intensification: 53 (2012) 1-9.

[55] C. C. C. M. Silva, F. P. N. B. Ribeiro , M. M. V. M. Souza , D. A. G. Aranda, Biodiesel production from soybean oil and methanol using hydrotalcites as catalyst, Fuel Process. Technol. 91 (2010) 205–210.

[56] J. M. Dias , M. C.M. A. Ferraz, M. F. Almeida, Comparison of the performance of different homogeneous alkali catalysts during transesterification of waste and virgin oils and evaluation of biodiesel quality, Fuel 87 (2008) 3572–3578.

[57] A. P. S. Dias, J. Bernardo, P. Felizardo, M. J. N. Correia, Biodiesel production by soybean oil methanolysis over SrO/MgO catalysts. The relevance of the catalyst granulometry, Fuel Process. Technol. 102 (2012) 146–155.

[58] M. Fan, P. Zhang, Q. Ma, Enhancement of biodiesel synthesis from soybean oil by potassium fluoride modification of a calcium magnesium oxides catalyst, Bioresour. Technol. 104 (2012) 447–450.

[59] F. Guo, N. N. Wei, Z. Xiu, Z. Fang, Transesterification mechanism of soybean oil to

biodiesel catalyzed by calcined sodium silicate, Fuel 93 (2012) 468–472.

[60] R. Guzatto, T. L. Martini, D. Samios, The use of a modified TDSP for biodiesel production from soybean, linseed and waste cooking oil, Fuel Process. Technol. 92 (2011) 2083–2088.

[61] X. Li, G. Lu, Y. Guo, Y. Guo, Y. Wang, Z. Zhang, X. Liu, Y. Wang, A novel solid superbase of Eu_2O_3 /Al_2O_3 and its catalytic performance for the transesterification of soybean oil to biodiesel, Catal. Commun. 8 (2007) 1969–1972.

[62] Y. Li, F. Qiu, D. Yang, X. Li, P. Sun, Preparation, characterization and application of heterogeneous solid base catalyst for biodiesel production from soybean oil, Biomass Bioenerg. 35 (2011) 2787–2795.

[63] X. Liang, G. Gong, H. Wu, J. Yang, Highly efficient procedure for the synthesis of biodiesel from soybean oil using chloro–aluminate ionic liquid as catalyst, Fuel 88 (2009) 613–616.

[64] X. Liu, X. Piao, Y. Wang, S. Zhu, Calcium Ethoxide as a Solid Base Catalyst for the Transesterification of Soybean Oil to Biodiesel, Energy. Fuels 22 (2008) 1313–1317.

[65] X. Liu, H. He, Y. Wang, S. Zhu, Transesterification of soybean oil to biodiesel using SrO as a solid base catalyst, Catal. Commun. 8 (2007) 1107–1111

[66] X. Liu, H. He, Y. Wang, S. Zhu, X. Piao, Transesterification of soybean oil to biodiesel using CaO as a solid base catalyst, Fuel 87 (2008) 216–221.

[67] G. R. Moradi, S. Dehghani, F. Khosravian, A. Arjmandzadeh, the optimized operational conditions for biodiesel production from soybean oil and application of artificial neural networks for estimation of the biodiesel yield, Renew. Energ. 50 (2013) 915–920.

[68] N. Pasupulety, K. Gunda, Y. Liu, G. L. Rempel, F. T. T. Ng, Production of biodiesel from soybean oil on CaO/Al2O3solid base catalysts, Appl. Catal. A 452 (2013) 189–202.

[69] E. Rashtizadeh, F. Farzaneh, M. Ghandi, A comparative study of KOH loaded on

double alumina silicate layers, microporous and mesoporous materials as catalyst for biodiesel production via transesterification of soybean oil, Fuel 89 (2010) 3393–3398.

[70] C. Samart, C. Chaiya, P. Reubroycharoen, Biodiesel production by methanolysis of soybean oil using calcium supported on mesoporous silica catalyst, Energy Conversion and Management 51 (2010) 1428–1431.

[71] Q. Shu, B. Yang, H. Yuan, S. Qing, G. Zhu, Synthesis of biodiesel from soybean oil and methanol catalyzed by zeolite beta modified with La_3^+, Catal. Commun. 8 (2007) 2159–2165.

[72] G. F. Silva, F. L. Camargo, A. L. O. Ferreira, Application of response surface methodology for optimization of biodiesel production by transesterification of soybean oil with ethanol, Fuel Process. Technol. 92 (2011) 407–413.

[73] S. M. P. Meneghetti, M. R. Meneghetti,T. M. Serra, D. C. Barbosa, C. R. Wolf, Biodiesel Production from Vegetable Oil Mixtures: Cottonseed, Soybean, and Castor Oils, Energ Fuel 2007 (21) 3746–3747.

[74] S. Tang, H. Zhao, Z. Song, O. Olubajo, Glymes as benign co–solvents for CaO–catalyzed transesterification of soybean oil to biodiesel, Bioresour. Technol. 139 (2013) 107–112.

[75] W. Xie, T. Wang, Biodiesel production from soybean oil transesterification using tin oxide–supported WO3catalysts, Fuel Process. Technol. 109 (2013) 150–155.

[76] W. Xie, L. Zhao, Production of biodiesel by transesterification of soybean oil using calcium supported tin oxides as heterogeneous catalysts, Energ. Convers. Manag. 76 (2013) 55–62.

[77] W. Xie, L. Zhao, Aminopropyl silica as an environmentally friendly and reusable catalyst for biodiesel production from soybean oil, Fuel 103 (2013) 1106–1110.

[78] A. Kalva, T. Sivasankar, V. S. Moholkar, Physical Mechanism of Ultrasound–

Assisted Synthesis of Biodiesel, Ind. Eng. Chem. Res. 48 (2009) 534–544.

[79] L. Batistella, L. A. Lerin, P. Brugnerotto, A. J. Danielli, C. M. Trentin, A. Popiolski, H.. Treichel, J. V. Oliveira, D. de Oliveira, Ultrasound assisted lipase catalyzed trans–esterification of soybean oil in organic solvent system, Ultrason. Sonochem. 19 (2012) 452–458.

[80] P. Chand, V. R. Chintareddy, J. G. Verkade, D. Grewell, Enhancing Biodiesel Production from Soybean Oil Using Ultrasonics, Energ. Fuel. 24 (2010) 2010–2015.

[81] P. Cintas, S. Mantegna, E. C. Gaudino, G. Cravotto, A new pilot flow reactor for high–intensity ultrasound irradiation. Application to the synthesis of biodiesel, Ultrason. Sonochem. 17 (2010) 985–989.

[82] F. F. P. Santos, S. Rodrigues, F. A. N. Fernandes, Optimization of the production of biodiesel from soybean oil by ultrasound assisted methanolysis, Fuel Process. Technol. 90 (2009) 312–316.

[83] W. Guo, H. Li, G. Ji, G. Zhang, Ultrasound–assisted production of biodiesel from soybean oil using Brønsted acidic ionic liquid as catalyst, Bioresour. Technol. 125 (2012) 332–334.

[84] P. A. Parkar, H. A. Choudhary, V. S. Moholkar, Mechanistic and kinetic investigations in ultrasound assisted acid catalyzed biodiesel synthesis, Chem. Eng. J. 187 (2012) 248–260.

[85] N. N Mahamuni, Y. G. Adewuyi, Application of Taguchi method to investigate the effects of process parameters on the transesterification of soybean oil using high frequency ultrasound, Energ. Fuel. 2010, 24, 2120–2126.

[86] D. Yu, L. Tian, H. Wu, S. Wang, Y. Wang, D. Ma, X. Fang, Ultrasonic irradiation with vibration for biodiesel production from soybean oil by *Novozym 435*, Process Biochem. 45 (2010) 519–525.

[87] S. Jain, M. P. Sharma, Kinetics of acid base catalyzed transesterification of *Jatropha curcas* oil, Bioresour. Technol. 101 (2010) 7701–7706.

[88] H. J. Berchmans, K. Morishita, T. Takarada, Kinetic study of hydroxide–catalyzed methanolysis of *Jatropha curcas*–waste food oil mixture for biodiesel production, Fuel 104 (2010) 46–52.

[89] H. J. Berchmans, S. Hirata, Biodiesel production from crude *Jatropha curcas* L. seed oil with a high content of free fatty acids, Bioresour. Technol. 99 (2008) 1716–1721.

[90] G. Corro, U. Pal, N. Tellez, Biodiesel production from *Jatropha curcas* crude oil using ZnO/SiO_2 photocatalyst for free fatty acids esterification, Appl. Catal. B 129 (2013) 39–47.

[91] G. Corro, N. Tellez, E. Ayala, A. M. Ayala, Two–step biodiesel production from *Jatropha curcas* crude oil using SiO_2-HF solid catalyst for FFA esterification step, Fuel 89 (2010) 2815–2821

[92] X. Deng, Z. Fang, Y. H. Liu, C. L. Yu, Production of biodiesel from Jatropha oil catalyzed by nanosized solid basic catalyst, Energy 36 (2011) 777–784.

[93] A. K. Endalew, Y. Kiros, R. Zanzi, Heterogeneous catalysis for biodiesel production from *Jatropha curcas* oil (JCO), Energy 36 (2011) 2693–2700.

[94] F. Guo, Z. Fang, X. F. Tian, Y. D. Long, L. Q. Jiang, One–step production of biodiesel from Jatropha oil with high–acid value in ionic liquids, Bioresour. Technol. 102 (2011) 6469–6472.

[95] K. H. Kay, S. M. Yasir, Biodiesel Production from Low Quality Crude Jatropha Oil Using Heterogeneous Catalyst, APCBEE Procedia 3 (2012) 23–27.

[96] N. S. Kitakawa, K. Kanagawa, K. Nakashima, T. Yonemoto, Simultaneous production of high quality biodiesel and glycerine from Jatropha oil using ion–exchange resins as catalysts and adsorbent, Bioresour Technol. 142 (2013) 732–736.

[97] Z. Helwani, N. Aziz , M.Z.A. Bakar , H. Mukhtar , J. Kim, M.R. Othman, Conversion of Jatropha curcas oil into biodiesel using re-crystallized hydrotalcite, Energ. Convers. Manag. 92 (2011) 2420–2428.

[98] P. Mazumdar, V. B. Borugadda, V. V. Goud, L. Sahoo, Physico–chemical characteristics of *Jatropha curcas* L. of North East India for exploration of biodiesel, Biomass Bioenerg. 46 (2012) 546–554.

[99] K. F. Yee, K. T. Lee, R. Ceccato, A. Z. Abdullah. Production of biodiesel from *Jatropha curcas* L. oil catalyzed by SO_4^{2-} /ZrO_2 catalyst: Effect of interaction between process variables, Bioresour. Technol. 102 (2011) 4285–4289.

[100] Y. H. T. Yap, H. V. Lee, M. Z. Hussein, R. Yunus, aluminum–based mixed oxide catalysts for methanolysis of *Jatropha curcas* oil to biodiesel, Biomass Bioenerg. 35 (2011) 827–834.

[101] A. F. Zanette, R. A. Barella, S. B. C. Pergher, H. Treichel, D. Oliveira, M. A. Mazuttib, E. A. Silva, J. V. Oliveira, Screening, optimization and kinetics of *Jatropha curcas* oil transesterification with heterogeneous catalysts, Renew. Energ. 36 (2011) 726–731.

[102] A. S. Badday, A. Z. Abdullah, K. T. Lee, Optimization of biodiesel production process from Jatropha oil using supported heteropolyacid catalyst and assisted by ultrasonic energy, Renew. Energ. 50 (2013) 427–432.

[103] A. S. Badday, A. Z. Abdullah, K. T. Lee, Ultrasound–assisted transesterification of crude Jatropha oil using cesium doped heteropolyacid catalyst: Interactions between process variables, Energy 60 (2013) 283–291.

[104] A. S. Badday, A. Z. Abdullah, K. T. Lee, Ultrasound–assisted transesterification of crude Jatropha oil using alumina–supported heteropolyacid catalyst, Appl. Energ. 105 (2013) 380–388.

[105] X. Deng, Z. Fang, Y. H. Liu, Ultrasonic transesterification of *Jatropha curcas* L. oil

to biodiesel by a two–step process, Energ. Convers. Manag. 51 (2010) 2802–2807.

[106] D. Kumar, G. Kumar, R. Johari, P. Kumar, Fast, easy ethano–methanolysis of *Jatropha curcas* oil for biodiesel production due to the better solubility of oil with ethanol in reaction mixture assisted by ultrasonication, Ultrason. Sonochem. 19 (2012) 816–822.

[107] D. Kumar, G. Kumar, Poonam, C. P. Singh, Ultrasonic–assisted transesterification of *Jatropha curcus* oil using solid catalyst, Na/SiO_2, Ultrason. Sonochem. 17 (2010) 839–844.

[108] H. Zou, M. Lei, Optimum process and kinetic study of *Jatropha curcas* oil pre–esterification in ultrasonical field, J. Tai. Inst. Chem. Eng. 43 (2012) 730–735.

[109] S. H. Shuit, K. T. Lee, A. H. Kamaruddin, S. Yusup, Reactive extraction and *in–situ* esterification of *Jatropha curcas* L. seeds for the production of biodiesel, Fuel 89 (2010) 527–530.

[110] S. Tamalampudi, M. R. Talukder, S. Hama, T. Numata, A. Kondo, H. Fukuda, Enzymatic production of biodiesel from Jatropha oil: a comparative study of immobilized–whole cell and commercial lipases as a biocatalyst, Biochem. Eng. J. 39 (2008) 185–189.

[111] S. Shah, M. N. Gupta, Lipase catalyzed preparation of biodiesel from Jatropha oil in a solvent free system, Process Biochem. 42 (2007) 409–414.

[112] H. J. Berchmans, S. Hirata, Biodiesel production from crude *Jatropha curcas* L. seed oil with a high content of free fatty acids, Bioresour. Technol. 99 (2008) 1716–1721.

[113] S. Jain, M. P. Sharma, Kinetics of acid base catalyzed transesterification of *Jatropha curcas* oil, Bioresour. Technol. 101 (2010) 7701–7706.

[114] A. K. Tiwari, A. Kumar, H. Raheman, Biodiesel production from Jatropha oil (*Jatropha curcas*) with high free fatty acids: an optimized process, Biomass Bioenerg. 31 (2007) 569–575.

[115] P. D. Patil, S. Deng, Optimization of biodiesel production from edible and non–edible vegetable oils, Fuel 88 (2009) 1302–1306.

[116] H. Lu, Y. Liu, H. Zhou,Y. Yang, M. Chen, B. Liang, Production of biodiesel from *Jatropha curcas* L. Oil, Comp. Chem. Eng. 33 (2009) 1091–1096.

[117] G. Corro, N. Tellez, E. Ayala, A. M. Ayala, Two–step biodiesel production from *Jatropha curcas* crude oil using SiO_2-HF solid catalyst for FFA esterification step, Fuel 89 (2010) 2815–2821.

[118] A. F. Zanette, R. A. Barella, S. B. C. Pergher, H. Treichel, D. Oliveira, M. A. Mazutti, Screening, optimization and kinetics of *Jatropha curcas* oil transesterification with heterogeneous catalysts, Renew. Energ. 36 (2011) 726–731.

[119] G. Kafuku, K. T. Lee, M. Mbarawa, The use of sulfated tin oxide as solid superacid catalyst for heterogeneous transesterification of *Jatropha curcas* oil, Chem. Papers 64 (2010) 734–40.

[120] A. K. Endalew, Y. Kiros, R. Zanzi, Heterogeneous catalysis for biodiesel production from *Jatropha curcas* oil (JCO), Energy 36 (2011) 2693–2700.

[121] K. F. Yee, K. T. Lee, R. Ceccato, A. Z. Abdullah, Production of biodiesel from *Jatropha curcas* L. oil catalyzed by SO_4^{2-}/ZrO_2 catalyst: Effect of interaction between process variables, Bioresour. Technol. 102 (2011) 4285–4289.

[122] H. V. Lee, R. Yunus, J. C. Juan, Y. H. Taufiq–Yap, Process optimization design for jatropha–based biodiesel production using response surface methodology, Fuel Process. Technol. 92 (2011) 2420–2428.

[123] P. Chadha, A. K. Arora, S. Prakash, M. K. Jha, S. K. Puri, D. K. Tuli, R. K. Malhotra, Ultrasonic assisted *in–situ* transesterification of Jatropha seed to biodiesel, J. Sci. Ind. Res. 71 (2012) 290–294.

[124] I. Worapun, K. Pianthong, P. Thaiyasuit, Two step biodiesel synthesis from crude *Jatropha curcas* L. oil using ultrasonic irradiation assisted, J. Oleo Sci. 61(2012)165–172.

[125] D. Kumar, G. Kumar, R. Johari, P. Kumar, Fast, easy ethano-methanolysis of

Jatropha curcas oil for biodiesel production due to the better solubility of oil with ethanol in reaction mixture assisted by ultrasonication, Ultrason. Sonochem. 19 (2012) 816–822.

[126] A. P. Vyas, J. L. Verma, N. Subrahmanyam, Effects of molar ratio, alkali catalyst concentration and temperature on transesterification of Jatropha oil with methanol under ultrasonic irradiation, Adv. Chem. Eng. Sci. 1 (2011) 45–50.

[127] G. Kumar, D. Kumar, Poonam, R. Johari, C. P. Singh, Enzymatic transesterification of *Jatropha curcas* oil assisted by ultrasonication, Ultrason. Sonochem. 18 (2011) 923–927.

[128] D. Kumar, G. Kumar, Poonam, C. P. Singh, Ultrasonic–assisted transesterification of *Jatropha curcas* oil using solid catalyst, Na/SiO_2, Ultrason. Sonochem, 17 (2010) 839–844.

[129] Y. Zhang, M. A. Dube, D. D. McLean, M. Kates, M. Biodiesel production from waste cooking oil: 1. Process design and technological assessment, Bioresour. Technol. 89 (2003) 1–16.

[130] D. Rattanaphra, A. Harvey, P. Srinophakun, Simultaneous conversion of triglyceride/free fatty acid mixtures into biodiesel using sulfated zirconia, Topics Catal., 53(2010) 773-782.

[131] K. S. Suslick, Ultrasound: Its physical, chemical and biological effects, VCH, New York, 1988.

[132] D. Ensminger, Ultrasonics: Fundamentals, technology, applications, Marcel Dekker: New York, 1988.

[133] A. D. Pierce, Acoustics: An introduction to its physical principles and applications, Acoustical Society of America, New York, 1989.

[134] F. R. Young, Cavitation. McGraw Hill, London, 1989.

[135] Y. T. Shah, A. B. Pandit, V. S. Moholkar, Cavitation reaction engineering, Plenum Press, New York, 1999.

[136] T. G. Leighton, The acoustic bubble, Academic Press, San Diego, 1994.

[137] T. J. Mason, J. P. Lorimer, Applied sonochemistry: The uses of power ultrasound in chemistry and processing, Wiley-VCH, Coventry, 2002.

[138] H. H. Flynn, Physics of acoustic cavitation in liquids. In: Physical Acoustics (Ed. W. P. Mason), Academic Press, New York, pp. 57–172, 1964.

[139] M. S. Plesset, A. Prosperetti, Bubble dynamics and cavitation, Ann. Rev. Fluid Mech. 9 (1977) 145–185.

[140] E. A. Neppiras, Acoustic cavitation, Phys. Rep. 61 (1980) 159–251.

[141] M. Brenner, S. Hilgenfeldt, D. Lohse, Single-bubble sonoluminescence, Rev. Mod. Phys. 74 (2002) 425–484.

[142] P. M. Morse, K. U. Ingard, Theoretical acoustics. Princeton University Press, Princeton, New Jersey, 1987.

[143] L. Rayleigh, On the pressure developed in a liquid during the collapse of spherical cavity, Phil. Mag. 34 (1917) 94–98.

[144] W. Besant, Hydrostatics and hydrodynamics. Deighton-Bell, Cambridge, 1889.

[145] M. S. Plesset, Dynamics of cavitation bubbles, J. Appl. Mech. (Trans. ASME) 16 (1949) 277–282.

[146] H. Poritsky, The collapse or growth of a spherical bubble or cavity in a viscous fluid. Proc. 1st US National Cong. Appl. Mech. (Ed. E. Sternberg) 813–821, 1952.

[147] B. E. Noltingk, E. A. Neppiras, Cavitation produced by ultrasonics, Proc. Phys. Soc. B63 (1950) 674–685.

[148] F. R. Gilmore, Hydrodynamic Laboratory Report. California Institute of Technology, 26–4, 1954.

[149] J. G. Kirkwood, H. A. Bethe, The pressure wave produced by an under water explosion. Office of Science Research and Development, Rep. 558, 1942.

[150] J. B. Keller, I. I. Kolodner, Damping of underwater explosion bubble oscillations, J.

Appl. Phys. 27 (1956) 1152–1161.

[151] J. B. Keller, M. J. Miksis, Bubble oscillations of large amplitude, J. Acoust. Soc. Am. 68 (1980) 628–633.

[152] A. Prosperetti, A. Lezzi, Bubble dynamics in a compressible liquid. Part 1. First order theory, J. Fluid Mech. 168 (1986) 457–477.

[153] C. E. Brennen, Cavitation and bubble dynamics, Oxford University Press, Oxford, 1995.

[154] R. Lofstedt, K. Weninger, S. J. Puttermann, B. P. Barber, Sonoluminescing bubbles and mass diffusion, Phys. Rev. E 51 (1995) 4400–4410.

[155] B. P. Barber, R. A. Hiller, R. Lofstedt, S. J. Putterman, K. R. Weninger, Defining the unknowns of sonoluminescence, Phys. Rep. 281 (1997) 65–143.

[156] S. Hilgenfeldt, D. Lohse, M. P. Brenner, Phase diagrams for sonoluminescing bubbles, Phys. Fluids 8(11) (1996) 2808–2826.

[157] D.-Y. Hsieh, M. S. Plesset, Theory of rectified diffusion of mass into gas bubbles, J. Acoust. Soc. Am. 33 (1961) 206–215.

[158] A. I. Eller, H. G. Flynn, Rectified diffusion through non-linear pulsations of cavitation bubbles, J. Acoust. Soc. Am. 37 (1965) 493–503.

[159] M. H. Safar, Comments on the paper concerning rectified diffusion of cavitation bubbles, J. Acoust. Soc. Am. 43 (1968)1188–1189.

[160] L. A. Crum, Measurements of the growth of air bubbles by rectified diffusion, J. Acoust. Soc. Am. 68 (1980) 203–211.

[161] M. M. Fyrillas, A. J. Szeri, Surfactant dynamics and rectified diffusion of microbubbles, J. Fluid Mech. 311 (1996) 361–378.

[162] D. V. Prasad Naidu, R. Rajan, R. Kumar, K. S. Gandhi, V. H. Arakeri, S. Chandrasekaran, Modeling of a batch sonochemical reactor, Chem. Eng. Sci. 49 (1994) 877–

888.

[163] C. Gong, D. P. Hart, Ultrasound induced cavitation and sonochemical yields, J. Acoust. Soc. Am. 104 (1998) 2675–2682.

[164] S. Sochard, A. M. Wilhelm, H. Delmas, Modeling of free radicals production in a collapsing gas-vapor bubble, Ultrason. Sonochem. 4 (1997) 77–84.

[165] W. C. Moss, D. A. Young, J. A. Harte, J. L. Levalin, B. F. Rozsnyai, G. B. Zimmerman, I. H. Zimmerman, Computed optical emissions from sonoluminescing bubbles, Phys. Rev. E 59 (1999) 2986–2992.

[166] S. J. Krishnan, P. Dwivedi, V. S. Moholkar, Numerical investigation into the chemistry induced by hydrodynamic cavitation. Ind. Eng. Chem. Res. 45 (2006) 1493–1504.

[167] K. Yasui, Alternative model for single-bubble sonoluminescence, Phys. Rev. E 56 (1997) 6750–6760.

168] K. Yasui, Chemical reactions in a sonoluminescing bubble, J. Phys. Soc. Jpn. 66 (1997) 2911–2920.

[169] B. D. Storey, A. J. Szeri, Water vapor, sonoluminescence and sonochemistry, Proc. R. Soc. Lond. Ser. A 456 (2000) 1685–1709.

[170] B. D. Storey, A. J. Szeri, A reduced model of cavitation physics for use in sonochemistry, Proc. R. Soc. Lond. Ser. A 457 (2001) 1685–1700.

[171] R. Toegel, B. Gompf, R. Pecha, D. Lohse, Does water vapor prevent upscaling sonoluminescence?, Phys. Rev. Lett. 85 (2000) 3165–3168.

[172] H. G. Flynn, Cavitation dynamics I. A mathematical formulation, J. Acoust. Soc. Am. 57 (1975) 1379–1396.

[173] E. A. Neppiras, Acoustic cavitation, Phys. Rep. 61 (1980) 159–251.

[174] R. E. Apfel, Possibility of micro-cavitation from diagnostic ultrasound. IEEE Trans. Ultrasonics Ferroelectrics Freq. Control UFFC 33 (1986) 139–142.

[175] C. K. Holland, R. E. Apfel, An improved theory for prediction of microcavitation thresholds. IEEE Trans. Ultrasonics Ferroelectrics Freq. Control 36 (1989) 204–208.

CHAPTER 3

Ultrasonic Biodiesel Synthesis from Soybean Oil with Basic Heterogeneous (CaO) Catalyst

3.1 Introduction

In Chapter 1, we presented the energy scenario of India, which clearly shows that development and deployment of a renewable and carbon neutral liquid transportation fuel is an urgent need of the hour in view of both energy and environmental security. In previous chapter, we presented review of representative literature that has addressed different aspects of biodiesel synthesis. The economy of biodiesel is not attractive due to high production cost, which is at par with petroleum-derived diesel. The major contribution to the production cost of biodiesel comes from cost of feedstock. Many European and Latin American countries have been using either soybean or palm oil as the feedstock due to very large scale production of these oil seeds. As far as India is concerned, scarcity as well as high cost of edible oil prohibits use of soybean and palm oil for biodiesel synthesis. Another solution to boost the economy of biodiesel is to market the side products of biodiesel manufacture. Glycerol is the

major side product of transesterification process. Glycerol resulting from transesterification with homogeneous catalyst has contaminations of alkali and alcohol, and thus, fetches very low price. The cost of purification of crude glycerol originating from trans–esterification process is prohibitively high [1]. Use of heterogeneous catalyst can marked reduce the contamination of glycerol (as it can be simply filtered out from reaction mixture [2]), and thus increase its sale value. In this chapter, we have studied the transesterification process with a basic heterogeneous catalyst (calcium oxide) with soybean oil as the feedstock.

For feed–stocks with low free fatty acid content, solid base catalysts like basic zeolites, alkali and alkali earth oxides and carbonates, hydrotalcites etc. are preferred for relatively higher reaction rates. Among alkali and alkaline earth oxides, CaO has been known to be one of the most active catalysts. High alkalinity, activity and poor solubility in methanol makes CaO an ideal solid base catalyst for biodiesel production; however, with a much slower kinetics as compared to homogeneous base catalysts [3–8]. Numerous studies have been published that report use of CaO (either in pure form or with promoters such as Zn or Li or supports like zeolite or carbon nanotubes) for biodiesel synthesis [3, 9–15]. As noted in Chapter 2, slow kinetics of heterogeneous catalyzed transesterification is a consequence of mass transfer limitation in that the reaction mixture is triphasic system comprising of oil (organic phase), alcohol (aqueous phase) and catalyst (solid phase). Possible solutions to enhancing mass transfer, and hence, reaction kinetics are: intense agitation or stirring, application of high pressure and temperature, use of a co–solvent [16] or phase transfer catalysts. Recently, ultrasound irradiation or sonication has been attempted as a means of intensification of kinetics of transesterification. Compared to the conventional homogeneous catalysis, relatively few studies have been published in intensification of heterogeneous catalyzed biodiesel synthesis with ultrasound. In Chapter 2, we have reviewed some papers in this subject. Recently, some papers have been published from University Sains Malaysia that

treats this subject. Mootabadi et al. [17] have investigated ultrasound–assisted transesterification of palm oil in presence of three alkaline earth metal oxide catalysts, viz. CaO, SrO and BaO. Effect of parameters such as sonication time, alcohol to oil molar ratio and catalyst loading was investigated and results have been correlated with basic strength of catalyst. In another paper, Salamatania et al. [18] have reported optimization of biodiesel synthesis using BaO and SrO as catalysts using statistical approach of response surface methodology. In addition to characterization of the catalyst, Salamatania et al. [18] have optimized same parameters as addressed by Mootabadi et al. [17]. Although both of these papers have experimental rigor, no attempt has been made by authors to identify the physical mechanism of the enhancement caused by ultrasound and cavitation.

In our study, we have adopted a dual approach in that we have devised experiments on the basis of statistical Box–Behnken design with analysis using response surface methodology. We have also carried out simulations of cavitation bubble dynamics in the reaction mixture, and have estimated the extent of physical and chemical effects of cavitation bubble at different experimental conditions. The correlation between experimental and simulations results, although qualitative in nature, has highlighted many interesting physical aspects of ultrasound–assisted heterogeneous catalyzed transesterification process, as elucidated in subsequent sections.

3.2 Experimental and Mathematical Modelling

3.2.1 Approach

As mentioned earlier, the experiments in our study have been devised on Box–Behnken statistical design. The following experimental parameters (or independent variables) have been chosen for optimization: catalyst loading (C), temperature (T), and alcohol to oil molar ratio (R). The time of the sonication was kept constant for 60 min based on our initial

experimental results. The exact experimental design, formulated using Minitab 15 trial version software, indicating range and levels of the independent variables is shown in Table 3.1. The response variable (%FAME) was fitted with a full quadratic model (given in equation 1) in order to correlate it to the experimental parameters or independent variables.

$$Y = \beta_0 + \sum_{i=1}^{3} \beta_i x_i + \sum_{i=1}^{3} \beta_{ii} x_i^2 + \sum_{i=1}^{2} \sum_{j=i+1}^{3} \beta_{ij} x_i x_j \qquad (3.1)$$

where Y is the response variable, i.e. %FAME yield. β_0 is a constant and β_i, β_{ii} and β_{ij} are the regression coefficients. x_i and x_j are coded independent variables.

Table 3.1: Experimental range and levels of independent variables

Independent Variables (or Factors)	Symbol coded	Levels of Factors Coded Value (Actual value)		
Catalyst concentration (wt%)	C	–1 (1)	0 (4)	1 (7)
Temperature (^oC)	T	–1 (40)	0 (52.5)	1 (65)
Alcohol to oil molar ratio (R)	M	–1 (6:1)	0 (12:1)	1 (18:1)

3.2.2 Material and methods

***Materials*:** Fortune® soybean oil (edible grade, procured from local market) with acid value of 0.2 mg KOH/g and average molecular weight of 884.65 g/mole was used in all experiments. Other chemicals used in experiments are: methanol (AR grade 99%, Merck India), CaO (AR grade 92%, Merck India), Na_2CO_3 (AR grade 99%, Merck India). Anhydrous methanol was obtained by further vacuum distillation.

Catalyst preparation and characterization: The CaO catalyst, as received from Merck, was calcined in a programmed muffle furnace at 900^{o}C for 3 h with an increasing temperature rate of 10^{o}C/min. After calcination, the catalyst was cooled to ambient temperature in a vacuum desiccator. Later it was characterized using X–ray diffractometer (Bruker, Model: D8 Advance, Cu–K_α (λ = 1.5406 Å), Range: 0.3–120^o, 40 kV 40 mA), Delsa^{TM} Nano C particle size analyzer (Beckman Coulter, Model: A53878) and BET surface area analyzer (Beckman

Coulter, Model No. SA 3100).In each experiment, freshly calcined catalyst was used so as to avoid problem of carbonate formation due to reaction of CaO with CO_2 present in ambient air.

3.2.3 Experimental setup and protocol

The experiments were conducted in two categories, viz. control and test. The control experiment was performed with mechanical stirring in a 50 mL two-neck round bottom flask. A magnetic stirrer was used to agitate reaction mixture (with total volume of 25 mL) at 600 rpm for 5 h. The catalyst concentration was 8% w/v oil (1.3 g), with alcohol to oil molar ratio of 12:1, and the temperature of the reaction being 65^{o}C. Samples of the reaction (500 μL aliquots) were withdrawn at 1 h interval to assess the conversion of the triglycerides (analysis of the procedure is described subsequently). The time data of conversion is depicted in Fig. 3.1. The total conversion obtained in the control experiment (at the end of 5 h) was approx. 56%. This value is significantly lesser than the conversion reported by Liu et al. [3]. We conjectured that this is an effect of presence of inert carbonate phase in the catalyst. To affirm this, we have conducted XRD analysis of the calcined calcium oxide, results of which have been described subsequently. Another probable cause behind this effect is improper mixing and distribution of the catalyst particles in the reaction mixture.

A schematic of the experimental setup is given in Fig. 3.2. An ultrasound bath (Elma Trans–sonic T–460 type, Germany, capacity: 2 L, frequency: 35 kHz, power: 35 W) was used for sonication of the transesterification reaction mixture. 2/3rd of bath volume was filled with water, which acted as medium for transmission of ultrasound. All experiments were carried out in a 50 mL two neck round bottom flask made of borosilicate glass. Since the temperatures of the transesterification reaction system were near or even at the boiling point of methanol, a reflux condenser was employed so as to condense the methanol vapors and return them to reaction mixture.

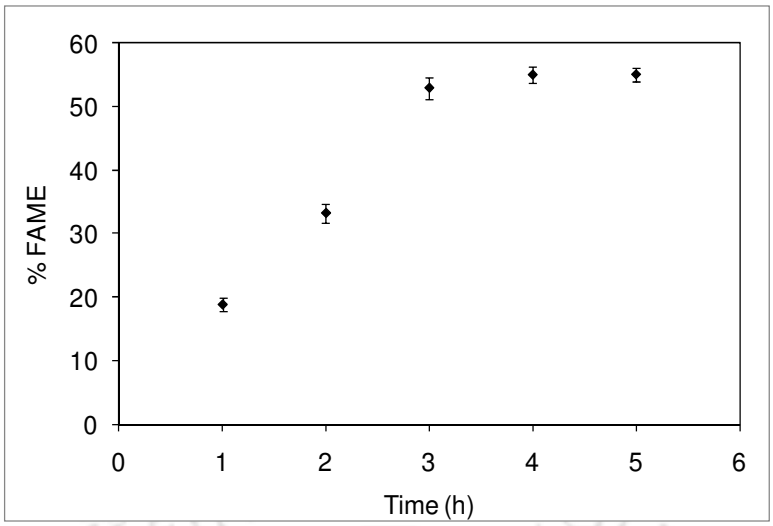

Figure 3.1: Results of the control experiments with mechanical stirring (reaction parameters: alcohol to oil molar ratio = 12:1, temperature = 65°C, catalyst concentration = 8 wt% oil, agitation speed = 600 rpm)

The temperature of water in the bath was maintained at desired levels by means of a variable energy input heating element. The bath was sealed to minimize as much heat loss as possible from the medium. The intensity (or pressure amplitude) of the ultrasound wave field shows significant spatial variation [19], and hence, the position of the reaction flask was maintained carefully the same in all experiments. The actual energy dissipation and pressure amplitude of the ultrasound wave in the bath was characterized using calorimetry [20].

As per the Box–Behnken statistical experimental design for 3 factors and 3 levels, 15 sets of experiments have been conducted for different combinations of the parameters. The experimental conditions in these sets are given in Table 3.2A, while the exact composition of reaction mixture in each set is given in Table 3.2B. Prior to performing the Box–Behnken experimental design, preliminary studies on the effect of time in the transesterification reaction was investigated and based on these results the time of sonication in all experiments was fixed as 60 min. The reaction mixture was intermittently stirred to avoid settling of large catalyst particles. In each set, experiments have been done in triplicate (3 runs) so as to assess

the reproducibility of results. The progress of the transesterification reaction was monitored by withdrawing 500 mL aliquots of the reaction mixtures after every 12 min. These aliquots were immediately mixed with hot aqueous suspension of Na_2CO_3 and centrifuged at 9000 rpm for 10 min to separate the solid catalyst as well as the aqueous (or glycerol and alcohol) phase. The organic or biodiesel layer was then analyzed to determine the yield of FAME or biodiesel.

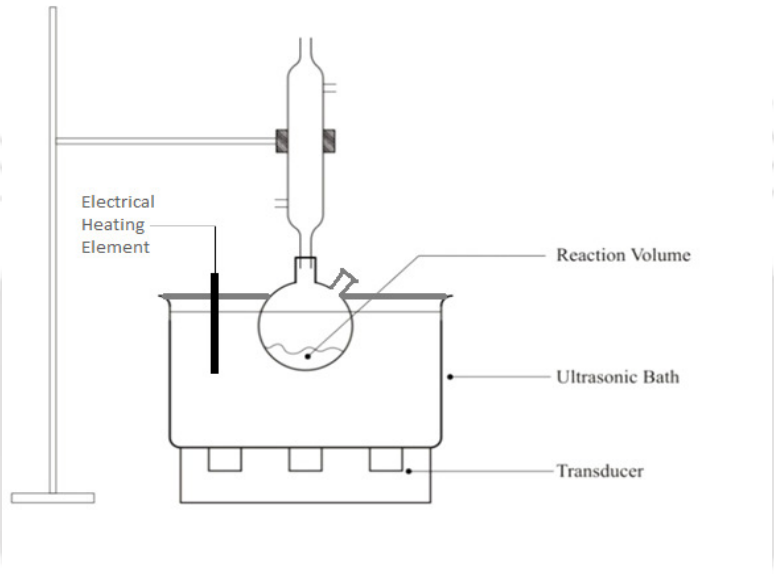

Figure 3.2: Schematic of the experimental setup

***Determination of reaction kinetics and %FAME yield*:** The gross conversion of triglycerides in soybean oil was determined using ^{1}H NMR (Varian 400 MHz FT–NMR) spectroscopic analysis with $CDCl_3$ as solvent and TMS (tetramethyl silane) as internal standard [21, 22]. The conversion (X) of triglycerides in soybean oil to fatty acid methyl esters is determined using following equation: $X = (2 \times A_{ME}) \times 100 / (3 \times A_{\alpha-CH_2})$, where, A_{ME} = integration value of the protons of the methyl esters (the strong singlet peak at 3.6 ppm), $A_{\alpha-CH2}$ = integration value of the methylene protons at 2.3 ppm.

Table 3.2

(A) Box–Behnken experimental design matrix

Sl. No.	Temperature (K)	Molar ratio	Catalyst (wt% oil)	% FAME yield with standard deviation	Fitted % FAME yield
1	313.15	6	4	15.8 ± 0.26	15.8
2	338.15	6	4	71 ± 0.83	71.3
3	313.15	18	4	9.2 ± 0.11	8.9
4	338.15	18	4	40.1 ± 0.65	40.1
5	313.15	12	1	1.5 ± 0.47	1.3
5	338.15	12	1	29.9 ± 0.8	29.5
7	313.15	12	7	26.3 ± 0.62	26.8
8	338.15	12	7	85.2 ± 0.4	85.4
9	325.65	6	1	13.8 ± 0.82	13.9
10	325.65	18	1	2.1 ± 0.25	2.5
11	325.65	6	7	62.7 ± 0.75	62.3
12	325.65	18	7	35.8 ± 0.45	35.6
13	325.65	12	4	75.1 ± 0.95	75.0
14	325.65	12	4	74.9 ± 1.07	75.0
15	325.65	12	4	75.1 ± 0.95	75.0

(B) Composition of reaction mixture in Box–Behnken experimental design matrix

Sl No.	Temperature (^{o}C)	Molar ratio	Catalyst (wt% oil)	Oil Volume (ml)	Methanol Volume (ml)	Methanol / Oil volume ratio	Catalyst added (g)
1	40.0	6	4	20	5	0.25	0.73
2	65.0	6	4	20	5	0.25	0.73
3	40.0	18	4	14.2	10.8	0.76	0.52
4	65.0	18	4	14.2	10.8	0.76	0.52
5	40.0	12	1	16.6	8.4	0.51	0.15
5	65.0	12	1	16.6	8.4	0.51	0.15
7	40.0	12	7	16.6	8.4	0.51	1.06
8	65.0	12	7	16.6	8.4	0.51	1.06
9	52.5	6	1	20	5	0.25	0.18
10	52.5	18	1	14.2	10.8	0.76	0.13
11	52.5	6	7	20	5	0.25	1.27
12	52.5	18	7	14.2	10.8	0.76	0.91
13	52.5	12	4	16.6	8.4	0.51	0.6
14	52.5	12	4	16.6	8.4	0.51	0.6
15	52.5	12	4	16.6	8.4	0.51	0.6

***Determination of transesterification kinetics*:** The time data of conversion of triglycerides obtained with help of ^{1}H NMR spectroscopy, as described above was used to determine the kinetic parameters of the process. The transesterification reaction progresses in three consecutive and reversible reactions steps as follows: (1) reaction of triglyceride (TG) and methanol to produce diglycerides (DG) and 1 molecule of methyl ester, (2) further reaction of diglycerides to yield monoglycerides (MG) and another molecule of methyl ester, and finally (3) reaction of monoglyceride to yield one mole of methyl ester and one mole of glycerol. In our analysis, we have determined the kinetic constant of the overall reaction, without accounting for the intermediate steps. The overall reaction is assumed to be governed by pseudo 1st order kinetics [23], and the following equation has been fitted to the conversion–time (X vs. t) data so as to obtain the kinetic constant:

$$\ln(1-X) = -kt \tag{3.2}$$

where X = conversion of triglyceride at any time t. Plot of $-\ln(1-X)$ vs t gives the kinetic constant k as the slope.

***Determination of activation energy (Arrhenius plot)*:** The Arrhenius equation gives a relationship between the specific reaction rate constant (k), absolute temperature (T) and the energy of activation (E_a) as: $k = A \times \exp(-E_a/RT)$ where A is the frequency factor and R is universal gas constant (J mol^{-1} K^{-1}). This equation is rewritten as:

$$\ln(k) = \frac{-E_a}{RT} + \ln(A) \tag{3.3}$$

We have used three reaction temperatures (as mentioned in Table 3.1) in our statistical experimental design. Experiments have been conducted using optimum values of catalyst loading and alcohol to oil molar ratio (as determined from the statistical experimental design) at these three reaction temperatures. Plot of ln (k) vs $1/T$ gives slope equal to ($-E_a/R$) from which activation energy can be determined.

3.2.4 Mathematical modelling of cavitation bubble dynamics

To get a quantitative estimate of the physical and chemical effects induced by ultrasound and cavitation bubbles in the system, we resort to simulations of cavitation bubble dynamics using the diffusion limited (ordinary differential equation) ODE model (using boundary layer approximation) proposed by Toegel et al. [24] for our analysis. This model is derived from the comprehensive (partial differential equation) PDE model of Storey and Szeri [25], which showed that vapor entrapment in the cavitation bubble, leading to formation of radicals is essentially a diffusion limited process. This model has been extensively described in our previous papers [20, 26, 27]. For the convenience of the reader, we reproduce here only the main components of the model and relevant data / boundary conditions. The main components of the model summarized in Table 3.3A are set of 4 ODEs as follows:

(1) Keller–Miksis equation for the radial motion of the bubble [28].

(2) Equation for Diffusive flux of methanol vapor and heat conduction through bubble wall.

(3) Overall energy balance treating the cavitation bubble as an open system.

Thermodynamic data for various species is given in Table 3.3B. The transport parameters for the heat and mass transfer (thermal conductivity and diffusion coefficient) are determined using Chapman–Enskog theory using Lennard–Jones 12–6 potential at the bulk temperature of the liquid medium [29-30]. Thermal and diffusive penetration depths are estimated using dimensional analysis. This model ignores the diffusion of gas across bubble interface on the basis that time scale for the diffusion of gases is much higher than the time scale of bubble dynamics. The set of ODEs in the bubble dynamics model can be solved simultaneously using Runge–Kutta adaptive step size method [31]. The reaction system in the present study is of liquid–liquid heterogeneous type, viz. methanol and oil. However, as per results of our earlier studies [26, 32], the energetics of the dynamics of cavitation bubbles in the oil phase is

too weak to produce any significant physical or chemical effect. This is mainly attributed to high viscosity of the oil. We have therefore considered and simulated only the bubble dynamics in methanol. Various parameters used in the simulation of bubble dynamics equation (for an air bubble) and their numerical values are as follows: Ultrasound frequency (f) = 35 kHz; Ultrasound pressure amplitude (P_A) = 1.5 bar; Equilibrium bubble radius (R_o) = 5 μm. Vapor pressure (in bar) of methanol at various reaction temperatures has been calculated using following Antoine type correlation (NIST Data Gateway, 2013): $\log_{10} P = 5.15853 - \frac{1569.613}{T - 34.846}$. Physical properties of methanol are [23]: density = 790 kg/m^3, kinematic viscosity = 6.829×10^{-7} Pa–s, surface tension = 0.02355 N/m and velocity of sound = 1103 m/s.

Estimation of physical and chemical effects of ultrasound and cavitation

Physical effect of ultrasound: Ultrasound propagates through the medium in the form of longitudinal wave with series of compression and rarefaction, and causes rapid oscillatory motion of fluid elements called as microstreaming. This motion gives rise to intense micro–mixing in the medium. The magnitude of the microstreaming velocity is given as: $u = P_A / \rho c$. Substituting values of P_A as 1.5×10^5 Pa, ρ = 790 kg/m^3, and c = 1103 m/s, gives u = 0.17 m/s.

Chemical effect of cavitation bubbles (sonochemical effect): The numerical solution of bubble dynamics model can give the temperature and pressure reached in the cavitation bubble at transient collapse, and also the number of gas and solvent molecules inside the bubble. Due to extreme conditions reached in the bubble, the solvent as well as gas molecules undergo dissociation to form numerous chemical species, which also react among themselves. Due to very high temperature as well as concentration (due to extremely small volume of the bubble), the kinetics of the reactions among these species is several orders of magnitude

higher than the time scale of bubble dynamics [27, 33]. Therefore, thermodynamic equilibrium can be assumed to prevail inside the bubble. The equilibrium mole fraction of different chemical species in the bubble at the peak conditions reached at transient collapse can be calculated using Gibbs free–energy minimization technique [34].

Physical effect of cavitation bubbles: Radial motion of cavitation bubbles generates intense convection in the medium through two phenomena, viz. micro–convection, shock or acoustic waves. Magnitudes of these entities can be determined using numerical result of bubble dynamics model as:

Micro–convection [35]*:*
$$V_{turb}(r,t) = \frac{R^2}{r^2}\left(\frac{dR}{dt}\right) \tag{3.4}$$

Shock waves (or Acoustic waves) [36, 37]:
$$P_{AW}(r,t) = \frac{\rho_L}{4\pi r}\frac{d^2V_b}{dt^2} = \rho_L\frac{R}{r}\left[2\left(\frac{dR}{dt}\right)^2 + R\frac{d^2R}{dt^2}\right] \tag{3.5}$$

where V_b is the volume of the bubble. A representative value of r is taken as 1 mm.

3.3 Results and Discussion

We shall present our results and discussion in four sections. To start with, results on characterization of the solid catalyst will be presented, following results of transesterification experiments based on statistical design and its analysis using Response Surface methodology. Finally, the results on simulations of cavitation bubble dynamics will be presented. In the fourth section, we shall correlate the experimental and simulations results so as get the physical insight into the solid catalyzed transesterification and also to identify the optimized process condition for maximum yield based on this insight.

Table 3.3

(A) Model for the Radial Motion of Cavitation Bubble

Model Component	Equation	Initial Value
1. Radial motion of the cavitation bubble	$\left(1-\frac{dR/dt}{c}\right)R\frac{d^2R}{dt^2}+\frac{3}{2}\left(1-\frac{dR/dt}{3c}\right)\left(\frac{dR}{dt}\right)^2=\frac{1}{\rho_L}\left(1+\frac{dR/dt}{c}\right)(P_i-P_t)+\frac{R}{\rho_L c}\frac{dP_i}{dt}-4\nu\frac{dR/dt}{R}-\frac{2\sigma}{\rho_L R}$ Internal pressure in the bubble: $P_i=\frac{N_{tot}(t)\,kT}{\left[4\pi\left(R^3(t)-h^3\right)/3\right]}$ Pressure in bulk liquid medium: $P_t=P_0-P_A\sin(2\pi ft)$	At $t = 0$, $R = R_o$, $dR/dt = 0$
2. Diffusive flux of solvent (methanol) molecules	$\frac{dN_S}{dt}=4\pi R^2 D_S\left.\frac{\partial C_S}{\partial r}\right\|_{r=R}\approx 4\pi R^2 D_S\left(\frac{C_{S,R}-C_S}{l_{diff}}\right)$ Instantaneous diffusive penetration depth: $l_{diff}=\min\left(\sqrt{\frac{RD_S}{\lvert dR/dt\rvert}},\frac{R}{\pi}\right)$	At $t = 0$, $N_S = 0$
3. Heat conduction across bubble wall	$\frac{dQ}{dt}=4\pi R^2\lambda\left.\frac{\partial T}{\partial r}\right\|_{r=R}\approx 4\pi R^2\lambda\left(\frac{T_0-T}{l_{th}}\right)$ Thermal diffusion length: $l_{th}=\min\left(\sqrt{\frac{R\kappa}{\lvert dR/dt\rvert}},\frac{R}{\pi}\right)$	At $t = 0$, $Q = 0$
4. Overall energy balance	$C_{V,mix}dT/dt=dQ/dt-P_i dV/dt+(h_S-U_S)dN_S/dt$ Mixture heat capacity: $C_{V,mix}=\sum C_{V,i}N_i$ (i = N_2/O_2/Solvent) Molecular properties of solvent: Enthalpy: $h=\left(1+\frac{f_i}{2}\right)kT_o$ Internal energy: $U_S=N_S kT\left(3+\sum_{i=1}^{3}\frac{\theta_i/T}{\exp(\theta_i/T)-1}\right)$ Heat capacity of various species (i = N_2/O_2/Solvent): $C_{V,i}=N_i k\left(f_i/2+\sum\left((\theta_i/T)^2\exp(\theta_i/T)\Big/\left(\exp(\theta_i/T)-1\right)^2\right)\right)$	At $t = 0$, $T = T_0$

(B) Thermodynamic properties of various species

Species	Degrees of freedom (translational + rotational) (f_i)	Lennard–Jones force constants		Characteristic vibrational temperatures θ (K)
		σ (10^{-10} m)	ε/k (K)	
N_2	5	3.68	92	3350
O_2	5	3.43	113	2273
CH_3OH	6	3.626	481.8	500.59, 1674.41, 1708.94, 1854.22, 2169.26, 2356.26, 2376.4, 2392.22, 4581.62, 4649.23, 4752.8, 5923.74

* – Data taken from Toegel [24]; Hirschfelder *et al.* [29], Reid *et al.* [38], Davis [43].

Notations: R – radius of the bubble; dR/dt – bubble wall velocity; c – velocity of sound in bulk liquid medium; ρ_L – density of the liquid; ν – kinematic viscosity of liquid; σ – surface tension of liquid; λ – thermal conductivity of bubble contents; κ – thermal diffusivity of bubble contents; θ – characteristic vibrational temperature(s) of the species; N_S – number of solvent molecules in the bubble; N_{N2} – number of nitrogen molecules in the bubble; N_{O2} – number of oxygen molecules in the bubble; t – time, D_S – diffusion coefficient of solvent vapor; C_S – concentration of solvent molecules in the bubble; $C_{S,R}$ – concentration of solvent molecules at the bubble wall or gas–liquid interface; Q – heat conducted across bubble wall; T – temperature of the bubble contents; T_o – ambient (or bulk liquid medium) temperature; k – Bolzmann constant; h_S – molecular enthalpy of solvent; U_S – internal energy of solvent molecules; f_i – translational and rotational degrees of freedom; $C_{V,i}$ – heat capacity at constant volume for species i; N_{tot} – total number of molecules (gas + vapor) in the bubble; h – van der Waal's hard core radius; P_o – ambient (bulk) pressure in liquid; P_A – pressure amplitude of ultrasound wave; f – frequency of ultrasound wave.

3.3.1 XRD and BET data of the solid catalyst

The phase purity of the catalyst before the transesterification reaction was examined by powder X–ray diffraction (XRD). The XRD spectrum is shown in Fig. 3.3A. The pattern of the catalyst matches well with the standard patterns of calcium oxide and calcium carbonate (JCPDS file No. 04–0777 and 75–2230). The catalyst contains both CaO and $CaCO_3$ phases in the solid catalyst sample. The results of particle size analysis and BET surface area are shown in Fig. 3.3B and 3.3C.

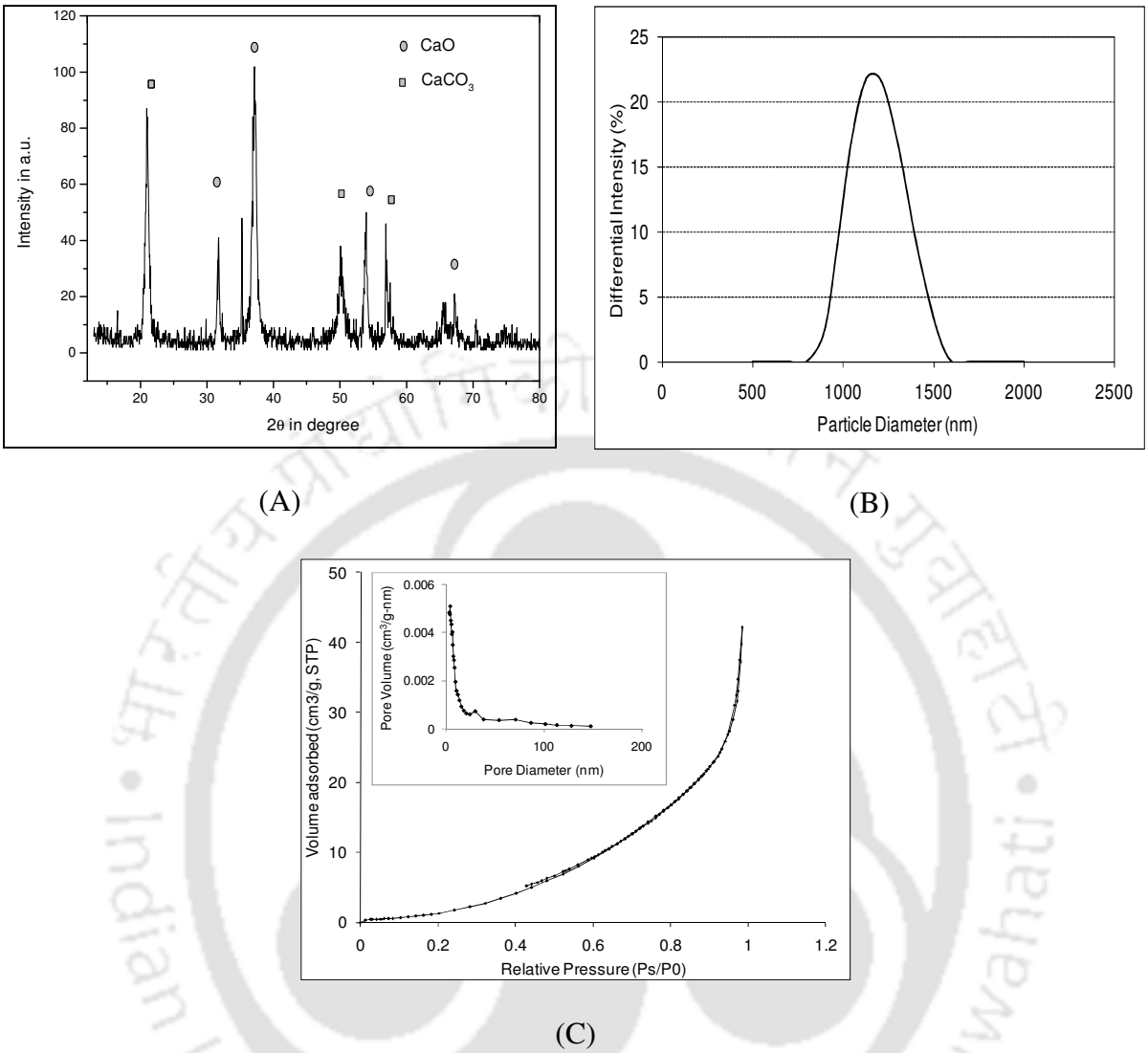

Figure 3.3: (A) XRD spectrum of the CaO catalyst Characterization of catalyst, (B) Particle size distribution of the CaO catalyst. Summary of distribution: D(10%) – 957.2 nm, D(50%) – 1124.7 nm, D(90%) – 1325.2 nm, Average- 1176.7 nm, (C) N_2 adsorption–desorption isotherms for the CaO catalyst and the corresponding BJH pore size distribution curve.

Fig. 3.3B shows the particle size analysis results. The average particle size of CaO catalyst was 1.176 microns. Fig. 3.3C shows N_2 adsorption–desorption isotherms for the CaO catalyst and the corresponding BJH pore size distribution curve. The BET surface area and total pore volume of the CaO was 7.114 m^2/g and 0.0607 cm^3/g, respectively. BJH pore radius obtained

from the adsorption isotherm is about 20 nm for the CaO catalyst, which is in the mesoporous range.

3.3.2 NMR analysis of reaction mixture

Fig. 3.4 shows ^{1}H NMR spectrum of fatty acid methyl esters (FAME) of soybean oil. The characteristic peak of FAME in ^{1}H NMR spectra is marked by presence of a peak at 3.6 ppm, as visible in Fig. 3.4. This peak corresponds to the presence of methyl ester protons of biodiesel. Various peaks in the ^{1}H NMR spectrum have been identified as follows: the triplet at 2.3 ppm corresponds to presence of α–carbonyl methylene, while peaks related to unsaturation in soybean oil are 2.0, 2.8 and 5.3 ppm, typically assigned to allylic, bis–allylic and olefinic hydrogen, respectively. A strong singlet signal at 1.2 ppm represents methylene groups of the carbon chain. The terminal methyl protons are associated with the triplet arising at 0.8 ppm. The multiplet at 1.6 ppm is assigned to α–carbonyl methylenes. A peak at 2.72 ppm denotes polyunsaturated fatty acids, which arises from the methylene group between two double bonds of a higher polyunsaturated fatty acid chain.

3.3.3 Experimental results and statistical analysis

The result of each experiment in the Box–Behnken statistical design is given Table 3.2A. The average FAME yield in each experiment is given along with standard deviation of the three trial runs in each experiment. A quadratic regression model (given in equation 3.1) was fitted to the results using coded values for the experimental parameters (Minitab 15 software, trial version). The fitted model is as follows:

$$Y = 75.028 + 21.686T - 9.522M + 20.341C - 16.918T^2 - 24.078M^2 - 22.369C^2 - 6.062T \times M - 3.818M \times C + 7.606T \times C \quad (3.6)$$

Notation: T – temperature, M – molar ratio and C – catalyst loading. The significant of each coefficient in the model equation was determined by standard t–test and p–values, also

indicated in Table 3.4A. It should be noted that the fitted model equation 3.6 is for the coded values of parameters (i.e. +1, 0 and –1), and not for the actual or absolute values of the parameters. Therefore, the regression coefficients of fitted model are only mathematical parameters and their significance is to be judged only the basis of *F*-value and *p*-value [39, 40]. A high *F*-value and *p*-value less than 0.05 indicate the significance level of the coefficient. For example, the coefficients for parameters *M*, *C* and ($M \times C$) indicate the individual influence of molar ratio, catalyst concentration and the interaction between these two parameters. The *p*-value of all three regression coefficients is 0.0, as indicated in Table 3.4A and the *F*-value of the regression coefficients, as given in Table 3.4B, is 8412.22 for overall model, 15582.11 for linear coefficients and 872.62 for interaction coefficient. This essentially means that the individual influence of molar ratio and catalyst concentration is relatively more significant than the interaction effect. The physical meaning of these values is that both molar ratio and catalyst concentration affect the transesterification yield, but these are rather independent parameters, in that there is no inter-link between the mechanisms of effects of these parameters. Values of FAME yield calculated using this model matched very well with the experimental results. The significance of regression is indicated by the coefficient of determination (R^2) which was 99.95%. This essentially means that 99.95% of the effect on the yield for CaO catalyst was explained by the variation in process variables. Table 3.4B shows the (analysis of variance) ANOVA for the quadratic model. The Lack of Fit *F*–value of 2.55 and *p*-value of 0.073 implies that Lack of fit is not significant as compared to the pure error.

The response surface 3–D plots indicating effect of interaction between any two variables (temperature–molar ratio or catalyst loading–temperature or molar ratio–catalyst loading), while holding the third parameter of its center point are shown in Fig. 3.5.

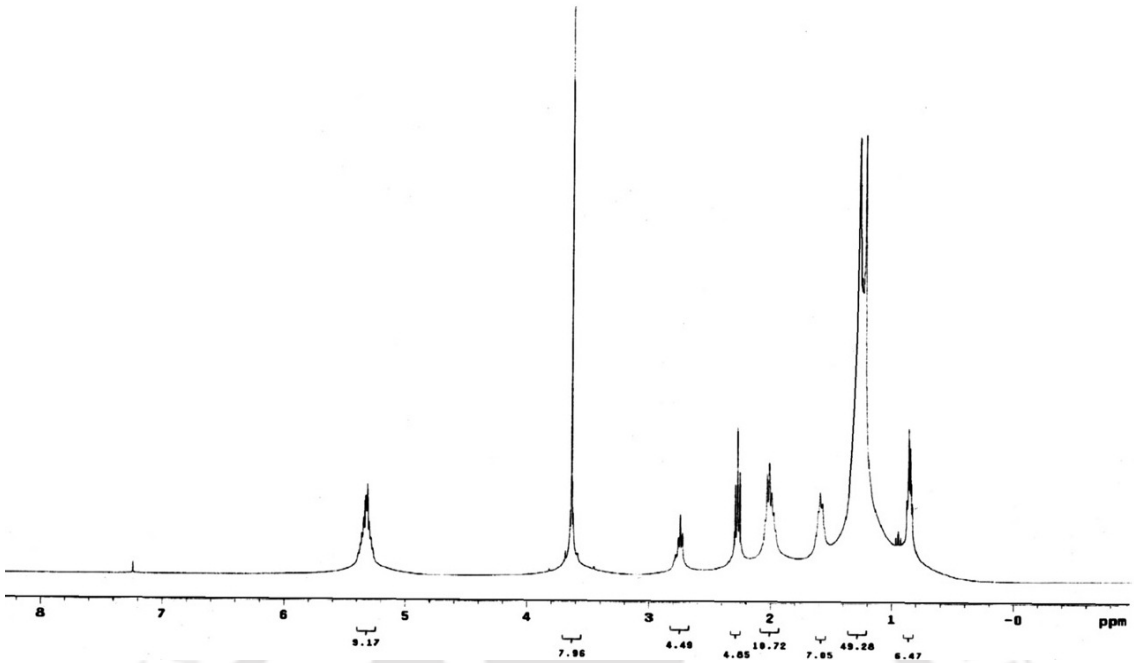

Figure 3.4: ^{1}H NMR spectrum of fatty acid methyl esters (FAME) of soybean oil

Table 3.4: Statistical analysis of experimental results

(A) Estimated Regression Coefficients for % FAME yield

Term	**Coefficients**	**SE coeff**	***t*–Stat**	***p*–value**
Constant (β)	75.028	0.2358	318.179	0.
Temperature (T)	21.686	0.1444	150.182	0.
Molar ratio (M)	–9.522	0.1444	–65.940	0.
Catalyst (C)	20.341	0.1444	140.868	0.
Temperature × Temperature (T^2)	–16.918	0.2126	–79.593	0.
Molar ratio × Molar ratio (M^2)	–24.078	0.2126	–113.283	0.
Catalyst × Catalyst (C^2)	–22.369	0.2126	–105.242	0.
Temperature × Molar ratio (TM)	–6.062	0.2042	–29.683	0.
Temperature × Catalyst (TC)	7.606	0.2042	37.245	0.
Molar ratio × Catalyst (MC)	–3.818	0.2042	–18.698	0.

Fig. 3.5A indicates that the FAME yield shows a maximum for catalyst concentration & molar ratio, especially for medium values of molar ratios. For lower molar ratios, however, the yield monotonically increases with catalyst concentration.

Table 3.4: Statistical analysis of experimental results (*continued*….)

(B) Analysis of variance (ANOVA) for transesterification of soybean oil using ultrasound

Source	DF	Sq SS	Adj SS	Adj MS	F	*p*–value
Regression	9	37887.6	37887.6	4209.74	8412.22	0.
Linear	3	23393.3	23393.3	7797.78	15582.11	0.
Square	3	13184.2	13184.2	4394.75	8781.92	0.
Interaction	3	1310.1	1310.1	436.69	872.62	0.
Residual Error	35	17.5	17.5	0.50	—	—
Lack–of–Fit	3	3.4	3.4	1.13	2.55	0.073
Pure Error	32	14.1	14.1	0.44	—	—
Total	44	37905.2			—	—

R^2 = 99.95%; R^2 (adj) = 99.94%

(C) Analysis of surface plots

(Values of variable parameters for maximum yield for center point value of third parameter)

Fixed Parameter (Center point value)	**Variable parameter**		**FAME Yield (%)**
Catalyst loading = 4 wt%	Temperature = 61.2^{o}C	Molar ratio = 10.3	83.89%
Temperature = 52.5^{o}C	Molar ratio = 10.6	Catalyst loading = 5.4 wt%	80.98%
Molar ratio = 12:1	Temperature = 62.2 ^{o}C	Catalyst loading = 5.8 wt%	89.36%

Similar behaviour is also seen for the variables temperature and molar ratios as evident from surface plot shown in Fig. 3.5B. However, for lower molar ratios, the FAME yield monotonically increases with temperature. The values of variables in Fig. 3.6A and 3.6B for which maximum in yield occurs is seen are listed in Table 3.4C, along with the value of the yield as predicted by the model. For combination of catalyst concentration (or loading) and temperature as variable (Fig. 3.5C), however, we do not see any maxima.

Again the values of catalyst loading and temperature for which maximum yield is seen for center point molar ratio of 12:1 are given in Table 3.4C. The FAME yield increases monotonically for all reaction temperature with increasing catalyst concentration.

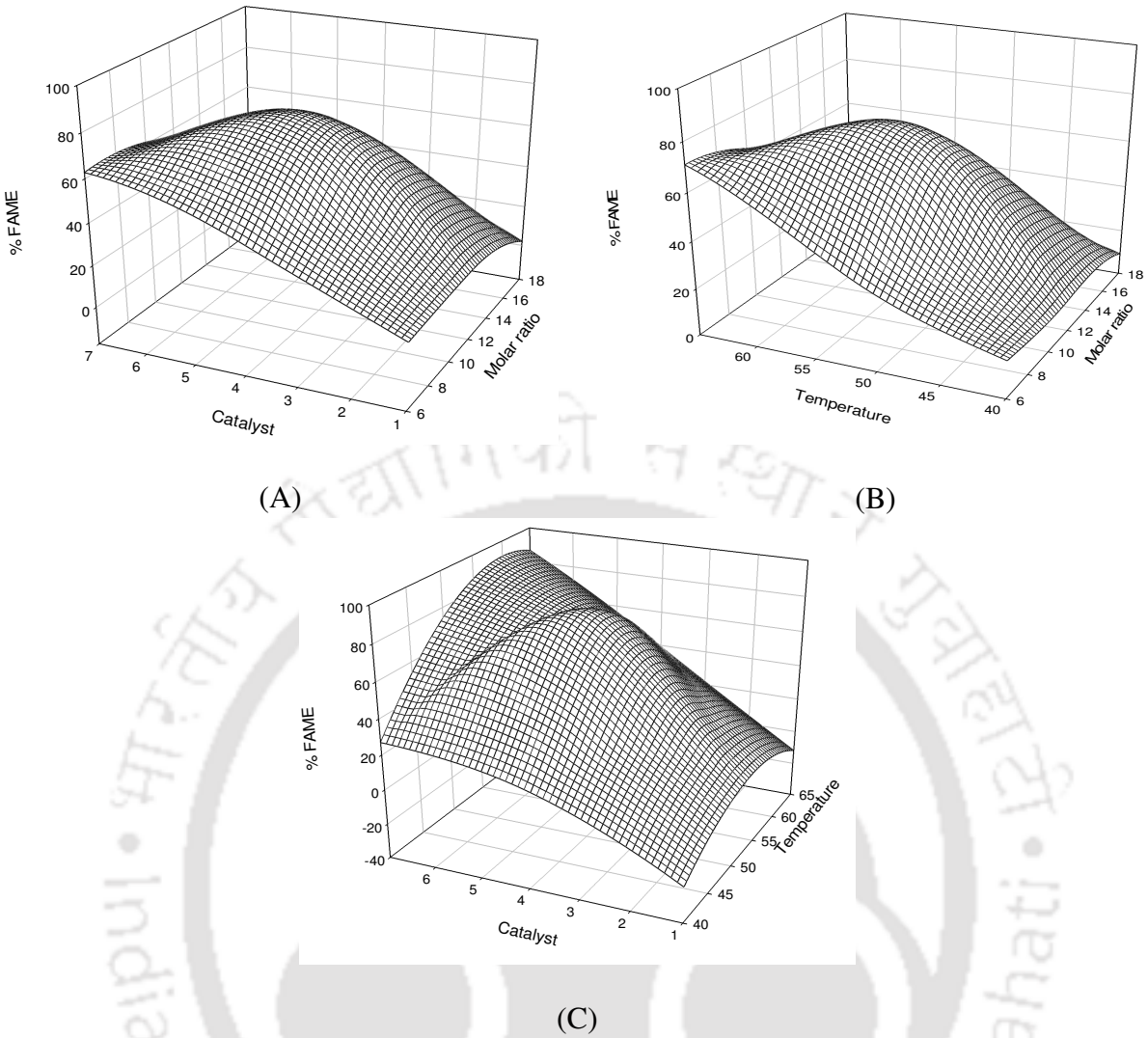

Figure 3.5: Response surface plots for % FAME yield as a function of reaction temperature, catalyst loading and methanol-to-oil molar ratio.

Results given in Table 3.4C clearly indicate that temperature is a dominant variable of the process, followed by catalyst loading and molar ratio. The highest yield of 89.36% is seen for high value of molar ratio of 12:1, high temperature of 62.2^{o}C and catalyst loading of 5.8%. An important observation is that no plateau is observed in any of the surface plots (the plateau is essentially indicative of nullification of interactive effect of variables on the FAME yield). The *p*–values of the ANOVA corroborate this result. Zero *p*–values of all individual

(linear and quadratic) as well as interaction coefficients indicate that all parameters have strong influence on the FAME yield; and moreover the influence of these parameters is strongly inter–related.

3.4. Optimization of the Process

The model equation 3.6 fitted the data (using coded values of variables) can be used to find the optimum values of parameters, for which the FAME yield is maximum. The optimization was carried out using Microsoft Excel solver that uses the quasi–Newton as well as conjugate gradient method for finding the solution using all three parameters as variables. The coded optimum values of variables are: temperature = 0.846, molar ratio = –0.354 and catalyst loading = 0.629. The actual values of parameters corresponding to these coded values are: temperature = 63^{o}C, alcohol to oil molar ratio = 9.8 (approximated as ~ 10) and catalyst loading = 5.9 wt% (approximated as ~ 6 wt%).

3.5 Kinetic Analysis of the Process

The results of the kinetic study of experiments performed with optimum values of molar ratio of 10 and catalyst loading of 6 wt% at different temperatures are depicted in Fig. 3.6A and B. Fig. 3.6A gives the time history of FAME yield, while Fig. 3.6B gives the conversion fitted through pseudo 1st order kinetic model. The regression coefficient values shown in Fig. 3.6B reveal that pseudo 1st order model fits quite well to the transesterification reaction. The pseudo 1st order kinetic constant of the reaction shows interesting trend with reaction temperature. With rise of temperature from 40 to 52 ^{o}C the kinetic constant shows a sharp increase of 7× as shown in the Table 3.5. However, further rise in temperature to 62 ^{o}C results in marginal 18% rise. Fig. 3.6C shows the Arrhenius plot for the reaction from which the activation energy can be determined. High activation energy of 82.3 kJ/mol observed in

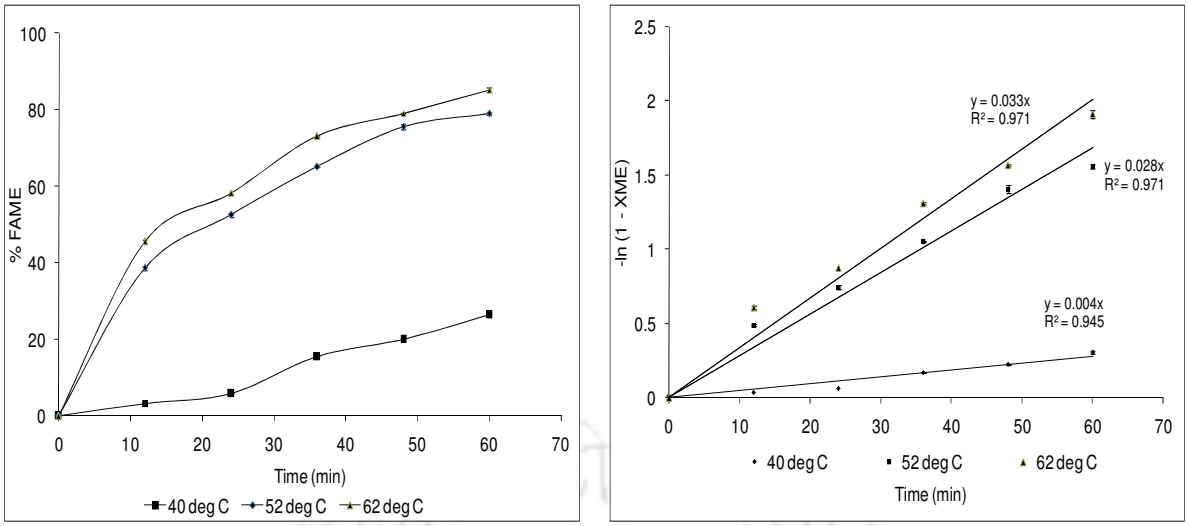

(A) (B)

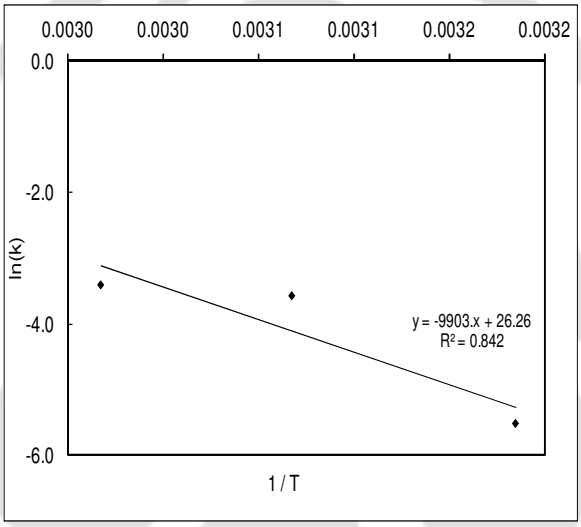

(C)

Figure 3.6: Kinetic analysis of experiment under optimum conditions. (A) Time history of conversion of triglycerides at different temperatures for methanol to oil molar ratio of 10:1 and catalyst concentration 6 wt%, (B) First order kinetic model fitted to the conversion data for determination of kinetic constants, (C) Arrhenius plot of ln (*k*) vs 1/T for the transesterification for methanol to oil molar ratio of 10:1 with catalyst concentration of 6 wt%

the present case is attributed to 3 phase heterogeneity (liquid–liquid–solid) of the reaction system. Our own previous study [32] with homogeneous acid catalyst of soybean oil–methanol transesterification, which essentially is a biphasic system, has reported activation energy of 27.5 kJ/mol for molar ratio of 12:1. The reaction system of oleic acid–methanol (which is a homogeneous mixture) with solid tungstophosphoric acid on SBA15 catalyst is

also a biphasic system and it is reported to have an activation energy of 44.6 kJ/mol [41]. These values compared to the activation energy observed in the present study clearly reveal the adverse effect of 3–phase heterogeneity in the system (that leads to the mass transfer limitation) on the activation energy.

Table 3.5: Kinetic analysis of reaction data

Temperature (^oC)	Rate constant$^{\#}$ (k) (min^{-1})
40	0.004 (R^2 = 0.945)
52	0.028 (R^2 = 0.971)
62	0.033 (R^2 = 0.971)

1st order kinetic constants at different temperature for methanol to oil molar ratio of 10:1 at 6 wt% of catalyst concentration

3.6 Simulation Results

Representative simulation results of radial dynamics of air bubble in methanol are shown in Fig. 3.7. The summary of entire simulation results for bubble dynamics in methanol at different reaction temperature used in the studies is given in Table 3.6, which lists the magnitude of convection produced by cavitation bubbles (i.e. sono–physical effects) and peak temperature/pressure conditions reached in the bubble along with the equilibrium composition of bubble contents at the transient collapse (i.e. sono–chemical effects).

We can observe that the extent of evaporation methanol in cavitation bubble increased very rapidly (almost the two orders of magnitude) as the temperature of reaction rises from 313 to 338 K. The bubble is supersaturated with methanol molecules with increasing extent of entrapment of methanol molecules in bubble. The net heat capacity of the bubble increases, leading to reduction in the peak temperature at collapse. The methanol vapor causes cushioning of collapse, and hence the pressure reached inside the bubble at collapse also reduces by almost four times.

Although the methanol vapor undergoes thermal dissociation at collapse resulting in

numerous species, the temperature peak at collapse is too small to result in generation of radical species. All species generated are molecular species.

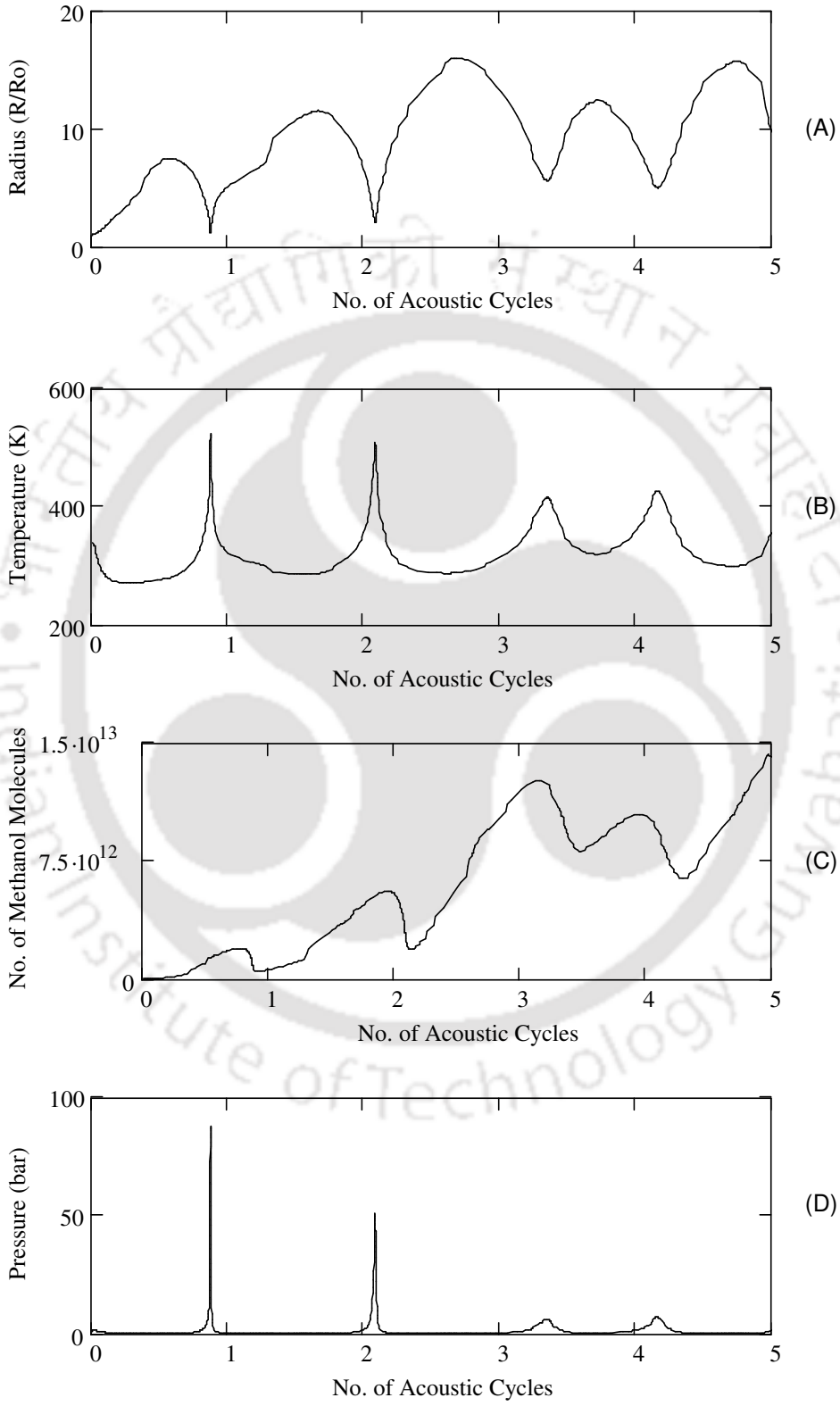

Figure 3.7

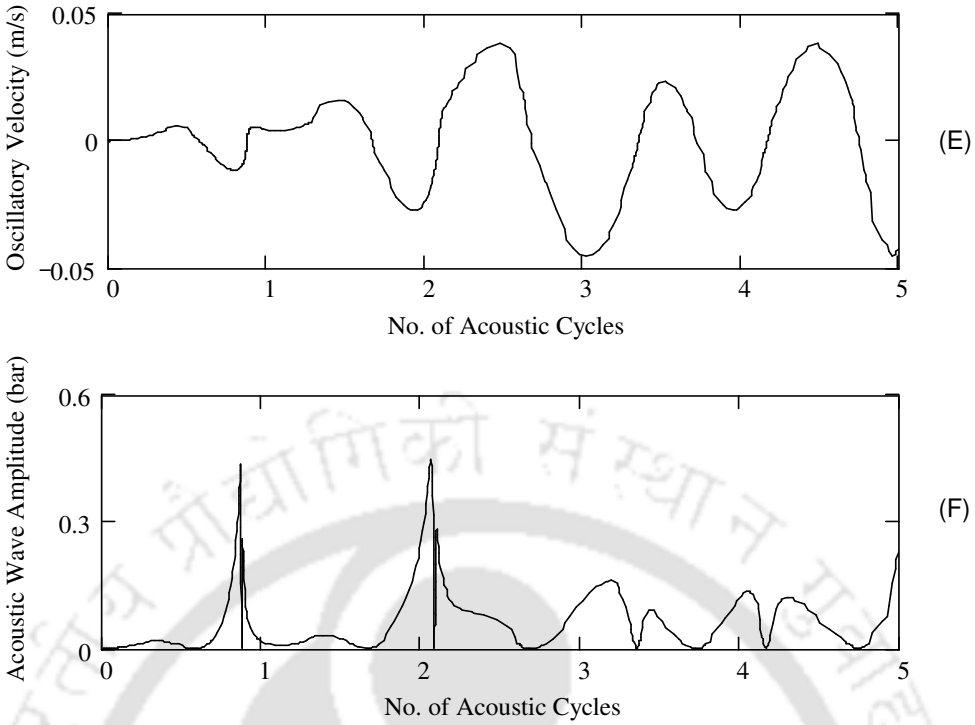

Figure 3.7 (*continued…*). Simulation results for radial motion of a 5 μm cavitation bubble (air) in methanol at 65°C. Time variation of (A) normalized bubble radius (R/R_o), (B) temperature in the bubble, (C) number of methanol molecules in the bubble, (D) pressure inside the bubble; (E) micro-convection (or oscillatory liquid velocity) generated by the cavitation bubble, (F) acoustic (or shock) waves emitted by the bubble.

Therefore, the cavitation bubbles are not capable of inducing any sonochemical effect. This result is in concurrence with our own previous papers [26, 32]. As far as sonophysical effect is concerned, an interesting trend with reaction temperature is observed. The amplitude of acoustic or shockwaves emitted by the bubbles decreases with increasing temperature (which essentially is a consequence of lesser compressions of bubble due to vapor cushioning). However, the magnitude of micro turbulence velocity increases with temperature, which could be attributed to greater expansion of bubbles as a consequence of larger solvent evaporation. However, comparing the magnitude of V_{turb} (~ 0.04 m/s) with the micro–streaming velocity (0.17 m/s) that the contribution of latter to convection is much higher.

Table 3.6: Summary of the simulation results

	Parameters for simulations		
	R_o = 5 µm T_o = 313 K	R_o = 5 µm T_o = 325.5 K	R_o = 5 µm T_o = 338 K
	Conditions at the first collapse of the bubble		
	T_{max} = 701.5 K P_{max} = 33.3 MPa V_{turb} = 0.01 m/s P_{AW} = 428 kPa	T_{max} = 598.5 K P_{max} = 36.3 MPa V_{turb} = 0.04 m/s P_{AW} = 138 kPa	T_{max} = 523.9 K P_{max} = 8.9 MPa V_{turb} = 0.0415 m/s P_{AW} = 44.7 kPa
	N_{N2} = 1.06 E+10 N_{O2} = 2.81 E+9 N_{ME} = 2.67 E+10	N_{N2} = 1.02 E+10 N_{O2} = 2.7 E+9 N_{ME} = 2.95 E+11	N_{N2} = 9.8 E+9 N_{O2} = 2.6 E+9 N_{ME} = 9.09 E+11
Species	**Equilibrium composition of different species in the bubble at transient collapse**		
H_2O	3.94E-01	2.36E-01	3.80E-01
CH_4	2.94E-01	7.00E-01	5.82E-01
N_2	1.96E-01	4.81E-02	1.24E-02
CO_2	1.04E-01	1.09E-02	2.35E-02
H_2	1.02E-02	4.34E-03	2.46E-03
NH_3	1.39E-03	9.67E-04	2.20E-04
CO	2.84E-04	6.83E-06	1.69E-06
C_2H_6	4.32E-05	7.33E-05	1.26E-05

Notations: The number format is as follows: 1.06 E+10 should be read as 1.06×10^{10} Various notations used are as follows: R_o – initial radius of the cavitation bubble; V_{turb} – average velocity of the micro–turbulence in the medium generated by ultrasound and cavitation in the medium (estimated at 1 mm distance from bubble center); P_{AW} – pressure amplitude of the acoustic wave generated by the cavitation bubble; T_{max} – temperature peak reached in the bubble at the time of first collapse; P_{max} – pressure peak reached in the bubble at the time of first collapse; N_{ME} – number of methanol molecules trapped in the bubble; N_{N2} – number of N_2 molecules in the bubble; N_{O2} – number of oxygen molecules in the bubble

3.7 Discussion and analysis

Concurrent analysis of simulations and experimental results helps us identify various facets of physical mechanism of the process. Sonication of reaction mixture induces intense micro-mixing in the medium that significantly boosts the conversion of triglycerides, as seen from comparison of the test and control experiments. Ultrasound induced micro-mixing is capable of producing finer emulsion than mechanical stirring (even at as high rpm as 600) that results in much faster kinetics and greater conversion (~ 90% conversion in 1 h in test experiments

as compared to ~56% conversion in 5 h in control experiments) at optimized conditions. The CaO catalyst being hydrophilic in nature preferably stays in the aqueous phase (or methanol). As explained in scheme 3.1 showing mechanism of the process, the methoxy ions are generated as a result of adsorption of methanol molecule on the catalyst surface.

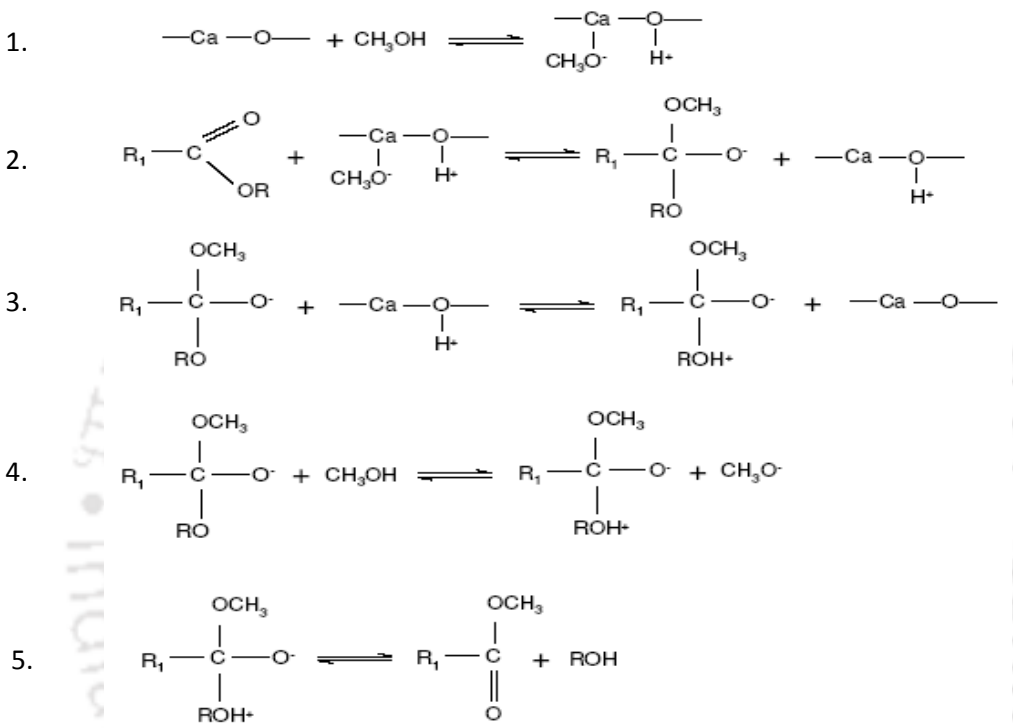

Scheme 3.1: Chemical mechanism of calcium oxide catalyzed trans-esterification for biodiesel synthesis.

These methoxy ions are then transferred to the organic phase at the interface between the two phases. As revealed in our previous paper [42], ultrasound can enhance the rate of adsorption and hence, the rate of CH_3O^- ions production. Convection generated by both ultrasound and cavitation helps dispersion of the aqueous and organic phases into each other, causing formation of emulsion that has high interfacial area. All three components of the convection (micro–streaming, micro–convection and acoustic shockwaves) contribute to emulsion

formation. Due to high viscosity of oil, the micro–streaming and micro–convection in methanol mostly contributes to the convection generated in the reaction system. As mentioned in previous section, the contribution of micro–streaming due to ultrasound to convection is much higher due to higher velocity. Moreover, the micro–streaming velocity is independent of temperature of the medium. Cavitation bubbles also contribute to convection through generation of acoustic waves that generate emulsion of the two phases. However, the magnitude of these waves reduces significantly at higher temperature. It could thus be expected that convection level in the medium should reduce with temperature. Conversely, that maximum yield is obtained at 62.5^{o}C (which is close to boiling point of methanol) indicates that role of cavitation bubble in process is rather negligible, and the system is dominated by intrinsic kinetics. This effect is clearly attributed to large activation energy of the reaction, which essentially is a manifestation of 3–phase heterogeneity of the reaction system, as stated earlier. The statistical design also predicts molar ratio for the highest FAME yield as 10:1, which is higher than that observed for homogeneous system (6:1) [22]. Again, this is a manifestation of the mass transfer limitation in the system. At low alcohol to oil molar ratio, the volume fraction of oil in the reaction mixture is high, due to which the convection intensity is low. This leads to non–uniform distribution of catalyst particles in the reaction mixture as well as lower interfacial area, and hence, lowers convection. Very high alcohol to oil molar ratios also results in lower interfacial area due to smaller volume of oil in reaction mixture, due to which interfacial area is smaller. The statistical model also predicts strong interaction between effects of all these process parameters on FAME yield. The parameters catalyst loading–molar ratio, and temperature–molar ratio are related through the variation in convection level in the medium that in turn are related to the cavitation bubble dynamics and ultrasound wave phenomena. The parameters catalyst loading & temperature are related through intrinsic kinetics of the process.

3.8 Conclusion

In this chapter, we have assessed mechanistic features of solid–based catalyzed soybean oil biodiesel synthesis, with approach of coupling experimental results based statistical design to simulation of ultrasound and cavitation bubble dynamics. One study has revealed several important physical features of this process which are significantly different from homogeneous catalyst process (both basic as well acidic). Due to 3–phase heterogeneity, the reaction system has strong mass transfer limitation. The reaction system is also found to be dominated by intrinsic kinetics due to large activation energy. Maximum yield is seen for the highest reaction temperature – close to boiling point of methanol. The effect of cavitation bubble on the system is found to be negligible and micro–streaming due to ultrasound provides the necessary convection. The most optimum contribution of parameters is found to be catalyst loading 6 wt%, temperature 62^{o}C, and molar ratio 10:1. The statistical analysis predicted that effect of all three parameters on the FAME yield was significant, and influence of all parameters was strongly interrelated. Catalyst composition is also an important factor. Our catalyst contained the inert carbonate phase, due to which the activity is expectedly reduced. Use of purer version of catalyst can yield even higher conversions. We believe that revelations of our study will be useful for further research in this area. Moreover, the methodology adopted in present work can also be extended to other transesterification system with different catalyst, alcohols and oils.

References

[1] X. Liu, X. Piao, Y. Wang, S. Zhu, Model study on transesterification of soybean oil to biodiesel with methanol using solid base catalyst, J. Phys. Chem. A 114 (2010) 3750–3755.

[2] M. L. Granados, D. M. Alonso, A. C. Alba–Rubio, R. Mariscal, M. Ojeda, P. Brettes, Transesterification of triglycerides by CaO: Increase of the reaction rate by biodiesel

addition, Energ. Fuel 23 (2009) 2259–2263.

[3] X. J. Liu, H.Y. He, Y. J. Wang, S. L. Zhu, X. L. Piao, Transesterification of soybean oil to biodiesel using CaO as a solid base catalyst, Fuel 87 (2008) 216–221.

[4] M. Zabeti, W. Daud, M. K. Aroua, Biodiesel production using alumina–supported calcium oxide: an optimization study, Fuel Proc. Technol. 91 (2010) 243–248.

[5] L. B. Wen, Y. Wang, D. L. Lu, S. Y. Hu, H.Y. Han, Preparation of KF/CaO nanocatalyst and its application in biodiesel production from Chinese tallow seed oil, Fuel 89 (2010) 2267–2271.

[6] D. M. Alonso, R. Mariscal, M. L. Granados, P. Maireles–Torres, Biodiesel preparation using Li/CaO catalysts: activation process and homogeneous contribution, Catal. Today 143 (2009) 167–171.

[7] H. Liu, L. Y. Su, Y. Shao, L. B. Zou, Biodiesel production catalyzed by cinder supported CaO/KF particle catalyst, Fuel 97 (2012) 651–657.

[8] Y. Tang, M. Meng, J. Zhang, Y. Lu, Efficient preparation of biodiesel from rapeseed oil over modified CaO, Appl. Energ. 88 (2011) 2735–2739.

[9] I. Lukic, J. Krstic, D. Jovanovic, D. Skala, Alumina/silica supported K_2CO_3 as a catalyst for biodiesel synthesis from sunflower oil, Bioresour. Technol. 100 (2009) 4690–4696.

[10] M. D. Machado, J. Perez–Pariente, E. Sastre, D. Cardoso, A.M. Guerenu, Selective synthesis of glycerol monolaurate with zeolitic molecular sieves, Appl. Catal. A 203 (2000) 321–328.

[11] S. Gryglewicz, Rapeseed oil methyl esters preparation using heterogeneous catalysts, Bioresour. Technol. 70 (1999) 249–253.

[12] H. Wu, J. Zhang, Q. Wei, J. Zheng, J. Zhang, Transesterification of soybean oil to biodiesel using zeolite supported CaO as strong base catalysts, Fuel Proc. Technol. 109(2013)

13–18.

[13] A. Zieba, A. Pacuła, A. Drelinkiewicz, Transesterification of triglycerides with methanol catalyzed by heterogeneous zinc hydroxy nitrate catalyst. Evaluation of variables affecting the activity and stability of catalyst, Energ. Fuels 24 (2010) 634–645.

[14] J. F. Puna, J. F. Gomes, M. Joana N. Correia, A. P. Soares Dias, J.C. Bordado, Advances on the development of novel heterogeneous catalysts for transesterification of triglycerides in biodiesel, Fuel 89 (2010) 3602–3606

[15] Y. Zu, G. Liu, Z. Wang, J. Shi, M. Zhang, W. Zhang, M. Jia, CaO supported on porous carbon as highly efficient heterogeneous catalysts for transesterification of triacetin with methanol, Energ. Fuels 24 (2010) 3810–3816.

[16] D. G. B. Boocock, S. K. Konar, V. Mao, H. Sidi, Fast one phase oil–rich process for the preparation of vegetable oil methyl esters, Biomass Bioenerg. 11 (1996) 43–50.

[17] H. Mootabadi, B. Salamatinia, S. Bhatia, A. Z. Abdullah, Ultrasonic–assisted biodiesel production process from palm oil using alkaline earth metal oxides as the heterogeneous catalysts, Fuel 89 (2010) 1818–25.

[18] B. Salamatinia, H. Mootabadi, S. Bhatia, A. Z. Abdullah, Optimization of ultrasonic–assisted heterogeneous biodiesel production from palm oil: a response surface methodology approach. Fuel Proc. Technol. 91 (2010) 441–448.

[19] V. S. Moholkar, S. P. Sable, A. B. Pandit, Mapping the cavitation intensity in an ultrasonic bath using the acoustic emission, AIChE J. 46 (2000) 684–694.

[20] T. Sivasankar, A.W. Paunikar, V. S. Moholkar, Mechanistic approach to enhancement of the yield of a sonochemical reaction. AIChE J. 53 (2007), 1132–1143

[21] G. Gelbard, O. Brès, R. M. Vargas, F. Vielfaure, U. F. Schuchardt, ^{1}H nuclear magnetic resonance determination of the yield of the transesesterification of rapeseed oil with methanol, J. Am. Oil Chem. Soc. 72 (1995) 1239–1241.

[22] G. Knothe, Analytical methods used in the production and fuel quality assessment of biodiesel, Trans. ASAE 44 (2001) 193–200.

[23] X. Liu, X. Piao, Y. Wang, S. Zhu, Calcium Ethoxide as a Solid Base Catalyst for the Transesterification of Soybean Oil to Biodiesel, Energ. Fuels 22 (2008) 1313–1317.

[24] R. Toegel, B. Gompf, R. Pecha, D. Lohse, Does water vapor prevent upscaling sonoluminescence? Phys. Rev. Lett. 85 (2000) 3165–3168.

[25] B. D. Storey, A. J. Szeri, Water vapor, sonoluminescence and sonochemistry. Proc. R. Soc. Lond. Ser. A 456 (2000) 1685–1709.

[26] A. Kalva, T. Sivasankar, V. S. Moholkar, Physical mechanism of ultrasound assisted synthesis of biodiesel, Ind. Eng. Chem. Res. 48 (2009) 534–544.

[27] S. J. Krishnan, P. Dwivedi, V. S. Moholkar, Numerical investigation into the chemistry induced by hydrodynamic cavitation. Ind. Eng. Chem. Res. 45 (2006) 1493–1504.

[28] J. B. Keller, M. J. Miksis, Bubble oscillations of large amplitude, J. Acoust. Soc. Am. 68 (1980) 628–633.

[29] J. O. Hirschfelder, C. F. Curtiss, R. B. Bird, Molecular Theory of Gases and Liquids, Wiley, New York, 1954.

[30] E. U. Condon, H. Odishaw, Handbook of physics. McGraw Hill, New York, 1958.

[31] W. H. Press, S. A. Teukolsky, B. P. Flannery, W. T. Vetterling, Numerical Recipes (2nd Ed.). Cambridge University Press, New York, 1992.

[32] P. A. Parkar, H. A. Choudhary, V. S. Moholkar, Mechanistic and kinetic investigations in ultrasound assisted acid catalyzed biodiesel synthesis. Chem. Eng. J. 187 (2012) 248– 260

[33] T. Sivasankar, V. S. Moholkar, Physical insights into the sonochemical degradation of recalcitrant organic pollutants with cavitation bubble dynamics, Ultrason. Sonochem. 16 (2009) 769–781.

[34] G. Eriksson, Thermodynamic studies of high temperature equilibria—XII: SOLGAMIX, a computer program for calculation of equilibrium composition in multiphase systems. Chem. Scr. 8 (1975) 100–103.

[35] Y. T. Shah, A. B. Pandit, V. S. Moholkar, Cavitation Reaction Engineering. Plenum Press, New York, 1999.

[36] S. Grossmann, S. Hilgenfeldt, M. Zomack, D. Lohse, Sound radiation of 3 MHz driven gas bubbles, J. Acoust. Soc. Am. 102 (1997) 1223–1227.

[37] V. S. Moholkar, M. M. C. G. Warmoeskerken, An integrated approach to optimization of an ultrasonic processor, AIChE J. 49 (2003) 2918–2932.

[38] R. C. Reid, J. M. Prausnitz, B. E. Poling, Properties of gases and liquids. McGraw Hill, New York, 1987.

[39] V. Brahmkhatri, A. Patel, 12–Tungstophosphoric acid anchored to SBA–15: An efficient, environmentally benign reusable catalysts for biodiesel production by esterification of free fatty acids, Appl. Catal. A 403 (2011) 161–172.

[40] D. C. Montgomery, Design and analysis of experiments (5th ed.). John Wiley & Sons (Asia) Pte. Ltd., Singapore, 2004.

[41] D. C. Montgomery, G. C. Runger, Applied statistics and probability for engineers (4th ed.). John Wiley & Sons, Inc., U.K., 2007.

[42] V. R. Midathana, V. S. Moholkar, Mechanistic studies in ultrasound–assisted adsorption for removal of aromatic pollutants, Ind. Eng. Chem. Res. 48 (2009) 7368–7377.

[43] S. L. Davis, Vibrational Modes of Methanol. (http://classweb.gmu.edu/sdavis/research/ modes.htm).

CHAPTER 4

Ultrasonic Synthesis of Biodiesel from Jatropha Oil with Basic Heterogeneous (CaO) Catalyst

4.1 Introduction

In the preceding chapter, we have presented optimization of biodiesel synthesis process form soybean oil. In this chapter, we extend the theme to the non–edible feedstock of *Jatropha Curcas* oil. Among the non–edible oil sources, *Jatropha Curcas* has been identified as one of the most prominent plant that can be potential feedstock for biodiesel production. The main merits of *Jatropha* plant are in terms of faster growth, higher fruit yield and lesser water requirement [1]. Despite these distinct merits, the major shortcoming of Jatropha oil is its high free fatty acid (FFA) content. Typically, the FFA content of Jatropha ranges from 10–20 wt% depending on source and species, and this is far higher than 1% limit for the transesterification reaction with conventional alkali catalyst. Reaction of FFA with alkali renders formation of soap that reduces biodiesel yield as well as creates problem of separation and purification [2–4]. Therefore, conventional transesterification process with alkali catalyst cannot be employed for Jatropha oil. To alleviate this problem, a two–step

approach for biodiesel synthesis has been reported by several researchers, in which the first step is esterification by sulfuric acid, and second step is transesterification by homogeneous alkali catalyst, viz. NaOH or KOH. However, use of NaOH or KOH has adverse effect on economy of biodiesel production. The alkali catalyst ends up in the glycerol side product of transesterification and contaminates it [5]. A solution to this problem is use of heterogeneous alkali catalyst like CaO, which can be easily separated from reaction mixture by filtration [6–13]. Solid CaO is well known for its high activity, high alkalinity and poor solubility in methanol among other heterogeneous alkali catalysts, which makes it an ideal solid base catalyst for biodiesel production. However, addition of the solid catalyst into oil–methanol transesterification reaction mixture renders it a 3–phase system, in which mass transfer limitations come into picture. The advantages of the solid CaO catalyst are outweighed by slower reaction kinetics as compared to homogeneous catalysts [14–19]. Intense agitation, application of high pressure and temperature, use of a co–solvent or phase transfer catalysts are possible solutions for enhancement of mass transfer and reaction kinetics [20]. In this thesis work, we have adopted sonication or ultrasound irradiation of the reaction mixture as a means of enhancement of mass transfer.

The study presented in this Chapter attempts to provide physical insight into the heterogeneous base catalyzed biodiesel synthesis employing CaO as solid catalyst for Jatropha oil. The process is in two steps: (1) esterification with sulfuric acid using conventional stirring method, and (2) transesterification with CaO using statistical experimental design (Box–Behnken method). The analysis has been done using Response Surface Methodology (RSM). In addition, we have done simulations of cavitation bubble dynamics in the reaction mixture. These simulations give quantitative estimate of the physical and chemical effects induced by ultrasound and cavitation under different experimental conditions used in statistical design. Concurrent analysis and correlation between the

statistical experimental design and bubble dynamics simulations has shed light on many physical aspects of the Jatropha oil based biodiesel synthesis.

4.2 Approach, Materials, Methods and Analysis

***Materials*:** Virgin *Jatropha curcas* oil was purchased from local farmers. This oil was in crude form and was used as received without any further purification or refining. The acid value (AV) and saponification value (SV) of the oil was determined as 21.57 mg KOH/g and 201.2 mg KOH/g using standard methods described in literature [21]. The average molecular weight of oil was determined as 932 g/mol using the equation 4.1 [22]:

$$M = (56.1 \times 3 \times 1000) / (SV - AV) \qquad (4.1)$$

where, 56.1 g/mol is the molecular weight of KOH, while number 3 denotes the number of fatty acids per triglyceride. Other chemicals used in the experiments are: analytical reagent (AR) grade methanol (purity 99%, Merck, India), sulfuric acid (98%, Merck, India), CaO (AR grade 92%, Merck India), Na_2CO_3 (AR grade 99%, Merck India). Anhydrous methanol was prepared by distillation.

Catalyst preparation and characterization: The fine powder of CaO catalyst, as received from supplier, was calcined in a programmed muffle furnace (Labtech, Korea) at 900^{o}C for 3 h with an increasing temperature rate of 10^{o}C/min. The calcination catalyst was cooled to ambient temperature in a vacuum desiccator. Characterization of the calcined catalyst was done using X–ray diffractometer (Bruker, Model: D8 Advance, Cu–K_α, λ = 1.5406 Å, Range: 7–75^{o}, 40 kV 40 mA), Delsa^{TM} Nano C particle size analyzer (Beckman Coulter, Model: A53878) and BET surface area analyzer (Beckman Coulter, Model No. SA 3100). Freshly calcined catalyst was used in each experiment so as to evade carbonate and hydroxide formation due to reaction of CaO with CO_2 and moisture present in ambient air.

4.3 Experimental Setup

Magnetic stirrer with hot plate (Tarson–spinot digital model MC–02) was used for esterification step. An oil bath (silicone oil) was used to maintain desired temperature. A 50 ml two neck round bottom flask was immersed in the oil bath, and reaction mixture was refluxed with a double walled condenser. For transesterification step, an ultrasound bath (Elma Transsonic T–460 type, Germany, capacity: 2 L, frequency: 35 kHz, power: 35 W) was used for sonication of the transesterification reaction mixture. 2/3rd of bath volume was filled with water, which acted as medium for transmission of ultrasound. A schematic of the experimental setup for trans–esterification reaction is given in Fig. 4.1. All experiments were carried out in a 50 mL two–neck round bottom flask made of borosilicate glass. A reflux condenser was employed so as to condense the methanol vapors and return them to reaction mixture. Reaction mixture was stirred continuously (100 rpm) with the help of a digitally controlled motor to prevent the settling of catalyst particles. A variable energy input heating element was used to raise the temperature of water in the bath at a desired levels. The bath was sealed at the top to minimize heat loss due to convection. Position of the reaction flask was kept same carefully in all experiments, since the intensity (or pressure amplitude) of the ultrasound wave field shows significant spatial variation [22]. The actual energy dissipation and pressure amplitude of the ultrasound wave in the bath was characterized using calorimetry [23].

4.4 Experimental Protocol

Preliminary assessments: Protocol of esterification was designed on the basis of results published by Deng et al. [24]. To estimate the efficacy of sonication in esterification of FFA, we attempted to perform esterification using both sonication and mechanical stirring in our

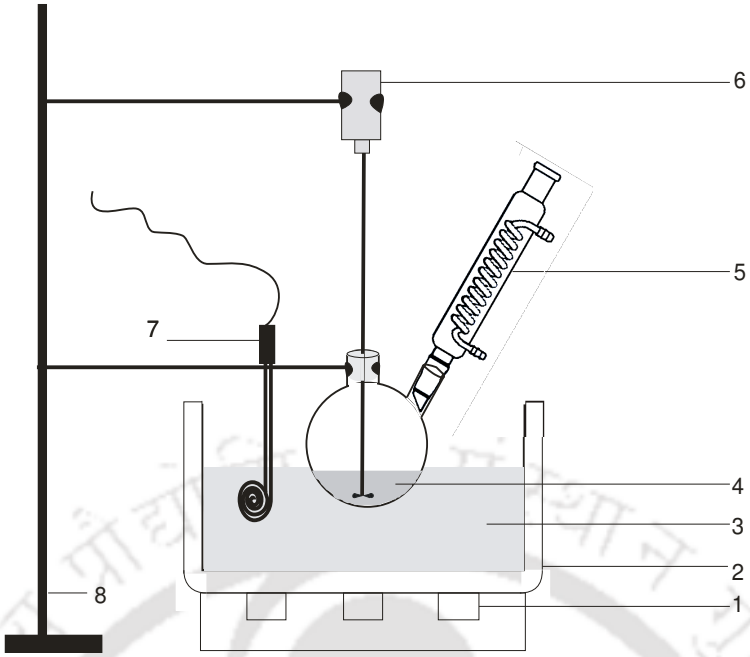

Figure 4.1: Schematic of experimental setup: (1) Transducers, (2) Sonication bath, (3) Sonication medium (water), (4) Reaction mixture, (5) Reflux condenser, (6) Electrical motor, (7) Electrical immersion heater, (8) Stand holder

preliminary experiments. However, we found that almost same time was required for complete esterification (> 90%, as observed from the reduction in acid value of oil) in both mechanical stirring and sonication. A complete reduction of acid value was obtained within 1 h with FAME yield in the range of 17–20% for both cases. These results are analogous to the result reported by Deng et al. [24], which essentially means that the rate of the esterification reaction may not be enhanced by sonication. Based on this initial study, we decided to carry out esterification step by conventional stirring instead of sonication.

Esterification: *Jatropha curcas* oil has high acid value of 21.57 mg KOH/g (indicating high free fatty acid content), and therefore, in the first step sulfuric acid catalyzed esterification reaction was carried out in two–neck round bottom flask fitted with a reflux condenser.

Table 4.1: Composition of reaction mixture for esterification reaction

Sl No.	Temperature (^{o}C)	Molar ratio	Catalyst (wt% oil)	Oil Volume (ml)	Methanol Volume (ml)	Methanol / Oil volume ratio	Catalyst added (ml)	Acid value mg KOH/g	% reduction in acid value*
1.	65	10	1	10.78	4.22	0.39	0.05	15.58	27.8
2.	65	10	3	10.78	4.22	0.39	0.16	7.22	66.5
3.	65	10	5	10.78	4.22	0.39	0.28	6.46	70.1
4.	65	15	1	9.44	5.56	0.59	0.05	9.12	57.7
5.	**65**	**15**	**3**	**9.44**	**5.56**	**0.59**	**0.14**	**2.85**	**86.8**
6.	**65**	**15**	**5**	**9.44**	**5.56**	**0.59**	**0.24**	**2.66**	**87.7**
7.	65	20	1	8.41	6.59	0.78	0.04	16.72	22.5
8.	65	20	3	8.41	6.59	0.78	0.13	14.25	33.9
9.	65	20	5	8.41	6.59	0.78	0.22	11.97	44.5

- *In comparison with the initial acid value of 21.57 mg/g

The important parameters for esterification reaction were alcohol to oil molar ratio and catalyst concentration at a fixed temperature of 65 ± 2°C with a reaction time of 1 h. Experiments were performed in nine sets, with duplicate runs in each set in order to assess the reproducibility of the results. The values of experimental parameters were decided from the previously published literature [24]. The exact composition of the reaction mixture in each set is given in Table 4.1. The total reaction volume was 15 mL. After the reaction, the reaction mixture was allowed to stand in a separating funnel to split the organic and aqueous phases. The organic layer was separated and washed with hot water to remove traces of acid and alcohol. The acid value (AV) of the organic layer (which essentially is the final esterification product) was again determined by titration method. The experimental set in which the acid value of the product was the lowest was selected for next set of experiments. The same experimental set was then conducted at increased reaction volume of 200 mL, and the results were found consistent which essentially means that the reaction characteristics did not change with scale of the reaction. The product of this large–scale reaction was preserved for further transesterification reaction.

***Transesterification*:** Experiments were conducted in two categories, viz. control and test. In control experiments, the reaction mixture was mechanically stirred in 50 mL two–neck round bottom flask. A magnetic stirrer was employed to blend the reaction mixture (total volume 15 mL) at 600 rpm for 6 h. The catalyst concentration was 4% w/v oil (0.38 g), with alcohol to oil molar ratio of 12:1 and temperature of the reaction being ~ 65°C. Samples of the reaction mixture (500 µL aliquots) were withdrawn at 1 h interval to assess the conversion of the triglycerides (analysis procedure is described subsequently). The time data of conversion is depicted in Fig.4.2.

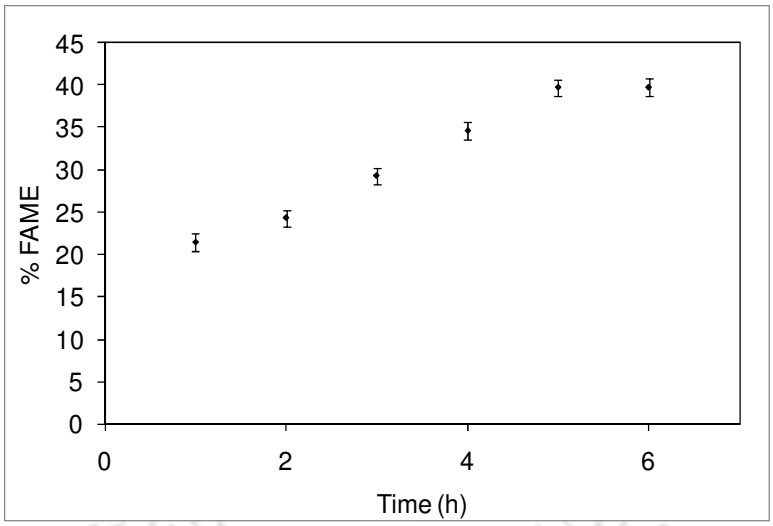

Figure 4.2: Time history of conversion of triglycerides with mechanical agitation for methanol to oil molar ratio of 12:1 and catalyst concentration 4 wt% at 65^{o} C.

The total conversion obtained in the control experiment (at the end of 6 h) was approx. 40%. This value is significantly lesser than the conversion reported by Taufiq–Yap et al. [25], in which nano–sized CaO (40 nm) catalyst has been used. We conjecture that this is an effect of presence of inert carbonate phase in the catalyst. To confirm this, we have carried out XRD analysis of the calcined calcium oxide and described the results subsequently. Another probable reason behind this effect could be improper mixing due to bigger particle size of the catalyst used in this study and inhomogeneous distribution of the catalyst particles in the reaction mixture. After completion of the transesterification reaction, the catalyst was separated by centrifugation at about 6000 rpm. The catalyst was then washed with hexane three times to remove the *Jatropha Curcas* oil. Further catalyst was dried in hot air oven for overnight for 12 h and then calcined at 900^{o}C for 3 h for reuse.

Box–Behnken statistical design has been used to devise the transesterification experiments. The FFA reduced Jatropha oil (as obtained from esterification) has been used as reactant in all the transesterification experiments. The following experimental parameters (or independent variables) have been chosen for optimization: catalyst loading (*C*), temperature

(*T*), and alcohol to oil molar ratio (*R*). The experiments were conducted in ultrasound bath for a fixed sonication time of 2 h, based on our initial experiments. The exact experimental design, formulated using Minitab 15 trial version software, indicating range and levels of the independent variables is shown in Table 4.2A. The response variable, i.e. % FAME yield, was fitted with a full quadratic model (given in equation 4.2) in order to correlate it to the experimental parameters or independent variables.

$$Y = \beta_0 + \sum_{i=1}^{3} \beta_i x_i + \sum_{i=1}^{3} \beta_{ii} x_i^2 + \sum_{i=1}^{2} \sum_{j=i+1}^{3} \beta_{ij} x_i x_j \qquad (4.2)$$

Various notations in above equation are as follows: Y = response variable (i.e. %FAME yield); β_0 = constant; β_i, β_{ij} and β_{ij} = regression coefficients; x_i and x_j = coded independent variables. The Box–Behnken statistical design of experiments comprises of 15 sets with (3 factors and 3 levels) with different combinations of the parameters. The experimental conditions in these sets are given in Table 4.2B, while the exact composition of reaction mixture in each set is given in Table 4.2C. The progress of the transesterification reaction was monitored by withdrawing 500 µL aliquots of the reaction mixtures after every 20 min. These aliquots were immediately mixed with hot aqueous suspension of 5% Na_2CO_3 and centrifuged at 6000 rpm for 10 min to separate the solid catalyst as well as the aqueous (or glycerol and alcohol) phase. The organic layer was then analyzed by ^{1}H NMR to determine the yield of FAME.

Table 4.2

(A) Experimental range and levels of independent variables

Independent Variables (or Factors)	Symbol coded	Levels of Factors Coded Value (Actual value)		
Catalyst concentration (wt%)	C	–1 (3)	0 (5)	1 (7)
Temperature (^{o}C)	T	–1 (45)	0 (60)	1 (75)
Alcohol to oil molar ratio (R)	M	–1 (6:1)	0 (12:1)	1 (18:1)

Table 4.2 (*Cont...*)

(B) Box–Behnken experimental design matrix*

Sl. No.	Temperature (°C)	Molar ratio	Catalyst (wt% oil)	% FAME yield	Fitted % FAME yield
1.	45 (–1)	6 (–1)	5 (0)	34.83 ± 0.44	34.84
2.	45 (–1)	18 (1)	5 (0)	21.77 ± 0.63	21.96
3.	75 (1)	6 (–1)	5 (0)	58.28 ± 0.55	58.09
4.	75 (1)	18 (1)	5 (0)	41.73 ± 0.56	41.72
5.	60 (0)	6 (–1)	3 (–1)	25.82 ± 0.28	25.98
6.	60 (0)	18 (1)	3 (–1)	24.26 ± 0.55	24.25
7.	60 (0)	6 (–1)	7 (1)	55.87 ± 0.58	55.88
8.	60 (0)	18 (1)	7 (1)	28.53 ± 0.65	28.36
9.	45 (–1)	12 (0)	3 (–1)	28.03 ± 0.27	27.85
10.	75 (1)	12 (0)	3 (–1)	49.57 ± 0.66	49.59
11.	45 (–1)	12 (0)	7 (1)	45.11 ± 0.70	45.09
12.	75 (1)	12 (0)	7 (1)	66.19 ± 0.53	66.36
13.	**60 (0)**	**12 (0)**	**5 (0)**	**93.90 ± 0.17**	**93.39**
14.	**60 (0)**	**12 (0)**	**5 (0)**	**93.04 ± 0.71**	**93.39**
15.	**60 (0)**	**12 (0)**	**5 (0)**	**93.22 ± 0.63**	**93.39**

* Coded variables are given in bracket. The bold rows identify maximum yields.

(C): Composition of reaction mixture in Box–Behnken experimental design matrix

Sl No.	Temperature (°C)	Molar ratio	Catalyst (wt% oil)	Oil Volume (ml)	Methanol Volume (ml)	Methanol / Oil volume ratio	Catalyst added (g)*
1	45	6	5	12.15	2.86	0.24	0.58
2	45	18	5	8.80	6.20	0.71	0.42
3	75	6	5	12.15	2.86	0.24	0.58
4	75	18	5	8.79	6.20	0.71	0.42
5	60	6	3	12.15	2.86	0.24	0.34
5	60	18	3	8.79	6.20	0.71	0.25
7	60	6	7	12.15	2.86	0.24	0.83
8	60	18	7	8.79	6.20	0.71	0.60
9	45	12	3	10.2	4.8	0.47	0.28
10	75	12	3	10.2	4.8	0.47	0.28
11	45	12	7	10.2	4.8	0.47	0.69
12	75	12	7	10.2	4.8	0.47	0.69
13	60	12	5	10.2	4.8	0.47	0.48
14	60	12	5	10.2	4.8	0.47	0.48
15	60	12	5	10.2	4.8	0.47	0.48

* Calcined CaO

***Determination of reaction kinetics and %FAME yield*:** ^{1}H NMR (Varian 400 MHz FT–NMR) spectroscopic analysis have been carried out to determine the gross conversion of triglycerides using $CDCl_3$ as solvent and TMS (tetramethyl silane) as internal standard [26, 27]. The following equation was used to determine the conversion (X) of triglycerides in Jatropha oil to fatty acid methyl esters:

$$X = \left(2 \times A_{ME}\right) \times 100 \Big/ \left(3 \times A_{\alpha - CH_2}\right) \tag{4.3}$$

where, A_{ME} = integration value of the protons of the methyl esters (the strong singlet peak at 3.6 ppm), $A_{\alpha-CH2}$ = integration value of the methylene protons at 2.3 ppm.

***Determination of transesterification kinetics*:** The time history of conversion of triglycerides obtained with help of ^{1}H NMR spectroscopy was analyzed using integral approach to determine the kinetic parameters of the process. Progress of any transesterification reaction occurs in three consecutive and reversible reactions steps, in which the triglyceride (TG) molecule is successively converted into di– and mono–glyceride molecule yielding one mole of ester in each conversion. In the third and final step, reaction of mono–glyceride with methanol yields one mole of methyl ester and one mole of glycerol. Thus, the net product of transesterification reaction is three molecules of methyl ester and one molecule of glycerol. In our analysis, we have determined the kinetic constant of the overall reaction, without accounting for the intermediate steps. The time history of reaction conversion has been analyzed using integral approach to determine the order of reaction with respect to triglyceride and the kinetic constant. The basic kinetic equation assumed is as follows where the subscript A denotes triglyceride:

$$\frac{dC_A}{dt} = -kC_A^n \tag{4.4}$$

As per differential analysis, the above equation can be converted in following form:

$$\ln\left(-\frac{dC_A}{dt}\right) = \ln k + n \ln C_A \qquad (4.5)$$

Plot of $\ln(-dC_A/dt)$ vs. $\ln C_A$ gives the order of reaction as slope and kinetic constant as y–intercept. However, we have monitored the reaction on the basis of conversion of triglyceride. In order to help fit the experimental to the model, we convert the equations 4.4 and 4.5 in terms of conversion (X) as follows:

$$C_A = C_{Ao}(1-X) \qquad (4.6)$$

$$-C_{Ao}\left(\frac{dX}{dt}\right) = -k\left[C_{Ao}(1-X)\right]^n \qquad (4.7)$$

Integration between limits ($t = 0$, $x = 0$) and ($t = t$, $x = X$), after separation of variables gives:

$$\ln(1-X) = \left\{\frac{\ln(n-1) + \ln k + (n-1)\ln C_{A_0}}{1-n}\right\} + \frac{1}{(1-n)}\ln t \qquad (4.8)$$

Plot of ln (1–X) vs ln t has slope of 1/(1–n) from which the order of reaction can be determined. The y–intercept gives the kinetic constant (for condition that $n > 1$). The initial concentration of triglyceride was determined as follows: the organic layer obtained after esterification step has density of 0.87 g/mL. As per the NMR analysis, it contains about 20 wt% ester. Therefore, the net quantity of triglyceride per mL of organic layer is 0.87 × 0.8 = 0.696 g/mL. The molecular weight of triglyceride (assuming that triglyceride molecule is mainly made up of oleic acid groups) is determined as 885 g/mol. Taking a ratio of weight of triglyceride per liter of organic layer, and the molecular weight of triglyceride yields the initial concentration of triglyceride (denoted as C_{Ao}) as 0.786 g/L.

***Determination of activation energy* (*Arrhenius plot*):** The Arrhenius equation gives a relationship between the specific reaction rate constant (k), absolute temperature (T) and the energy of activation (E_a) as: $k = A\exp\left(-E_a/RT\right)$ where A is the frequency factor and R is

universal gas constant (J mol^{-1} K^{-1}). This equation is rewritten as:

$$\ln(k) = \frac{-E_a}{RT} + \ln(A) \qquad (4.9)$$

It should be noted that Arrhenius analysis assumes that kinetic constant is a sole function of temperature only, and does not depend on the concentration of reactants or the reaction order. As will be revealed in the subsequent sections, the order of the transesterification reaction (with respect to triglyceride) changes with temperature. However, for calculation of activation energy we have assumed an average order of reaction with respect to triglyceride. Plot of ln (k) vs 1/T gives slope as ($-E_a/R$), from which activation energy can be determined. Experiments have been conducted using optimum values of catalyst loading and alcohol to oil molar ratio (as determined from the statistical experimental design) at three temperatures, viz. 45°, 55° and 65°C.

4.5 Mathematical Modelling of Cavitation Bubble Dynamics

The results of our previous papers have shown that transesterification reaction system is mainly influenced by the physical effects of ultrasound and cavitation, and the beneficial effect is in terms of intense micro–convection generated in the medium that enhances the emulsification of the oil and methanol phases. As a result, the interfacial area between the phases increases markedly, leading to better and faster transfer of the methoxy (CH_3O^-) ions from aqueous to organic phase. There is no sonochemical effect involved in the enhancement effect of ultrasound and cavitation, which engages formation of radical species. In view of this, we have used a different bubble dynamics model in this paper than our earlier papers [28–30]. This model is a modified form of classical Rayleigh–Plesset equation with inclusion of the compressibility effects (for greater details we refer the reader to these papers [31–33]). We have chosen the following bubble dynamics equation [34–36], which is essentially a modified form of the original Rayleigh–Plesset equation [37] with inclusion of the

compressibility effect [38–39]:

$$R\frac{d^2R}{dt^2}+\frac{3}{2}\left(\frac{dR}{dt}\right)^2=\frac{1}{\rho}\left(p(R,t)-P_o-P(t)\right)+\frac{R}{\rho c}\frac{d}{dt}\left[p(R,t)-P(t)\right]-\frac{4\mu}{\rho R}\frac{dR}{dt}-\frac{2\sigma}{\rho R} \quad (4.10)$$

Various notations are as follows: R = radius of the bubble at any time; dR/dt = velocity of bubble wall; P_o = ambient or static pressure in bulk liquid; ρ = density of bulk liquid; c = sonic speed in bulk liquid; μ = viscosity of the bulk liquid; σ = surface tension of bulk liquid. $p(R,t)$ and $P(t)$ are the pressures inside the cavitation bubble and the time variant pressure of the acoustic wave, respectively; and are written as:

$$p(R,t)=\left(P_o+\frac{2\sigma}{R_o}-P_v\right)\left(\frac{R_o^3-h^3}{R^3-h^3}\right)^v+P_v \quad (4.11)$$

$$P(t)=P_A\cos(2\pi ft)=P_A\cos(\omega t) \quad (4.12)$$

Various notations are as follows: R_o = initial or equilibrium radius of the bubble; P_o = vapor pressure of bulk liquid; h = van der Waal's hard core radius; r = polytropic constant of bubble content; P_A = pressure amplitude of ultrasound wave; f = frequency of ultrasound wave; ω = angular frequency of ultrasound waves. The numerical solution of the equations 4.10–4.12 using Runge–Kutta adaptive step size method [40], yields time series of R and dR/dt, using which the magnitude of the convective effects of cavitation bubble are calculated as follows:

Physical effect of cavitation bubbles: Radial motion of cavitation bubbles generates intense convection in the medium through two phenomena, viz. micro–convection, shock or acoustic waves. Magnitudes of these entities can be determined using numerical result of bubble dynamics model as:

Micro–convection [41]*:* $$V_{turb}(r,t)=\frac{R^2}{r^2}\left(\frac{dR}{dt}\right) \quad (4.13)$$

Shock waves (*or Acoustic waves*) [42, 43]:

$$P_{AW}(r,t) = \frac{\rho}{4\pi r}\frac{d^2V_b}{dt^2} = \rho\frac{R}{r}\left[2\left(\frac{dR}{dt}\right)^2 + R\frac{d^2R}{dt^2}\right] \tag{4.14}$$

where V_b is the volume of the bubble. A representative value of r is taken as 1 mm.

Table 4.3 Simulations of Cavitation Bubble Dynamics

(A) Parameters of simulations [27]

Sr. No.	Physical / Process Parameter	Value
1.	Ultrasound frequency (f)	35 kHz
2.	Ultrasound pressure amplitude (P_A)	1.5 bar
3.	Equilibrium bubble radius (R_o)	5 μm
4.	Vapor pressure (in bar) of methanol [50]	$\log_{10} P = 5.15853 - \frac{1569.613}{T - 34.846}$
	Physical properties of methanol:	
5.	Density	790 kg/m^3
6.	Kinematic viscosity	6.829×10^{-7} Pa–s
7.	Surface tension	0.02355 N/m
8.	Velocity of sound	1103 m/s

(B) Results of simulations

Sr. No.	Reaction Temperature (^{o}C)	Pressure amplitude of acoustic waves (bar)	Velocity of micro–convection (mm/s)
1.	45	49.3	2.55
2.	55	28.4	1.74
3.	65	64.9	1.51

Physical effect of ultrasound [44]**:** Ultrasound propagates through the medium in the form of longitudinal wave with series of compression and rarefaction, and causes rapid oscillatory motion of fluid elements called microstreaming. This motion gives rise to intense micro–mixing in the medium. The magnitude of the microstreaming velocity is given as: $u = P_A/\rho c$. Substituting values of P_A as 1.5×10^5 Pa, ρ = 790 kg/m^3, and c = 1103 m/s, gives u = 0.17 m/s. In addition to the micro–streaming due to ultrasound, some additional micro–streaming is also created by circulatory currents generated near the phase boundaries like surface of solid catalyst or the bubble wall (or gas liquid interface). This micro–streaming is analyzed

by Nyborg [45]. Although the magnitude of this micro–streaming is similar to that due to the ultrasound, this phenomena is highly localized and decreases extremely rapidly away from the phase boundary (with proportion of r^{-5}). This may also contribute to some extent to the local convection present in the reaction system.

Cavitation bubble dynamics in methanol versus in oil: The transesterification reaction system is of liquid–liquid heterogeneous type, viz. methanol and oil. The catalyst is in solid phase. Thus, the overall system is a triphasic system. The catalyst being hydrophilic is mostly suspended in the methanol phase, although some fraction may also be present in oil phase. Thus, the motion of cavitation bubbles in both oil and methanol are likely to influence the mass transfer characteristics of the system. However, our earlier studies [28–29] have shown that the energetics of the dynamics of cavitation bubbles in the oil phase is too weak to produce any significant physical or chemical effect. This is mainly attributed to high viscosity of the oil. For the same reasons, the micro turbulence velocity in the oil phase is also relatively much smaller than that in methanol. Thus, the physical effects of cavitation and ultrasound rendered in methanol phase are responsible for the enhancement effect. We have therefore considered and simulated only the bubble dynamics in methanol. Various parameters used in the simulation of bubble dynamics equation (for an air bubble) and their numerical values are listed in Table 4.3A.

4.6 Results and Discussion

4.6.1 Characterization of CaO catalyst

The phase purity of the catalyst before the transesterification reaction was examined by powder X–ray diffraction (XRD). The comparison of XRD spectrum is shown in Fig. 4.3.

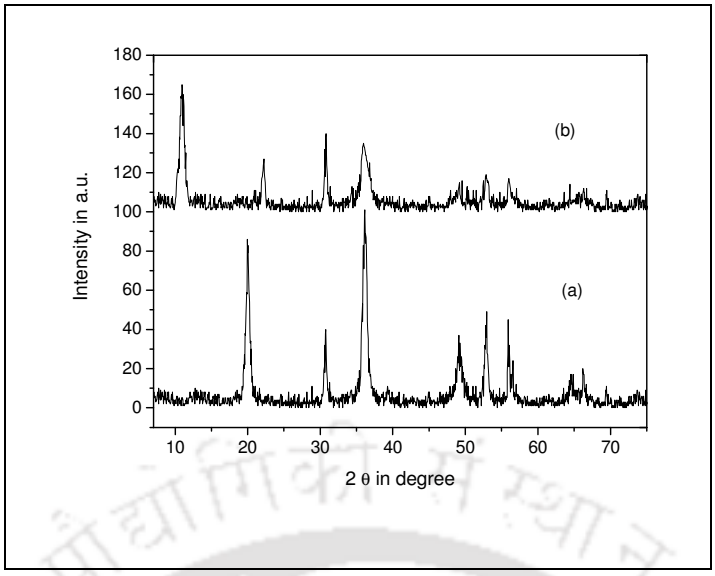

Figure 4.3: XRD spectrum of (a) CaO and (b) $Ca(OMe)_2$

Fig. 4.3a is the XRD spectra of freshly calcined CaO catalyst that matches well with the standard patterns of calcium oxide and calcium carbonate (JCPDS file No. 04–0777 and 75–2230). The catalyst contains both CaO and $CaCO_3$ phases in the solid catalyst sample. Fig. 4.3b is the XRD spectrum of freshly calcined CaO catalyst after the reaction with MeOH at 65°C for 1 h under sonication. This spectrum clearly shows growth of two new peaks at 10°, 21° angle along with the diminishing peak of CaO. The pattern of the Fig.4.3b closely resembles with JCPDS file No. 20–1565 which is the phase of the $Ca(OMe)_2$. In addition to this, we have also performed the particle size analysis and BET surface area of the catalyst. For brevity, we give herewith the final results of this analysis. The average particle size of CaO catalyst was determined as 1.176 microns. The BET surface area and total pore volume of the catalyst was 7.114 m^2/g and 0.0607 cm^3/g, respectively. BJH pore radius obtained from the adsorption isotherm is about 20 nm for the CaO catalyst, which is in the mesoporous range.

4.6.2 NMR analysis

Figs. 4.4A, B and C show ^1H NMR spectra of virgin *Jatropha Curcas* oil, product of

esterification reaction and the final reaction mixture after transesterification, respectively. The peak at 3.6 ppm in ^{1}H NMR spectra corresponds to the characteristic peak of FAME. This peak corresponds to methyl ester protons of biodiesel. It is absent in Fig. 4.4A. It is visible in Fig. 4.4B only to a small extent, while Fig. 4.4C shows a prominent peak. .This is essentially a confirmation of the progress of transesterification with formation of larger quantities of FAME. Various other peaks in the ^{1}H NMR spectrum have been identified as follows: the triplet at 2.3 ppm corresponds to α–carbonyl methylene, while peaks related to unsaturation in *Jatropha Curcas* oil are at 2.0, 2.8 and 5.3 ppm, typically assigned to allylic, bis–allylic and olefinic hydrogen, respectively. A strong singlet signal at 1.2 ppm represents methylene groups of the carbon chain. The terminal methyl protons are associated with the triplet arising at 0.8 ppm. Multiplet at 1.6 ppm is assigned to α–carbonyl methylenes. Polyunsaturated fatty acids are identified by peak at 2.72 ppm. This peak arises from methylene group between two double bonds of a higher polyunsaturated fatty acid chain.

4.6.3 Experimental results and statistical analysis

The results of esterification reactions indicated in Table 4.1 show an interesting facet that for molar ratio of 15:1 and temperature of 65^{o}C, the maximum esterification occurs with the highest reduction in acid value. However, the reduction in acid value does not reveal any significant effect of acid concentration. For doubling of acid concentration from 3 wt% to 5 wt%, the reduction in acid value remains practically unaltered. Higher acid concentration, on the other hand, can lead to formation of sulfones that could poison the catalyst. Moreover, higher acid concentration in the reaction mixture makes it more corrosive.

Results of Box–Behnken transesterification experimental design are given Table 4.2B. The statistical analysis of the experimental results is given in Table 4.4A using Minitab 15 software (trial version).

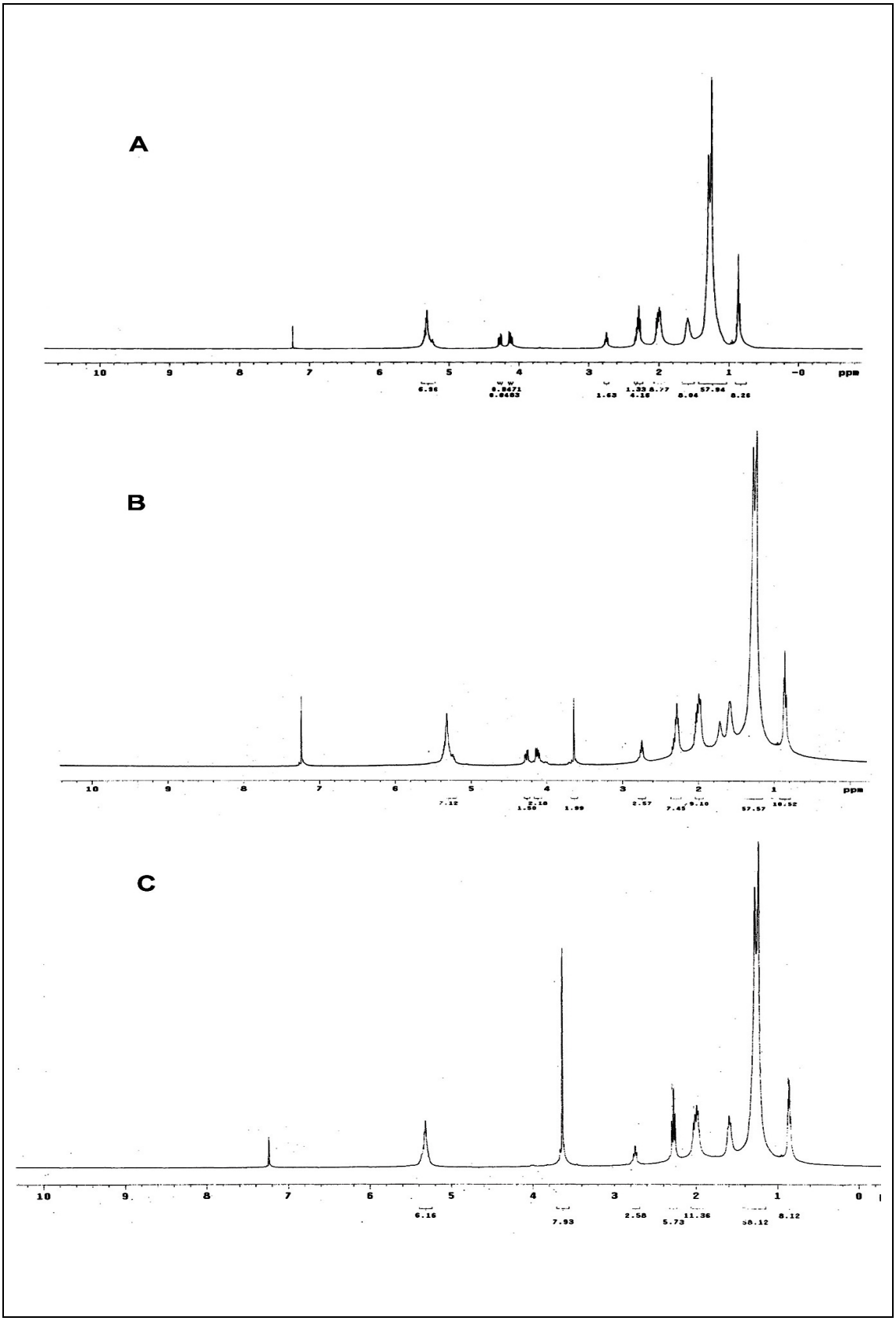

Figure 4.4: ^{1}H NMR spectrum of (A) pure *Jatropha Curcas* oil, (B) esterification product with 18% FAME and (C) fatty acid methyl ester (FAME) of *Jatropha Curcas* oil after trans–esterification

A quadratic regression model (given in equation 4.2) was fitted to the results using coded values for the experimental parameters. The model is fitted as follows:

$$Y = 93.387 + 10.753\ T - 7.314\ M + 8.501\ C - 20.315\ T^2 - 33.92\ M^2 - 25.847\ C^2 - 0.874\ T \times M - 6.446\ M \times C - 0.117\ T \times C \quad (4.17)$$

Notation: T – temperature, M – molar ratio and C – catalyst loading.

This equation contains 3 linear, square and interaction coefficients (or model parameters) whose significance is determined using standard *t*–test and *p*–values. The fitted equation is in terms of the coded values of parameters and not absolute values.

The significance of these variables is adjudged on the basis of *t*–test, *F*–values and *p*–values. A large *t*–stat value and *p*–value < 0.05 indicates significance of the coefficient and the process parameters to which this coefficient belongs. Relative *F*–values of linear interaction and quadratic coefficient indicate the significance of the individual effect of the parameter as well as the extent of interaction between them. As can be seen from results of ANOVA given in Table 4.4B, *F*–value of overall regression is 9971.75, while *F*–value of linear coefficient is 6201.77. Moreover, the *p*–values of all linear coefficients is < 0.05, which indicates that these variables have a significant effect on the transesterification yield in the range of these parameters considered in the experiments. Coefficients of determination (R^2) is another measure of significance of regression, i.e. R^2 = 99.96% not only indicate excellent fit of the model to the experimental data but also that 99.96% of the effect on the yield for CaO catalyst was explained by variation of the process parameters. The Lack of Fit *F*–value of 0.59 and *p*–value of 0.629 implies that Lack of Fit is not significant as compared to the pure error or in other words the model was significant. It should be noted that the quadratic regression model valid only within the experimental range applied in the present study.

Table 4.4: Statistical analysis of experimental results

(A) Estimated Regression Coefficients for % FAME yield

Term	Coefficients	SE coeff	*t*–stat	*p*–value
Constant (β)	93.38	0.186	502.042	0.
Temperature (T)	10.753	0.113	94.404	0.
Molar ratio (M)	–7.314	0.113	–64.210	0.
Catalyst (C)	8.5013	0.113	74.632	0.
Temperature × Temperature (T^2)	–20.315	0.167	–121.160	0.
Molar ratio × Molar ratio (M^2)	–33.92	0.167	–202.307	0.
Catalyst × Catalyst (C^2)	–25.846	0. 167	–154.152	0.
Temperature × Molar ratio (TM)	–0.874	0.161	–5.426	0.
Temperature × Catalyst (TC)	–0.116	0.161	–0.724	0.474
Molar ratio × Catalyst (MC)	–6.445	0.161	–40.013	0.

(B): Analysis of variance (ANOVA) for transesterification of soybean oil using ultrasound

Source	DF	Sq SS	Adj SS	Adj MS	F	*p*–value
Regression	9	27947.7	27947.7	3105.30	9971.75	0.
Linear	3	5793.9	5793.9	1931.29	6201.77	0.
Square	3	21645.9	21645.9	7215.30	23169.80	0.
Interaction	3	507.9	507.9	169.31	543.68	0.
Residual Error	35	10.9	10.9	0.31	—	—
Lack–of–Fit	3	0.6	0.6	0.19	0.59	0.629
Pure Error	32	10.3	10.3	0.32	—	—
Total	44	27958.6			—	—

R^2 = 99.96%; R^2 (adj) = 99.95%

Figs. 4.5A, B, C show the contour plots indicating effect of interaction of any two variables on the yield of transesterification process. The contour plots essentially are graphical representation of regression equation. An infinitive number of combinations of two test variables with the other two maintained at their respective zero level is represented by each of the contour curve.

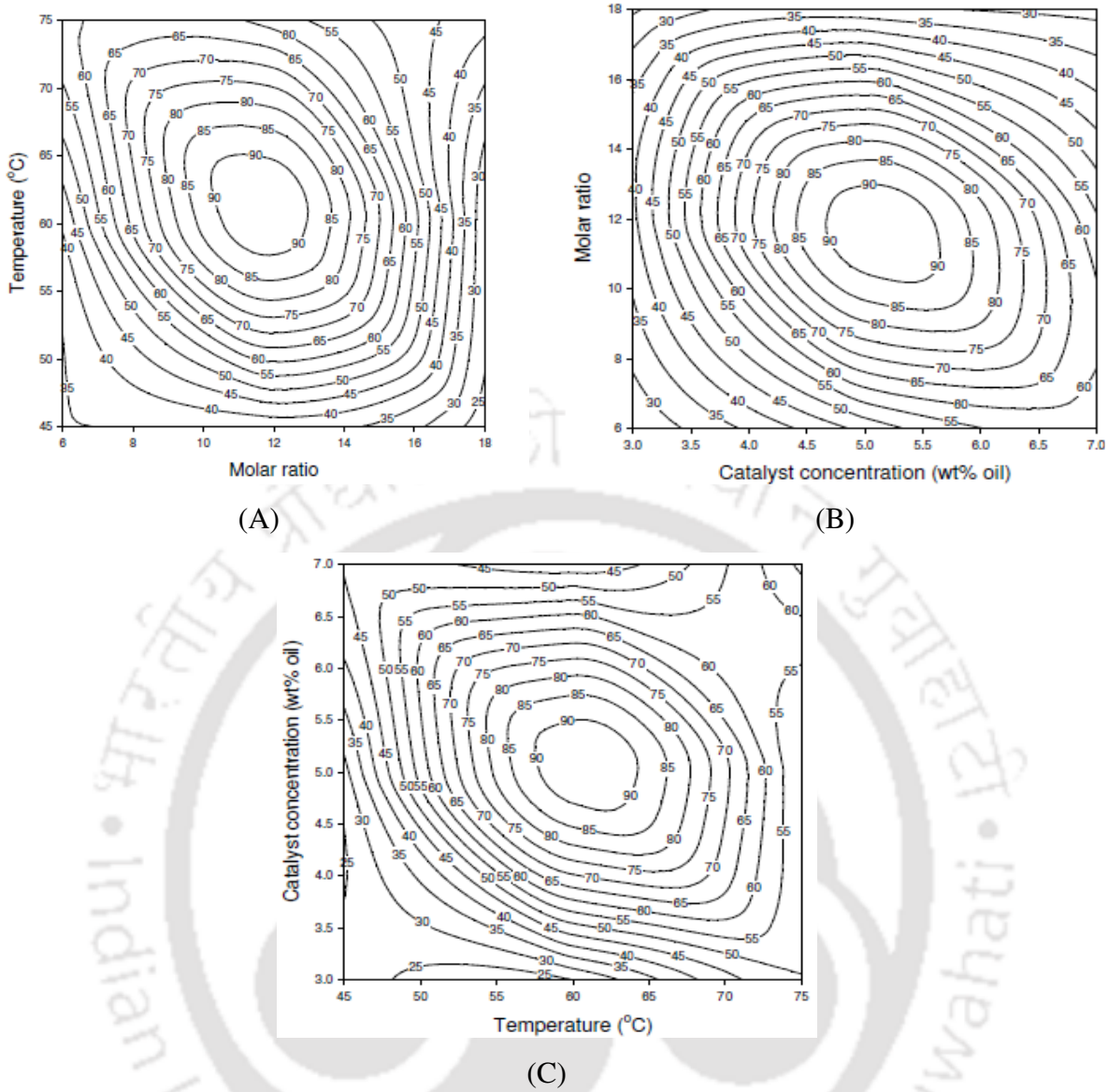

Figure 4.5: Contour plots showing variation of transesterification yield (or % FAME yield) as a function of any two experimental parameters. (A) temperature & molar ratio, (B) molar ratio & catalyst concentration, (C) catalyst concentration and temperature.

Table 4.4(C): Analysis of contour plots

Fixed Parameter (Center point value)	Variable parameter		FAME Yield (%)
Catalyst loading = 5	Temperature = 63.4	Molar ratio = 11.3	95.23
Temperature = 60	Molar ratio = 11.3	Catalyst loading = 4.3	94.6
Molar ratio = 12:1	Temperature = 56	Catalyst loading = 4.3	95.5

Units: Temperature in degree Celsius, catalyst loading in wt% oil.

The interaction between the variables may be predicted from the nature of the response surface contours, whether elliptical, circular, or saddle point [46–47]. The surface confined in the smallest ellipse in the contour diagram indicates the maximum predicted value. Only for a good interaction between the independent variables, perfect elliptical contours are obtained. The contour plots in Figs. 4.5A (temperature & molar ratio) and 4.5B (molar ratio & catalyst concentration) are elliptical indicting good interaction between the parameters, and the maximum point is obtained at the point of intersection of major and minor axes of the ellipse. The significance of interaction between parameters can also be judged from the *p*–value 0.00 given in Table 4.4A. Contour plot in Fig. 4.5C (catalyst concentration & temperature) has more circular nature indicating relatively insignificant interaction between the parameters. This is also confirmed by insignificant *p*–value (i.e. 0.474) of the interaction coefficient of catalyst concentration and temperature. The contour plots help us identify range of parameters for which the highest yield of transesterification is obtained. The ranges of the parameters are: temperature ≈ 57–65^{o}C, catalyst concentration ≈ 4.5–5.5 wt%, molar ratio ≈ 10–12.

4.6.4 Optimization of the Process

The model equation 4.17 fitted the data (using coded values of variables) can be used to find the set of optimum values of parameters, for which the FAME yield is maximum. This optimization (which is essentially the global optimum for the dependent variable *Y* of equation 4.2), was carried out using C program. Table 4.4C gives the optimum values of any two process parameters with the value of third parameters fixed at its center point. The global optimum values of parameters have also been determined with the C program as: temperature = 0.266, molar ratio = –0.128 and catalyst loading = 0.18. Actual values of parameters corresponding to these coded values are: temperature = 64^{o}C, alcohol to oil molar ratio = 11.23 (approximated as ~ 11) and catalyst loading = 5.36 wt%. The maximum yield= 96%.

4.6.5 Kinetic analysis of the process

Order of a reaction is essentially the dependence of the rate of reaction/conversion of the reactants on the concentration of reactant. In case of a tri–phasic catalytic reaction like transesterification, the net reaction depends on adsorption of CH_3OH molecule on the surface of catalyst (refer to scheme 4.1 showing possible reaction mechanism), the formation of methoxide ion (CH_3O^-) and the transfer of this ion to the organic phase (i.e. attack of methoxide ion to triglyceride molecule) at the interface of the organic aqueous phases, and finally the intrinsic rate of reaction $k = A \exp(-E_a/RT)$, which is a major function of temperature.

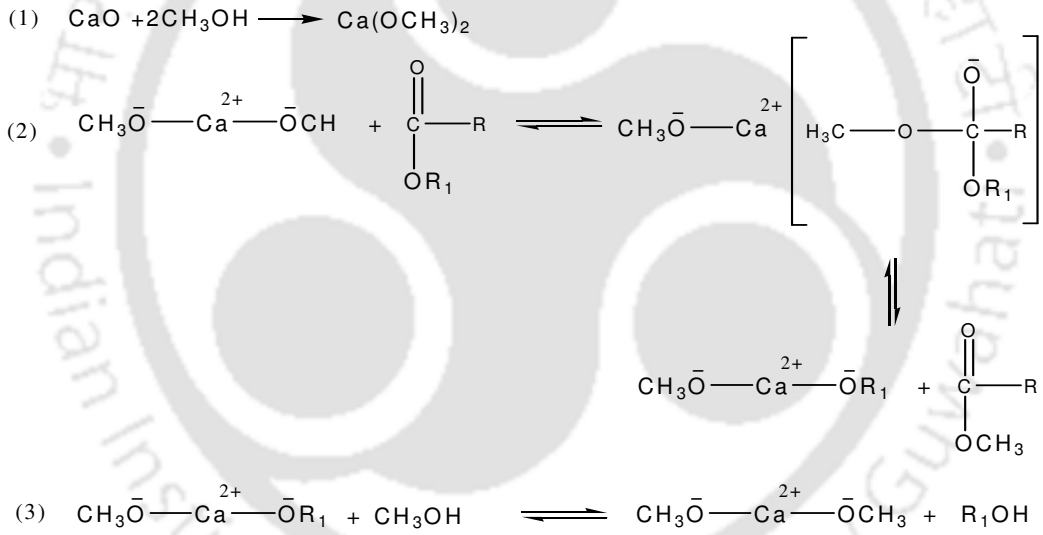

Scheme 4.1: Proposed mechanism of calcium oxide catalyzed trans–esterification reaction.

At lower temperature, k is smaller, and hence, the yield of transesterification depends on rate of reaction between triglyceride molecule and methoxide ions. Thus, at lower reaction temperature, the reaction becomes kinetically controlled. At higher temperature, k becomes higher, and hence, the yield of the reaction depends on the interaction between the methoxide

ion and triglyceride molecule. This interaction occurs at the interface between oil and methanol, and thus, is dependent on the convection in the system or mass transfer characteristics of the system. Results of our kinetic analysis for determination of order (with respect to triglyceride) and rate constant of the reaction are shown in Fig. 4.6 and the summary of results is given in Table 4.5A. It can be observed that order of the reaction decreases with the increase of the reaction temperature. For determination of activation energy using Arrhenius equation, we have to consider an average value of reaction order, as the Arrhenius analysis assumes that the kinetic constant is merely a function of temperature.

However, in our kinetic analysis we have seen that reaction order varies from 1.48 for 60°C to 4.5 for 45°C. We assume an average reaction order of 3 for all temperatures used in activation energy determination. The rate expression for a 3rd order reaction can be determined from the general expression (equation $dC_A/dt = -kC_A^n$ for $n = 3$) as:

$$\frac{1}{(X-1)^2} = 2kC_{A_0}^2 t + 1 \qquad (4.18)$$

Rate constants for different reaction temperatures determined using a 3rd order kinetics (or equation 4.18) are presented in Table 4.5B. The results of the kinetic study of experiments performed with optimum values of molar ratio of ~ 11 and catalyst loading of ~ 5.5 wt% at different temperatures are depicted in Fig. 4.7A and B. Fig. 4.7A gives the time history of FAME yield, while Fig. 4.7B gives the conversion fitted through 3rd order kinetic model. The 3rd order kinetic constant of the reaction shows interesting trend with reaction temperature. With rise of temperature from 45 to 65°C, the kinetic constant shows a sharp increase of 100×. Fig. 4.7C shows the Arrhenius plot for the reaction, from which the activation energy can be determined. High activation energy of 133.5 kJ/mol observed in the present case is attributed to 3–phase heterogeneity (liquid–liquid–solid) of the reaction system resulting in higher mass transfer limitations.

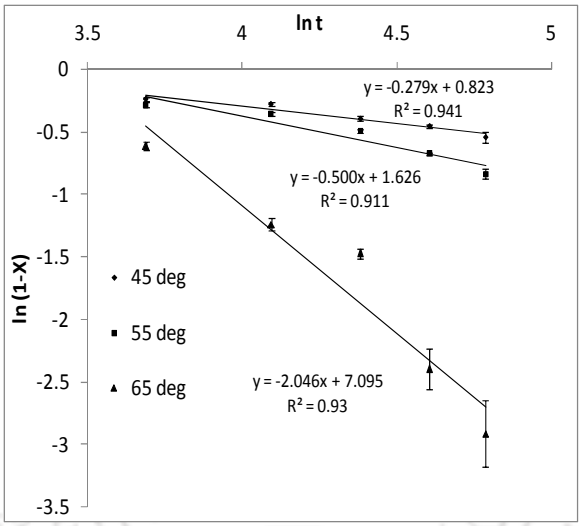

Figure 4.6: Results of integral analysis of the kinetic data for determination of kinetic constant and order of transesterification (with respect to triglycerides)

Table 4.5:.Kinetics of transesterification reaction

(A) Results of integral analysis of reaction kinetics data

Temperature (°C)	Reaction order (n)	Rate constant ($L^{n-1}mol^{1-n}s^{-1}$)
65	1.488	0.065
55	3	0.031
45	4.58	0.037

(B) Kinetic analysis for 3rd order# reaction

Temperature (°C)	Rate constant (k) ($L^2\ mol^{-2}\ s^{-1}$)
45	8.26×10^{-5} ($R^2 = 0.86$)
55	1.66×10^{-4} ($R^2 = 0.81$)
65	1.46×10^{-3} ($R^2 = 0.78$)

This is an average of the orders seen at different temperatures.

These impurities might poison the catalyst by adsorbing over it and reducing its activity. Despite these limitations of the present study, the beneficial effect of ultrasound could be realized by comparing our results with those of Vujicic et al. [48], who reported an activation energy of 162 kJ/mol for biodiesel synthesis from sunflower oil using CaO catalyst in a mechanically stirred reactor in the temperature range of 60 to 120°C and pressure of 5–15 bar.

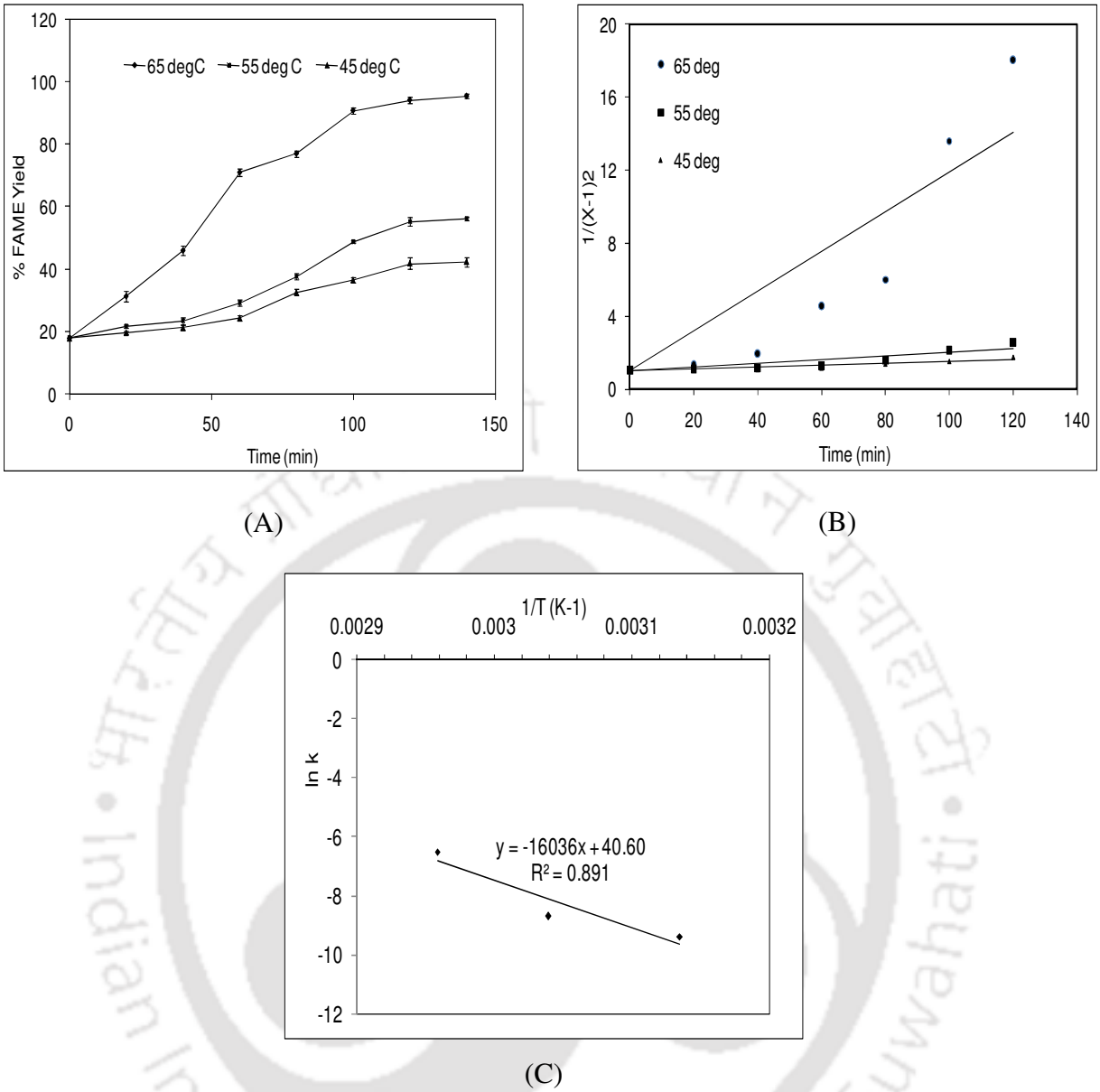

Figure 4.7: Kinetic analysis of transesterification under optimum conditions determined from statistical analysis. (A) Time history of conversion of triglycerides at different temperatures for methanol to oil molar ratio of 11:1 and catalyst concentration 5.5 wt%, (B) Fitting of 3rd order kinetics to the transesterification data to determine the kinetic constant of the reactions, (C) Arrhenius plot of ln (*k*) vs 1/T for transesterification reaction considering 3rd order reaction kinetics (with respect to triglyceride) for optimum conditions of methanol to oil molar ratio (11:1) and catalyst concentration (5.5 wt%) as determined by statistical analysis.

The difference in activation energy calculated in this study and that reported by Vujicic et al. [48] could be attributed to the marked enhancement of mass transfer characteristics of the system by ultrasound.

4.7 Simulation Results

Representative simulation results of radial dynamics of air bubble in methanol are shown in Fig. 4.8. The summary of entire simulation results for bubble dynamics in methanol at different reaction temperature used in the studies is given in Table 4.3B, which lists the magnitudes of the acoustic waves and micro–convection produced by cavitation bubbles (i.e. sono–physical effects) leading to emulsification of the oil and methanol phase. By comparing the magnitudes of the acoustic waves and micro–convection velocity, it could be easily perceived that the contribution of the former is much higher. However, the micro–streaming due to ultrasound also contributes to the net mixing of the phases, and this factor remains practically constant at all reaction temperatures. Comparing the magnitudes of acoustic waves and micro–convection velocities for reaction temperature of 45^{o}, 55^{o} and 65^{o}C, one can conjecture that overall extent of convection induced in the system due to sonication changes only marginally with temperature. However, there is large variation in kinetic constant of transesterification observed at these temperatures. The causes leading to this effect will be discussed in next section.

Our previous study [30] on heterogeneous CaO catalyzed transesterification of soybean oil–methanol, we have reported activation energy 82.3 kJ/mol for optimum molar ratio of 10:1. Another probable cause leading to effect of higher activation energy observed in the present study could be the impure nature of the crude *Jatropha Curcus* oil used.

4.8 Analysis

Prior to the main analysis section, we describe herewith briefly the chemical mechanism of the process as a preamble. CaO catalyst being hydrophilic in nature preferably stays in the aqueous phase (or methanol).

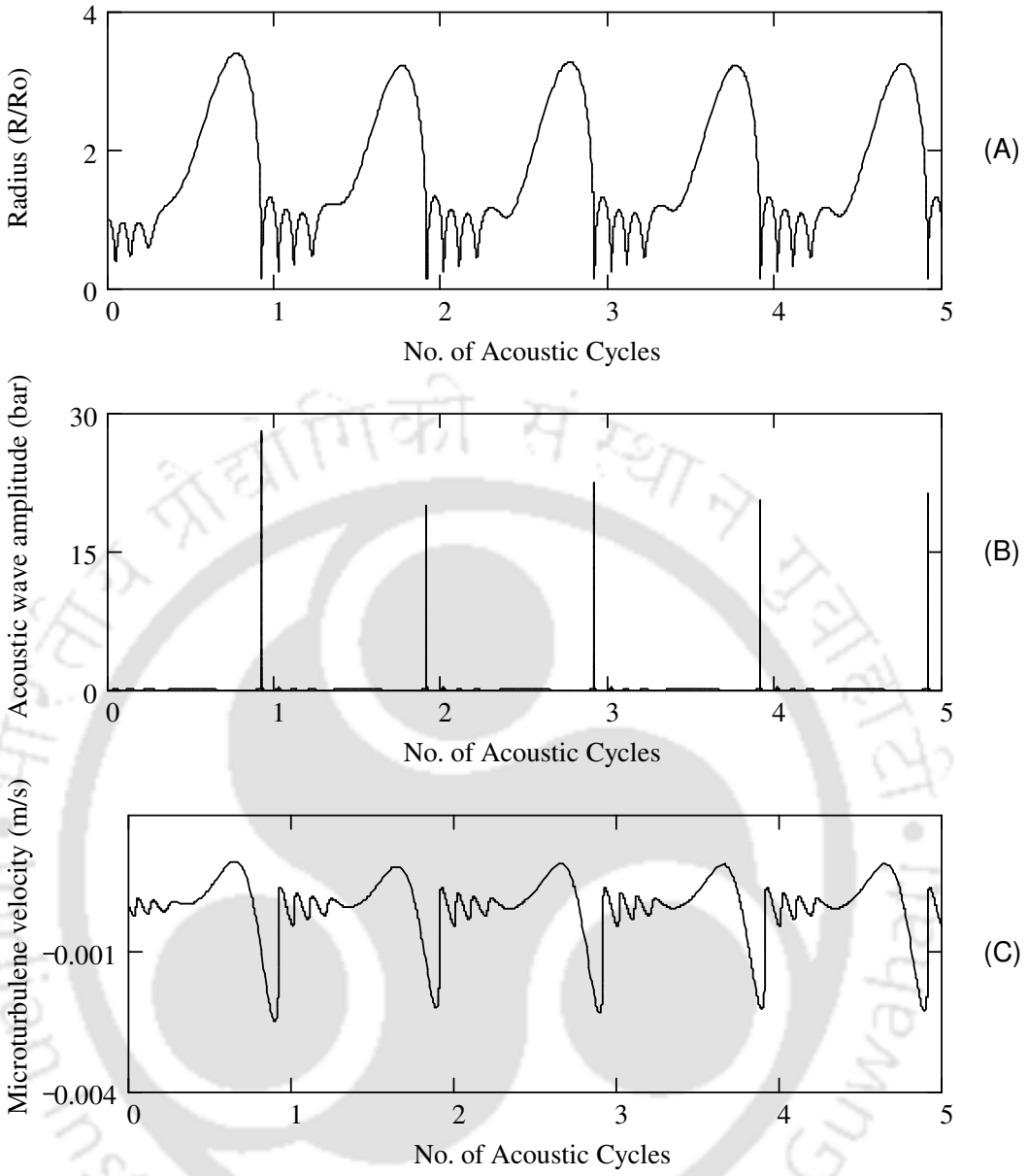

Figure 4.8: Simulation results for radial motion of a 5 µm cavitation bubble (air) in methanol at 55°C. Time variation of (A) normalized bubble radius (R/R_o), (B) acoustic (or shock) waves emitted by the bubble, (C) micro–convection (or oscillatory liquid velocity) generated by the cavitation bubble.

As explained in mechanism of the process (scheme 4.1), calcium methoxide $Ca(CH_3O)_2$ formed on the surface of CaO is the actual catalyst for alcoholysis of triglyceride. As noted earlier, formation of calcium methoxide has been confirmed by XRD data of Fig. 4.3B.

Sonication of freshly calcined CaO under reflux of methanol for 1 h shows growth of fresh peaks of calcium methoxide. $Ca(CH_3O)_2$ transfer one of its methoxy groups to the carbonyl carbon of the triglyceride forming an insoluble organic salt of $Ca(CH_3O)_2$ and triglyceride. Alkoxy group of triglyceride is adsorbed by the calcium methoxide to give alkoxy calcium methoxide and a fatty acid methyl ester. Finally, alkoxy calcium methoxide react with excess methanol to regenerate the actual catalyst calcium methoxide and alcohol [49]. At the end of reaction, the catalyst precursor CaO is regenerated by separation of solid phase by filtration, washing with n–hexane, drying for 12 h at 100°C, and finally calcination at 900°C.

Concurrent analysis of simulations and experimental results helps us identify various facets of physical mechanism of the process. Some peculiar features of the transesterification process can be observed from the results of the Box–Behnken experimental design:

The least yield of 21.96% is seen in set 2 for the lowest temperature (45°C), highest molar ratio (18) and moderate catalyst (5 wt%).

Yield in similar range, i.e. 25.98% amd 24.25% is obtained in sets 5 and 6 for combinations of 60°C temperature, molar ratios of 6 and 18 (respectively), and catalyst concentration of 3 wt%. Interestingly, yield in similar range (27.85%) is obtained in set 9 for which the molar ratio is moderate (12), while temperature reduces to 45°C with catalyst concentration remaining the same at 3 wt%.

Comparison of yields of set 7 and 8 also gives interesting observation. The molar ratio reduces 3 times in set 7 as compared to set 8. Nonetheless, the yield of set 7 is approx. 2× higher. This is completely contradictory to the expectation that yield would increase with molar ratio. This observation becomes even more remarkable as the temperature of both sets is 60°C and the catalyst concentration is the highest, i.e. 7 wt%.

Similar trend of reduction in yield with rise in molar ratio is also seen in sets 3 and 4, although in this case the yield reduces by ~ 30% with 3× rise in the molar ratio.

The relative effect of temperature and catalyst can also be deduced from results of experimental sets 10 and 11. Lowest temperature of 45°C at the highest catalyst concentration of 7 wt% in set 11 gives almost similar yield as in set 10 for the highest temperature of 75°C and the lowest catalyst concentration of 3 wt%.

Comparing results of set 10 and 12 reveals that at the highest temperature of 75°C (which is well above the b.p. of methanol), doubling of catalyst concentration results in mere 30% rise in the yield of transesterification.

The highest yield is obtained for sets 13 to 15 in which the temperature is just below the b.p. of methanol and both catalyst concentration and molar ratio are moderate.

Above results indicate that all three process parameters, viz. molar ratio, temperature and catalyst concentration have a significant influence on the transesterification yield. Nonetheless, as noted earlier, the combination of optimum process parameters for the highest yield is temperature = 64°C, alcohol to oil molar ratio = 11.23 (approximated as ~ 11) and catalyst loading = 5.36 wt%, which are the middle or moderate values used in statistical design. We justify these values as follows:

1. Since the transesterification reaction occurs in the liquid phase, it is essential that both methanol and oil remain in liquid phase at the reaction temperature. The boiling point of methanol is 65°C. The optimum temperature obtained in our experiment is close to boiling point of methanol, for which methanol exists in liquid phase. At the highest temperature used in our experimental design, i.e. 75°C, the methanol in the reaction mixture vaporizes resulting in reduction in interfacial area for reaction.

2. The influence of molar ratio and catalyst concentration is inter–related. For very low catalyst concentrations (~ 3 wt%), the amount of methoxy ions generated are low giving smaller yields. Interfacial area between oil and methanol depends on extent of dispersion of these liquids in each other. Since the intensity of cavitation bubble motion is higher in

methanol, one would expect higher dispersion and interfacial area for the highest molar ratio, and consequently higher yield. However, contrary to this expectation, we see reduction in yield at highest molar ratio. The probable cause leading to this effect is that catalyst particles being hydrophilic stay preferentially in methanol phase. The methoxy ions that induce the transesterification reaction are generated at the catalyst surface. As the volume fraction of methanol in the total reaction mixture increases with molar ratio, these ions have to diffuse through larger volume so as to reach the interface and react with triglyceride. On the other hand, if the molar ratio is too low, the volume fraction of oil in the reaction mixture is high and some catalyst particle may also stay in oil phase. The oil competitively wets the catalyst surface, thus reducing formation of methoxy ions. As a result of these competing phenomena, the highest yield is obtained at moderate alcohol to oil molar ratios.

4.9 Conclusion

The major findings and conclusion of this chapter are summarized as under:

(1) Due to very high FFA content of Jatropha oil, the single step synthesis of biodiesel thorough transesterification is not possible. Therefore, a two step methodology of esterification followed by transesterification was adopted.

(2) The esterification reaction catalyzed by H_2SO_4 does not show any beneficial influence of ultrasound, either in terms of kinetic or in terms of yield.

(3) XRD analysis confirms that reaction between CaO and MeOH generates $Ca(OMe)_2$ which is the active catalyst for transesterification reaction.

(4) Maximum yield is seen for the reaction temperature – close to boiling point of methanol. The optimum values of parameters for the highest yield of transesterification have been determined as follows: alcohol to oil molar ratio ≈ 11, catalyst concentration ≈ 5.5 wt% and temperature ≈ 64^{o}C. The activation energy of the reaction is calculated as 133.5 kJ/mol.

(5) Comparison of activation energy obtained for the present system with that for the homogeneous catalyst system (assisted with sonication) reveals that the heterogeneity of the system increases mass transfer constraints resulting in approx. 4× increase in activation energy. Obviously, the rise in activation energy is manifested in terms of high reaction temperature (as compared the homogeneous system) required to obtain high yields (typically ≥ 90%).

(6) On the other hand, comparison of activation energy obtained in the present study with that of Vujicic et al.[48] reveals that intense micro–convection induced by ultrasound enhances the mass transfer characteristics of the system with ~ 20% reduction in activation energy, as compared to mechanically agitated systems.

(7) Influence of catalyst concentration and alcohol to oil molar ratio on the trans–esterification yield is inter–linked through formation of methoxy ions, and their diffusion to the oil–alcohol interface, which in turn is determined by the volume fractions of the two phases in the reaction mixture. As a result, the highest transesterification yield is obtained at the moderate values of catalyst concentration and alcohol to oil molar ratio.

References

[1] M. Y. Koh, T. I. Mohd. Ghazi, A review of biodiesel production from *Jatropha curcas* L. oil, Renew. Sust. Energ. Rev. 15 (2011) 2240–2251.

[2] V. C. Pandey, K. Singh, J. S. Singh, A. Kumar, B. Singh, R. P. Singh, *Jatropha curcas*: A potential biofuel plant for sustainable environmental development, Renew. Sust. Energ. Rev. 16 (2012) 2870–2883.

[3] S. Lim, K. T. Lee, Influences of different co–solvents in simultaneous supercritical extraction and transesterification of *Jatropha curcas* L. seeds for the production of biodiesel, Chem. Eng. J. 221 (2013) 436–445.

[4] F. H. Kasim, A. P. Harvey, Influence of various parameters on reactive extraction of *Jatropha curcas* L. for biodiesel production, Chem. Eng. J. 171 (2011) 1373– 1378

[5] X. Liu, X. Piao, Y. Wang, S. Zhu, Model study on transesterification of soybean oil to biodiesel with methanol using solid base catalyst, J. Phys. Chem. A 114 (2010) 3750–3755.

[6] M. L. Granados, D. M. Alonso, A. C. Alba–Rubio, R. Mariscal, M. Ojeda, P. Brettes, Transesterification of triglycerides by CaO: Increase of the reaction rate by biodiesel addition, Energ. Fuel 23 (2009) 2259–2263.

[7] X. J. Liu, H. Y. He, Y. J. Wang, S.L. Zhu, X.L. Piao, Transesterification of soybean oil to biodiesel using CaO as a solid base catalyst, Fuel 87 (2008) 216–221.

[8] M. D. Machado, J. Perez–Pariente, E. Sastre, D. Cardoso, A.M. Guerenu, Selective synthesis of glycerol monolaurate with zeolitic molecular sieves, Appl. Catal. A 203 (2000) 321–328.

[9] S. Gryglewicz, Rapeseed oil methyl esters preparation using heterogeneous catalysts, Bioresour. Technol. 70 (1999) 249–253.

[10] H. Wu, J. Zhang, Q. Wei, J. Zheng, J. Zhang, Transesterification of soybean oil to biodiesel using zeolite supported CaO as strong base catalysts, Fuel Proc. Technol. 109 (2013) 13–18.

[11] A. Zieba, A. Pacuła, A. Drelinkiewicz, Transesterification of triglycerides with methanol catalyzed by heterogeneous zinc hydroxy nitrate catalyst. Evaluation of variables affecting the activity and stability of catalyst, Energ. Fuels 24 (2010) 634–645.

[12] J. F. Puna, J. F. Gomes, M. Joana N. Correia, A. P. Soares Dias, J. C. Bordado, Advances on the development of novel heterogeneous catalysts for transesterification of triglycerides in biodiesel, Fuel 89 (2010) 3602–3606

[13] Y. Zu, G. Liu, Z. Wang, J. Shi, M. Zhang, W. Zhang, M. Jia, CaO supported on porous carbon as highly efficient heterogeneous catalysts for transesterification of triacetin

with methanol, Energ. Fuels 24 (2010) 3810–3816.

[14] M. Zabeti, W. Daud, M. K. Aroua, Biodiesel production using alumina–supported calcium oxide: an optimization study, Fuel Proc. Technol. 91 (2010) 243–248.

[15] L. B. Wen, Y. Wang, D. L. Lu, S. Y. Hu, H. Y. Han, Preparation of KF/CaO nanocatalyst and its application in biodiesel production from Chinese tallow seed oil, Fuel 89 (2010) 2267–2271.

[16] D. M. Alonso, R. Mariscal, M. L. Granados, P. Maireles–Torres, Biodiesel preparation using Li/CaO catalysts: activation process and homogeneous contribution, Catal. Today 143 (2009) 167–171.

[17] H. Liu, L.Y. Su, Y. Shao, L.B. Zou, Biodiesel production catalyzed by cinder supported CaO/KF particle catalyst, Fuel 97 (2012) 651–657.

[18] Y. Tang, M. Meng, J. Zhang, Y. Lu, Efficient preparation of biodiesel from rapeseed oil over modified CaO, Appl. Energ. 88 (2011) 2735–2739.

[19] I. Lukic, J. Krstic, D. Jovanovic, D. Skala, Alumina/silica supported K_2CO_3 as a catalyst for biodiesel synthesis from sunflower oil, Bioresour. Technol. 100 (2009) 4690–4696.

[20] D. G. B. Boocock, S. K. Konar, V. Mao, H. Sidi, Fast one phase oil–rich process for the preparation of vegetable oil methyl esters, Biomass Bioenerg. 11 (1996) 43–50.

[21] S. Suzanne Nielsen (Ed.), Food Analysis Laboratory Manual, fourth ed., Springer-Verlag New York Inc., New York, 2010.

[22] X. Deng, Z. Fang, Y. Liu, Ultrasonic transesterification of *Jatropha curcas* L. oil to biodiesel by a two–step process, Energ. Conver. Manage. 51 (2010) 2802–2807.

[23] V. S. Moholkar, S.P. Sable, A.B. Pandit, Mapping the cavitation intensity in an ultrasonic bath using the acoustic emission, AIChE J. 46 (2000) 684–694.

[24] Xin Deng, Zhen Fang, Yun–hu Liu, Chang–Liu Yu, Production of biodiesel from

Jatropha oil catalyzed by nanosized solid basic catalyst, Energy 36 (2011) 777–784.

[25] T. Sivasankar, A. W. Paunikar, V. S. Moholkar, Mechanistic approach to enhancement of the yield of a sonochemical reaction, AIChE J. 53 (2007), 1132–1143.

[26] G. Gelbard, O. Brès, R.M. Vargas, F. Vielfaure, U.F. Schuchardt, 1H nuclear magnetic resonance determination of the yield of the transesesterification of rapeseed oil with methanol, J. Am. Oil Chem. Soc. 72 (1995) 1239–1241.

[27] G. Knothe, Analytical methods used in the production and fuel quality assessment of biodiesel, Trans. ASAE 44 (2001) 193–200.

[28] P. A. Parkar, H. A. Choudhary, V.S. Moholkar, Mechanistic and kinetic investigations in ultrasound assisted acid catalyzed biodiesel synthesis, Chem. Eng. J. 187 (2012) 248– 260

[29] A. Kalva, T. Sivasankar, V. S. Moholkar, Physical mechanism of ultrasound assisted synthesis of biodiesel, Ind. Eng. Chem. Res. 48 (2009) 534–544.

[30] H. A. Choudhury, S. Chakma, V. S. Moholkar, Mechanistic insight into sonochemical biodiesel synthesis using heterogeneous base catalyst, Ultrason. Sonochem. 21 (2014) 169–181.

[31] V. S. Moholkar, M. M. C. G. Warmoeskerken, Integrated approach to optimization of an ultrasonic processor, AIChE .J. 49 (2003) 2918–2932.

[32] A. Ranjan , C. Patil , V. S. Moholkar, Mechanistic assessment of microalgal lipid extraction, Ind. Eng. Chem. Res. 49 (2010) 2979–2985.

[33] K. Suresh, A. Ranjan, S. Singh, V.S. Moholkar, Mechanistic investigations in sono–hybrid techniques for rice straw pretreatment, Ultrason. Sonochem.21 (2013) 200–207.

[34] R. Lofstedt, K. Weninger, S. J. Puttermann, B. P. Barber, Sonoluminescing Bubbles and Mass Diffusion, Phys. Rev. E 51, (1995) 4400–4410.

[35] S. Hilgenfeldt, D. Lohse, M. P. Brenner, Phase Diagrams for Sonoluminescing Bubbles, Phys. Fluids.8, (1996) 2808–2826.

[36] B. P. Barber, R. A. Hiller, R. Lofstedt, S. J. Putterman, K. R. Weninger, Defining the Unknowns of Sonoluminescence, Phys. Rep. 281, (1997) 65–143.

[37] M. Plesset, The Dynamics of Cavitation Bubbles, J. Appl. Mech. (Trans. ASME), 16, (1949) 277–282.

[38] A. Prosperetti, A. Lezzi, Bubble Dynamics in a Compressible Liquid. Part 1. First Order Theory, J. Fluid Mech., 168, (1986) 457–477.

[39] J. B. Keller, M. J. Miksis, Bubble Oscillations of Large Amplitude, J. Acoust. Soc. Am. 68, (1980) 628–633.

[40] W. H. Press, S. A. Teukolsky, B. P. Flannery, W. T. Vetterling, Numerical Recipes (2nd Ed.), Cambridge University Press: New York, 1992.

[41] Y. T. Shah, A. B. Pandit, V. S. Moholkar, Cavitation Reaction Engineering, Plenum Press, New York, 1999.

[42] S. Grossmann, S. Hilgenfeldt, M. Zomack, D. Lohse, Sound radiation of 3 MHz driven gas bubbles, J. Acoust. Soc. Am. 102 (1997) 1223–1227.

[43] V. S. Moholkar, M.M.C.G. Warmoeskerken, An integrated approach to optimization of an ultrasonic processor, AIChE J. 49 (2003) 2918–2932.

[44] A. D. Pierce, Acoustics: An introduction to its physical principals and applications, Acoustical Society of America, New York, 1989.

[45] W. L. Nyborg, Acoustic streaming near a boundary, J. Acoust. Soc. Am. 30 (1958) 329–339.

[46] M. S. Tanyildizi, D. Ozer, M. Elibol, Optimization of a–amylase production by Bacillus sp. using response surface methodology, Process Biochem. 40 (2005) 2291–2296.

[47] K. Ravikumar, K. Pakshirajan, T. Swaminathan, K. Balu, Optimization of batch process parameters using response surface methodology for dye removal by a novel adsorbent, Chem. Eng. J. 105 (2005) 131–138.

[48] Dj. Vujicic, D. Comic, A. Zarubica, R. Micic, G. Boskovic, Kinetics of biodiesel synthesis from sunflower oil over CaO heterogeneous catalyst, Fuel 89 (2010) 2054–2061.

[49] S. Gryglewicz, Rapeseed oil methyl esters preparation using heterogeneous catalysts, Bioresour. Technol. (70) 1999 249–253.

[50] NIST Data Gateway (Chemistry Webbook) Home Page. http://webbook.nist.gov/ chemistry (accessed June 2013).

CHAPTER 5

Ultrasonic Jatropha Oil Biodiesel Synthesis Using Sulfuric Acid Catalyst

5.1. Introduction

In the last chapter, we presented results of ultrasonic biodiesel synthesis with *Jatropha curcas* oil using heterogeneous base catalyst. Due to high FFA content of crude *Jatropha curcas* oil, direct transesterification was not possible with solid base catalyst as it would lead to saponification. Therefore, we had used a two step process in which the FFA content of the oil was lowered by esterification with H_2SO_4 catalyst in the first step. In the second step, transesterification was carried out using the CaO base catalyst. In this chapter, we have extended this theme using sulphuric acid catalyst through out ultrasonic biodiesel synthesis, i.e. in both steps of esterification and transesterification. The feedstock used is same as the previous chapter, i.e. Jatropha oil. Use of same acid catalyst in both steps lowers the time of the entire process. Secondly, although intrinsic kinetics of the acid catalyst is far slower than base catalyst, due to the homogeneous nature of acid catalyst, the overall process

is likely to have same batch time as for the heterogeneous base catalyst (in which the limitations of mass transfer are more marked, as outlined earlier). The ultrasound irradiation of the reaction mixture is going to boost the kinetics of the acid catalyzed transesterification.

The approach and methodology adopted in this chapter is same as earlier in that we essentially try to find link between chemistry of transesterification /esterification reaction and physics of ultrasound and cavitation to establish the physical mechanism of this process. The second aim is to optimize the process in terms of experimental parameters. For this purpose, we have devised our experimental protocols on a statistical experimental design (Box–Behnken method), and the analysis has been done using Response Surface Methodology (RSM). Simulations of the cavitation bubble dynamics in the reaction mixture have been done to estimate the physical and chemical effects induced by ultrasound and cavitation, under different experimental conditions used in statistical design. Concurrent analysis and correlation between the statistical experimental design and bubble dynamics simulations has shed light on many physical aspects of the Jatropha oil based biodiesel synthesis that could form vital inputs for further research in this area and could also give useful guidelines for scale–up of the process.

5.2 Materials and Methods

5.2.1 Materials

Jatropha curcas oil was procured from local market. The acid value (AV) and saponification value (SV) of the oil was determined as 21.57 mg KOH/g and 201.2 mg KOH/g using standard methods described in the Chapter 4. Other chemicals used in experiments are methanol (AR grade 99%, Merck, India) and sulfuric acid (AR grade 98%, Merck, India). Anhydrous methanol was obtained by further vacuum distillation. Other chemicals were used as received without any further treatment.

5.2.2 Experimental setup

An ultrasound bath (Elma Trans–sonic T–460 type, Germany, capacity: 2 L, frequency: 35 kHz, power: 35 W) was used for sonication of the transesterification reaction mixture. 2/3rd of bath volume was filled with water, which acts as medium for transmission of ultrasound. All experiments were carried out in a 50 mL two–neck round bottom flask made of borosilicate glass. Since the temperatures of the transesterification reaction system were near or even higher than the boiling point of methanol, a reflux condenser was employed for methanol vapours. A digital thermometer was inserted in the second neck of the reaction flask to monitor the temperature of the reaction mixture continuously. The temperature of water in the bath was maintained at desired levels by means of a variable energy input heating element. The bath was sealed to minimize as much heat loss as possible from the medium. The intensity (or pressure amplitude) of the ultrasound wave field shows significant spatial variation [1], and hence, the position of the reaction flask was maintained carefully the same in all experiments. The actual energy dissipation and pressure amplitude of the ultrasound wave in the bath was characterized using calorimetry [2].

5.2.3 Experimental Protocol

The experimental protocol reported below is based on several preliminary experiments. One important variable that was assessed was the temperature of transesterification. No product was seen at temperatures below 50^{o}C. To decide the protocol for esterification step, we have compared our preliminary results on esterification with those of Deng et al. [3]. In our preliminary experiments, we attempted to perform esterification using both sonication and mechanical stirring. However, we found that the time for almost complete esterification (> 90%, as indicated by reduction in acid value of oil) was same for both mechanical stirring and sonication, in that almost complete reduction of acid value was obtained within 1 h with FAME yield in the range of 17–20%. This result matches with the result reported by Deng et

al. [3]. This essentially means that the kinetics of the esterification reaction was rather insensitive to sonication.

Esterification: Sulfuric acid catalyzed esterification reaction of crude *Jatropha curcas* oil (AV = 21.57 mg KOH/g indicating high free fatty acid content) was carried out in the first step in two–neck round bottom flask fitted with a reflux condenser. This protocol was similar to that described in the Chapter 4. Based on the results of this study which revealed that sonication had practically no effect on enhancement of kinetics of esterification, and that esterification was dominated by intrinsic kinetics, we have carried out the esterification with mechanical stirring. The optimization parameters for esterification reaction were alcohol to oil molar ratio and catalyst concentration, with two fixed parameters, viz. temperature of reaction fixed at 65 ± 2°C, and the reaction time being 1 h. These parameters were fixed on the basis of our preliminary experiments. 9 sets of experiments were performed with duplicate runs in each set in order to assess the reproducibility of the results. *Jatropha curcas* oil has high acid value of 21.57 mg KOH/g (indicating high free fatty acid content), and therefore, in the first step sulfuric acid catalyzed esterification reaction was carried out in two–neck round bottom flask fitted with a reflux condenser. The important parameters for esterification reaction were alcohol to oil molar ratio and catalyst concentration at a fixed temperature of 65 ± 2°C with a reaction time of 1 h. Experiments were performed in nine sets, with duplicate runs in each set in order to assess the reproducibility of the results. The values of experimental parameters were decided from the previously published literature [4]. The exact composition of the reaction mixture in each set is given in Table 4.1 in Chapter 4. The total reaction volume was 15 mL. After the reaction, the reaction mixture was allowed to stand in a separating funnel to split the organic and aqueous phases. The organic layer was separated and washed with hot water to remove traces of acid and alcohol.

Table 5.1: Levels of independent variables in statistical design of experiments

Independent Variables (or Factors)	Symbol coded	Levels of Factors Coded Value (Actual value)		
Catalyst concentration (wt%)	C	–1 (3)	0 (6)	1 (9)
Temperature (^oC)	T	–1 (55)	0 (70)	1 (85)
Alcohol to oil molar ratio (R)	M	–1 (4:1)	0 (7:1)	1 (10:1)

The acid value (AV) of the organic layer (which essentially is the final esterification product) was again determined by titration method. The experimental set in which the acid value of the product was the lowest was selected for next set of experiments. The same experimental set was then conducted at increased reaction volume of 200 mL, and the results were found consistent which essentially means that the reaction characteristics did not change with scale of the reaction. The product of this large–scale reaction was preserved for further transesterification reaction.

Transesterification: The transesterification experiments have been devised using Box–Behnken statistical design. The product of esterification experiments described above was used as reactant in the transesterification experiments. The following experimental parameters (or independent variables) have been chosen for optimization: catalyst loading (*C*), temperature (*T*), and alcohol to oil molar ratio (*R*). These experiments were carried out in the ultrasound bath described earlier with time of sonication fixed as 2 h, based on our initial experiments. The exact experimental design, formulated using Minitab 15 trial version software, indicating range and levels of the independent variables is shown in Table 5.1. The response variable, i.e. % FAME yield, was fitted with a full quadratic model (given in equation 5.1) in order to correlate it to the experimental parameters or independent variables.

$$Y = \beta_0 + \sum_{i=1}^{3} \beta_i x_i + \sum_{i=1}^{3} \beta_{ii} x_i^2 + \sum_{i=1}^{2} \sum_{j=i+1}^{3} \beta_{ij} x_i x_j \qquad (5.1)$$

Various notations are as follows: Y = response variable (i.e. %FAME yield); β_0 = constant; β_i, β_{ij} and β_{ij} = regression coefficients; x_i and x_j = coded independent variables. The Box–Behnken statistical experimental design for 3 factors and 3 levels (with different combinations of the parameters), comprises of 15 sets of experiments. The experimental conditions in these sets are given in Table 5.2A, while the exact composition of reaction mixture in each set is given in Table 5.2B. In each set, experiments have been done in triplicate (3 runs) so as to assess the reproducibility of results. The progress of the transesterification reaction was monitored by withdrawing 500 µL aliquots of the reaction mixtures after every 20 min. These aliquots were mixed with 1 mL of 0.05 M NaOH to neutralize the homogeneous acid catalyst, and centrifuged at 6000 rpm for 10 min to separate the homogenous catalyst as well as the aqueous (or glycerol and alcohol) phase. The organic or biodiesel layer was then analyzed to determine the yield of FAME or biodiesel.

Table 5.2: (A) Box–Behnken experimental design matrix

Sl. No.	Temperature (^oC)	Molar ratio	Catalyst (wt% oil)	% FAME yield#	Fitted % FAME yield
1	55	4	6	22.04	24.49
2	85	4	6	18.00	15.75
3	55	10	6	30.70	32.94
4	85	10	6	38.97	36.51
5	55	10	3	40.85	37.45
5	85	7	3	32.97	34.27
7	55	7	9	42.40	42.09
8	85	7	9	35.7	39.09
9	70	4	3	32.05	32.99
10	70	10	3	36.40	37.55
11	70	4	9	28.33	27.17
12	70	10	9	52.77	51.82
13	70	7	6	79.48	79.48
14	70	7	6	79.01	79.48
15	70	7	6	79.95	79.48

– This is average result of 3 experimental runs or trials in each set.

(B) Composition of reaction mixture in Box–Behnken experimental design matrix

Sl No.	Temperature (°C)	Molar ratio	Catalyst (wt% oil)	Oil Volume (ml)	Methanol Volume (ml)	Methanol / Oil volume ratio	Catalyst added (ml)
1	55	4	6	12.97	2.03	0.16	0.20
2	85	4	6	12.97	2.03	0.16	0.20
3	55	10	6	10.78	4.22	0.39	0.34
4	85	10	6	10.78	4.22	0.39	0.34
5	55	10	3	10.78	4.22	0.39	0.16
5	85	7	3	11.77	3.23	0.27	0.18
7	55	7	9	11.77	3.23	0.27	0.57
8	85	7	9	11.77	3.23	0.27	0.57
9	70	4	3	12.97	2.03	0.16	0.20
10	70	10	3	10.78	4.22	0.39	0.16
11	70	4	9	12.97	2.03	0.16	0.63
12	70	10	9	10.78	4.22	0.39	0.52
13	70	7	6	11.77	3.23	0.27	0.37
14	70	7	6	11.77	3.23	0.27	0.37
15	70	7	6	11.77	3.23	0.27	0.37

5.2.4 Analysis

Determination %FAME yield: The gross conversion of triglycerides in *Jatropha curcas* oil was determined using ^{1}H NMR (Varian 400 MHz FT–NMR) spectroscopic analysis with $CDCl_3$ as solvent and TMS (tetramethyl silane) as internal standard . The conversion (X_{ME}) of triglycerides in *Jatropha curcas* oil to fatty acid methyl esters is determined using following equation: $X_{ME} = 2A_{ME} \times 100/3 \times A_{\alpha-CH2}$, where A_{ME} = integration value of the protons of the methyl esters (the strong singlet peak at 3.6 ppm), $A_{\alpha-CH2}$ = integration value of the methylene protons at 2.3 ppm.

Determination of transesterification kinetics: The time data of conversion of triglycerides obtained with help of ^{1}H NMR spectroscopy, as described above was used to determine the kinetic parameters of the process. The transesterification reaction progresses in three consecutive and reversible reactions steps as follows: (1) reaction of triglyceride (TG) and methanol to produce diglycerides (DG) and 1 molecule of methyl ester, (2) further reaction of diglycerides to yield monoglycerides (MG) and another molecule of methyl ester, and finally

(3) reaction of monoglyceride to yield one mole of methyl ester and one mole of glycerol. In our analysis, we have determined the kinetic constant of the overall reaction, without accounting for the intermediate steps. The overall reaction is assumed to be governed by pseudo 1st order kinetics, and the following equation has been fitted to the conversion–time (X_{ME} vs t) data so as to obtain the kinetic constant: $\ln(1-X_{ME}) = -kt$, where X_{ME} = conversion of triglyceride at any time t. Plot of $-\ln(1-X_{ME})$ vs t gives the kinetic constant k as the slope.

Determination of activation energy (*Arrhenius plot*): The Arrhenius equation gives a relationship between the specific reaction rate constant (k), absolute temperature (T) and the energy of activation (E_a) as: $k = A\exp(-E_a/RT)$, where A is the frequency factor and R is universal gas constant (8.314 J mol^{-1} K^{-1}). This equation is rewritten as:

$\ln k = -E_a/RT + \ln A$. We have used 3 reaction temperatures (as mentioned in Table 5.2) in our statistical experimental design. Experiments have been conducted using optimum values of catalyst loading and alcohol to oil molar ratio (as determined from the statistical experimental design) at these three reaction temperatures. Plot of ln k vs $1/T$ gives slope equal to $(-E_a/R)$ from which activation energy can be determined.

5.2.5 Simulations of cavitation bubble dynamics

As noted in the Introduction section, we have carried out simulations of cavitation bubble dynamics to estimate the physical and chemical effects induced by ultrasound and cavitation bubbles in the system. We have used the diffusion limited model proposed by Toegel et al. [5] based on boundary layer approximation for our analysis. This model is essentially the ordinary differential equation (ODE) approximation of comprehensive partial differential equation (PDE) model of Storey and Szeri [6], which is based on the principal result that vapor transport and entrapment in the cavitation bubble during its radial motion is essentially a diffusion limited process. The entrapped vapor and gas molecules inside the bubble at

transient collapse are subjected to the extreme conditions generated at the collapse, leading to formation of radicals. This model has been extensively described in our previous papers [7–9]. The reaction system in the present study is of liquid–liquid heterogeneous type, viz. methanol and oil. Our earlier studies [7, 10] have shown that the energy intensity of the dynamics of cavitation bubbles in the oil phase is too weak to produce any significant physical or chemical effect, as a result of high viscosity of oil. Therefore, any contribution of sonication towards the intensification of transesterification reaction is from the bubble dynamics in methanol. We have used following parameters for simulations of an air bubble: Ultrasound frequency (f) = 35 kHz; Ultrasound pressure amplitude (P_A) = 150 kPa; Equilibrium bubble radius (R_o) = 10 μm. Vapor pressure (in bar) of methanol at various reaction temperatures has been calculated using following

$$\log_{10} P\ (\text{bar}) = 5.15853 - \frac{1569.613}{T - 34.846} \tag{5.2}$$

Physical properties of methanol are [25, 28]: density = 790 kg/m^3, kinematic viscosity = 6.829×10^{-7} Pa–s, surface tension = 0.02355 N/m, and velocity of sound = 1103 m/s.

Effect of ultrasound on reaction system: Ultrasound wave is a longitudinal wave that in the form of longitudinal wave with series of compression and rarefaction accompanied by rapid oscillatory motion of fluid elements around a mean position called as micro–streaming. Due to finite viscosity of the medium, some momentum of the wave is dissipated and is manifested in the form of low–velocity (few mm/s) unidirectional liquid currents, known as acoustic streaming. The phenomenon of micro–streaming gives rise to intense micro–mixing in the medium. The magnitude of the micro–streaming velocity is given as:

$$u = P_A / \rho c \tag{5.3}$$

Substituting values of P_A as 150 kPa, ρ = 790 kg/m^3, and c = 1103 m/s, gives u = 0.17 m/s.

Physical and chemical effect of cavitation bubbles: The numerical solution of bubble

dynamics model can be used for estimation of physical and chemical effects of cavitation bubbles. The numerical solution of model equations gives the temperature and pressure reached in the cavitation bubble at transient collapse, and also the number of gas and solvent molecules inside the bubble. As noted earlier, at extreme conditions reached in the bubble during transient collapse, the solvent as well as gas molecules undergo dissociation to form numerous chemical species, which also react among themselves. Due to very high temperature as well as concentration (due to extremely small volume of the bubble), the kinetics of the reactions among these species is several orders of magnitude higher than the time scale of bubble dynamics [8]. As a consequence, the bubble contents can be expected to be at thermodynamic equilibrium at the moment of collapse. The equilibrium mole fraction of different chemical species in the bubble at the peak conditions reached at transient collapse can be calculated using Gibbs free–energy minimization technique [11]. The physical effect of cavitation bubbles is generation of intense convection in the medium through micro–convection and shock or acoustic waves. Magnitudes of these entities can be determined from numerical solution of bubble dynamics model [12].

5.3. Results and Discussion

5.3.1 NMR analysis of reaction mixture

The ^{1}H NMR spectrum of fatty acid methyl esters (FAME) of *Jatropha curcas* oil is shown in Fig. 5.1. The characteristic peak at 3.6 ppm in the spectrum represents the FAME. This peak essentially corresponds to the presence of methyl ester protons of biodiesel or FAME molecule. The other peaks in the ^{1}H NMR spectrum have been identified as follows: the triplet at 2.3 ppm corresponds to presence of α–carbonyl methylene, while peaks corresponding to unsaturation in *Jatropha curcas* oil are at 2.0, 2.8 and 5.3 ppm, and these are assigned to allylic, bis–allylic and olefinic hydrogen, respectively. A strong singlet signal

at 1.2 ppm represents methylene groups of the carbon chain. The terminal methyl protons are associated with the triplet arising at 0.8 ppm. The multiplet at 1.6 ppm is assigned to α–carbonyl methylenes. The peak at 2.72 ppm corresponds to polyunsaturated fatty acids, which arise from the methylene group between two double bonds of a higher polyunsaturated fatty acid chain.

5.3.2 Experimental results

Esterification with sulfuric acid: Initially, we conjectured that H_2SO_4 being a strong acid catalyst could bring out both esterification and transesterification reaction simultaneously. Varying acid catalyst concentration from 1 to 10 wt% transesterification reaction of virgin Jatropha oil was attempted at 12:1 alcohol to oil molar ratio at 65°C. It was observed that the highest percentage yield of FAME with this procedure was only up to 20%, even after prolonged sonication period of 5 h. Mechanical stirring for 5 h of the same reaction mixture could not yield FAME in the range of 17–20%. These results, as mentioned earlier section 5.2.3 corroborate that the esterification kinetics is relatively insensitive to method of providing convection in the reaction mixture, either through stirring or through sonication. The probable reason for failure in the production of higher yield of FAME with H_2SO_4 could be water inhibition of transesterification process. Large amount of water produced (due to presence of high free fatty acid in oil) during the esterification reaction can inhibit the transesterification reaction [3,13]. In view of this, the esterification and transesterification was carried out in consecutive steps in the subsequent experiments. Our preliminary experiments have already indicated that the kinetics of esterification reaction was rather insensitive to ultrasound irradiation, as almost same yield was obtained with mechanical stirring also.

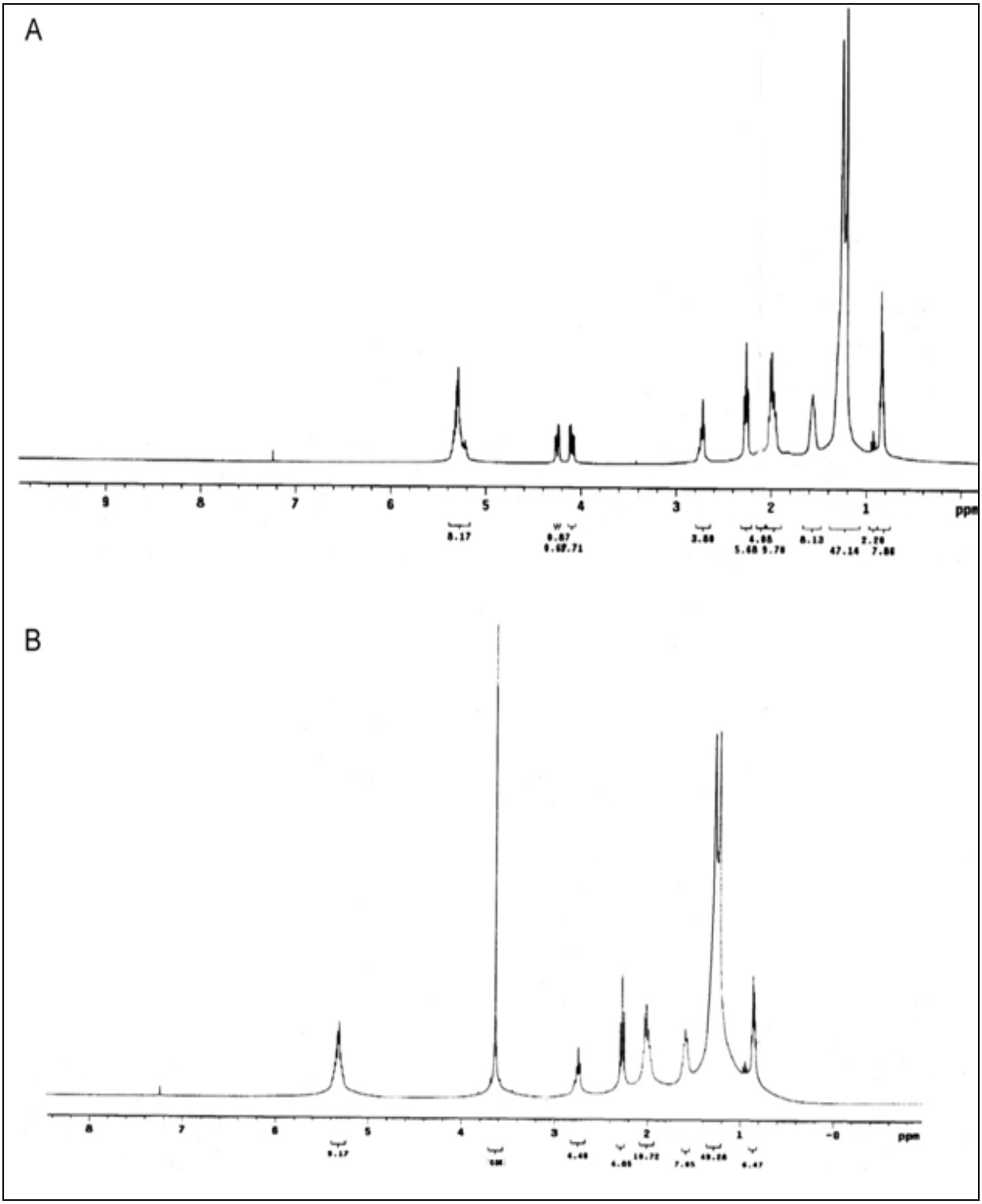

Figure 5.1: ^{1}H NMR spectrum of (A) pure Jatropha oil, and (B) fatty acid methyl ester(FAME) of Jatropha oil after trans–esterification.

Moreover, the initial experiments also indicated that intrinsic kinetics of the esterification and transesterification dominated the overall yield of the process, and mere sonication of reaction mixture was not enough to drive the reaction more towards product side. Intermediate removal of water and other impurities formed as reaction side product was essential prior to final transesterification experiments. Therefore, the esterification reactions (prior to transesterification) were carried out at 65^{o}C employing three molar ratios of alcohol to oil (viz. 10, 15 and 20) and three H_2SO_4 concentrations (viz. 1, 3 and 5 wt % of oil) with mechanical stirring instead of sonication.

***Transesterification experiments*:** The results of transesterification experiments in the Box–Behnken statistical design are given Table 5.2A. A quadratic regression model (given in equation 5.1) was fitted to the results using coded values for the experimental parameters (Minitab 15 software, trial version). The fitted model is:

$$Y = 79.48 + 7.30T + 2.11C - 1.29M - 26.32T^2 - 15.77C^2 - 25.73M^2 + 5.02\ T{\times}C + 0.29\ M{\times}C + 3.077M{\times}T \quad (5.4)$$

Notation: T – temperature, M – molar ratio and C – catalyst loading. The significant of each coefficient in the model equation was determined by standard t–test and p–values, which have also been given in Table 5.3A. Values of FAME yield calculated using this model matched very well with the experimental results. The significance of regression is indicated by the coefficient of determination (R^2), which was 99.09%. This essentially means that 99.09% of the effect on the yield for H_2SO_4 catalyst was explained by the variation in process variables. Table 5.3B shows the ANOVA for the quadratic model. The response surface 3–D plots indicating effect of interaction between any two variables (temperature–molar ratio or catalyst loading–temperature or molar ratio–catalyst loading), while holding the third parameter at its center point are shown in Fig. 5.2. Fig. 5.2A indicates that the FAME yield

shows a maximum for catalyst concentration & molar ratio, especially for medium values of both molar ratio and catalyst concentration. Similar behaviour is also seen for the variables temperature and molar ratios as evident from surface plot shown in Fig 5.2B. The values of variables in Fig.5.2A and B, corresponding to the maxima in yield are listed in Table 5.3C, along with the value of the yield as predicted by the model. It could be seen from results of Table 5.3C that for each of the plot 5.2 A, B, C, in which one variable was held at its center point, the optimum values of the other two variables are also near the center point. The global optimum values of the variables are: catalyst loading = 6.27 wt%, molar ratio = 6.96, temperature = 72.3^{o}C, and these values match quite closely with the optimum values of the plots 5.2 A, B, C. This is a very interesting result that optimum values of all three variables are near the center point, and the maximum FAME yield seen in Figs. 5.2 A, B, C, and the yield at globally optimum variables are almost same. An important observation is that no plateau is observed in any of the surface plots (the plateau is essentially indicative of nullification of interactive effect of variables on the FAME yield). The *p*–values of the ANOVA corroborate this result. Lowest *p*–value for temperature (0.001) indicates that it is more significant variable than the other two variables, viz. catalyst concentration (*p*–value 0.127) and alcohol to oil molar ratio (*p*–value 0.314). Thus, temperature has the strongest influence on the FAME yield. Among the *p*–values of regression coefficients for interactions of variables, the interaction between temperature and catalyst is most significant, as indicated by *p*–value of 0.028.

An inspection of Table 5.2A gives an idea of the relative influence and inter–relation of each of the variable on yield of transesterification. We cite below some examples:

For experiment set 2, the temperature (85^{o}C) is above optimum, catalyst concentration (6 wt%) is at optimum, however molar ratio (4:1) is below optimum, and the yield drops to 18%.

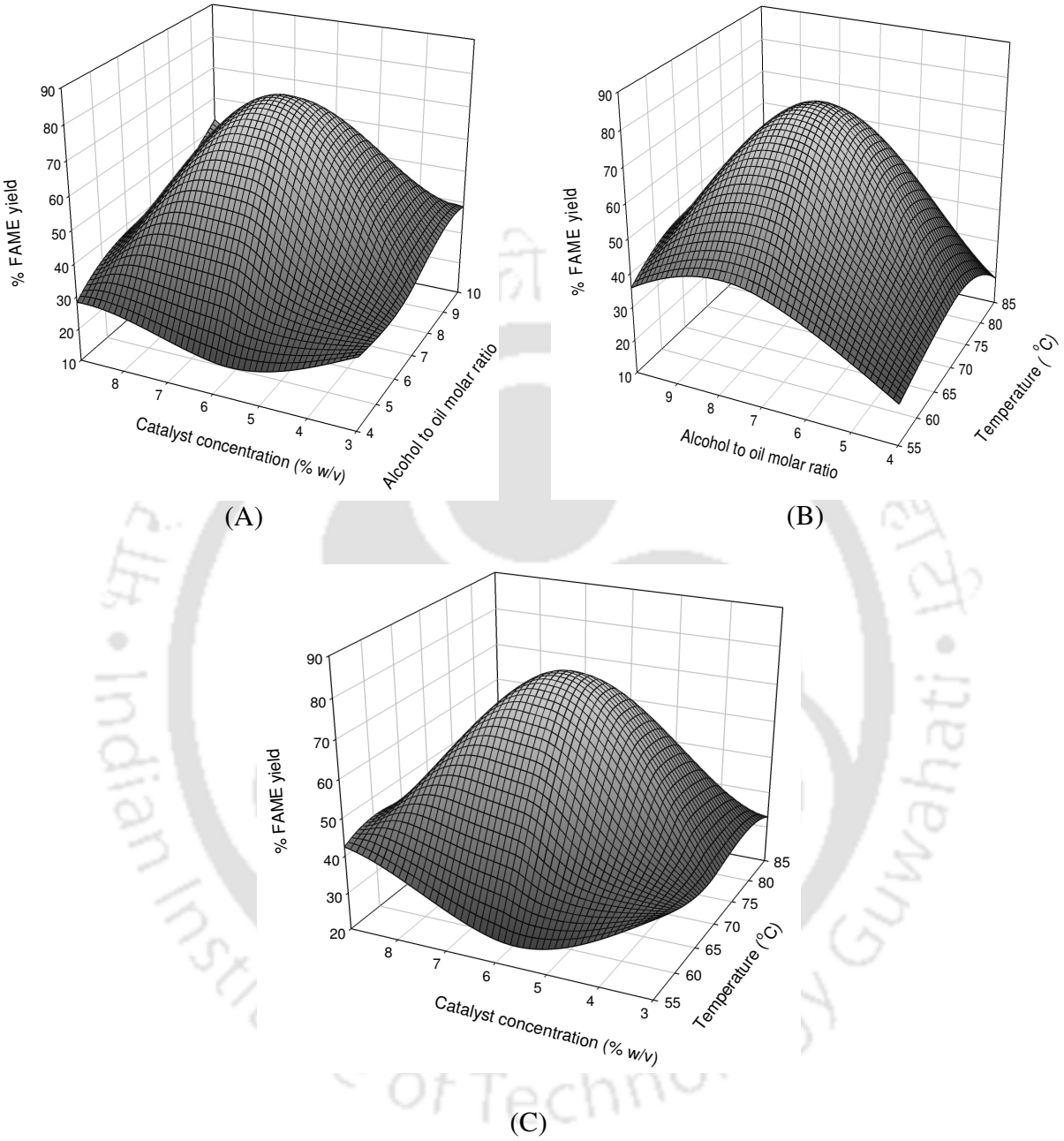

Figure 5.2: Response surface plots for % FAME yield as a function of reaction temperature, catalyst loading and methanol–to–oil molar ratio.

Table 5.3: Statistical analysis of experimental results

(A) Estimated Regression Coefficients for % FAME yield

Term	Coefficients	SE coeff	*t*–Stat	*p*–value
Constant (β)	79.480	1.889	42.079	0.
Temperature (T)	7.302	1.157	6.313	0.001
Molar ratio (M)	–1.293	1.157	–1.119	0.314
Catalyst (C)	2.116	1.157	1.830	0.127
Temperature × Temperature (T^2)	–26.322	1.703	–15.461	0.
Molar ratio × Molar ratio (M^2)	–25.730	1.703	–15.113	0.
Catalyst × Catalyst (C^2)	–15.770	1.703	–9.263	0.
Temperature × Molar ratio ($T{\cdot}M$)	3.077	1.636	1.881	0.119
Temperature × Catalyst ($T{\cdot}C$)	5.022	1.636	3.070	0.028
Molar ratio × Catalyst ($M{\cdot}C$)	0.295	1.636	0.180	0.864

(B) Analysis of variance (ANOVA) for transesterification of *Jatropha curcas* oil

Source	DF	Sq SS	Adj SS	Adj MS	F	*p*–value
Regression	9	5802.73	5802.73	644.75	60.24	0.
Linear	3	475.83	475.83	158.61	14.82	0.006
Square	3	5187.76	5187.76	1729.25	161.57	0.
Interaction	3	139.13	139.13	46.38	4.33	0.074
Residual Error	5	53.07	53.07	10.70	–	–
Lack–of–fit	3	53.07	53.07	17.69	80.08	0.012
Pure Error	2	0.44	0.44	0.22	–	–
Total	14	5856.24			–	–

(C) Analysis of surface plots

(Values of variable parameters for maximum yield for center point value of third parameter)

Fixed Parameter (Center point value)	Variable parameter		FAME Yield (%)
Catalyst loading = 6 wt%	Temperature = 72.1°C	Molar ratio = 6.95	80%
Temperature = 70°C	Molar ratio = 6.93	Catalyst loading = 6.2 wt%	79.6%
Molar ratio = 7	Temperature = 72.2 °C	Catalyst loading = 6.3 wt%	80.1%

Global optimized values: R^2 = 99.09%; R^2 (adj) = 99.44%, Molar ratio = 6.96 (–0.01581), Temperature = 72.3 °C (0.146341), Catalyst concentration = 6.27 wt% (0.09), Yield = 80.12%

- For experiment set 11, the temperature (70°C) is near optimum, catalyst concentration (9 wt%) is above optimum, however molar ratio (4:1) is below optimum, and the yield drops to 28%.
- For experiment set 12, the temperature (70°C) is near optimum, catalyst concentration (9 wt%) and molar ratio (10:1) are above optimum, the yield is relatively higher, i.e. 52.77%.
- For experiment set 9, the temperature (70°C) is near optimum; however, catalyst concentration (3 wt%) and molar ratio (4:1) is below optimum, and the yield drops to 32%.
- For experiment set 3, the temperature (55°C) is below optimum, catalyst concentration (6 wt%) is at optimum and molar ratio (10:1) is above optimum, and the yield drops to 30.7%.

The above results essentially show that the influence of all three variables on FAME yield is strongly inter–related. We try to seek physical explanation for the above trends after presentation of simulations results.

***Kinetic analysis of transesterification reaction*:** The kinetic study of the transesterification was carried out at the optimum conditions obtained from statistical analysis. This was aimed to find the pseudo 1st order kinetic constant and the activation energy of the reaction system. Keeping two variables, viz. catalyst concentration and molar ratio, at their optimum values, viz. 6 wt% and 7:1, respectively, the third variable of temperature was varied at three levels close to the optimum value, viz. 55, 62 and 70°C. The results of this study are shown in Figs. 5.3. Time history of conversion of triglycerides in the reaction mixture at different temperatures is shown in Fig. 5.3A, while analysis of the conversion data using pseudo first order kinetic model to determine the kinetic constants of reaction at different temperatures is shown in Fig. 5.3B. The kinetic constants obtained from the plot have been summarized in Table 5.4.

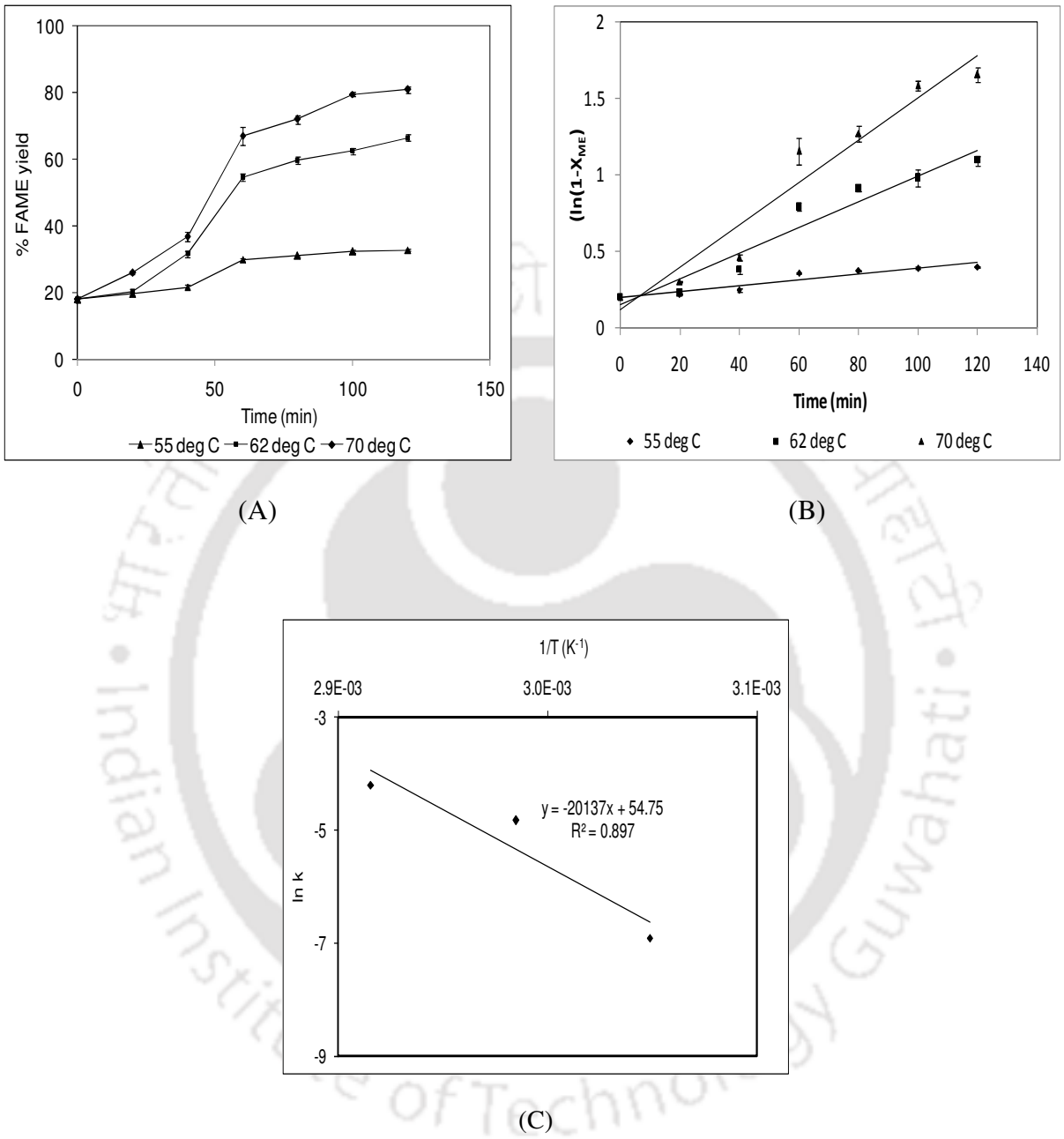

Figure 5.3: Kinetic analysis of transesterification of Jatropha oil under sonication. (A) Time history of conversion of triglycerides at different temperatures for methanol to oil molar ratio of 7:1 and catalyst concentration 6 wt%, (B) Pseudo 1st order kinetic model fitted to the conversion data for determination of kinetic constants at different reaction temperatures, (C) Arrhenius plot of ln (k) vs 1/T for the transesterification for methanol to oil molar ratio of 7:1 with catalyst loading of 6 wt%.

Table 5.4: Kinetic analysis of reaction data

Temperature (^oC)	Rate constant# (k) (min^{-1})
55	0.001 (R^2 = 0.903)
62	0.008 (R^2 = 0.938)
70	0.013 (R^2 = 0.943)

Pseudo 1st order kinetic constants at different temperature for methanol to oil molar ratio of 7:1 at 6 wt% of catalyst concentration

Interestingly, the kinetic constant shows a maximum with temperature at 70°C. With further rise in temperature above boiling point of methanol, the rate constant decreases and we attribute this anomaly to the phase of methanol (as most of methanol stays in vapor phase, while the transesterification reaction is in liquid phase). We have ascertained this hypothesis in an experiment carried out at 85°C. In this experiment, we have observed a kinetic constant of 0.002 min^{-1}. If methanol stays in vapor phase, the interaction between electrophillic carbonyl carbon of triglyceride and methanol reduces, thus decreasing the yield of the reaction. The Arrhenius plot of the experiments is given Fig. 5.3C to determine the activation energy of the reaction. The value of activation energy for transesterification reaction was found to be 167.419 kJ/mol. High activation energy for homogenous acid catalyzed transesterification (compared to homogenous base catalyst) probably results in slower reaction kinetics. This value is in accordance with previously reported value of 162 kJ/mol reported by Vujicic et al. [14] for biodiesel synthesis from sunflower oil over CaO heterogeneous catalyst.

5.3.3 Simulations results

The results of simulation of dynamics of a 10 micron air bubble are described in Figure 5.4, and the summary of simulations is given in Table 5.5.

The radial bubble motion in methanol at temperature near its boiling point is quite weak. There is very large evaporation of methanol into the bubble and the bubble contents at the collapse are dominated by methanol vapors (as indicated by the number of methanol molecules entrapped in the bubble). This vapor cushions the collapse of the bubble, at the same time increases the heat capacity of the bubble contents. Due to these two effects, the temperature and pressure peaks reached at the collapse of cavitation bubble are rather moderate. The species generated from dissociation of methanol vapor (CH_4, H_2O, CO_2) are essentially of molecular type. Thus, there is no sonochemical effect (i.e. generation of highly reactive radical species) involved. Moreover, the magnitudes of the microturbulence and acoustic waves generated by the bubble are also quite small to create any strong convection in the system. For example, if we compare the magnitudes of micro–turbulence velocity (0.038 m/s) and micro–streaming velocity (0.17 m/s, as noted earlier), we can perceive that the contribution of ultrasound to total convection in the medium is far higher.

5.4 Analysis

Analysis of the experimental and simulation results reveals some important facets of the physical mechanism of the acid esterification / transesterification process. The augmentation effect of ultrasound is marginal on esterification reaction. As far as transesterification is concerned, the reaction system seems to be dominated by its intrinsic kinetics. The simulations results reveal that there is no sonochemical effect involved – as there is no formation of any radical species from cavitation bubbles. Therefore, the beneficial effect of ultrasound on the reaction system is through strong micro–mixing and emulsification of oil and alcohol phases [12,15]. Moreover, contribution of convection due to ultrasound to emulsification is more predominant than cavitation bubbles.

Table 5.5: Summary of simulation results

Species	**Parameters for simulations**
	R_o = 10 μm, T_o = 328 K
	Results
	T_{max} = 566 K P_{max} = 21.9 MPa V_{turb} = 0.038 m/s P_{AW} = 78.7 kPa
	N_{N2} = 7.73 E+10 N_{O2} = 2.06 E+10 N_{MeOH} = 7.37 E+11
	Equilibrium composition of bubble at transient collapse
H_2O	2.68E-01
CH_4	5.85E-01
N_2	1.27E-01
CO_2	1.46E-02
H_2	3.14E-03
NH_3	1.07E-03
CO	3.72E-06
C_2H_6	3.19E-05

The viscosity of oil is quite high, and hence, the intensity of bubble motion is too low to create sufficient convection. The micro–streaming velocity is also expected to be quite small. Thus, the major contribution to the overall convection in the system is through micro–streaming in methanol.

An assessment of the results depicted in section 5.3.2 corroborates the above conclusion. We can see that even for high reaction temperatures (70^o or 85^{o}C), and also high catalyst concentration (6 or 9% w/w oil), the yield is low if the molar ratio is low (4:1). This is an obvious consequence of low convection intensity in the medium with low alcohol content, which is manifested in terms of less emulsification and lower interfacial area, due to which the protonation of carbonyl oxygen of triglyceride is reduced. Quite interestingly, the FAME yield reduces at temperature of 55^{o}C, while molar ratio being as high as 10:1. This could be a consequence of dilution of acid concentration in methanol at high molar ratio.

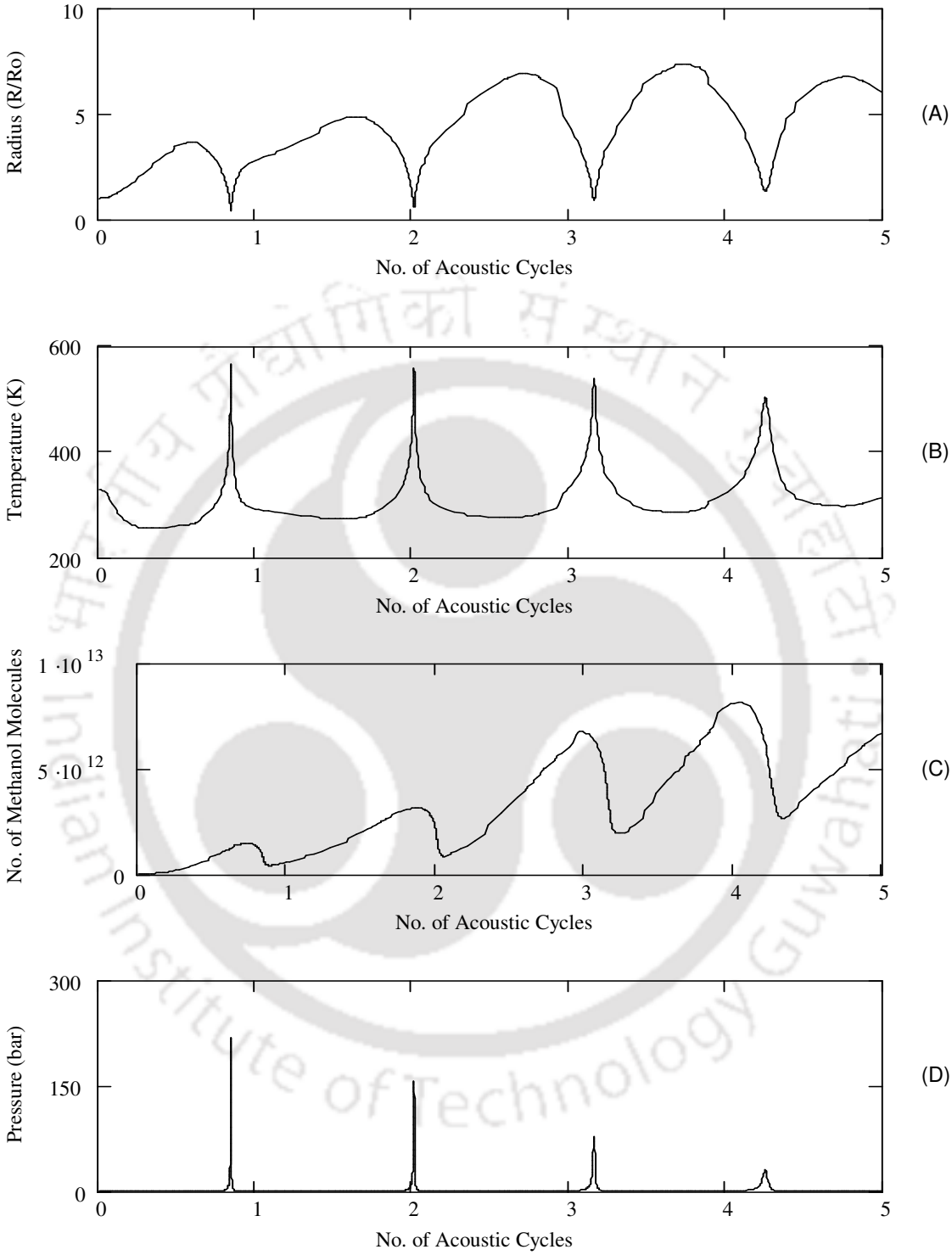

Figure 5.4

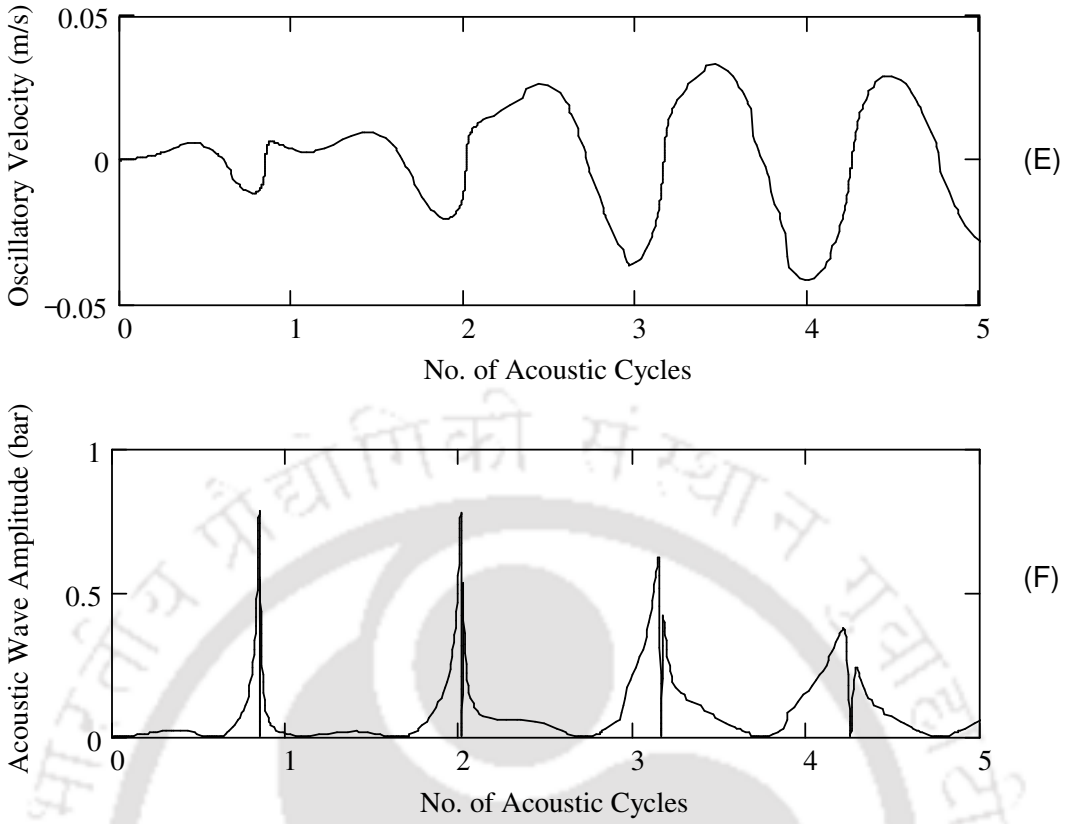

Figure 5.4 (*continued*….): Simulation results for radial motion of a 10 μm cavitation bubble (air) in methanol at 55°C. Time variation of (A) normalized bubble radius (R/R_o), (B) temperature in the bubble, (C) number of methanol molecules in the bubble, (D) pressure inside the bubble, (E) micro–convection (or oscillatory liquid velocity) generated by the cavitation bubble, (F) acoustic (or shock) waves emitted by the bubble.

Thus, although the convection in the reaction system is high due to larger quantity of alcohol, the net probability of interaction of proton in aqueous phase with carbonyl oxygen could be lower, leading to smaller yield. A rise of catalyst concentration to 9 wt% and temperature to 70°C almost doubles this yield. These results clearly show the relative influence of mass transfer and intrinsic kinetics on the transesterification reaction system. Mere enhancement of mass transfer with ultrasound is not sufficient to boost the overall kinetics of the process leading to high FAME yield. It also depends on factors such as catalyst concentration and temperature that determine the intrinsic kinetics of the reaction. Therefore, for maximum

yield of the transesterification process, an overall optimization in terms of all parameters is necessary and mere elimination of mass transfer limitation with sonication will not suffice. In this paper, we have addressed this issue and have given an overall optimization of the process with statistical approach.

Comparing these results with the base catalyzed system [7], in which the effect of sonication was far more marked, we present the following conjecture: In case of base catalyzed systems, the methoxide (CH_3O^-) is formed in the methanol phase, which attacks the carbonyl carbon of triglyceride at the interface between two phases. In case of acid catalyzed systems, it is the proton (H^+) that is produced by the acid attacks the carbonyl oxygen to protonate it, which is followed by the nucleophilic attack of methanol at the interface between two phases. Methanol being poor nucleophile, its intrinsic rate of reaction is much slower than the methoxide ion. Sonication can cause intense mixing between phases leading to high interfacial area, but it cannot alter the intrinsic reactivity of methoxide ion as well as methanol. Thus, the kinetics of acid catalyzed process does not get boosted with sonication as much as the base catalyzed process.

5.5 Conclusions

In this chapter, we have explored the acid catalyzed esterification / transesterification of Jatropha oil (which has high free fatty acid content) with mechanical stirring and sonication. The results of this study have revealed that kinetics of acid catalyzed esterification was relatively insensitive to ultrasound irradiation. On the other hand, the beneficial effect of sonication on transesterification reaction was only through the intense micro–mixing induced by ultrasound, and cavitation bubble did not render any impressive effect on boosting the kinetics. The transesterification system was revealed to be strongly controlled by intrinsic kinetics and mass transfer resistance. Simultaneous esterification / transesterification with

sonication did not succeed due to formation of water in the former step, and sonication alone could not overcome this snag. The most optimum values of different experimental variables have been determined as: alcohol to oil molar ratio ≈ 7, catalyst concentration ≈ 6 wt% and temperature ≈ 70°C. The influence of these variables is highly involved and interlinked, and any deviation of a parameter from its optimum value leads to sharp reduction in the FAME yield. The results of this study thus lead us to conclusion that the sonication of reaction mixture does not change the chemistry of the process and the beneficial effect is only of physical nature, which is further limited by the intrinsic kinetics and mass transfer.

References

[1] V. S. Moholkar, S. P. Sable, A. B. Pandit, Mapping the cavitation intensity in an ultrasonic bath using the acoustic emission, AIChE J. 46 (2000) 684–694.

[2] T. Sivasankar, A. W. Paunikar, V. S. Moholkar, Mechanistic approach to enhancement of the yield of a sonochemical reaction, AIChE J. 53 (2007) 1132–1143.

[3] X. Deng, Z. Fang, Y. Liu, Ultrasonic transesterification of *Jatropha curcas* L. oil to biodiesel by a two–step process, Energ. Conver. Manage. 51 (2010) 2802–2807.

[4] S. Jain, M. P. Sharma, Biodiesel production from *Jatropha curcas* oil, Renew. Sust. Energ. Rev. 14 (2010) 3140–3147.

[5] R. Toegel, B. Gompf, R. Pecha, D. Lohse, Does water vapor prevent upscaling sonoluminescence, Phys. Rev. Lett. 85 (2000) 3165–3168.

[6] B. D. Storey, A. J. Szeri, Water vapor, sonoluminescence and sonochemistry. Proc. R. Soc. Lond. Ser. A 456 (2000) 1685–1709.

[7] A. Kalva, T. Sivasankar, V. S. Moholkar, Physical mechanism of ultrasound assisted synthesis of biodiesel, Ind. Eng. Chem. Res. 48 (2009) 534–544.

[8] K. S. Kumar, V. S. Moholkar, Conceptual design of a novel hydrodynamic cavitation reactor, Chem. Eng. Sci. 62(10) (2007) 2698–2911.

[9] S. J. Krishnan, P. Dwivedi, V. S. Moholkar, Numerical investigation into the chemistry induced by hydrodynamic cavitation, Ind. Eng. Chem. Res. 45 (2006) 1493–1504.

[10] P. A. Parkar, H. A. Choudhary, V. S. Moholkar, Mechanistic and kinetic investigations in ultrasound assisted acid catalyzed biodiesel synthesis, Chem. Eng. J. 187 (2012) 248– 260.

[11] G. Eriksson, Thermodynamic studies of high temperature equilibria—XII: SOLGAMIX, a computer program for calculation of equilibrium composition in multiphase systems. Chem. Scr. 8 (1975) 100–103.

[12] Y. T. Shah, A. B. Pandit, V. S. Moholkar, Cavitation Reaction Engineering, Plenum Press, New York, 1999.

[13] M. A. Khan, S. Yusup, M. M. Ahmad, Acid esterification of a high free fatty acid crude palm oil and crude rubber seed oil blend: Optimization and parametric analysis, Biomass Bioenerg. 34 (2010) 1751–1756.

[14] Dj. Vujicic, D. Comic, A. Zarubica, R. Micic, G. Boskovic, Kinetics of biodiesel synthesis from sunflower oil over CaO heterogeneous catalyst, Fuel 89 (2010) 2054–2061.

[15] K. M. Rajkovic, J. M. Avramovic, P. S. Milic, O. S. Stamenkovic,V. B. Veljkovic, Optimization of ultrasound–assisted base–catalyzed methanolysis of sunflower oil using response surface and artificial neural network methodologies, Chem. Eng. J. 215–216 (2013) 82–89.

CHAPTER 6

Ultrasonic Jatropha Oil Biodiesel Synthesis Using Chlorosulfonic acid

6.1 Introduction

In the previous two chapters, viz. Chapter 4 and Chapter 5, we presented our studies in synthesis of biodiesel form *Jatropha Curcas* oil using heterogeneous base catalyst and homogenous acid catalyst. However, both of these processes were a two-step process of esterification followed by transesterification, which was necessitated by high FFA content of Jatropha Curcas oil. In case of base catalyst, high FFA content leads to formation of soap, while in case of homogeneous acid catalyst two-step process was necessary because water formed in the esterification step hydrolyze the TG, in addition to inhibiting and deactivating the proton. This lowers the kinetics of the process. Thus, an intermediate separation and purification of the oil phase after initial esterification was necessary prior to subsequent trans-esterification.

In this Chapter, we have presented a novel process for synthesis of Jatropha oil

biodiesel in a single step using a non-conventional acid catalyst without any intermittent purification and separation. This catalyst brings about in–situ removal of water formed during esterification process, thus, counteracting the inhibition. The esterification / transesterification process with chlorosulfonic acid thus obviates the need of intermediate purification of reaction mixture, giving high yields of biodiesel (comparable to those using base catalyst) in reasonable reaction periods. Our approach in this Chapter is same as earlier chapters in that we use a statistical experimental design (Box–Behnken method and fitted quadratic model with ANOVA) to determine the optimum reaction conditions. Moreover, we have also done Arrhenius and thermodynamic analysis of the process to determine the kinetics and thermodynamic parameter such as pseudo first order kinetic constant, activation energies, enthalpy and entropy change. This analysis has revealed interesting features of the chlorosulfonic acid catalyzed esterification/ transesterification process.

6.2 Theoretical Contemplation

Before proceeding to the experimental section we present herewith the theoretical contemplations that formed basis of the present study. As noted in the preceding section, the major problem with acid catalyzed esterification of free fatty acids in *Jatropha curcas* oil is the inhibition of the catalyst caused by the water formed in the esterification process. A discussion is given below regarding the mechanism through which this inhibition occurs.

Inhibition of acid catalyst during transesterification: The mechanism of the inhibition of homogenous acid catalyst in presence of water has been explained by Liu et al. [1] and Ataya et al. [2]. During esterification process, the protonation of the carbonyl oxygen is a fast quasi–equilibrium step. The subsequent nucleophilic attack of alcohol on the protonated carboxylic acid, resulting in formation of tetrahedral intermediate, is the rate determining step. Dissociation of sulphuric acid in aqueous medium results in formation of H_3O^+

(hydroxonium) ion and HSO_4^- (bisulphate) ions. Since H_3O^+ is strongly acidic species, the water content of the medium doesn't change the H_3O^+ concentration, or the rate limiting step. The inhibition effect of water on H_2SO_4 catalyst could be an effect of two causes, viz. decrease in acid strength and / or loss of catalyst accessibility. The protons H^+ generated from dissociation of H_2SO_4 can form either H_3O^+ ion or $CH_3OH_2^+$ (methoxonium) ion. Bronsted acid theory suggests $CH_3OH_2^+$ to be more acidic than H_3O^+ [3]. However, according to solvation chemistry of protons, it is the solvation state of the protons that determines the strength of strong acid like H_2SO_4 than the extent of dissociation. Greater solvation of protons results in lowering of its chemical and catalytic activity. Comparing among $CH_3OH_2^+$ and H_3O^+ ions, without taking into consideration solvation characteristics, a lower acidity for $CH_3OH_2^+$ is expected due to higher inductive effect of methyl group, which is in contradiction with the Brønsted acid theory. The solvation state of proton is determined by contribution of all solvating molecules. Strong hydrogen bond networks formed by water molecule can delocalize the charge on the H_3O^+ ion, thus stabilizing it. Comparing on this basis, the $CH_3OH_2^+$ ion (where steric hindrance of $-CH_3$ group comes into picture) has less ability to form hydrogen bonds. Secondly, comparing the solvation generated by H_2O and CH_3OH molecules, we see that H_2O is a better donor of electron pair than methanol. Therefore, contribution to solvation of protons by water molecule is much higher than methanol. Greater enthalpy release occurs during solvation of H_3O^+ and CH_3OH^+ in water than in methanol. On this basis, Liu et al. [1] and Pines and Fleming [4] hypothesize water as proton sponge that accommodates protons inside a self–assembled water network with lower entropic state. On the other hand, the solvation of proton by methanol molecules is hindered due to their smaller orientational polarizability, and lesser symmetry of the CH_3OH molecule than H_2O.

Ataya et al. [2] have put the reduction in catalytic activity of H_2SO_4 in a slightly

different context on the basis of hypothesis of Gileadi and Kirowa–Eisner, [5] which states that water molecule in presence of methanol acts as scavenger for proton to form H_3O^+ cation. Therefore, in an emulsion of reaction mixture comprising of CH_3OH, H_2O, H_2SO_4 and any FFA, a core of H_3O^+ cations and their sulphate anions can form micelles, with FFA molecule on the exterior. The hydrophilic end of FFA (containing the –OH tail) would be close to H_3O^+ core and the hydrocarbon end in the methanol phase. This phenomenon will result in formation of micelles of FFA–H_3O^+ with acid cores in the polar CH_3OH phase. However, these micelles are shielded from the bulk methanol phase. Formation of FFA–H_3O^+ micelles in the TG phase has also been proposed by Lotero et al. [6] who showed that acidic species are distributed in both alcohol and oil (or triglyceride) phase. The micelle in the triglyceride (TG) phase shields and reduces the accessibility of the acid catalyst by the TG molecules.

In summary, solvation of protons with water, higher energy is need for protonation of carbonyl oxygen in the FFA or TG by H_3O^+ proton carrier. Protonation of FFA/TG results in greater reduction in entropy that generates more geometric configuration for nucleophilic attack of methanol, thus increasing the collision efficiency.

Counter action of water inhibition during biodiesel synthesis by chlorosulfonic acid: Biodiesel synthesis in presence of chlorosulfonic acid occurs in three steps as given below.

(1) *Esterification*: As shown in scheme 6.1(A), reaction of a free fatty acid molecule with methanol in presence of chlorosulfonic acid catalyst results in formation of an ester and a water molecule [7].

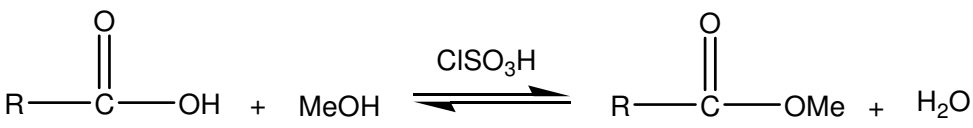

Scheme 6.1(A): Reaction of chlorosulfonic acid induced esterification process.

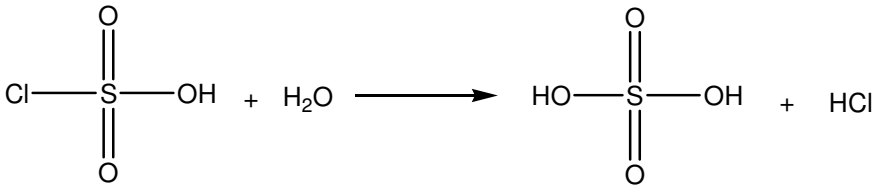

Scheme 6.1(B): Removal of water formed during esterification by chlorosulfonic acid

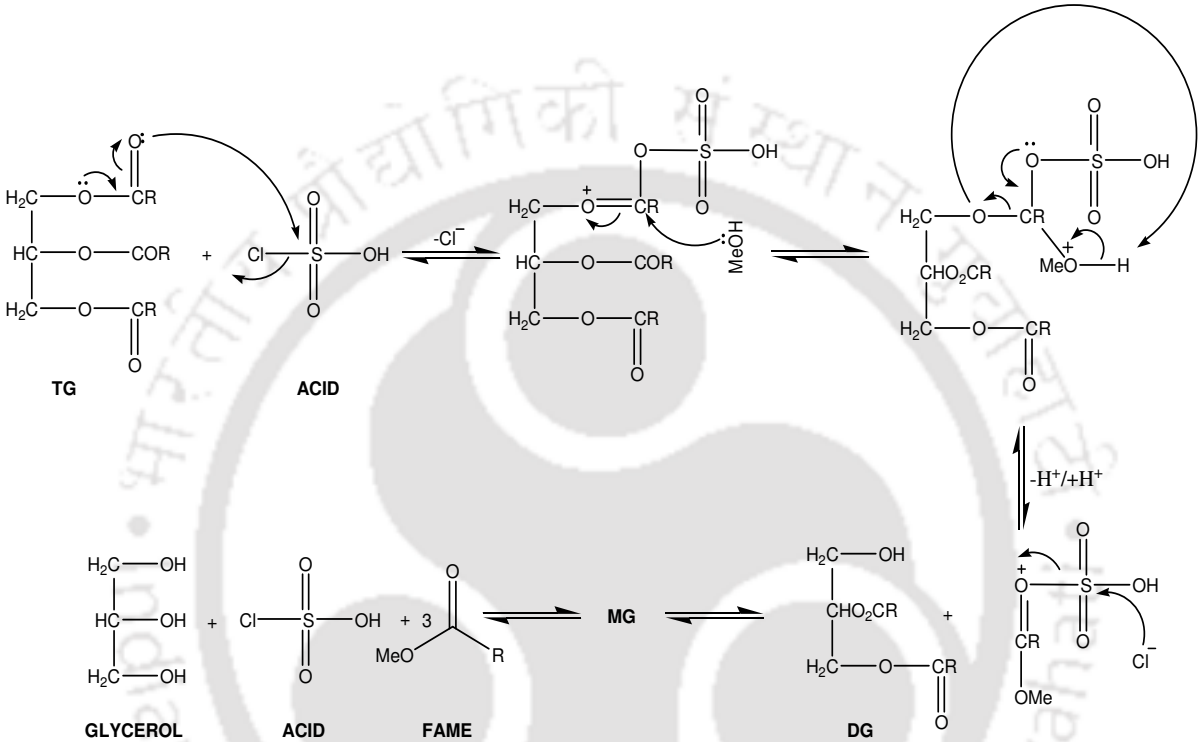

Scheme 6.1(C): Plausible mechanism of chlorosulfonic acid induced trans–esterification process.

(2) *In–situ removal of water by chlorosulfonic acid***:** The water produced in the esterification process reacts with chlorosulfonic acid molecule to produce H_2SO_4, as shown in scheme 6.1(B) [8]. Dissociation of H_2SO_4 thus produced can generate additional protons that catalyze the esterification /transesterification reaction. However, generation of H_2SO_4 is accompanied by in–situ removal of water molecule that solvate the H_3O^+ ion and reduce its activity. Although H_2O formed during esterification breaks the chlorosulfonic acid, resulting species of H_2SO_4 is strongly acidic that maintains the overall catalyst activity more or less constant.

The mechanism of H_2SO_4 catalyzed transesterification has been explained in Chapter 2 proposed by Lotero et al. [6].

(3) *Transesterification*: Scheme 6.1(C) shows the mechanism proposed for transesterification of TG in presence of chlorosulfonic acid catalyst. The initial transesterification is induced by scission of S–Cl bond of the chlorosulfonic acid creating electropositive centre on sulfur, which is attacked by the nonbonding electron of carbonyl oxygen. This generates an intermediate 'A' with electrophillic centre at the carbonyl–carbon of triglyceride, which is followed by nucleophilic attack of methanol on carbonyl–carbon of triglyceride. Rearrangement of intermediates with abstraction of proton by TG moiety produces diglyceride and catalyst bound ester. The attack of Cl^- ion on this intermediate regenerates chlorosulfonic acid catalyst with release of one FAME molecule. Consecutive reaction of di–glyceride (DG) and mono–glyceride (MG) then further produces two more molecules of FAME and regenerates the acid catalyst.With this conjectures and contemplation devised our transesterification experiments using statistical design.

6.3 Materials and Methods

6.3.1 Materials

Jatropha curcas oil (in crude form) was procured from local market. The acid value (AV) and saponification value (SV) of the oil was determined as 21.57 mg KOH/g and 201.2 mg KOH/g using standard methods described in the Chapter 4.Other chemicals used in experiments are methanol (Merck, India, AR grade 99%) and chlorosulfonic acid (Sigma Aldrich, India, AR grade 99%). These chemicals were also used as received without any further treatment.

6.3.2 Experimental setup

The schematic diagram of the experimental setup is given in Fig.6.1. Trans–esterification reaction was carried out in 100 mL beakers made of borosilicate glass. In order to conduct reactions at different temperatures, the beaker was submerged in the reservoir of a refrigerated circular bath (Jeio Tech, Model: Lab Companion RW 0525G) filled with water.

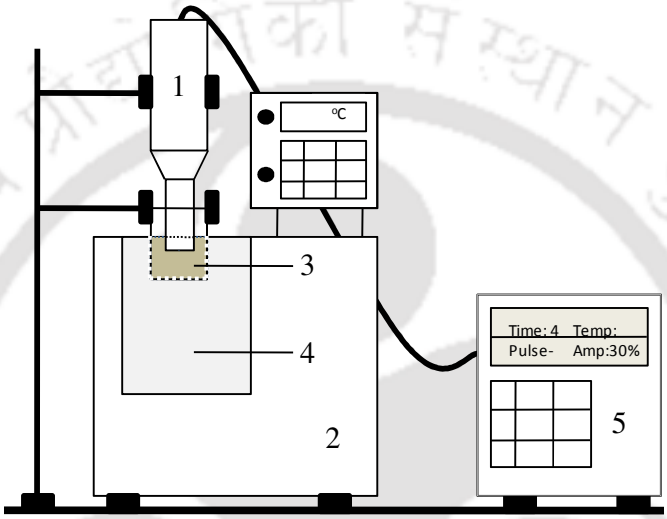

Figure 6.1: Experimental setup: (1) ultrasound probe, (2) refrigerated and heating bath circulator, (3) reaction mixture, (4) water in the refrigerated bath, (5) ultrasonic processor

The temperature of the water in reservoir was maintained at different levels, viz. 30, 45 and 60^{o}C. Internal circulation of water was provided so as to maintain a constant temperature. The temperature of reaction mixture was monitored with a digital thermometer, and was found to be same as that of the water in the reservoir. A programmable microprocessor based ultrasonic processor (Sonics and Materials Inc., Model: VCX 500) was used for sonication .This processor had operating frequency of 20 kHz with a sonicator probe of 25 mm diameter. It was fabricated from high grade titanium alloy (Ti–6Al–4V). The processor was facilitated with automatic tuning and frequency control and automatic

amplitude compensation. The amplitude for all the experiments was set to 25% corresponding to a power input of 125 W (theoretical maximum power). The actual acoustic pressure amplitude was determined using calorimetric measurement with methanol as the medium as 1.6 bar [11].

6.3.3 Experimental Protocol

Base case experiment: Initially, as the base case of experiments, esterification / transesterification was carried out using mechanical stirring of reaction mixture. This reaction was conducted at 65°C for 16 h with 20:1 alcohol to oil molar ratio and catalyst concentration of 5 wt% oil with total reaction volume of 15mL. The progress of the reaction was monitored by withdrawing aliquots (500 µL) of reaction mixture every 4 h and analyzing for conversion of triglyceride and free fatty acid with ^{1}H NMR (Varian 400 MHz FT–NMR) spectrometry with $CDCl_3$ as solvent and TMS (tetramethylsilane) as internal standard [12–13].

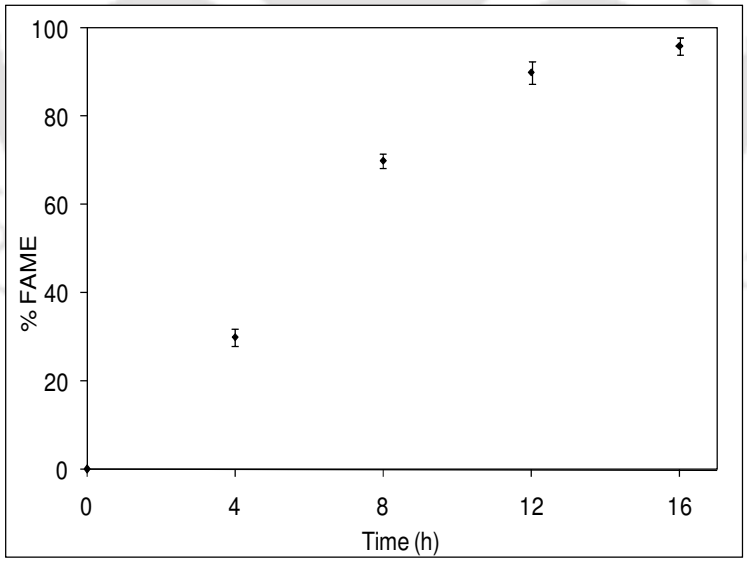

Figure 6.2: Control experiment for transesterification with mechanical agitation. Reaction conditions: temperature = 65°C, molar ratio = 20:1, catalyst concentration = 5 wt% oil, Agitation = 300 rpm. Reaction mixture: Oil = 13.6 mL, MeOH = 11.4 mL, Catalyst = 0.4 mL

This method gives the gross conversion (X) of TG and FFA to their corresponding ester. We have termed this conversion as percentage yield of FAME (100×) and all kinetic and thermodynamic analysis has been made on this basis. The results of base case experiments revealed percentage FAME yield of ~ 90% after 16 h given in Fig. 6.2. The slow kinetics of acid catalyzed biodiesel synthesis, as mentioned earlier, is evident from this result.

Statistical experimental design (single step esterification–transesterification): Further experiments were carried out using sonication (or ultrasound irradiation) of the reaction mixture (total reaction volume 15 mL) so as to boost its kinetics, as noted earlier. These experiments were devised as per the statistical experimental design (Box–Behnken method). The following experimental parameters (or independent variables) have been chosen for optimization: catalyst loading (C), temperature (T), and alcohol to oil molar ratio (R). The experiments were conducted with a fixed sonication time of 4 h, based on our initial experiments. The actual and coded values of different experimental parameters (i.e. levels of the independent variables) used in the Box–Behnken design are shown in Table 6.1. The response variable, i.e. % FAME yield (or percentage conversion of TG and FFA), was fitted with a full quadratic model (given in equation 6.1) in order to correlate it to the experimental parameters or independent variables.

$$Y = \beta_0 + \sum_{i=1}^{3} \beta_i x_i + \sum_{i=1}^{3} \beta_{ii} x_i^2 + \sum_{i=1}^{2} \sum_{j=i+1}^{3} \beta_{ij} x_i x_j \qquad (6.1)$$

Notations are as follows: Y = response variable (i.e. % FAME yield); β_0 = constant; β_i, β_{ii} and β_{iii}= regression coefficients; x_i and x_j = coded independent variables. The Box–Behnken statistical design of experiments, devised using Minitab 15 software (trial version) comprises of 15 sets with (3 factors and 3 levels) with different combinations of parameters. The experimental conditions in these sets are given in Table 6.2A, while exact composition of reaction mixture in each set is given in Table 6.2B. The progress of the esterification–

transesterification reaction was monitored by withdrawing 500 µL aliquots of the reaction mixtures every 30 min. In order to quench the reaction, the aliquots were immediately mixed with 1 mL 0.05 N NaOH, and centrifuged at 6000 rpm for 10 min to separate the acid catalyst and aqueous phase (comprising of glycerol and alcohol). The organic layer was then analyzed by ^{1}H NMR to determine the percentage yield of FAME.

Table 6.1: Experimental range and levels of independent variables

Independent Variables (or Factors)	Symbol coded	Levels of Factors Coded Value (Actual value)		
Catalyst concentration (wt% oil)	C	–1 (1)	0 (5)	+1 (9)
Temperature (^{o}C)	T	–1 (30)	0 (45)	+1 (60)
Alcohol to oil molar ratio (R)	M	–1 (10:1)	0 (20:1)	+1 (30:1)

Table 6.2A: Box–Behnken experimental design matrix

Sl. No.	**Catalyst (wt% oil)**	**Molar ratio**	**Temperature (^{o}C)**	**% FAME yield**	**Fitted % FAME yield**
1	1 (–1)	10(–1)	45(0)	15.09 ± 0.67	12.01
2	5 (0)	10(–1)	60 (+1)	69.91 ± 1.67	65.04
3	9 (+1)	20(0)	30(–1)	59.99 ± 1.29	52.05
4	1(–1)	20(0)	60(+1)	24.68 ± 0.75	32.61
5	5(0)	30(+1)	30(–1)	32.70 ± 0.68	37.56
6	5(0)	20(0)	45(0)	80.12 ± 3.5	76.66
7	5(0)	30(+1)	60(+1)	53.56 ± 0.51	54.48
8	1(–1)	30(+1)	45(0)	27.67 ± 0.49	18.80
9	1(–1)	20(0)	30(–1)	15.20 ± 1.11	19.20
10	9(+1)	30(+1)	45(0)	53.65 ± 1.14	56.72
11	9(+1)	10(–1)	45(0)	56.87 ± 0.87	65.73
12	5(0)	20(0)	45(0)	76.56 ± 1.46	76.66
13*	**9(+1)**	**20(0)**	**60(+1)**	**95.4 ± 1.03**	**91.4**
14	5(0)	10(–1)	30(–1)	30.13 ± 1.19	29.2
15	5(0)	20(0)	45(0)	73.31 ± 3.5	76.66

* The bold values indicate experimental set with the highest FAME yield.

Conventional two–step experiments: As noted in previous section, one of the contemplations underlying this study was that chlorosulfonic acid causes in–situ removal of water formed during esterification process, thus eliminating the water inhibition to acid catalyzed transesterification.

Table 6.2B: Composition of reaction mixture in Box–Behnken experimental design matrix

Sl No.	Catalyst (wt% oil)	Molar ratio	Temperature (^oC)	Oil Volume (ml)	Methanol Volume (ml)	Catalyst added (g)
1	1	10	45	17.5	7.5	0.1
2	5	10	60	17.5	7.5	0.5
3	9	20	30	13.5	11.5	0.7
4	1	20	60	13.5	11.5	0.07
5	5	30	30	11	14	0.3
5	5	20	45	13.5	11.5	0.4
7	5	30	45	11	14	0.3
8	1	30	45	11	14	0.06
9	1	20	30	13.5	11.5	0.07
10	9	30	45	11	14	0.6
11	9	10	45	17.5	7.5	0.9
12	5	20	45	13.5	11.5	0.4
13	9	20	60	13.5	11.5	0.7
14	5	10	30	17.5	7.5	0.5
15	5	20	45	13.5	11.5	0.4

In order to ascertain this conjecture, we have also carried out biodiesel synthesis with crude *Jatropha curcas* oil with conventional two–step approach of separate esterification and transesterification, with intermediate purification of the reaction mixture to remove water formed during esterification. In these set of experiments, the esterification experiments were carried out for 1 h using H_2SO_4 catalyst (3 wt% oil) at 65^oC and 15:1 molar ratio. These values were decided on the basis of our earlier study [14]. This process essentially converts almost all FFA (> 95%) into corresponding esters. This reaction mixture was neutralized by

addition of 0.05 M NaOH solution. The organic layer was separated and washed 3 times with hot water to remove all traces of acid and alcohol. This layer was dried on activated silica to remove traces of water. This layer is essentially FFA free Jatropha oil containing triglycerides. The transesterification of this layer with sonication was then carried out using chlorosulfonic acid catalyst. The experimental parameters (viz. molar ratio and catalyst concentration) used in this transesterification reaction were essentially same as the optimized conditions obtained from statistical experimental design, as described in previous section. The reaction temperature, however, was varied at three levels, viz. 30, 45 and 60^{o}C for kinetic and thermodynamic analysis with a fixed reaction time of 3 h. The comparison of yield and kinetics of these experiments with the single step experiments (based on statistical design described in previous section) give an estimate of the beneficial effect of in–situ removal of chlorosulfonic acid.

Determination of transesterification kinetics: Synthesis of biodiesel in single step reactions with chlorosulfonic acid catalyst occurs in four consecutive and reversible reactions steps. The first step is the reaction of free fatty acid (FFA) with methanol to give one molecule of FAME and water. The chlorosulfonic acid reacts with water molecule to yield H_2SO_4 which itself can catalyse both esterification and transesterification steps. The ensuing transesterification step begins with the reaction of triglyceride (TG) and methanol to produce diglycerides (DG) and one molecule of FAME this is followed by reaction of diglyceride with methanol yields monoglycerides (MG) and another molecule of FAME. In final step, monoglyceride reacts with methanol to yields third molecule of FAME and one mole of glycerol. Thus, four molecules of FAME (one from esterification of an FFA molecule and three from transesterification of a TG molecule) and one molecule each of glycerol is formed after completion of the reaction. In our analysis, we have determined the kinetic constant of the overall reaction, without accounting for the intermediate steps.

Since the FFA content of the *Jatropha curcas* oil is rather low, it is the kinetics of transesterification step that governs the overall process time and yield of biodiesel. Based on our previous studies, we have assumed the transesterification reaction to follow pseudo 1st order kinetics and the equation fitted to the conversion data is:

$$\ln(1-X) = -kt \qquad (6.2)$$

where X = conversion of triglyceride at any time t. Plot of $-\ln(1-X)$ vs t gives the kinetic constant k as the slope.

Determination of activation energy (Arrhenius plot): A relationship between the specific reaction rate constant (k), absolute temperature (T) and the energy of activation (E_a) is given by the Arrhenius equation as: $k = A \times \exp(-E_a/RT)$ where A is the frequency factor and R is universal gas constant (J mol^{-1} K^{-1}).

To determine the activation energy of the single step process (involving both esterification and transesterification), experiments were conducted at three different temperatures viz. 30, 45 and 60°C. The catalyst concentration and molar ratio in these experiments were same as the global optimum values obtained from statistical experimental design. In order to deduce the change in activation energy from conventional double step process to single step process, experiment were conducted in two step procedure at same three temperatures as that of the single step process. The Plot of ln (k) vs $1/T$ gives slope equal to ($-E_a/R$) from which activation energy can be determined.

6.4 Result and Discussion

6.4.1 Statistical analysis

Single step transesterification experiments: As noted earlier, these experiments were based on Box–Behnken statistical design. The results of the 15 sets of experiments in this design are given in the Table 6.2A. The quadratic regression model fitted to these results using equation

6.1 is given below:

$$Y = 76.66 + 13.19T - 0.55M + 22.90C - 9.79T^2 - 20.29M^2 - 18.05C^2 - 4.73T \times M - 3.95M \times C + 6.48T \times C \quad (6.3)$$

where, *T*, *M* and *C* indicates temperature, molar ratio and catalyst concentration respectively. The significance of coefficients corresponding to each parameter is estimated by the *t*–test and *p*–value given in Table 6.3A. Table 6.3B shows the ANOVA for the quadratic model. The values of FAME yield predicted by this model are in excellent agreement with the experimental values. The overall R^2 value of the regression is 0.95, which reveals excellent fit of the model to the experimental data and point that 95.5% of the effect on the yield for chlorosulfonic acid catalyst was explained by the variation in process variables.

The fitted quadratic equation is in terms of the coded values of the parameters and not in absolute values. A *p*–value of < 0.05 of any coefficient (either linear or quadratic interaction) designates it as significant or insignificant. On this basis molar ratio is relatively insignificant than the other two parameters, viz. temperature and catalyst concentration. Moreover, the interaction effects between process parameters were found to be insignificant. The response surface plots depicting variation in FAME yield as a function of any two process parameters (as independent variable parameters), with the value of third process parameter (fixed parameter) held at its center point in the Box–Behnken design are given Fig. 6.3. These plots are representatives of the interactive effect of the two process parameter on the yield. It could be seen from surface plots that the yield shows a maxima for a particular combination of two process parameters that are treated as variables for the plot. Table 6.3C gives the exact values of the process parameter in each of the three surface plots (either from combination of temperature–molar ratio, molar ratio–catalyst concentration and catalyst concentration and temperature) for which maxima in yield is obtained.

Table 6.3: Statistical analysis of experimental results

(A) Estimated regression coefficients for % FAME yield

Term	**Coefficients**	**SE coeff**	***t*–Stat**	***p*–value**
Constant (β)	76.66	5.2	14.73	0.
Temperature (T)	13.19	3.18	4.14	0.
Molar ratio (M)	–0.55	3.18	–0.17	0.869
Catalyst (C)	22.9	3.18	7.19	0.001
Temperature × Temperature (T^2)	–9.79	4.69	–2.09	0.091
Molar ratio × Molar ratio (M^2)	–20.29	4.69	–4.33	0.008
Catalyst × Catalyst (C^2)	–18.05	4.69	–3.85	0.012
Temperature × Molar ratio (TM)	–4.73	4.5	–1.05	0.342
Temperature × Catalyst (TC)	6.48	4.5	1.44	0.21
Molar ratio × Catalyst (MC)	–3.95	4.5	–0.88	0.421

(B) Analysis of variance (ANOVA) for transesterification of Jatropha oil

Source	DF	Sq SS	Adj SS	Adj MS	F	*p*–value
Regression	9	8629.32	8629.32	958.81	11.8	0.007
Linear	3	5593.	5593.	1864.33	22.95	0.002
Square	3	2716.32	2716.32	905.44	11.15	0.012
Interaction	3	319.99	319.99	106.66	1.31	0.368
Residual Error	5	406.15	406.15	81.23	—	—
Lack–of–Fit	3	382.95	382.95	127.65	11.	0.084
Pure Error	2	23.2	23.2	11.6	—	—
Total	14	9035.47			—	—

$R^2 = 0.955$; R^2 (adj) = 0.874

(C) Analysis of surface plots

(Values of variable parameters for maximum yield for center point value of third parameter)

Fixed parameter (Center point value)	**Variable parameter**		**FAME Yield (%)**
Catalyst concentration = 5 wt% oil	Temperature = 55.4 °C	Molar ratio = 19.1	81.3%
Temperature = 45°C	Molar ratio = 19.3	Catalyst concentration = 7.6 wt% oil	84%
Molar ratio = 20:1	Temperature = 59.1 °C	Catalyst concentration = 8.2 wt% oil	92%

GLOBAL OPTIMUM: Catalyst = 8.35, Molar ratio = 17.89, Temperature = 60 °C, Yield = 93%

Inspection of the Table 6.3C, which gives the optimum combination of process parameters for the highest yield in the three surface plots, reveals that the optimum value of molar ratio (whether considered as fixed or variable parameter) for the highest yield remains the same. The highest yield of 92% is obtained when both transesterification temperature and catalyst concentration is high. The temperature 59.1^{o}C for the highest yield is close to the boiling point of methanol. The yield drops marginally if either temperature or the catalyst concentration is lowered. An interesting observation is that the molar ratio required for high yield with chlorosulfonic acid catalyst (20:1) is more than double that of the molar ratio required for sulphuric acid catalyst in a two step process. The probable causes for large requirement of alcohol are as follows:

(1) The transesterification process in case of chlorosulfonic acid begins with activation of carbon–oxygen bond of the carbonyl carbon of TG by acid rather than direct protonation for the case of H_2SO_4 as reported by Lotero et al. [6]. The intermediate 'A' formed after the activation of carbon–oxygen bond by chlorosulfonic acid is a very large molecule. As a result the methanol molecule trying to access the electrophillic centre is likely to face significant steric hindrance. Therefore, large quantities of alcohol are required to over populate the hindered site and to drive the reversible transesterification reaction towards forward direction.

(2) All the water formed during the esterification of FFA may not be removed from the reaction medium by chlorosulfonic acid immediately. Thus, traces of water present in the reaction mixture at any point of time can drive the reversible reaction of acid catalysed aqueous hydrolysis. To counteract this large amount of alcohol is required to drive forward the esterification reaction.

The global maximum of the FAME yield (93%) as per the quadratic regression model is obtained for conditions: Catalyst concentration ≈ 8.35, molar ratio ≈ 18:1 and temperature ≈ 60 ^{o}C.

Table 6.2A gives comparative analysis of FAME yield results in different experimental set that helps us to deduce the relative influence of each of the process parameters under study.

Comparison of results of experimental sets 4 and 9 reveals the influence of temperature. With a low catalyst concentration of 1 wt% and molar ratio of 20:1, the FAME yield show as 75% increase as the temperature is doubled from 30^{o}C to 60^{o}C.

Comparison of results of sets 1and 11 reveals that increasing catalyst concentration from 1 to 9 wt% can take yield to significantly high value of ~ 66%.

Comparison of results of sets 2 and 7 reveals the insignificant influence of the molar ratio. Even with 3× increase in molar ratio at catalyst concentration of 5 wt% and temperature of 60 ^{o}C, the FAME yield shows a trivial rise of ~ 20%. Similar trend is also seen from the result of experimental set 1 and 8.

The above results clearly identify catalyst concentration and temperature as the most significant variable of the process affecting FAME yield. The highest yield is therefore seen for catalyst concentration of 9 wt%, temperature of 60 ^{o}C and moderate molar ratio of 20:1. Lower FAME yield at very large molar ratio of 30:1 could be a consequence of rather dilute acid concentration in aqueous phase.

Intrinsic kinetics vs. mass transfer: Comparison of biodiesel yield with ultrasound under optimized conditions of molar ratio, temperature and catalyst concentration with the base case experiment (under mechanical agitation) reveals that fine emulsification generated by micro–convection induced by ultrasound and cavitation reduces the mass transfer limitations, thus boosting the gross kinetics of the reaction. As regards to physical mechanism of the ultrasonic process, we have shown in our earlier papers [14, 15–17] that convection generated by ultrasound/cavitation in methanol phase is mainly responsible for formation of emulsion.

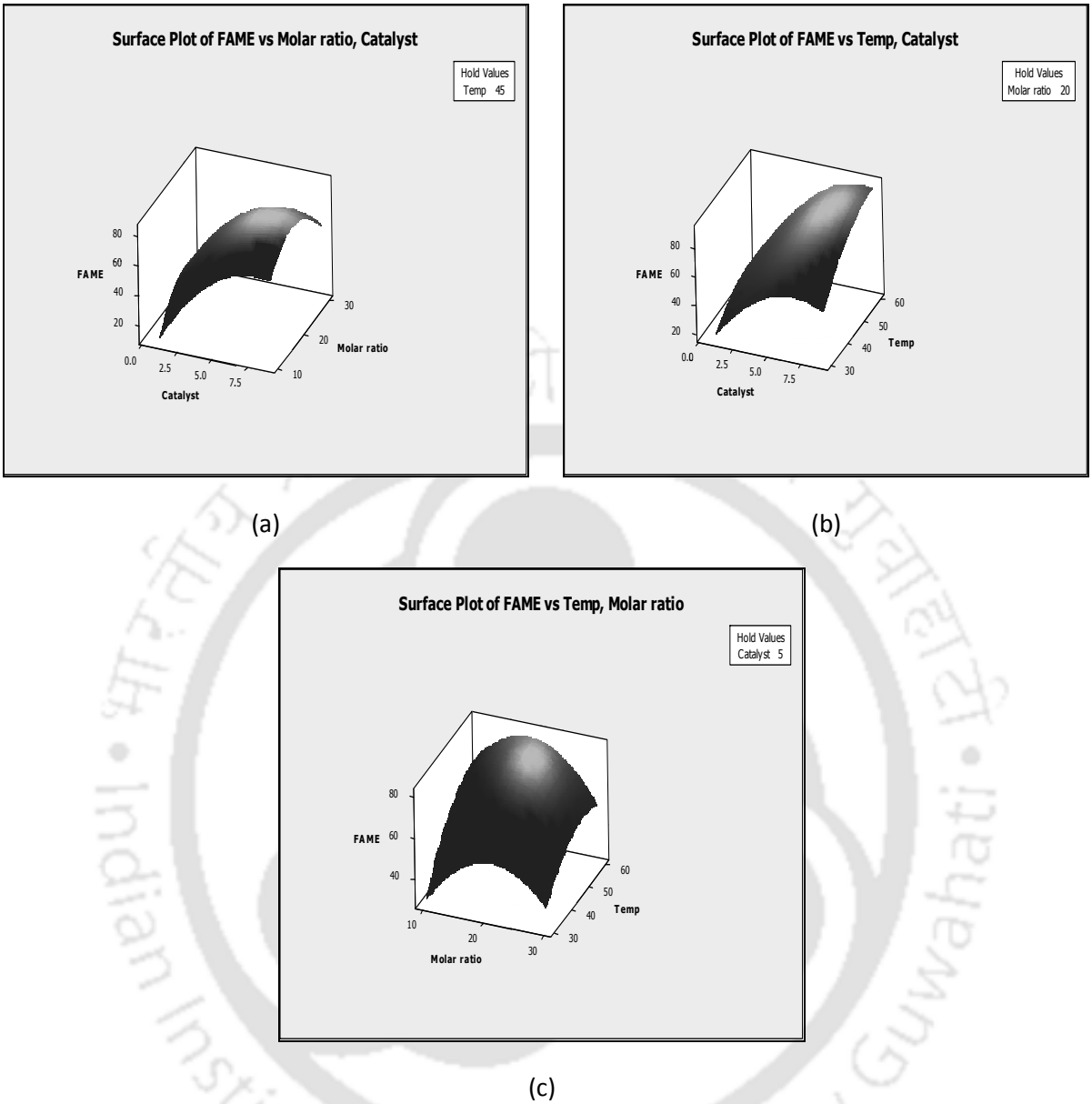

Figure 6.3: Response surface plots for % FAME yield as a function of reaction temperature, catalyst loading and methanol–to–oil molar ratio

Given this result, in the Box–Behnken experimental design, the net interfacial area between oil/methanol phases is likely to be in the reactions in which the highest for molar ratio of 30:1 is employed. However, as discussed earlier, the FAME yield in Box–Behnken experiments reduces at very high molar ratio of 30:1. These results clearly reveal the relative roles of mass transfer and intrinsic kinetics on the reaction system. Subsequent to formation of fine

emulsion with ultrasonication, the reaction system is controlled by intrinsic kinetics, which in turn depends on catalyst concentration (that determines the activation energy) and the temperature. It should also be pointed out that probability of interaction between acid and triglyceride molecule reduces at higher molar ratios due to lower concentration of acid, and this factor also contributes to lowering of the gross kinetics of the process leading to smaller yields.

6.4.2 Kinetic and thermodynamic analysis

The kinetics of the single step biodiesel synthesis was studied at three temperatures for global optimum conditions of molar ratio and catalyst concentrations. The time history of the FAME yield and the pseudo 1st order kinetic model fitted to the data is shown in Fig. 6.4A and 6.4B. In order to compare kinetic behaviour of the single step and double step process experiment have been conducted with two–step procedure also. The temperature of experiment of the second step (i.e. transesterification) was kept at same values, i.e. 30, 45 and 60^{o}C. The catalyst concentration and molar ratio were same as the global optimum of single step process with fixed reaction time of 3 h. The time history and the pseudo 1st order kinetic model fit to the kinetic data are shown in Figs. 6.4C and 6.4D.

Table 6.4 lists the pseudo 1st order kinetic constants and activation energy for both single and double–step experiments at three temperatures, while Fig. 6.5 shows the corresponding Arrhenius plots. It could be seen that the kinetic constants for both single and double step processes at different temperatures do not show significant variation. The activation energy for single step biodiesel synthesis is 57.3 kJ/mol, and interestingly it shows a reduction of ~ 40% to 31.3 kJ/mol for the double–step process. We attribute this reduction of activation energy to almost complete absence of water in the reaction mixture in the transesterification in double step process.

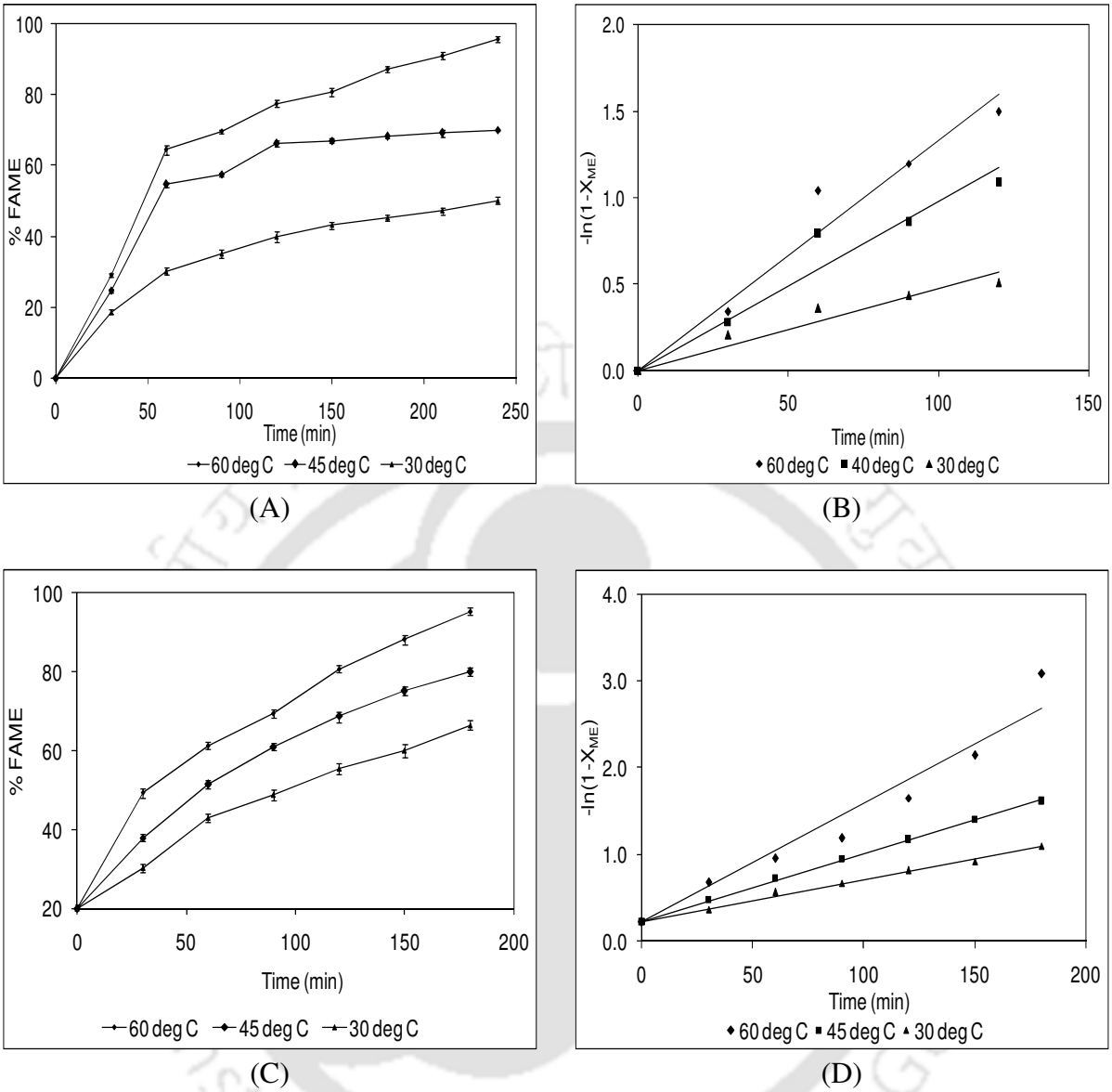

Figure 6.4: (A) Time history of FAME yield at different reaction temperatures for single–step transesterification process, (B) Fitting of pseudo first order kinetic model to the conversion data for single–step transesterification process. Best fit equations: For 30^{o}C, y = 0.00472 x, R^2 = 0.92; For 45 ^{o}C, y = 0.00976 x, R^2 = 0.94; For 60 ^{o}C, y = 0.0133 x, R^2 = 0.954, (C) Time history of FAME yield at different reaction temperature for 2–step transesterification process, (D) Fitting of pseudo first order kinetic model to the conversion data for 2–step transesterification process. Best fit equations: For 30 ^{o}C, y = 0.00485 x + 0.22, R^2 = 0.99; For 45 ^{o}C, y = 0.00787 x + 0.22, R^2 = 0.99; For 60 ^{o}C, y = 0.0137 x + 0.22, R^2 = 0.945.

Table 6.4: Kinetic analysis of transesterification process

Temperature in ^{o}C (K)	Single step process		Double step process	
	pseudo 1st order kinetic constant (min^{-1})	Activation Energy (kJ/mol)	pseudo 1st order kinetic constant (min^{-1})	Activation Energy (kJ/mol)
65 (333)	0.0133		0.0137	
45(318)	0.0096	57.33	0.0078	31.29
30(303)	0.0047		0.0048	

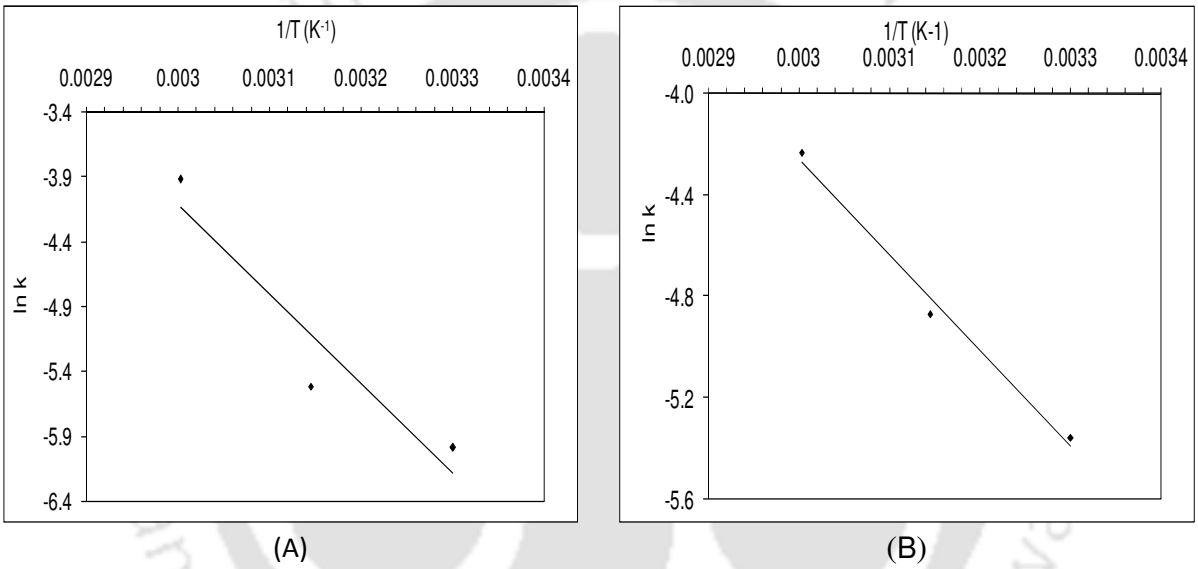

Figure 6.5: Arrhenius plot for determination activation energy of transesterification process. (A) Single step process, Best fit: $y = -6895.1\ x + 16.57$, $R^2 = 0.89$, (B) Double step process with intermediate water removal after esterification, Best fit: $y = -3764.2\ x + 7.0357$, $R^2 = 0.99$.

Contrary to this, despite in–situ water removal by chlorosulfonic acid, some traces of water may be left out in the reaction mixture in the single step process, which contribute to catalyst inhibition and rise in the activation energy. Comparing the values of activation energy for chlorosulfonic acid catalyzed biodiesel synthesis with the activation energy observed with that of H_2SO_4 catalyzed biodiesel synthesis gives a very interesting result. In our own

experiments with H_2SO_4 catalyzed esterification/transesterification of crude *Jatropha curcas* oil, we have observed an activation energy of 169.4 kJ/mol. Freedman et al have also reported relatively higher activation energies (> 80 kJ/mol) for acid catalyzed transesterification reactions [18]. However, with chlorosulfonic acid catalyst, the activation energies are 3 × lower than the H_2SO_4 catalyzed biodiesel synthesis. Although at this juncture, we are unable to provide a justification for result. It is likely to be consequence of basic difference in the mechanism of transesterification reaction with H_2SO_4 and chlorosulfonic acid catalyst.

6.4.3 Thermodynamic analysis

Using the result of kinetic analysis we have also determined the thermodynamic characteristic of the single step and double step process of biodiesel synthesis with chlorosulfonic acid catalyst. For this purpose, we have used the Eyring equation.

$$\ln\frac{k}{T} = -\frac{\Delta H}{R}\frac{1}{T} + \ln\frac{k_b}{h} + \frac{\Delta S}{R} \tag{6.4}$$

where, k is the rate constant at temperatures T and ΔH and ΔS are the activation enthalpy and entropy, k_b, h and R are Boltzmann, Planck and universal gas constant, respectively. ΔH and ΔS for the process can be determined from the slope and y–intercept of the Eyring plot (ln k/T vs $1/T$). The Eyring plots for the single and double step process are shown in Fig. 6.6. Table 6.5 lists the value of ΔH, ΔS and ΔG (Gibbs energy change) for the process, determined using equation $\Delta G = \Delta H - T\Delta S$. A slight increase of activation enthalpy is seen for single step process as compared to the double step, which in turn is compensated by greater reduction of activation entropy for double step process. Again, a possible cause of this trend is due to the absence of water in the reaction mixture for the double step process. The result of these inverse variations is that the overall Gibbs energy change for both single–step and double step protocol is practically same.

Table 6.5: Thermodynamic analysis

Temperatur in ^{o}C(K)	Single step process			Double step process		
	ΔH (kJ/mol)	−ΔS (kJ/mol K)	ΔG (kJ/mol)	ΔH (kJ/mol)	−ΔS (kJ/mol K)	ΔG (kJ/mol)
65(333)			94.07			96.1
45(318)	33.45	0.18	91.34	28.65	0.2	93.06
30(303)			88.61			90.02

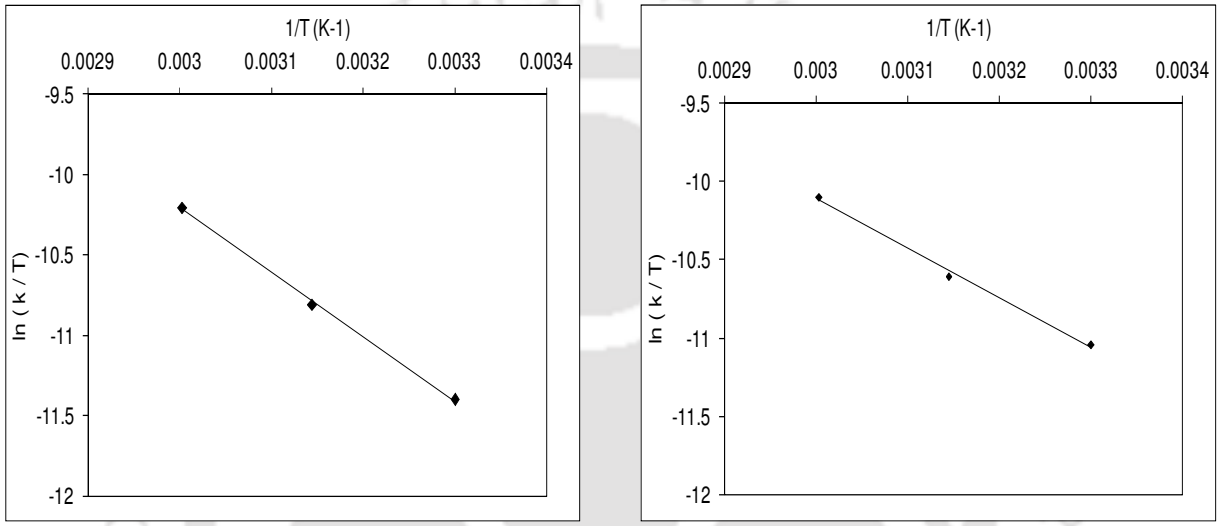

(A) (B)

Figure 6.6: Eyring plots to determine change in enthalpy (ΔH) and change in entropy (ΔS) during transesterification process. (A) Single–step process, Best fit: $y = -4023\ x + 1.8621$, $R^2 = 0.99$, (B) Double step process (with intermediate removal of water after esterification), Best fit: $y = -3168.8\ x - 0.603$, $R^2 = 0.99$.

6.5 Conclusion

Economic production of biodiesel necessitates use of cheap feedstocks that have high FFA content. In this chapter, we have reported a novel single step process for biodiesel synthesis from such feed stocks (with *Jatropha curcas* oil as the model) using chlorosulfonic acid catalyst. Chlorosulfonic acid catalyzes both esterification and transesterification reactions, and also counteracts the inhibition caused by water formed during esterification. The overall reaction time for single step biodiesel process is obviously much smaller than the

conventional double step process comprising of esterification and transesterification with intermediate purification of reaction mixture adopted for feedstocks with high FFA content. Statistical optimization of the process shows 93% yield at conditions of 8.5 wt% catalyst, 20:1 alcohol to oil molar ratio and temperature of 60^{o}C. Peculiar feature of this process is that high yield is seen at moderate temperature of 60^{o}C and a smaller reaction time of 4h, as compared to the much higher temperature (> 100^{o}C) and reaction time of 20h reported in literature for acid catalyzed transesterification reactions [18]. Same argument holds for molar ratio of 20:1 for optimum yield. This value is also much lower than the molar ratios exceeding 50 reported in literature for acid catalyzed transesterification [19]. The activation energy for the process is at least 3× lower than the energy (typically in the range of 140–170 kJ/mol) reported for H_2SO_4 catalyst with high FFA containing feedstocks [14, 15]. However, the thermodynamic analysis reveals that the net Gibbs energy change for the single step process is almost same as that for the conventional double step process. In summary, the chlorosulfonic acid based process for biodiesel has shown encouraging results, which deserve more in–depth investigation with different economic feedstock with high FFA content.

References

[1] Y. Liu, E. Lotero, J. G. Jr. Goodwin, Effect of water on sulfuric acid catalyzed esterification, J. Mol. Catal. A: Chem. 245 (2006) 132–140.

[2] F. Ataya, M. A. Dube, M. Ternan, Acid–catalyzed transesterification of Canola oil to biodiesel under single and two–phase reaction conditions, Energ Fuel. 21 (2007) 2450–2459.

[3] H. Sadek, M. S. A Elamayem, M. A. Elgeheit, Acid hydrolysis of ethyl acetate in presence of glycol or glycerol, Suom. Kemistil. 63 (1963) 115–123.

[4] E. Pines, G. R. Fleming, Proton transfer in mixed water–organic solvent solutions: Correlation between rate, equilibrium constant, and the proton free energy of transfer, J. Phys. Chem. 95 (1991) 10448–10457.

[5] E. Gileadi, E. Kirowa–Eisner, Electrolytic conductivitys – the hopping mechanism of the proton and beyond, Electrochim. Acta 51 (2006) 6003.

[6] E. Lotero E, Y. Liu, D. E. Lopez, K. Suwannakarn, D.A. Bruce, J. G. Jr.Goodwin Synthesis of biodiesel via acid catalysis, Ind. Eng. Chem. Res. 44 (2005) 5353–5363.

[7]. L. Xuarez, Z. Rodriguez, R. Gonzalez, M. Mesa, R. Pellon, New conditions for synthesis of diethyl acetonedicarboxylate, Revista CENIC, Ciencias Quimicas, 25–26 (1–2–3) (1994–1995) 13–14.

[8] R. J. Cremlyn, Chlorosulfonic Acid A Versatile Reagent, UK: Royal Society of Chemisty, 2002.

[9] S. S. Nielsen, Food Analysis Laboratory Manual. (4^{th} ed.). New York: Springer–Verlag, 2010.

[10] X. Deng, Z. Fang, Y. Liu, Ultrasonic transesterification of Jatropha curcas L. oil to biodiesel by a two–stepprocess. Energ. Convn. Manag. 51 (2010) 2802–2807.

[11] T. Sivasankar, A. W. Paunikar, V. S. Moholkar, Mechanistic approach to enhancement of the yield of a sonochemical reaction, AIChE J. 53 (2007) 1132–1143.

[12] G. Gelbard, O. Brès, R. M. Vargas, F. Vielfaure, U. F. Schuchardt, ^{1}H nuclear magnetic resonance determination of the yield of the transesterification of rapeseed oil with methanol, J. Am. Oil Chem. Soc. 72 (1995) 1239–1241.

[13] G. Knothe, Analytical methods used in the production and fuel quality assessment of biodiesel, Trans. ASAE 44 (2001) 193–200.

[14] H. A. Choudhury, R. S. Malani, V. S. Moholkar, Acid catalyzed biodiesel synthesis from Jatropha oil: Mechanistic aspects of ultrasound intensification, Chem. Eng. J. 231 (2013) 262–272.

[15] P. A. Parkar, H. A. Choudhary, V. S. Moholkar, Mechanistic and kinetic investigations in ultrasound assisted acid catalyzed biodiesel synthesis, Chem. Eng. J. 187 (2012) 248– 260.

[16] A. Kalva , T. Sivasankar, V. S. Moholkar, Physical mechanism of ultrasound assisted synthesis of biodiesel, Ind. Eng. Chem. Res. 48 (2009) 534–544.

[17] H. A. Choudhary, S. Chakma, V. S. Moholkar, Mechanistic insight into sonochemical biodiesel synthesis using heterogeneous base catalyst, Ultrason. Sonochem. 21 (2013) 169-81.

[18] B. Freedman, R. O. Butterfield, E. H. Pryde, Transesterification kinetics of soybean oil, J. Am. Oil Chem. Soc. 63 (1986) 1375–1380.

[19] S. Zheng, M. Kates, M.A. Dube, D. D. McLean, Acid–catalyzed production of biodiesel from waste frying oil, Biomass Bioenerg. 30 (2006) 267–272.

CHAPTER 7

Overview and Scope for Future Work

7.1 Overview

In the past one decade, world has observed tremendous growth of biofuels, which has been mainly enthused by concerns about global emission levels and energy security. Many countries including India have already implemented strong support policies for biofuels which have been mainly driven by energy security concerns. Additional drivers for these policies are the desire to sustain the agricultural sector and revitalise the rural economy. More recently, with rising issue of greenhouse gas emission and global warming, the reduction of CO2 emissions, especially in the transport sector has become an additional important driver for biofuel development. One of the obvious and most common policy is a blending mandate – which defines the proportion of biofuel that must be mixed with liquid transport fuel. Government funding, soft loans, tax incentives and other subsidies are some support measures for the biofuels policy. More than 50 countries have adopted blending targets or mandates. India has a mandate of implementing 20% blends of ethanol-gasoline and biodiesel-diesel by 2017 [1]. The global biofuel production has shown a marked growth from

16 billion litres in 2000 to more than 100 billion litres (volumetric) in 2010.As a result of these efforts, the biofuels today provide around 3% of total road transport fuel globally (on an energy basis). However, this is far lesser than the actual potential and considerably higher targets need to be achieved in near future [1].

The production of transport fuels from biomass, in either liquid or gaseous form, is a simultaneous solution to low net fossil-energy requirement and low life-cycle greenhouse gas (GHG) emissions. The main hurdles to the expansion of biofuels production are competition for agricultural commodities and land, and impacts on water resources and biodiversity. Conventional biofuels such as biodiesel and biobutanol are economically not competitive with petroleum derived diesel and gasoline at market prices, although competitiveness varies depending on feedstock costs and international crude oil prices. Large investments for commercial-scale production of biofuels can only be attracted if specific support measures such as tax waivers/concessions, subsidies, minimum support price or special financial support are available that sufficiently address the financial risks associated with scaling up innovative processes and the insecurity of product markets. The successful development of advanced biofuels technologies, using non-food biomass feedstocks that would provide also solve the fuel-versus-food controversy, could help overcome most barriers and achieve sustainable, very low CO_2, cost-effective biofuels.

The Energy Technology Policy division of International Energy Agency [1] has set a target of 50% reduction in energy-related CO_2 emissions by 2050 as compared to 2005 levels. This target can only be achieved with rapid development and deployment of low-carbon energy measures and technologies, such as improved energy efficiency, greater use of renewable energy sources, and effective implantation (or enforcement) of policy of CO_2 Capture and Sequestration. To achieve the targets of reduction in CO_2 emissions in the transport sector, it is necessary that biofuels share 27% of total transport fuel. With this, the

biofuel demand by 2050 is likely to reach 32 EJ, or 760 million tonne of oil equivalent (Mtoe).

The present thesis work was undertaken with aim of developing a new technology for biodiesel synthesis with non-edible oil feedstock that overcomes the demerits of conventional technology and at the same time boosts the economy of the process. We summarize herewith the major findings of our study addressing different facets of the ultrasound assisted biodiesel synthesis. These results, when viewed together at a glance (summarized in Table 7.1), give a coherent and interesting picture of the ultrasound assisted biodiesel synthesis process.

Chapter 1 gives the general introduction of the thesis theme and also describes the motivation for the same. In this chapter, we have tried to give a picture of the scenario of energy sector (especially the petroleum industry) in India supported with several statistical data. We have also described the efforts on renewable energy in India and India's biofuels policy. We have also given the information and data on GHG emissions and other environmental issues, which further emphasize the urgent need for use of biofuels for decarbonisation of the environment. On this basis, we have given the motivation of the present thesis.

Chapter 2 presents the literature review on various aspects of biodiesel synthesis with ultrasound using mainly two feedstock, viz. soybean oil and Jatropha oil. In view of the theme of the thesis, the literature on biodiesel synthesis with heterogeneous catalyst (using either ultrasonic synthesis or conventional synthesis techniques) has also been reviewed. We have also given a general introduction to basic principles and equations of ultrasound and cavitation bubble dynamics.

In Chapter 3, we have presented studies in ultrasound assisted synthesis of biodiesel from soybean oil using CaO as heterogeneous catalyst. In this chapter, we have attempted to identify the mechanistic features of ultrasound–enhanced biodiesel synthesis with solid CaO.

Table 7.1: Summary of results of different components of ultrasonic biodiesel process development as described in preceding chapters

Sl. No.	Oil Type	Oil / MeOH Ratio		Catalyst Type		Catalyst Loading (wt% of oil)		Reaction Temperature (°C)		Total Reaction Time	FAME Yield (% purity)
		Esterification	Transesterification	Esterification	Transesterification	Esterification	Transesterification	Esterification	Transesterification		
1	**Soybean**	NA	10:1	NA	CaO	NA	6	NA	~ 62	1 h	~ 89
2	***Jatropha curcas***	15:1	11:1	H_2SO_4	CaO	3	5.5	~65	~ 65	2 h /2 h	~ 95
3	***Jatropha curcas***	15:1	7:1	H_2SO_4	H_2SO_4	3	6	~65	~ 70	2 h/2 h	~ 80
4	***Jatropha curcas***	NA	20:1	NA	$ClSO_3H$	NA	9	NA	~ 60	4 h	~ 95

A statistical design of experiments (Box–Behnken) was used to identify the influence of temperature, alcohol to oil molar ratio and catalyst loading on transesterification yield. The optimum values of these parameters for the highest yield were identified through Response Surface Method (with a quadratic model) and ANOVA. The optimum values for transesterification of soybean oil were: temperature = 62°C, molar ratio = 10:1 and catalyst loading = 6 wt%. The activation energy was determined as 82.3 kJ/mol using pseudo 1st order reaction kinetics. The value of activation energy is higher than that for homogeneous catalyzed system (for both acidic and basic catalyst). The experimental results have been analyzed by simulations of cavitation bubble dynamics. Due to 3–phase heterogeneity of the system, the yield was dominated by intrinsic kinetics, and the optimum temperature for the highest yield was close to boiling point of methanol. At this temperature, the influence of cavitation bubbles (in terms of both sonochemical and sonophysical effect) is negligible, and ultrasonic micro–streaming provided necessary convection in the system. The influence of all parameters on the reaction system was found to be strongly inter–dependent.

In Chapter 4, we reported studies in ultrasound-assisted heterogeneous base catalyzed (CaO) synthesis of biodiesel from crude *Jatropha curcas* oil. The synthesis of biodiesel was carried out in two stages, viz. esterification and trans-esterification. The esterification process is not influenced by ultrasound. The transesterification process, however, shows marked enhancement with ultrasound. A statistical experimental design has been used to optimize the process conditions for the synthesis. The optimum values of parameters for the highest yield of transesterification have been determined as follows: alcohol to oil molar ratio ≈ 11, catalyst concentration ≈ 5.5 wt%, and temperature ≈ 64°C. Integral method was adopted to determine the order of the reaction and it was found to be close to 3rd order with respect to TG concentration. Hence 3rd order kinetic model was fitted to determine the rate constant and the activation energy. The activation energy of the reaction is calculated as 133.5 kJ/mol. The

heterogeneity of the system increases mass transfer constraints resulting in approx. 4× increase in activation energy, as compared to homogeneous alkali catalyzed system. It is also revealed that intense micro-convection induced by ultrasound enhances the mass transfer characteristics of the system with ~ 20% reduction in activation energy, as compared to mechanically agitated systems. XRD analysis confirms formation of $Ca(OMe)_2$, which is the active catalyst for transesterification reaction. The response surface studies were done and contour plots with elliptical nature were obtained. These plots revealed a good interaction among the reaction parameters selected for the study. The significance of interaction of the plots was also confirmed from their *p*-values of 0.00. Influence of catalyst concentration and alcohol to oil molar ratio on the transesterification yield were found to be inter-linked through formation of methoxy ions, and their diffusion to the oil-alcohol interface.

Chapter 5 presents studies in optimization of biodiesel synthesis from *Jatropha Curcas* oil with H_2SO_4 catalyst under ultrasonic irradiation. A statistical experimental design (Box–Behnken) is coupled to simulations of cavitation bubble dynamics. The transesterification system was revealed to be strongly controlled by intrinsic kinetics and mass transfer resistance. A pseudo 1^{st} order kinetic model was fitted to determine the rate constants and activation of acid catalyzed transesterification reaction. The activation energy for transesterification reaction was determined as 167.42 kJ/mol. High activation energy for homogenous acid catalyzed transesterification (compared to homogenous base catalyst) results in slower reaction kinetics. Sonication causes intense mixing between phases leading to high interfacial area, but it cannot alter the intrinsic reactivity of methoxide ion as well as methanol. Thus, the kinetics of acid catalyzed process does not show as much enhancement with sonication as the base catalyzed process. The optimum conditions for biodiesel synthesis have been determined as: alcohol to oil molar ratio ≈ 7, catalyst concentration ≈ 6% w/w oil and temperature ≈ 70°C. The influence of these variables is highly involved and interlinked,

and any deviation from its optimum value leads to sharp reduction in the FAME yield. Results of this study illustrate that sonication does not change the chemistry of acid–catalyzed transesterification, and the beneficial effect is only of physical nature, which is further limited by the intrinsic kinetics and mass transfer. Beneficial effect of sonication on transesterification reaction was found to be only through the intense micro–mixing induced by ultrasound.

Chapter 6 reports investigations in a novel single-step process with chlorosulfonic acid catalyst for biodiesel synthesis using *Jatropha curcas* oil as feedstock. The crude *Jatropha curcas* oil has high FFA content, and hence, its pre-treatment is necessary to remove the FFA, which interferes in transesterification reaction. Chlorosulfonic acid can handle high FFA content in the vegetable oils by catalyzing both esterification and transesterification reactions. Moreover, chlorosulfonic acid also counteracts inhibition caused by water formed during esterification, which is the cause for very slow kinetics of acid catalyzed transesterification. Statistical optimization has been done using Box–Behnken experimental design and the process shows 93% yield for 8.5 wt% catalyst, 20:1 alcohol to oil molar ratio and temperature of 65^{o}C. High yield is seen at moderate temperature and molar ratio, which are much smaller than that for conventional sulphuric acid catalyzed processes. The activation energy for the process (57 kJ/mol) is at least 3× lower than the energy for sulphuric acid catalyzed transesterification. The thermodynamic analysis reveals that the net Gibbs energy change for the single step process is almost same as that for sulphuric acid catalyzed process. These results show distinct merits of chlorosulfonic acid catalyzed biodiesel synthesis. In order to compare the result of transesterification a single step and two step transesterification reactions have been carried out and Arrhenius plot for determination of activation energy for both the process.

On a whole, this thesis has attempted to investigate mechanistic issues of ultrasonic

process for production of biodiesel from both edible and non edible oil source. Since conventional method of reaction, which involves mechanical agitation of the reaction mixture, is inefficient in biodiesel production due to mass transfer limitation, use of ultrasound has been put forward as remedy. The problems associated with homogeneous catalyst for biodiesel synthesis have been overcome with the use of heterogeneous base catalyst. The novel process of biodiesel synthesis with chlorosulfonic acid as catalyst has high potential for application on pilot and commercial scale. In this process, chlorosulfonic acid catalyses esterification and transesterification reactions simultaneously. The results of present thesis provide a mechanistic insight in the sonochemical biodiesel synthesis along with statistical optimization. We believe that this thesis would open new avenues for undertaking future research in this area. Some suggestions in this regard are given below:

7.2 Scope for Future Work

The work presented in this thesis can be extended in many ways which can have focus on further optimization with ultrasound parameters like frequency and intensity or development and use of better solid catalysts or biodiesel synthesis. It is also worth carrying out some of the optimized ultrasonic biodiesel synthesis processes in this work at higher scale. Some suggestions for the future work are as follows:

1. Synthesis of metal doped base catalyst for biodiesel production.

2. Development of new heterogeneous acid catalyst with silica and zirconia support for transesterification reaction.

3. Use of other cheap non edible feedstock available biodiesel synthesis.

4. Simultaneous extraction of oil from seed, esterification and transesterification with ultrasound.

5. Finally scaling up ultrasound assisted biodiesel production from lab-scale to industrial

scale. Up scaling may also include design of new ultrasonic reactors and optimum condition for the whole process.

References

[1] Technology Roadmap: Biofuels for Transport, IEA Renewable Energy Division, International Energy Agency, Paris, France, 2011.

Acknowledgments

It is my pleasure to thank those who made this thesis possible. I recollect numerous occasions and moments which make me proud to be a part of this world class Centre. It is my privilege to be amidst some intellectual genius, who guided in my pursuit of knowledge. I owe my deepest gratitude to all of them.

The first and foremost appreciation goes to my supervisor Prof. V. S. Moholkar for his valuable guidance throughout the research work. I thank him for his encouragement, guidance, and support from the initial to the final level, which enabled me to develop a better understanding of the subject and leads to a successful completion. I would like to acknowledge my sincere gratitude to my doctoral committee members, Prof. A.T. Khan, Prof. G.Das and Dr. B.P. Mandal for their insightful advices and suggestions throughout the research.

My sincere thanks go to the Center for Energy and also to the faculty members associated with Center for their constant inspiration and valuable suggestions. The kind and constant help of the staff members of the Center is also duly acknowledged. I am also thankful to the Indian Institute of Technology Guwahati for providing me with the infrastructure and facilities for advanced research.

I extend my sincerest thanks to staff members of Center for Energy for extending helping hands in various part of the research work. My special thanks go to Pankaj Kalita, Leepakshi, Borbora, Geetanjali Hazarika, Dhiren Huzuri, Krishna, and Dhulumoni for their constant encouragement and help during the course of the research.

I am also thankful to my colleague and friends Amrita Ranjan, Swati Khanna, Sankar, Suchi, Jay, Arup, Manish, Preetam for their constant help, motivation, and enthusiastic company and all the wonder ful time we spent in various events. I will specifically like to extend by sincere

thanks to my close friends Amrita Ranjan, Swati, Abu, Anil Shukla, Tauseef who were like an extended family for me during my stay at Guwahati.

I acknowledge Ministry of New and Renewable Energy for providing JRF and SRF -NRE fellowship during my PhD tenure. The infrastructural and analytical facilities provided by

Centre for Energy, Department of Chemical Engineering, and facility provided by CIF, IIT Guwahati are also acknowledged.

The episode of acknowledgement would remain incomplete without mentioning the care of my parents, my siblings and my wife, who are an inseparable part of my life. I owe my gratitude to all of them.

I would express my deepest gratitude to all my well wishers. Last but not the least, I express my thanks to Almighty for blessing me and giving the strength to complete this work.

Date: 26-05-2014

Hanif A. Choudhury

Guwahati

RESEARCH OUTPUT OF THE THESIS

- P. A. Parkar[1], **H. A. Choudhary[1]**, V. S. Moholkar, Mechanistic and kinetic investigations in ultrasound assisted acid catalyzed biodiesel synthesis, ***Chemical Engineering Journal***, 187 (2012) 248-260. ([1] Equal contribution).
- **H. A. Choudhury**, S. Chakma, V. S. Moholkar, Mechanistic insight into sonochemical biodiesel synthesis using heterogeneous base catalyst, ***Ultrasonic Sonochemistry*****,** 21 (2014) 169–181.
- **H. A. Choudhury**, R. S. Malani, V. S. Moholkar; Acid catalyzed biodiesel synthesis from Jatropha oil: mechanistic aspects of ultrasonic intensification, ***Chemical Engineering Journal***, 231 (2013) 262-272.
- **H. A. Choudhury**, P. P. Goswami, R. S. Malani, V. S. Moholkar, Ultrasonic biodiesel synthesis from *Jatropha curcas* oil with heterogeneous base catalyst: Mechanistic insight & statistical optimization, ***Ultrasonic Sonochemistry*****,** 21 (2014) 169–181.
- **H. A. Choudhury**, P. Srivastava, V. S. Moholkar; Single step acid catalyzed biodiesel synthesis from *Jatropha curcas* oil: Statistical optimization, ***AIChE Journal***, 60 (2014) 1572-1581.